

Lecture Notes in Civil Engineering

Rafid AlKhaddar  
Ram Karan Singh  
Subashisa Dutta  
Madhuri Kumari *Editors*

# Advances in Water Resources Engineering and Management

Select Proceedings of TRACE 2018

 Springer

# Lecture Notes in Civil Engineering

Volume 39

## Series Editors

Marco di Prisco, Politecnico di Milano, Milano, Italy

Sheng-Hong Chen, School of Water Resources and Hydropower Engineering,  
Wuhan University, Wuhan, China

Ioannis Vayas, Institute of Steel Structures, National Technical University of  
Athens, Athens, Greece

Sanjay Kumar Shukla, School of Engineering, Edith Cowan University, Joondalup,  
WA, Australia

Anuj Sharma, Iowa State University, Ames, IA, USA

Nagesh Kumar, Department of Civil Engineering, Indian Institute of Science  
Bangalore, Bangalore, Karnataka, India

Chien Ming Wang, School of Civil Engineering, The University of Queensland,  
Brisbane, QLD, Australia

**Lecture Notes in Civil Engineering (LNCE)** publishes the latest developments in Civil Engineering - quickly, informally and in top quality. Though original research reported in proceedings and post-proceedings represents the core of LNCE, edited volumes of exceptionally high quality and interest may also be considered for publication. Volumes published in LNCE embrace all aspects and subfields of, as well as new challenges in, Civil Engineering. Topics in the series include:

- Construction and Structural Mechanics
- Building Materials
- Concrete, Steel and Timber Structures
- Geotechnical Engineering
- Earthquake Engineering
- Coastal Engineering
- Hydraulics, Hydrology and Water Resources Engineering
- Environmental Engineering and Sustainability
- Structural Health and Monitoring
- Surveying and Geographical Information Systems
- Heating, Ventilation and Air Conditioning (HVAC)
- Transportation and Traffic
- Risk Analysis
- Safety and Security

To submit a proposal or request further information, please contact the appropriate Springer Editor:

- Mr. Pierpaolo Riva at [pierpaolo.riva@springer.com](mailto:pierpaolo.riva@springer.com) (Europe and Americas);
- Ms. Swati Meherishi at [swati.meherishi@springer.com](mailto:swati.meherishi@springer.com) (India);
- Ms. Li Shen at [li.shen@springer.com](mailto:li.shen@springer.com) (China);
- Dr. Loyola D'Silva at [loyola.dsilva@springer.com](mailto:loyola.dsilva@springer.com) (S-E Asia and Australia/NZ).

**Indexed by Scopus**

More information about this series at <http://www.springer.com/series/15087>

Rafid AlKhaddar · Ram Karan Singh ·  
Subashisa Dutta · Madhuri Kumari  
Editors

# Advances in Water Resources Engineering and Management

Select Proceedings of TRACE 2018

 Springer

المنارة للاستشارات

*Editors*

Rafid AlKhaddar  
Department of Civil Engineering  
Liverpool John Moores University  
Liverpool, UK

Subashisa Dutta  
Indian Institute of Technology Guwahati  
Guwahati, India

Ram Karan Singh  
King Khalid University  
Abha, Saudi Arabia

Madhuri Kumari  
Department of Civil Engineering  
Amity School of Engineering  
and Technology, Amity University  
Uttar Pradesh  
Noida, India

ISSN 2366-2557

Lecture Notes in Civil Engineering

ISBN 978-981-13-8180-5

<https://doi.org/10.1007/978-981-13-8181-2>

ISSN 2366-2565 (electronic)

ISBN 978-981-13-8181-2 (eBook)

© Springer Nature Singapore Pte Ltd. 2020

This work is subject to copyright. All rights are reserved by the Publisher, whether the whole or part of the material is concerned, specifically the rights of translation, reprinting, reuse of illustrations, recitation, broadcasting, reproduction on microfilms or in any other physical way, and transmission or information storage and retrieval, electronic adaptation, computer software, or by similar or dissimilar methodology now known or hereafter developed.

The use of general descriptive names, registered names, trademarks, service marks, etc. in this publication does not imply, even in the absence of a specific statement, that such names are exempt from the relevant protective laws and regulations and therefore free for general use.

The publisher, the authors and the editors are safe to assume that the advice and information in this book are believed to be true and accurate at the date of publication. Neither the publisher nor the authors or the editors give a warranty, expressed or implied, with respect to the material contained herein or for any errors or omissions that may have been made. The publisher remains neutral with regard to jurisdictional claims in published maps and institutional affiliations.

This Springer imprint is published by the registered company Springer Nature Singapore Pte Ltd.

The registered company address is: 152 Beach Road, #21-01/04 Gateway East, Singapore 189721, Singapore

# Preface

Water resources are of paramount importance for mankind. These irreplaceable resources are experiencing major stress due to depletion of quantity and degradation of quality. Global climate change is altering the basic hydrologic cycle, thus complicating the water resources management challenges. The issues related to water resources cannot be resolved in isolation by engineers or scientists, but it requires multidisciplinary and integrated understanding and approach. The recent technological advances are proving to be an effective tool for addressing the broad spectrum of water resources issues like rainfall prediction, glacier melting, river pollution, river ecosystem sustenance, flood disaster, and many more.

This book is a compilation of various research works carried out by a panel of esteemed experts in the area of water resources engineering and management. The objective of this compilation is to provide relevant and timely information to those who are striving to contribute to this domain by utilizing the latest technology. The content of this book is based on papers accepted during the Second International Conference on Trends and Recent Advances in Civil Engineering (TRACE 2018) held in Amity University, Noida, on August 23–24, 2018. It covers interdisciplinary innovative research in hydrometeorology, river ecology, reservoir, water pollution and treatment, and hydraulic structure. The topics include technological intervention and solution for climate change impacts on water resources, water security, clean water to all, sustainable water reuse, water loss through evapotranspiration, etc. The chapters present the latest areas of research like HEC, SWAT, GIS and remote sensing application for solving water resources issues. We are hopeful that it will prove to be of high value to graduate students, researchers, scientists, and practitioners of water resources system.

We owe our sincere gratitude to all our family members and friends who helped us through this journey of publishing the book. Special thanks to all the national and international reviewers who helped us in selecting the best of the works as different chapters of the book. Our appreciation goes to the research fellows who assisted us in preliminary follow-ups with authors and initial software-based plagiarism check. We thank our management team including Head of Institution, Head of the Department, and other faculty members for providing valuable suggestions

and support whenever it was required. We are very thankful to advisory committee and organizing committee of TRACE 2018 who believed in us and provided the opportunity for publishing the book. We wish to acknowledge and thank all the authors and co-authors of different chapters who cooperated with us at every stage of publication and helped us to sail through this mammoth task. Last but not least, we are grateful to the editing team of Springer who provided all guidance and support to us in the compilation of the book and also shaped up the book into a marketable product.

Liverpool, UK  
Abha, Saudi Arabia  
Guwahati, India  
Noida, India

Rafid AlKhaddar  
Ram Karan Singh  
Subashisa Dutta  
Madhuri Kumari

# Contents

<b>Performance Evaluation of Five Penman Forms of Models by Means of Lysimetric Evapotranspiration Under Water Stress Environments at New Delhi, India</b> .....	1
Ram Karan Singh, Javed Mallick and P. S. Pawar	
<b>A Methodology to Measure Flow Fields at Bridge Piers in the Presence of Large Wood Debris Accumulation Using Acoustic Doppler Velocimeters</b> .....	17
Iacopo Carnacina, Aleksandra Lescova and Stefano Pagliara	
<b>Real-Time Reservoir Operation Policy: A Case Study of Tanahu Hydropower Project</b> .....	27
Bhola N. S. Ghimire, Rabindra Nath Shrestha and Upendra Dev Bhatta	
<b>Nexus of Water Footprint with Energy and GDP of Saudi Arabia and Solution for Sustainable Water Usage</b> .....	43
Vineet Tirth	
<b>Statistical Parameters of Hydrometeorological Variables: Standard Deviation, SNR, Skewness and Kurtosis</b> .....	59
Chetan Sharma and C. S. P. Ojha	
<b>A New Approach to Analyze the Water Surface Profile Over the Trench Weir</b> .....	71
Swati Bhave and Sanjeev Kumar	
<b>Soil Loss Assessment in Imphal River Watershed, Manipur, North-East India: A Spatio-Temporal Approach</b> .....	81
Loukrakpam Chandramani and Bakimchandra Oinam	
<b>Analysis of the Extreme Rainfall Events Over Upper Catchment of Sabarmati River Basin in Western India Using Extreme Precipitation Indices</b> .....	103
Shivam Gupta, Ankit Gupta, Sushil K. Himanshu and Ronald Singh	



<b>Rainfall Runoff Modelling of Urban Area Using HEC-HMS: A Case Study of Hyderabad City</b> .....	113
Vinay Ashok Rangari, V. Sridhar, N. V. Umamahesh and Ajey Kumar Patel	
<b>Hydrodynamic Simulation of River Ambica for Riverbed Assessment: A Case Study of Navsari Region</b> .....	127
Darshan Jayeshbhai Mehta and Sanjay Madhusudan Yadav	
<b>Evaluation of the SWAT Model for Analysing the Water Balance Components for the Upper Sabarmati Basin</b> .....	141
Ankit Gupta, Sushil K. Himanshu, Shivam Gupta and Ronald Singh	
<b>Rainfall-Runoff Modelling and Simulation Using Remote Sensing and Hydrological Model for Banas River, Gujarat, India</b> .....	153
Anant Patel	
<b>GIS-Based Morphometric Analysis and Prioritization of Upper Ravi Catchment, Himachal Pradesh, India</b> .....	163
D. Khurana, S. S. Rawat, G. Raina, R. Sharma and P. G. Jose	
<b>Estimation of Domestic Water Demand and Supply Using System Dynamics Approach</b> .....	187
Bharti Chawre	
<b>Sustainable Development and Management of Groundwater in Varanasi, India</b> .....	201
Padam Jee Omar, S. B. Dwivedi and P. K. S. Dikshit	
<b>Applications of GIS in Management of Water Resources to Attain Zero Hunger</b> .....	211
Ashita Sharma, Manish Kumar and Nitasha Hasteer	
<b>Electrocoagulation as an Eco-Friendly River Water Treatment Method</b> .....	219
Khalid S. Hashim, Rafid AlKhaddar, Andy Shaw, P. Kot, Dhiya Al-Jumeily, Reham Alwash and Mohammed Hashim Aljefery	
<b>Wetland Dynamics Using Geo-Spatial Technology</b> .....	237
Nilendu Das, Anurag Ohri, Ashwani Kumar Agnihotri, Padam Jee Omar and Sachin Mishra	
<b>Inland Waterway as an Alternative and Sustainable Transport in Kuttanad Region of Kerala, India</b> .....	245
Madhuri Kumari, Sarath Syamaprasad and Sushmit Das	

## About the Editors

**Dr. Rafid AlKhaddar** has extensive experience in Water and Environmental Engineering, with special expertise in wastewater treatment methods. He graduated from the University of Basra, Iraq as a civil engineer, and obtained his Masters and PhD in Civil Engineering Hydraulics from the University of Strathclyde, Glasgow, UK. He is currently Professor and Head of the Department of Civil Engineering at Liverpool John Moores University where he manages 27 staff and over 780 students, who are enrolled in various courses such as HNC, BEng, MEng, MSc and PhD. He has maintained a very strong link with the UK Water and Environmental industry in order to stay involved with any new developments in the aforementioned fields. He was the President of the Chartered Institution of Water and Environmental Management (CIWEM) in 2015–16. He is also a Fellow of the Institution and an Honorary Vice President of the Institution. He has published over 160 articles in peer-reviewed journals and international conferences.

**Dr. Ram Karan Singh** is Professor of Civil Engineering in King Khalid University, Abha City, Kingdom of Saudi-Arabia. He has over 28 years of teaching, research and administrative experience in top institutions and universities in India and abroad. He completed his B.E.(Hons.) Civil Engineering, M.E. in Civil Engineering (with specialization in Hydraulics Engineering), and PhD in the area of hydraulics and water resources engineering from BITS-Pilani, Pilani, India. He was awarded a post-doctoral fellowship by the Japan Society for the Promotion of Science, Japanese Government from 2002–2004 to carry out “Diffuse pollution modeling of water environment of Japanese low land watersheds” at the Department of Hydraulics Engineering, NIRE, Tsukuba Science City, Japan. He has published over 150 research papers, four books and also supervised 10 PhD thesis. He is a recipient of several national and international awards and fellow of various professional societies in his area of work.

**Dr. Subashisa Dutta** received his Ph.D in Computational Hydraulics from the Indian Institute of Technology (IIT) Kharagpur. He completed his Master’s in Irrigation and Hydraulics Engineering and Bachelor’s in Civil Engineering from

Sambalpur University. Currently, he is Professor in the Department of Civil Engineering, Indian Institute of Technology (IIT) Guwahati. He has worked at the Scientist Space Applications Centre (ISRO), Ahmedabad prior to joining IIT Guwahati. His major research interests are hill-slope hydrology, distributed hydrological modeling, flood inundation modeling, geo-spatial technology, 2D river flow, sediment transport modeling, river bank protection and stormwater drainage design. He is leading multiple research works by Inland Waterways Authority of India. He is also working on dam break analysis of hydroelectric projects in Assam, India.

**Dr. Madhuri Kumari** received her PhD from The Energy Resource Institute (TERI) for her work on geostatistical modeling for prediction of rainfall in the Indian Himalayas. She completed her Master's in Hydraulics and Water Resources Engineering from Institute of Technology, Banaras Hindu University in 1999, and Bachelor's in Civil Engineering from Andhra University in 1997 and was recipient of Gold Medal. She is working as Professor in the Department of Civil Engineering, Amity School of Engineering and Technology, Amity University, Noida, India. She has a vast industry experience of 11 years and an academic experience of 9 years. Her research works in the area of rainfall modeling have been published in reputed journals. Her research interests include application of geographical information system in solving problems related to water resources engineering.

# Performance Evaluation of Five Penman Forms of Models by Means of Lysimetric Evapotranspiration Under Water Stress Environments at New Delhi, India



Ram Karan Singh, Javed Mallick and P. S. Pawar

**Abstract** A global scale has been recommended using the Penman–Monteith method of FAO (56) on reference water evapotranspiration ( $ET_o$ ) calculations or irrigation design, which provides good results under different climatic conditions. In addition to this method, various forms of popular Panamanian equations such as FAO 24 Penman (1977), Kimberly–Penman (1996), and Penman (1948) are widely used throughout the world including India. The evaporation in the Hydrology and Irrigation Committee of the American Society of Civil Engineers has formed a committee recommended by reference standard (standardized Penman–Monteith equation). This method works in a manner similar to that of FAO Penman–Monteith using the short reference station ( $ET_{os}$ ) used in the present study. The main objective of this study is to assess the performance of these five common forms of Penman forms of the equations established on the daily predictions of the ET indicators under climatic conditions in New Delhi. The ET ( $ET_c$ ) harvest can be obtained using crop factor ( $K_c$ ). One can develop and use different types of crop coefficients, i.e., single  $K_c$  and single  $K_c$  with weather correction. The choice of  $K_c$  depends on the accuracy required in the  $ET_c$  accounts. For the evaluation of the performance of five models, the use of selected data from seventeen harvest seasons from 1976 to 2006 of maize (*Zea mays* L.) was used. Each harvest season requires information on lysimetric ET along with other meteorological parameters and soil moisture monitoring. The statistical indicators used to evaluate the performance were the least squares difference (RMSD), mean bias error (MBE), and  $t$  count. From the study, we can conclude that the performance of the Penman–Monteith ASCE and FAO 56 Penman–Monteith is slightly higher than that of the other models under the above-mentioned water conditions, using all four types of crop coefficients.

**Keywords** Evapotranspiration · Lysimetric · Water stress conditions · Penman equations

---

R. K. Singh (✉) · J. Mallick  
King Khalid University, Abha, Kingdom of Saudi Arabia  
e-mail: [ram@kku.edu.sa](mailto:ram@kku.edu.sa); [ramkaran.singh@gmail.com](mailto:ramkaran.singh@gmail.com)

P. S. Pawar  
The Energy and Resources Institute, IHC, New Delhi, India

© Springer Nature Singapore Pte Ltd. 2020  
R. AlKhaddar et al. (eds.), *Advances in Water Resources Engineering and Management*, Lecture Notes in Civil Engineering 39,  
[https://doi.org/10.1007/978-981-13-8181-2\\_1](https://doi.org/10.1007/978-981-13-8181-2_1)

## 1 Introduction

The decline in water availability in recent decades is one of the major problems that could severely limit the industrial and agricultural growth of India. Irrigation is the leading sector of water use in India, which uses more than 80% of whole water. This trend is expected to continue in the future [9]. The needs of irrigation water depend on the rate of evaporation (ET). Therefore, this important information is required by decision makers, managers, farmers, or many related people such as naturalists and economists.

Many ET equations have been developed and used by researchers who have posed a question about the best method without answers [10]. The ET equations are available from simple temperature-based equations to a range of complex multilayered equations based on resistance. In addition, different versions of the basic equations are available to interested users, making their use more complex. The transferability of crop coefficients from one region to another raises questions again.

For these and other related reasons, evapotranspiration in the Hydrology and Irrigation Committee of the American Society of Civil Engineers, the Action Committee (AC) was set for standardize "Reference Evaporation Equations" [4, 10, 23]. The AC studied the problems in detail and recommended the adoption of two standard reference equations, one for  $ET_{os}$  representing short crop (i.e., natural vegetation like grass) and another for  $ET_{rs}$  representing a large crop (i.e., alfalfa); both day-to-day and hourly versions of the equations were undertaken. The purpose of the standard equation and the calculation of criteria is to standardize the ET methodology and use it as a basis for determining the crop factor for both agricultural use and landscape. The result of the ASCE Working Committee is the Uniform Equation Reference (Standard Penman-Monteith) [4, 23]. FAO Irrigation and Drainage Paper No. 56 recommends FAO Penman-Monteith method as the standard method. The results of ASCE standardized Penman-Monteith equation for daily ET calculations using short crop reference ( $ET_{os}$ ) are the same as FAO 56 Penman-Monteith equation. These two methods can predict the most correct ET in a wide range of climates and locations with maximum probability. However, besides these methods, other methods like Penman (1948), FAO 24 Penman, and Kimberly-Penman (1996) are also used widely in India.

ET is difficult to measure in field environments. To determine ET special equipment or to accurately measure different physical parameters and water balance, the lysimeters are required. These methods are costly and require qualified research staff. Even with these restrictions, the regular measurement of ET using these methods is critical compared to other indirect methods. The most common crop-based approach follows ET estimates worldwide, including India. As mentioned above, lysimetric ET data are rare and may be available for several years as cultures and sites. However, the assessment of indirect methods using these data is of utmost importance for accurate estimates and their applications. Current examples of such reviews can be found by Alexandris and Kerkides [1], Karam et al. [12, 13], Garcia et al. [7], Utset et al. [22], Medaires et al. [14], Pauwels and Samson [15], Brunel et al. [5],

Xinmin et al. [24], Suleiman et al. [21], Gavilan et al. [8], Pereira et al. [16], Sauer et al. [17], Singh and Islam [18, 19] and Singh et al. [20].

This work describes the results of the study, which was conducted to evaluate five advanced computational methods that are more widely used in a variety of water stress conditions using ET lysimetric technology. In contrast, research results help to estimate the exact amount of irrigation and scheduling of irrigation.

## 2 Reference ET Equations

As seen before, the different equations are available for estimating ET. The reference ET for Windows manual provides a detailed description of the most commonly used methods [3]. These details are also available in Dorrenbos and Pruitt [6], Jensen et al. [11], and Allen et al. [2] or other popular textbooks or research articles. In order to avoid duplication of these available works in general, the name of the method and its abbreviated form used in this publication are mentioned only here. In the study here, five methods were chosen that are most frequently used in the world plus India. These methods are ASCE standardized FAO 24 corrected Penman (24\_Pen), Penman–Monteith (St\_PM), Kimberly–Penman variable wind function (KP\_96), FAO 56 Penman–Monteith (56\_PM), and Penman (1948 and 1963) with original wind function (Pen\_48).

## 3 Materials and Methods

### 3.1 Location

Research Center at the Water Technology Center (WTC), Indian Institute of Agricultural Research (IARI), New Delhi, India. The latitude, longitude, and elevation of the study area are 28.67°, 77.17°, and 228 m (above sea level), respectively. The above-mentioned pilot site is a regular monitoring station of the lysimeter evaporation (ET) at the Indian Meteorological Service (IMD), India, and is maintained in accordance with WMO specifications.

### 3.2 Data Sources and Integrity

IMD is responsible for capturing agricultural data and high-quality weather. It has a wide network of 219 agricultural meteorological observatories, 40 ET observatories, and some private observatories. The well-maintained ET observation sites also have enough green space area. Fifteen years of crop data were collected from 1976 to 1991

by IMD, India. In addition, two crop year data were used from the field (2005 and 2006) conducted at the same site for the analysis provided. The total data include 17 ET harvest periods lysimetric with associated weather parameters and weekly moisture monitoring of the maize (*Zea mays* L.). The research results and data were used in addition to the studies presented here for further research on this topic. All data refer to the months of July to November when maize is grown. The use of daily or larger time steps, weekly or monthly, for ET analysis is common in India, and hourly steps are rarely used in ET analysis. Therefore, an analysis of the daily time step was performed.

### 3.3 Data Selection for Analysis

FAO's expert opinion on the review of FAO's crop water needs has adopted the following definition of crop selection. "A virtual reference station with a supposed plant height of 0.12 m, surface resistance of  $70 \text{ SM}^{-1}$ , and an albedo of 0.23." In order to maintain grouping with the definition of non-rainy days, the day should be cleared with the bright sun, days with appropriate soil moisture, and at least 75–80% soil cover, which is selected for the evaluation. According to this rule, the daily water balance in the soil was determined for 17 crop seasons using the method described in Annex 8 of FAO 56 [2]. Established on precipitation rates and soil moisture ratios available in the actual water balance, the data were divided into numerous groups. These data were then evaluated again for bright sunlight, vapor pressure, and wind speed situations.

### 3.4 Reference ET Calculations

Calculate forest reference criteria and ED code for day and hour increments using REF-ET for Windows version 2.0 (evapotranspiration). This is a program [3] precisely for standard ET accounts for a range of common equations. The five methods were developed to analyze specific reference areas. Of these five methods, the St\_PM method can calculate the ET reference for each of the surfaces. ET can reference a surface with a different reference surface using a specific  $ET_{os}/ET_{rs}$  ratio. In this analysis, however, the results of the singular single reference were used, because only for this reference were crop coefficients available.

### 3.5 Performance Indicators

Regression analysis using the best selection factor ( $R^2$ ) is used in the agricultural research model to evaluate the performance of the model. Sometimes, the standard deviation is used with or without these indicators. Two of the most commonly used statistical indicators in the literature dealing with environmental modeling are proposed by Jacovides and Kontoyiannis (1995) which can be well defined as follows:

$$\text{RMSD} = \sqrt{\left(\frac{1}{N} \sum_{i=1}^N d_i^2\right)} \quad (1)$$

$$\text{MBE} = \frac{1}{N} \sum_{i=1}^N d_i \quad (2)$$

where  $N$  is number of data pairs and  $d_i$  is the difference between  $i$ th predicted value and  $i$ th measured value.

The two most popular methods have been of those given by Page et al. (1979) and Davies et al. (1984). Equation forms of these indicators as described in Jacovides and Kontoyiannis (1995) are as follows:

According to Page et al. (1979),

$$\text{RMSD}_1 = \sqrt{\frac{1}{N} \sum_{i=1}^N \left(\frac{d_i}{F_i}\right)^2} \quad (3)$$

$$\text{MBE}_1 = \frac{1}{N} \sum_{i=1}^N \frac{d_i}{F_i} \quad (4)$$

And according to Davies et al. (1984),

$$\text{RMSD}_2 = \sqrt{\frac{1}{N} \sum_{i=1}^N d_i^2} \div \left(\frac{1}{N} \sum_{i=1}^N F_i\right) \quad (5)$$

$$\text{MBE}_2 = \left(\frac{1}{N} \sum_{i=1}^N d_i\right) \div \left(\frac{1}{N} \sum_{i=1}^N F_i\right) \quad (6)$$

where  $F_i$  is the  $i$ th measured value.

The  $t$ -statistics defined through MBE and RMSD is as follows:

$$t = \sqrt{\frac{(N-1) \times \text{MBE}^2}{\text{RMSD}^2 - \text{MBE}^2}} \quad (7)$$



The  $t$ -statistics revealed here is more informative as it uses RMSD and MBE. Moreover, the smaller the  $t$ -value, the better the performance of the model.

## 4 Results and Discussion

In this study, total data from the 17 harvest periods including ET lysimetric were used daily with corresponding weather parameters and weekly monitoring of soil moisture of the maize (*Z. mays* L.). First, the normal case data were selected using strict guidelines in FAO 56 [2], such as appropriate soil moisture conditions, possible plant yield, and at least 80% soil coverage.

From seventeen crop seasons, 266 days data were selected for normal class. Then by observing available soil water values, data for water stress condition (condition after depletion of 50% of available soil water) were selected. It was found out that because of soil water depletion from one area or soil layer, a different soil moisture status was formed. And sometimes, little amount of soil water becomes available for crop ET in such areas because of overnight redistribution of soil moisture and or capillary rise of water. Under this condition, the crop suffers from mild to moderate level of water stress. If such water was not available, then the crop suffers from severe water stress depending upon atmospheric conditions. Both moderate and severe water stress are very dynamic conditions and need careful attention under field condition. It was found out that during the study period (seventeen crop seasons), the crop was suffering from mild to moderate stress for 78 days. These days were classified as moderate stress period. Also, the crop was suffering from moderate to severe stress for 64 days. This period was classified as severe stress period. Rainy days and days with thick cloud cover were omitted from the analysis. Depending upon the quantity of rainfall, soil moisture will remain above field condition and soil will remain saturated for two to three days after heavy showers. Such saturated soil moisture condition days were classified under wet conditions. Out of seventeen years of crop season data, 208 days data were classified under wet condition.

Means of various climatic parameters across the four classes, viz. normal, moderate, severe, and wet, are shown in Fig. 1. Data labels for normal class of each weather parameter are shown in Fig. 1. The range of net radiation variation across the classes was 17.7–4.3 MJm<sup>-2</sup>d<sup>-1</sup> with means varying from 10.72 to 13.24 MJm<sup>-2</sup>d<sup>-1</sup>. The range of variation of maximum temperature during the analyzed period was from 26.1 to 39.6 °C with means varying from 32.17 to 35.58 °C. Also, the range of variation of minimum temperature during the analyzed period was from 12.9 to 28.5 °C with means varying from 21.26 to 25.02 °C. Average wind speed across different classes was varying from 3.81 (wet class) to 6.22 km/h (moderate class), while it was 4.13 km/h for normal class. Figure 1 reveals that VPD was the lowest for wet class which has value of 6.61 mbar, and for normal, severe, and moderate classes, the value of VPD was 13.13, 16.15, and 18.29 mbar, respectively. Figure 1 also shows that average moisture depletion of normal class and wet class was 29 and 15.22% which was much below than water stress limits (depletion of 50% of available water). Also,

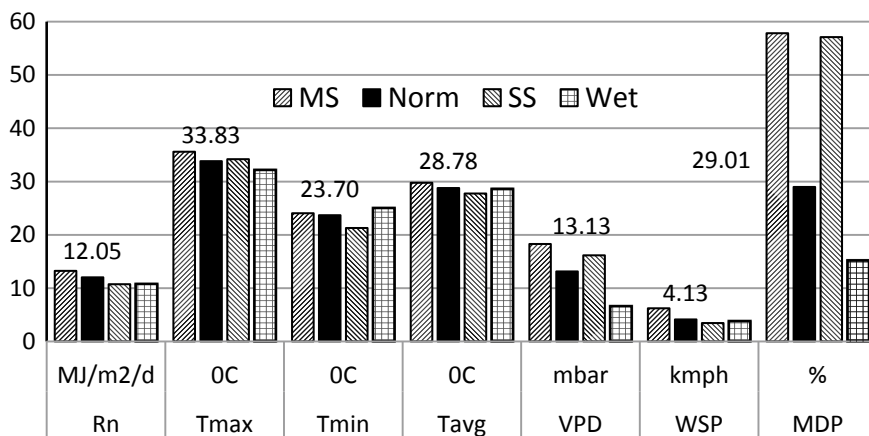


**Fig. 1** Comparison of different weather parameters over four classes

**Table 1** Pearson product-moment correlation coefficients between calculated ET with lysimetric ET for different models

No.	Model	Norm	SS	MS	Wet
1	St_PM	0.808	0.910	0.834	0.621
2	56_PM	0.808	0.910	0.834	0.621
3	KP_96	0.811	0.900	0.818	0.610
4	Pen_48	0.788	0.882	0.800	0.619
5	24_Pen	0.792	0.875	0.774	0.621

moisture depletion percentage of severe class and moderate stress class was 57.10 and 57.83%, respectively.

Pearson product-moment correlation coefficients ( $R$ ) worked out between predicted  $ET_c$  and lysimetric  $ET_c$  for five Penman versions of models for four classes are presented in Table 1. It is provided in Table 1 that the range of variation of  $R$  for normal class is 78.8–80.11%, and St-PM, 56\_PM, and KP\_96 models had the highest  $R$  for this class. Under severe stress conditions,  $R$  is varying from 87.5 to 91% with the highest  $R$  found out for St\_PM and 56\_PM model-predicted  $ET_c$ . As compared to this,  $R$  under moderate stress condition is less than severe stress condition but higher than normal condition as well as the range of variation of moderate class is higher (77.4–83.4%). Across the four classes and for all models, the lowest  $R$  is seen for wet class (61.8% class average) and the highest  $R$  is seen for severe stress class (89.5% class average). It is also provided in Table 1 that all the models are very closely tracking each other, among which three models St\_PM, 56\_PM, and KP\_96 have slightly better performance than Pen\_48 and 24\_Pen.

#### 4.1 Performance of Models Under Normal Condition

Table 2 provides the performance and ranks of five models using statistical performance indicators mentioned in previous sections for normal class. According to this table, RMSD of five models using single  $K_c$  is varying from 1.211 (St\_PM & 56\_PM) to 1.758 mm/d (24\_Pen). This difference is about 52–74% of individual average  $ET_c$  according to  $RMSD_1$  and about 28–40.6% of normal class average  $ET_c$  according to  $RMSD_2$ . MBE for this subclass (single  $K_c$  under normal class) is varying from 0.259 to 1.197 mm/d across different models. MBE is the lowest for St\_PM and 56\_PM models: 0.259 mm/d ( $MBE_1 = 17.4\%$  or  $MBE_2 = 6\%$ ), followed by KP\_96 model: 0.770 mm/d (30% or 17.8%) and Pen\_48 model: 0.848 mm/d (33.6% or 19.6%), and MBE is the highest for 24\_Pen model with 1.197 mm/d (41.6% or 27.7%). Positive MBE values indicate overprediction and vice versa. “ $t$ ” values for single  $K_c$  section reveal that the lowest  $t$ -values are for St\_PM and 56\_PM models. But these lowest values are above critical limits value of 2.33 for 99% probability one-tailed  $t$ -test with  $n = 220$ . These  $t$ -values indicate that the results are variable in a different set of observation with different experiments. Section two of Table 2 provides the performance of model-predicted  $ET_c$  against lysimetric  $ET_c$  using weather-adjusted  $K_c$  values. This section clearly indicates that the use of weather-adjusted  $K_c$  significantly improved the prediction of models. Even though RMSD value is decreased very slightly from 1.42 mm/d (single  $K_c$  subclass average) to 1.34 mm/d (weather-adjusted  $K_c$  subclass average), this slight improvement is responsible for a significant reduction in unsystematic errors. This has reflected in the MBE and  $t$ -values of this subclass. Two models in this subclass, viz. St\_PM and 56\_PM, show very small and significant  $t$ -values. Therefore, it can be said that  $ET_c$  predictions of these models are very stable and can be verified across different experiments with more than 99% probability. The lower section of the Table provides the performance of five Penman versions of models using dual crop coefficient. Pen\_48 model which was overpredicting using single  $K_c$  values shows a reduction in overpredicting using dual crop coefficient. St\_PM and 56\_PM models which performed better using weather-adjusted  $K_c$  show good performance using dual crop coefficients also. Even though RMSD of these models is very slightly increasing from 1.21 to 1.39 mm/d, biasness of these models is decreasing which is shown by highly significant  $t$ -values (3.29 compared to 0.8).

#### 4.2 Performance of Models Under Severe Stress Conditions

Table 3 provides the performance and ranks of five models using statistical performance indicators for severe stress class. Topmost section of Table 3 indicates the use of single  $K_c$  for  $ET_c$  predictions in the models. RMSD values for this subclass are varying from 2.127 (St\_PM and 56\_PM) to 3.037 mm/d (24\_Pen). This difference is about 143–194% of average  $ET_c$  according to  $RMSD_1$  and about 80–114% of average  $ET_c$  according to  $RMSD_2$ . The use of weather-adjusted  $K_c$ , dual  $K_c$ , and

Table 2 Performance of models under normal condition

No.	Model	Type of $K_c$	RMSD (mm/d)	RMSD <sub>1</sub> (%)	RMSD <sub>2</sub> (%)	MBE (mm/d)	MBE <sub>1</sub> (%)	MBE <sub>2</sub> (%)	$t$
1	St_PM	Single $K_c$	1.211	0.520	0.280	0.259	0.174	0.060	3.29
2	56_PM		1.211	0.520	0.280	0.259	0.174	0.060	3.29
3	KP_96		1.443	0.621	0.334	0.770	0.300	0.178	9.47
4	Pen_48		1.481	0.660	0.342	0.848	0.336	0.196	10.47
5	24_Pen		1.758	0.740	0.406	1.197	0.416	0.277	13.95
1	St_PM	Weather-adjusted $K_c$	1.203	0.482	0.278	0.042	0.120	0.010	0.52
2	56_PM		1.203	0.482	0.278	0.042	0.120	0.010	0.52
3	KP_96		1.341	0.571	0.310	0.528	0.241	0.122	6.42
4	Pen_48		1.372	0.607	0.317	0.603	0.276	0.139	7.34
5	24_Pen		1.596	0.680	0.369	0.934	0.351	0.216	10.83
1	St_PM	Dual $K_c$	1.395	0.502	0.323	-0.075	0.105	-0.017	0.80
2	56_PM		1.395	0.502	0.323	-0.075	0.105	-0.017	0.80
3	KP_96		1.486	0.588	0.343	0.395	0.223	0.091	4.14
4	Pen_48		1.534	0.626	0.355	0.477	0.259	0.110	4.90
5	24_Pen		1.705	0.693	0.394	0.793	0.332	0.183	7.88

water stress adjustment coefficient  $K_s$  in  $K_c$  is reducing RMSD of each subclass from 2.5 mm/d (single  $K_c$  class average) to 2.4, 2.2, and 1.7 mm/d, respectively. Biasness errors of five models are reducing from 123 to 75% according to  $MBE_1$ . Similar reductions are also observed for  $t$ -values, but  $t$ -values suggest that these results may vary in different experiments.

### 4.3 Performance of Models Under Moderate Stress Conditions

It was found out that even after depletion of 50% of available soil water, sometimes crop is transpiring water more vigorously than normal conditions. The probable reason for this might be the availability of little quantity of soil water due to overnight redistribution of soil moisture and capillary rise of water. Under this condition, the crop suffers from mild to moderate level of water stress in which the crop tries to compensate overheating by increasing  $ET_c$  rates. Therefore,  $ET_c$  under moderate stress sometimes exceeds than normal  $ET_c$ . Table 4 provides the performance and ranks of five models using statistical performance indicators for moderate stress class. Top portion of Table 4 indicates the use of single  $K_c$  for  $ET_c$  predictions in the models for which RMSD values are 1.392 (Pen\_48), 1.436 (St\_PM & 56\_PM), 1.615 (KP\_96), and 1.759 mm/d (24\_Pen). The use of weather-adjusted  $K_c$ , dual  $K_c$ , and water stress adjustment coefficient  $K_s$  in  $K_c$  is increasing RMSD of each subclass from 1.53 mm/d (single  $K_c$  subclass average) to 1.57, 1.54, and 2.24 mm/d, respectively. “ $t$ ” values for single  $K_c$  section reveal significant results for St\_PM, 56\_PM, Pen\_48, and KP\_96 models (2.38, for 99% probability one-tailed  $t$ -test with  $n = 78$ ).

### 4.4 Performance of Models Under Wet Conditions

Table 5 represents the performance indicators of five Penman versions of model-predicted  $ET_c$ , calculated using single  $K_c$ , weather-adjusted  $K_c$ , and dual  $K_c$  with lysimeter  $ET_c$ . RMSD values of wet condition predictions by five models show that the performance of these models within each subclass has a very slight difference between the models. The difference of first ranking model and fifth ranking model in each subclass has values of 0.15 (single  $K_c$ ), 0.39 (weather-adjusted  $K_c$ ), and 0.24 mm/d (dual  $K_c$ ).  $ET_c$  predictions using single  $K_c$  show significant predictions as all  $t$ -values are below a critical limit of 2.33 (for 99% probability one-tailed  $t$ -test with  $n = 208$ ). Table 5 also provides that the use of weather-adjusted  $K_c$  is decreasing RMSD and MBE values, but the use of dual  $K_c$  is increasing the RMSD and MBE values.

Table 3 Performance of models under severe stress condition

No.	Model	Type of $K_c$	RMSD (mm/d)	RMSD <sub>1</sub> (%)	RMSD <sub>2</sub> (%)	MBE (mm/d)	MBE <sub>1</sub> (%)	MBE <sub>2</sub> (%)	$t$
1	St_PM	Single $K_c$	2.127	1.434	0.803	1.842	1.048	0.696	12.74
2	56_PM		2.127	1.434	0.803	1.842	1.048	0.696	12.74
3	KP_96		2.548	1.628	0.962	2.286	1.246	0.863	14.93
4	Pen_48		2.686	1.761	1.014	2.448	1.344	0.925	16.30
5	24_Pen		3.037	1.937	1.147	2.784	1.497	1.052	16.87
1	St_PM	Weather-adjusted $K_c$	2.039	1.367	0.770	1.710	0.986	0.646	11.32
2	56_PM		2.039	1.367	0.770	1.710	0.986	0.646	11.32
3	KP_96		2.441	1.555	0.922	2.140	1.179	0.808	13.39
4	Pen_48		2.574	1.682	0.972	2.298	1.274	0.868	14.56
5	24_Pen		2.915	1.853	1.101	2.625	1.422	0.991	15.22
1	St_PM	Dual $K_c$	1.904	1.318	0.719	1.347	0.866	0.509	7.36
2	56_PM		1.904	1.318	0.719	1.347	0.866	0.509	7.36
3	KP_96		2.235	1.495	0.844	1.737	1.046	0.656	9.08
4	Pen_48		2.365	1.615	0.893	1.888	1.137	0.713	9.74
5	24_Pen		2.665	1.778	1.006	2.188	1.277	0.827	10.58
1	St_PM	Water stress-adjusted $K_s$	1.535	1.174	0.580	0.695	0.606	0.262	3.73
2	56_PM		1.535	1.174	0.580	0.695	0.606	0.262	3.73
3	KP_96		1.719	1.312	0.649	1.013	0.757	0.383	5.36
4	Pen_48		1.832	1.428	0.692	1.146	0.838	0.433	5.89
5	24_Pen		2.053	1.572	0.775	1.397	0.960	0.528	6.82

**Table 4** Performance of models under moderate stress condition

No.	Model	Type of $K_c$	RMSD (mm/d)	RMSD <sub>1</sub> (%)	RMSD <sub>2</sub> (%)	MBE (mm/d)	MBE <sub>1</sub> (%)	MBE <sub>2</sub> (%)	$t$
1	Pen_48	Single $K_c$	1.392	0.215	0.203	0.198	0.047	0.029	1.20
2	St_PM		1.436	0.205	0.210	-0.390	-0.044	-0.057	2.35
3	56_PM		1.436	0.205	0.210	-0.390	-0.044	-0.057	2.35
4	KP_96		1.615	0.245	0.236	0.390	0.072	0.057	2.07
5	24_Pen		1.759	0.277	0.257	0.851	0.142	0.124	4.60
1	Pen_48	Weather-adjusted $K_c$	1.425	0.216	0.208	0.039	0.022	0.006	0.23
2	St_PM		1.523	0.217	0.222	-0.535	-0.066	-0.078	3.11
3	56_PM		1.523	0.217	0.222	-0.535	-0.066	-0.078	3.11
4	KP_96		1.634	0.246	0.239	0.229	0.047	0.033	1.18
5	24_Pen		1.730	0.270	0.253	0.679	0.115	0.099	3.54
1	Pen_48	Dual $K_c$	1.408	0.215	0.206	-0.229	-0.012	-0.033	1.37
2	KP_96		1.552	0.232	0.227	-0.051	0.011	-0.007	0.27
3	24_Pen		1.566	0.251	0.229	0.382	0.078	0.056	2.09
4	St_PM		1.595	0.222	0.233	-0.783	-0.097	-0.114	4.68
5	56_PM		1.595	0.222	0.233	-0.783	-0.097	-0.114	4.68
1	24_Pen	Water stress-adjusted $K_s$	1.903	0.285	0.278	-1.265	-0.164	-0.185	7.39
2	KP_96		2.101	0.301	0.307	-1.621	-0.219	-0.237	10.07
3	Pen_48		2.191	0.317	0.320	-1.733	-0.232	-0.253	10.74
4	St_PM		2.509	0.352	0.366	-2.180	-0.302	-0.318	14.60
5	56_PM		2.509	0.352	0.366	-2.180	-0.302	-0.318	14.60

Table 5 Performance of models under wet condition

No.	Model	Type of $K_c$	RMSD (mm/d)	RMSD <sub>1</sub> (%)	RMSD <sub>2</sub> (%)	MBE (mm/d)	MBE <sub>1</sub> (%)	MBE <sub>2</sub> (%)	$t$
1	St_PM	Single $K_c$	1.619	0.747	0.409	-0.270	0.142	-0.068	2.26
2	56_PM		1.619	0.747	0.409	-0.270	0.142	-0.068	2.26
3	Pen_48		1.646	0.846	0.416	0.127	0.261	0.032	1.04
4	KP_96		1.661	0.809	0.420	0.025	0.224	0.006	0.20
5	24_Pen		1.770	0.860	0.447	0.241	0.278	0.061	1.84
1	Pen_48	Weather-adjusted $K_c$	1.607	0.797	0.406	-0.055	0.206	-0.014	0.46
2	St_PM		1.630	0.708	0.412	-0.434	0.092	-0.110	3.70
3	56_PM		1.630	0.708	0.412	-0.434	0.092	-0.110	3.70
4	KP_96		1.632	0.763	0.412	-0.153	0.170	-0.039	1.26
5	24_Pen		1.707	0.810	0.431	0.054	0.222	0.014	0.42
1	St_PM	Dual $K_c$	1.696	0.955	0.434	-0.047	0.258	-0.012	0.37
2	56_PM		1.696	0.955	0.434	-0.047	0.258	-0.012	0.37
3	KP_96		1.785	1.039	0.423	0.265	0.348	0.067	2.01
4	Pen_48		1.787	1.080	0.413	0.375	0.389	0.095	2.87
5	24_Pen		1.938	1.100	0.435	0.494	0.407	0.125	3.53



## 5 Conclusions

The performance evaluation of  $ET_c$  predictions by five Penman versions of models has been carried out under normal, moderate stress, severe stress, and wet conditions using single, weather-adjusted, dual, and water stress-adjusted crop coefficient values for carefully selected data from seventeen maize (*Z. mays* L.) crop seasons at New Delhi locations using RMSD, MBE, and  $t$ -values. The performance evaluation of ET models using statistical indicators suggested by Jacovides and Kontoyiannis (1995) was found to be very promising and may be recommended for such evaluations. Penman–Monteith method (St\_PM and 56\_PM in our case) is considered as one of the accurate methods for ET prediction under well-established weather stations. The results of the presented study support this consideration, and these methods can be recommended for the estimation of crop water requirements or irrigation scheduling for New Delhi region or regions having similar climates for maize crop. The analysis of the results of the presented study reveals that the use of at least weather-adjusted  $K_c$  values is must for precise  $ET_c$  estimations. Extensive review of the literature on the presented topic shows that the use of weather-adjusted  $K_c$  or dual  $K_c$  is rarely done in India. The use of dual  $K_c$  is suggested for the scientific investigations which involve crop water requirements or related research for consistent and reliable predictions. It can also be concluded from the presented study that the use of water stress coefficient ( $K_s$ )-adjusted  $K_c$  under water stress conditions is improving the predictions considerably. But the use of  $K_s$  alone is not sufficient for water stress level quantification or identification of water stress on crop, and better methodologies are required for water stress representation.

## References

1. Alexandris S, Kerkides P (2003) New empirical formula for hourly estimates of reference evapotranspiration. *Agric Water Manage* 60:181–198
2. Allen RG, Pereira LS, Raes D, Smith M (1998) Crop evapotranspiration: guidelines for computing crop water requirements. Irrigation and Drainage Engineering Paper No 56, United Nations Food and Agriculture Organization, Rome, Italy
3. Allen RG (2000) REF-ET for Windows: reference evapotranspiration calculator version 2.0, University of Idaho Research and Extension Center, Kimberly, ID. Current online version: <http://www.kimberly.uidaho.edu/ref-et/>
4. Allen RG, Walter IA, Elliott R, Mecham B, Jensen ME, Itenfisu D, Howell TA, Snyder R, Brown P, Echings S, Spofford T, Hattendorf M, Cuenca RH, Wright JL, Martin D (2000) Issues, requirements and challenges in selecting and specifying a standard ET equation. In: Evans RG, Benham BL, Trooien TP (eds) Proceedings of the 4th decennial irrigation symposium (ASAE), 14–16 Nov 2000, Phoenix, AZ, U.S.A., pp 201–208
5. Brunel J, Ihab J, Droubi AM, Samaan S (2006) Energy budget and actual evapotranspiration of an arid oasis ecosystem: Palmyra (Syria). *Agric Water Manage* 84:213–220
6. Dorrenbos J, Pruitt WO (1977) Crop water requirements. Irrigation and Drainage Engineering Paper No 24, United Nations Food and Agriculture Organization, Rome, Italy
7. Garcia M, Raes D, Allen R, Herbas C (2004) Dynamics of evapotranspiration in Bolivian highlands (Altipano). *Agric Forest Meteorol* 25(1–2):67–82

8. Gavilan P, Berengena J, Allen RG (2007) Measuring versus estimating net radiation and soil heat flux: impact on Penman-Monteith reference ET estimates in semiarid regions. *Agric Water Manage* 89:275–286
9. Gupta SP (2002) India Vision 2020. Online document of Planning Commission, Govt. of India. [http://planningcommission.nic.in/plans/planrel/pl\\_vsn2020.pdf](http://planningcommission.nic.in/plans/planrel/pl_vsn2020.pdf)
10. Itenfisu D, Elliott R, Allen RG, Walter IA (2000) Comparison of reference evapotranspiration calculation across range of climates. In: Evans RG, Benham BL, Trooien TP (eds) Proceedings of the 4th decennial irrigation symposium (ASAE), 14–16 Nov 2000, at Phoenix, AZ., U.S.A., pp 216–227
11. Jensen ME, Burman RD, Allen RG (1990) Evapotranspiration and irrigation water requirements. ASCE Manuals and Reports on Engineering Practice No. 70, ASCE, New York, NY, U.S.A., pp 332
12. Karam F, Breidy J, Stephan C, Roupheal J (2003) Evapotranspiration, yield and water use efficiency of drip irrigated corn in the Bekka Valley, Lebanon. *Agric Water Manage* 63:125–137
13. Karam F, Masaad R, Steir T, Mounzer O, Roupheal Y (2005) Evapotranspiration and seed yield of field grown soyabean under deficit irrigation conditions. *Agric Water Manage* 75:226–244
14. Medaires GA, Arruda FB, Sakai E (2005) Crop coefficients for irrigated beans derived using three reference evapotranspiration methods. *Agric Forest Meteorol* 135(1–4):135–143
15. Pauwels VRN, Samson R (2006) Comparison of different methods to measure and model actual evapotranspiration rates for a wet sloping grasslands. *Agric Water Manage* 82:1–24
16. Pereira AR, Green SR, Nova NAV (2007) Sap flow, leaf area, net radiation and Priestley-Taylor formula for irrigated orchard and isolated trees. *Agric Water Manage* 92:48–52
17. Sauer TJ, Singer JW, Prueger JH, DeSutter TM, Hatfield JL (2007) Radiation balance and evaporation partitioning in a narrow-row soyabean canopy. *Agric Forest Meteorol* 145(3–4):206–214
18. Singh RK, Islam S (2013) Monitoring of potential evapotranspiration of Abha City, Kingdom of Saudi Arabia. *Int J Adv Innov Res* (2278-7844) /#269/ 2(12):269–272
19. Singh RK, Islam S (2014) Estimation of potential evapotranspiration of Asir Region, Kingdom of Saudi-Arabia: considering climate variability. *Int J Adv Innov Res* (2278-7844) /#194/ 3(1):194–199
20. Singh RK et al (2016) Analysis of potential evapotranspiration of different cities of Kingdom of Saudi Arabia. *Int J Adv Innov Res (IJAIR)* (ISSN: 2278-7844) /#48 5(02):48–51
21. Suleiman AA, Soler CMT, Hoogenboom G (2007) Evaluation of FAO-56 crop coefficient procedures for deficit irrigation management of cotton in a humid climate. *Agric Water Manage* 91:33–42
22. Utset A, Farre I, Martinez-Cob A, Cavero J (2004) Comparing Penman-Monteith and Priestley-Taylor approaches as reference-evapotranspiration inputs for modeling maize water-use under Mediterranean conditions. *Agric Water Manage* 66:205–219
23. Walter IA, Allen RG, Elliott R, Mecham B, Jensen ME, Itenfisu D, Howell TA, Snyder R, Brown P, Echings S, Spofford T, Hattendorf M, Cuenca RH, Wright JL, Martin D (2000) ASCE's standardized reference evapotranspiration equation. In: Evans RG, Benham BL, Trooien TP (eds) Proceedings of the 4th decennial irrigation symposium (ASAE), 14–16 Nov 2000, at Phoenix, AZ, U.S.A., pp 209–215
24. Xinmin Z, Lin H, Xiuju B, Bingxiang Z, Fahe C, Xinzhang S (2007) The most economical irrigation amount and evapotranspiration of the turfgrasses in Beijing City, China. *Agric Water Manage* 89:98–104

# A Methodology to Measure Flow Fields at Bridge Piers in the Presence of Large Wood Debris Accumulation Using Acoustic Doppler Velocimeters



Iacopo Carnacina , Aleksandra Lescova and Stefano Pagliara 

**Abstract** Bridge failure due to scour in flooding conditions has been at the center of attention of hydraulic engineers for decades. Large wood debris accumulation on bridge piers has been found as one of the main causes for bridge collapse. The combined action of enhanced scouring at the base of the pier and increased hydrodynamic load is viewed as the main force driving the enhanced failure probability. It is therefore fundamental to understand the distribution of the flow field around the accumulation and in the proximity of the pier, in order to be able to understand the potential acceleration and turbulence enhancement that could help understand what drives the failure and reduces its probability. However, this particular configuration poses physical constraints to flow measurements, as the accumulated mass of logs hinders a direct access to instrumentation directly immersed in water. This paper proposed a new methodology to measure the flow fields in the presence of debris accumulation using an acoustic Doppler velocimeter (ADV). The methodology consists in applying a matrix of rotation on the instantaneous velocity measured in the three dimensions to access locations underneath the debris that could not be accessed using the standard rotation of the debris. The methodology shows the potential to provide accurate measurements in the proximity of the debris and the groove and is able to maintain the statistics of the flow fields in terms of both average velocity and turbulence intensity.

**Keywords** Debris · Acoustic doppler velocimeter · Scour · Flow measurements · Bridges

---

I. Carnacina (✉)

Liverpool John Moores University, Liverpool L3 3AF, UK  
e-mail: [i.carnacina@ljmu.ac.uk](mailto:i.carnacina@ljmu.ac.uk)

A. Lescova

Department of Civil Engineering, Riga Technical University, Riga, Latvia

S. Pagliara

DESTEC, University of Pisa, Pisa, Italy

© Springer Nature Singapore Pte Ltd. 2020  
R. AlKhaddar et al. (eds.), *Advances in Water Resources Engineering and Management*, Lecture Notes in Civil Engineering 39,  
[https://doi.org/10.1007/978-981-13-8181-2\\_2](https://doi.org/10.1007/978-981-13-8181-2_2)

## 1 Introduction

Since the 1950s, numerous investigations were made to understand the possible mechanism of scour forming around a bridge pier and several studies focus on the analysis of scour and scour protection [1–4]. In conducting hydraulic studies for a bridge, it is desirable to understand the characteristics and behavior of the rivers in the vicinity of crossing and to be able to interpret them with the help of maps and aerial photographs. The physical characteristics of a stream are determined by a variety of factors, such as climate, topography, geology, and land use. Exploring flow conditions around bridge piers can help to provide different methods of protecting structures from failing [5–11]. In order to understand the scouring mechanics and the behavior of protection, it is important to understand the flow field around a bridge pier in the presence of debris accumulation, and it is necessary to make accurate flow measurements around the pier, where most of the turbulent structures form. Due to the presence of the debris accumulation, ADV measurement in its straight original position is impossible. This paper introduces a new algorithm to rotate ADV measurements and gain access to the area immediately next to the pier and below the debris.

## 2 Experimental Apparatus

All the experimental tests were carried out in 12-m-long, 0.61-m-wide, and 0.5-m-depth channel with glass walls (Fig. 1). The flow was supplied by means of a sluice gate provided with a flow straightener (0.25 cm mesh).

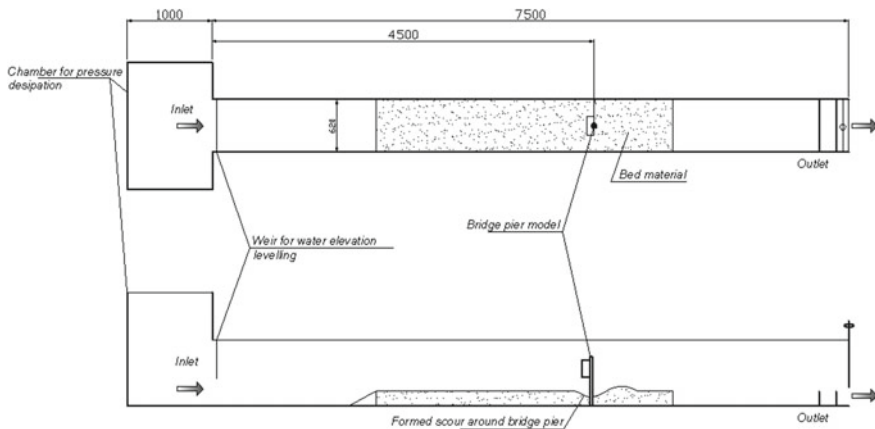


Fig. 1 Plan view

The discharge was measured by means of a KROHNE® electromagnetic flow meter, installed in the supply line. A false bottom was used to simulate the riverbed. In upstream area, steel box provided the transition between the mobile bed and the inlet sluice gate. A second steel box of the outlet side in the downstream area closed the false bottom. One cylindrical pier of diameter  $D = 0.03$  m has been used in the tests for modeling the bridge pier presence. The pier was placed at the false bottom in the center of the channel. A weir, positioned 2 m downstream from the last box, regulated the exact water depth for obtaining the permanence of the water level in the channel during the test. Point gauge with precision of 1 mm was used for measuring the bed average level which has to be taken as a zero point, and measurements were taken along the longitudinal section of the channel as well as cross section by centerline according to the model of bridge pier. The experimental flow rate was  $Q = 33.5$  l/s. For all the tests, a medium river sand has been used, with particle size characteristics are:  $d_{50} = 1$  mm,  $\sigma = (d_{84}/d_{16})^{0.5} = 1.2 =$  standard deviation of sediments,  $\varphi = 31^\circ$  and  $\varphi' = 36^\circ$  are the angles of repose of dry and wet sediment, and density of the sediment  $\rho_s = 2440$  kg/m<sup>3</sup>. Experimental tests have been carried out using debris accumulation model of frontal rectangular shape. In tests with the presence of debris accumulation percentage rough blockage ratio  $\Delta A = [(d_d - D) \cdot (t_d + d_f)] / (b \cdot h) \cdot 100 = 6\%$ ; for  $d_f = 0$  in which  $d_f =$  average logs diameter and  $b =$  channel width (0.60 m),  $h =$  water depth (0.17 m),  $t_d =$  debris thickness (0.16 m) and  $d_d =$  debris diameter (0.17 m),  $D =$  pier diameter (0.03 m), from which it can be made a conclusion that the porosity affects the scour evolution in not so sufficiently degree, while both  $\Delta A$  and roughness play an important role in  $z_{\max}/D$  temporal evolution [3].

## 2.1 Apparatus Used for Experiments

A Nortek acoustic Doppler velocimeter (ADV) was used to measure the three-dimensional components of the flow in each point of the flow field in the tests. The ADV provides high-precision flow velocity measurements in the three directions. The measurements are insensitive to water quality, which allows for a wide range of applications. Velocimeters are used in laboratories, wave basins, rivers, estuaries, and oceanographic research.

The ADV uses the Doppler effect to measure 3D flow in a small sampling volume (0.5 cm) geometrically located at a fixed distance (5 cm) from the probe.

The acoustic sensor is composed by two main elements: a signal transmit transducer and three receiving transducers. The sampling volume is located away from the sensor and provides undisturbed measurements. Small particles reflect the signal, which is picked up by the receiving transducers. The instrumental accuracy is of the order of cm/s, and the high sampling frequency (25 Hz) allows also for accurate turbulence intensity and temporal signal cross-correlation.

### 3 Methodology

The probe is attached to a brace that allows pitch, roll, and yaw rotations. In order to find the exact location of the probe in the rotated configuration, the methodology to measure the flow field in the proximity of the debris is divided into two steps.

The first step consists in finding the exact values for three angles of rotation using the velocity flow field in the original probe configuration and in the rotated configuration. The second step consists in finding the relation between the original coordinates in the reference system (the  $x$ -axis direction is along the channel by longitudinal section,  $y$ -axis accorded to the cross section, and the  $z$ -axis). Several configurations were tested in order to find the optimal angles that allowed for undisturbed measurement in the proximity of the debris or the pier bottom.

#### 3.1 Step 1: Rotational Matrices and Pitch, Roll, and Yaw Angles

The first step of calibration of the probe is obtaining data of the current point in the flow field with permanent coordinates  $x$ ,  $y$ , and  $z$  in one coordinate system using the standard position of the probe, which means no rotation or rolling, heading, and pitching; all angles around the three axes  $x$ ,  $y$ , and  $z$  are equal to  $0^\circ$ . The heading rotation is about the  $z$ -axis, and the rolling rotation is about the  $y$ -axis.

For example, the independent reference point of the area of the channel has the coordinates:  $X = 3.993$  m,  $Y = 0.545$  m, and  $Z = 510$  m.

The coordinates have been taken before the test started, and this point could be used as an initial position of the standard position for further rotation of any new position of the probe which will be used for obtaining all the necessary data in the flow field. Using the ADV, the three components of the flow field were measured in the original positions,  $U$ ,  $V$ , and  $W$ , where  $U$  = component of  $x$ -axis direction,  $V$  = component of the  $y$ -axis direction, and the third component  $W$  = velocity vector of the  $z$ -axis. For each point of the flow field data, the recording process lasted 40 s to provide more precise data results using the average value taken during this period.

For all the skewed positions, which have been used for obtaining data of the flow field, it is necessary to find out accurate rotational angles around the axis. Matrix multiplication leads to different results depending on the order of application of multiplication. In this work, all the further commutations about the rotational matrix and finding the angles are use first a rotating around the  $z$ -axis and after around the  $y$ -axis, hence, in case of other sequence of rotation other matrix has to be used. For computing and rotational processes, the MATLAB and ExploreV software were used, after collecting all the data in CollectV. There are three basic rotational matrices in three dimensions:

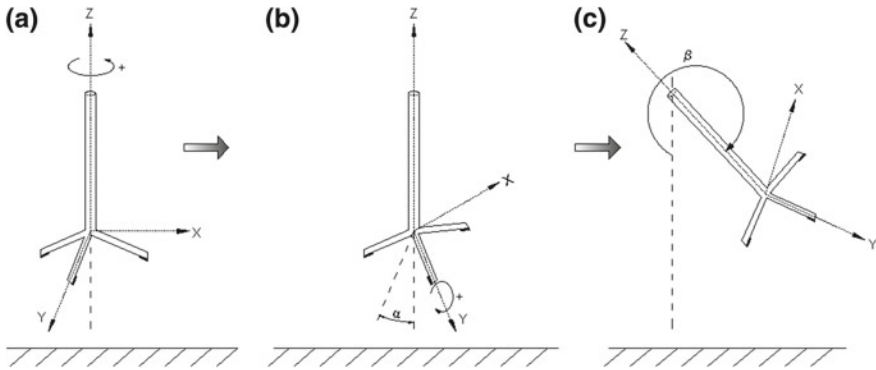


Fig. 2 Conditions of the ADV probe during rotation around z-axis and y-axis

$$A_Y(\alpha) = \begin{bmatrix} \cos \alpha & 0 & \sin \alpha \\ 0 & 1 & 0 \\ -\sin \alpha & 0 & \cos \alpha \end{bmatrix} \quad A_X(\alpha) = \begin{bmatrix} 1 & 0 & 0 \\ 0 & \cos \alpha & -\sin \alpha \\ 0 & \sin \alpha & \cos \alpha \end{bmatrix} \quad A_Z(\alpha) = \begin{bmatrix} \cos \alpha & -\sin \alpha & 0 \\ \sin \alpha & \cos \alpha & 0 \\ 0 & 0 & 1 \end{bmatrix}$$

The direction of the rotation is as follows:  $A_x$  rotates the y-axis toward the z-axis,  $A_y$  rotates the z-axis toward the x-axis, and  $A_z$  rotates the x-axis toward the y-axis. Figure 2 shows the order of the rotation of the ADV probe. The first condition A was first used to take measurements in the flow field. After rotation around the z-axis by angle  $\alpha$  (the positive direction is shown in figure), the position of the probe stays in condition B. After the second rotation around the y-axis by angle  $\beta$ , we obtain the third ADV condition C. It is important to follow the correct order of rotation to be able to rotate the measured data during elaboration.

A component of a vector is the modulus of that vector in a given direction. From the recorded data, we can form first a matrix with the initial velocity vector components obtained in the standard position of the ADV probe,  $U$  matrix  $U = [u, v, w]$ , and the second matrix of the skewed velocity vector components after rotating around z-axis and y-axis,  $U'$  matrix:  $U' = [u', v', w']$ . To facilitate the calculation of the rotational angles, it is necessary to calculate the norm of vectors  $V$  and  $V'$ , using algebraical expressions:

$$V = \sqrt{u^2 + v^2 + w^2}; \quad V' = \sqrt{u'^2 + v'^2 + w'^2}$$

With known  $V$  and  $V'$ , all the components of  $u, v, w, u', v',$  and  $w'$  can be normalized by dividing them by its norm  $V$  or  $V'$ ; therefore:

$$u_n = \frac{u}{V}; \quad v_n = \frac{v}{V}; \quad w_n = \frac{w}{V}; \quad u'_n = \frac{u'}{V'}; \quad v'_n = \frac{v'}{V'}; \quad w'_n = \frac{w'}{V'}$$

The normalized matrices  $U_{\text{norm}}$  and  $U'_{\text{norm}}$  of  $U$  and  $U'$  are  $U_{\text{norm}} = [u_n, v_n, w_n]; U'_{\text{norm}} = [u'_n, v'_n, w'_n]$ . Before using multiplication of matrices, it is nec-



essary to find the angles of rotation  $\alpha$  and  $\beta$ . To do so, we have to find the values of angles which can lead the transformation equation to zero:

$$f_1(\alpha) = u' \cdot \sin \alpha - v' \cdot \cos \alpha + w' \cdot 0 - v \rightarrow f_1(\alpha) = 0$$

$$f_2(\alpha, \beta) = u' \cdot \cos \alpha \cdot \cos \beta - v' \cdot \sin \alpha \cdot \cos \beta - w' \cdot \sin \beta - u \rightarrow f_2(\alpha, \beta) = 0$$

This provides four solutions of four couples of  $\alpha$  and  $\beta$  angle values. Using MATLAB, it is possible to check all the variants by comparing the expected results and find out the right solution. The last step consists in multiplying the normalized skewed matrix of velocity components  $U'_{\text{norm}}$  by  $A_{ZY}$ ; as a result, we obtain the matrix which is closely the same as the normalized matrix of the standard values  $U_{\text{norm}}$ .

Following the order the first rotation is around  $Z$  and, after that around  $Y$ , yields:

$$A_{ZY} = A_Y \cdot A_Z = \begin{bmatrix} \cos \alpha & 0 & \sin \alpha \\ 0 & 1 & 0 \\ -\sin \alpha & 0 & \cos \alpha \end{bmatrix} \cdot \begin{bmatrix} \cos \beta & -\sin \beta & 0 \\ \sin \beta & \cos \beta & 0 \\ 0 & 0 & 1 \end{bmatrix} = \begin{bmatrix} \cos \alpha \cdot \cos \beta & -\cos \beta \cdot \sin \alpha & -\sin \beta \\ \sin \alpha & \cos \alpha & 0 \\ \sin \beta \cdot \cos \beta & -\sin \alpha \cdot \sin \beta & \cos \beta \end{bmatrix}$$

### 3.2 Step 2: Offset from the Standard Position

Obviously, if we need to take measurements of the point in the flow field with coordinates  $X = 3.44$  m,  $Y = 0.35$  m, and  $Z = 320$  m, the ADV probe has to be put directly into the position with the same coordinates (evidently, if the initial coordinates of the reference point were taken using the ADV position). For any rotation and changed position of the probe, new coordinates and relative offset values have to be found to set the probe in the right location with the newly obtained coordinates in the rotated reference system. After changing the position using the rotation of the ADV, new coordinates for reference point have to be taken, to have  $X$ ,  $Y$ ,  $Z$  and  $X_1$ ,  $Y_1$ ,  $Z_1$ .

For example,  $X_1 = 4.191$ ,  $Y_1 = 0.549$ , and  $Z_1 = 251$ .

After the delta is found:

$$\Delta X_1 = X_1 - X \rightarrow \Delta X_1 = 4.191 - 3.993 = 0.198 \text{ m}$$

$$\Delta Y_1 = Y_1 - Y \rightarrow \Delta Y_1 = 0.549 - 0.545 = 0.004 \text{ m}$$

$$\Delta Z_1 = Z_1 - Z \rightarrow \Delta Z_1 = 2.51 - 5.10 = -2.59 \text{ m}$$

The new coordinates for the same point are as follows:

$$X' = X + \Delta X_1 \rightarrow X' = 3.44 + 0.198 = 3.638 \text{ m}$$

$$Y' = Y + \Delta Y_1 \rightarrow Y' = 0.35 + 0.004 = 0.354 \text{ m}$$

$$Z' = Z + \Delta Z_1 \rightarrow Z' = 3.20 + (-2.59) = 0.61 \text{ m}$$



Knowing simple mathematical transformations, it is easy to use each time more suitable coordinate system related to the known location of any point. As results, coordinates are changed for both the standard and skewed positions of the probes  $X, Y, Z$  and  $X', Y', Z'$  with an accuracy to 1 mm. This ensures that the obtained data shows the real condition of the flow in exact set point.

## 4 Application

As an example, we can make under review one case of rotation. It is important also to know which kinds of rotations were done before placing the ADV probe into the skewed position to be able to compare the obtained values of rotation angles with actual values while working to the experiment on the channel.

We have three components of the velocity vector, obtained from the standard position of the probe without any rotations: sampled  $u = 32.63$  cm/s,  $v = -0.11$  cm/s, and  $w = -1.08$  cm/s.

And the values measured with the skewed position of the probe after rotation are as follows: modified  $u' = 1.06$  cm/s,  $v' = -32.63$  cm/s, and  $w' = -0.15$  cm/s.

Calculating norms:

$$V = \sqrt{u^2 + v^2 + w^2} = \sqrt{32.63^2 + (-0.11)^2 + (-1.08)^2} = 32.647$$

$$V' = \sqrt{u'^2 + v'^2 + w'^2} = \sqrt{1.06^2 + (-32.63)^2 + (-0.15)^2} = 32.648$$

Getting normalized values:

$$u_n = \frac{u}{V} = 0.999447; \quad u'_n = \frac{u'}{V'} = 0.03246;$$

$$v_n = \frac{v}{V} = -0.00337; \quad v'_n = \frac{v'}{V'} = -0.99946;$$

$$w_n = \frac{w}{V} = -0.03308; \quad w'_n = \frac{w'}{V'} = -0.00459$$

Therefore, the normalized matrices are as follows:

$$U_{\text{norm}} = \begin{bmatrix} u_n \\ v_n \\ w_n \end{bmatrix} = \begin{bmatrix} 0.999447 \\ -0.00337 \\ -0.03308 \end{bmatrix} \quad U'_{\text{norm}} = \begin{bmatrix} u'_n \\ v'_n \\ w'_n \end{bmatrix} = \begin{bmatrix} 0.03246 \\ -0.99946 \\ -0.00459 \end{bmatrix}$$

Using functions  $f_1(\alpha)$  and  $f_2(\alpha, \beta)$  have been found four couples of angles, which meet necessary requirements:  $f_1(\alpha) = 0, f_2(\alpha, \beta) = 0$ .

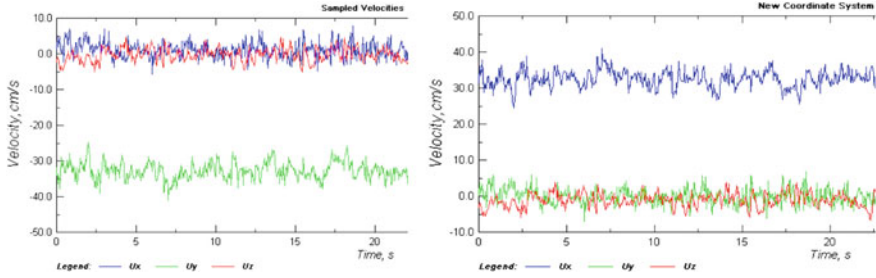


**Fig. 3** Velocity vector taken with the skewed position before and after rotation

$$\begin{aligned}\alpha_1 &= 88.00^\circ & \beta_1 &= 2.2^\circ \\ \alpha_2 &= 268.5^\circ & \beta_2 &= 177.9^\circ \\ \alpha_3 &= 88.00^\circ & \beta_3 &= 358.5^\circ \\ \alpha_4 &= 268.5^\circ & \beta_4 &= 181.7^\circ\end{aligned}$$

With the help of MATLAB, the obtained results were checked and found one solution for the pair of angles  $\alpha = 88.00^\circ$  and  $\beta = 358.5^\circ$ . The standard normalized vector  $U_{\text{norm}}$  has almost the same value as multiplication  $U'_{\text{norm}}$  by  $A_{ZY}$ , which shows that the angles of rotation were found correctly and can be used for rotating the components of the velocity vectors taken in this position (Fig. 3).

$$U'_{\text{norm}} \cdot A_{ZY} = \begin{bmatrix} 0.9994 \\ -0.0032 \\ -0.0339 \end{bmatrix} \quad U_{\text{norm}} = \begin{bmatrix} 0.9995 \\ -0.0034 \\ -0.0331 \end{bmatrix}$$

Owing to graphical visualization, it is easier to estimate the quality of taken data, if it was obtained correctly, without noises, and can be trusted. In case of spike and other troubles, it is possible to filter the data, after which results are more accurate. After rotating the velocity vectors by found angles, it is possible also to compare the values from ExploreV program data; therefore, we have:

Standard position: sampled  $u = 32.63$ ;  $v = -0.11$ ;  $w = -1.08$

Skewed position after rotation:  $u = 32.62$ ;  $v = -0.07$ ;  $w = -1.00$ .

## 5 Conclusions

The paper presented a methodology to measure flow velocity and turbulence next to bridge pier using the ADV and using the rotational matrix. The methodology has been validated in laboratory conditions and shows good accuracy in measuring flow velocities next to debris accumulating to bridge piers. The methodology proposed

can help understand the flow features around the pier in the presence of debris accumulation and help determine size and characteristics of protections to reduce catastrophic bridge failures.

## References

1. Hager WH (2007) Scour in hydraulic engineering. *Proc Inst Civ Eng Water Manag* 160(3):159–168
2. Melville BW, Dongol DM (1992) Bridge pier scour with debris accumulation. *J Hydraul Eng ASCE* 118(9):1306–1310
3. Pagliara S, Carnacina I (2010) Temporal scour evolution at bridge piers: effect of wood debris roughness and porosity. *J Hydraul Res* 48(1):3–13
4. Pagliara S, Carnacina I (2011) Influence of wood debris accumulation on bridge pier scour. *J Hydraul Eng ASCE* 137(2):254–261
5. Dey S, Raikar RV (2007) Characteristics of horseshoe vortex in developing scour holes at piers. *J Hydraul Eng ASCE* 133(4):399–413
6. Ettema R, Kirkil G, Muste M (2006) Similitude of large-scale turbulence in experiments on local scour at cylinders. *J Hydraul Eng ASCE* 132(1):33–40
7. Graf WH, Istiarto I (2002) Flow pattern in the scour hole around a cylinder. *J Hydraul Res* 40(1):13–20
8. Johnson KR, Ting FCK (2003) Measurements of water surface profile and velocity field at a circular pier. *J Eng Mech ASCE* 129(5):502–513
9. Melville BW, Raudkivi AJ (1977) Flow characteristics in local scour at bridge piers. *J Hydraul Res* 15(4):373–380
10. Muzzammil M, Gangadharaiah T, Gupta AK (2004) An experimental investigation of a horseshoe vortex induced by a bridge pier. *Proc Inst Civ Eng Water Manag* 157(2):109–119
11. Pagliara S, Carnacina I (2013) Bridge pier flow field in the presence of debris accumulation. *Proc Inst Civ Eng Water Manag* 166(4):187–198

# Real-Time Reservoir Operation Policy: A Case Study of Tanahu Hydropower Project



Bhola N. S. Ghimire, Rabindra Nath Shrestha and Upendra Dev Bhatta

**Abstract** For water resources engineering community, reservoir operation is a complex job. Real-time reservoir operation is furthermore complex as it has to consider the real-time hydrological uncertain events. In this paper, a real-time operation model is presented for Tanahu Hydropower Reservoir System in Nepal. To handle the real-time hydrology, it has to predict the reservoir inflow, which is done by using genetic programming (GP). For this, GP-based inflow forecasted models are developed. The reservoir optimization model is solved using EMPSO method for few years' inflow data, and the optimal solutions are obtained and used to generalize the operational policies. The release policies are used that obtained from EMPSO model and generalization is done with the function of initial storages and inflows to it by using GP model. Finally, the reservoir operation policies are formulated with the forecasted inflow. Performance of models is measured by using coefficient of determination ( $R^2$ ) and root mean squared error (RMSE) and found that the real-time operational model shows good accuracy.

**Keywords** Real-time reservoir operation · Genetic programming · Inflow forecasting · Tanahu hydropower project

## Notations

The following are the notations/abbreviations used in this article

$\beta_i$	Regression coefficient
$\gamma$	Unit weight of water
$\eta$	Overall generation efficiency

---

B. N. S. Ghimire (✉) · R. N. Shrestha · U. D. Bhatta  
Institute of Engineering, Tribhuvan University, Kathmandu, Nepal  
e-mail: [bholag@ioe.edu.np](mailto:bholag@ioe.edu.np)

$DQ_t$	Environmental flow provided in time period $t$
$DQ_{\min}$	Minimum environment flow required in various time periods
$E$	Hydropower energy
$EV_t$	Evaporation loss for any time period $t$
$E_t$	Evaporation loss for any time period $t, t - 1, \dots$
$e_t$	Rate of evaporation in time period $t$
$H_t$	Difference in elevation with water level at time $t$
$n$	Number of observations
$k$	Number of independent variables
$O_t$	Reservoir overflow during time period $t$
$P_{\min}$	Minimum power production limit per week
$P_{\max}$	Maximum power production limit per week
$P_t$	Power production at time period $t$
$Q_t$	Reservoir inflow at time period $t$
$R_t$	Water release at time period $t$
$R_{\min}$	Minimum limit of water releases from the reservoir in a week
$R_{\max}$	Maximum limits of water releases from the reservoir in a week
$sd(.)$	Standard deviation
$S_{\min}$	Allowable minimum storage volume
$S_{\max}$	Allowable maximum storage volume
$S_t$	Storage volume at the beginning of time period $t$
$S_{t+1}$	Reservoir storage volume at the end of time period $t$
$T$	Set of examples that reaches the node
$T_i$	Subset of examples that have the $i^{\text{th}}$ outcome of the potential set
$T_t$	Number of plant operating hours in a week
$t$	Time step
EC	Evolutionary Computation
FSL	Full Supply Level
GP	Genetic Programming
GWh	Giga Watt hour
IIL	Intake Invert Level
JJAS	June, July, August, and September
MLR	Multiple Linear Regression
MT	Model Tree
MOL	Minimum Operation Level
MW	Mega Watt
MWh	Mega Watt hour
PSO	Particle swarm optimization
RMSE	Root Mean Square Error
SDR	Standard Deviation Reduction
TWL	Tail water level

## 1 Introduction

For reservoir operation community, real-time reservoir is a challenging job. Since the operator should handle the river inflows, which is an uncertain event, the real-time phenomena become complex. In any hydropower projects, to generate the maximum power with fulfilling the constraints is important. This reflects the strength of real-time operation policy. The releases are often functions of forecasted reservoir inflows and the reservoir storage levels. The decisions are based on limited forecast information, thus it involves making release decisions in an uncertain environment. The process of making a decision (under uncertain environment) at a time period ' $t$ ' and updating the available information at the end of time period ' $t$ ' and making the next decision is a continuous process over the reservoir operational horizon.

During planning phase, the reservoir operation model assumes that the inflows at the beginning of each time period ' $t$ ' are known. But, in practice for real-time operation of reservoir, the exact value of the inflow is unknown at the beginning of time period ' $t$ '. This issue may be addressed by using a suitable inflow forecasting model. Time series models play a key role in forecasting the hydrologic variables. To know the future value of the variables such as reservoir inflows, it is very important to know their historical behavior. By using historical data, developing an accurate forecasting model is one of the most complicated tasks in hydrological modeling [1]. Therefore, through analysis of past data, the selection of most influencing variables is crucial steps in developing effective forecasting model. Real-time operation of reservoir system requires specific operating rules, in addition to inflow forecasting models. One of the conventional approaches widely used to operate the reservoirs is rule curve. Rule curve indicates the target storage at the end of each time period. These fixed rule curves do not consider the dynamic variation in the hydrologic variables and therefore often result in poor performance of reservoir system.

To improve the performance, a real-time reservoir operation model should consider all the variations in making decisions on releases. Mujumdar and Ramesh [2] presented a model for short-term reservoir operation for irrigation. The real-time operation model uses the forecasted inflows for the current period, for which a decision is sought. In hydropower reservoir system, real-time reservoir operation plays an important role. For real-time operation, its performance depends upon the accuracy of forecasting model. In this study, the real-time operation model for weekly time scale is developed and applied to the Tanahu Hydropower Reservoir System in Nepal.

## 2 Descriptions of the Methodologies

In this study, three regression models are used for generalizing the reservoir operation policies and their performance evaluated by using standard approaches. The methods used are: (i) Multiple linear regression (MLR), (ii) Model tree (MT), and (iii)

Genetic programming (GP). Brief details of these methods are given in the following subsections.

## 2.1 Multiple Linear Regression (MLR)

By the name, MLR is a regression model that involves more than one regressor variable. The model can be represented as:

$$y = \beta_0 + \beta_1x_1 + \beta_2x_2 + \beta_3x_3 + \dots + \beta_kx_k + \varepsilon \quad (1)$$

where  $y$  is response variable,  $k$  is index of predictor variables and  $\beta_i$  ( $i = 0, 1, 2, \dots, k$ ) are regression coefficients and  $\varepsilon$  is error term. Regression coefficients were estimated by using the least square methods.

## 2.2 Genetic Programming (GP)

Genetic programming (GP) [3] is an evolutionary computing method. GP is useful for regression calculations. While working, it starts with an initial population of randomly generated computer programs. There are several researchers used GP in different fields: for unit hydrograph determination [4]; for sediment discharge modeling [5]; for evaporation modeling [6]; for longitudinal dispersion coefficients in streams [7]; and for reservoir operation problems [8].

The working of genetic programming involves five steps:

- (i) Generate an initial population of random compositions of the functions and terminals,
- (ii) Execute each program in the population and assign a fitness value as per accuracy fitting in the program,
- (iii) Create a new population of computer programs by implementing mutation and crossover operations,
- (iv) Repeat steps (i) and (iii) over several iterations, and
- (v) Select the best computer program (either program form or equation form) that explored so far as the solution for given problem.

More details on GP and its workings can be found in Koza [3], Kisi, and Guvan [6].

Least mean square error is the main criterion used for model selection. In this study, the GP parameters set used to the program are: Population size = 500; Mutation frequency = 95%; Mutation rate = 0.01; Crossover frequency = 50%. The functions or operations used for GP program are: +, -, /, \*, power, sqrt, sin, cos, etc.

### 2.3 Model Tree (MT)

MT is a data-driven technique. Normally, MT handles continuous class problems. It provides structural representation of the data and piecewise linear fit to the subclasses. The details of MT can be found Quinlan [9], Wang, and Witten [10]. Reddy and Ghimire [5] used MT technique to predict the suspended sediment load in a river.

While selecting the model, the standard deviation reduction (SDR) is used. That is given as:

$$\text{SDR} = sd(T) - \sum_i \frac{|T_i|}{|T|} sd(T_i) \quad (2)$$

where  $T$  represents set of examples that reached the node;  $T_i$  represents the subset of examples that have the  $i$ th outcome of the potential set (i.e., the sets that result from splitting the node according to the chosen attribute); and  $sd(\cdot)$  represents the standard deviation.

## 3 Reservoir Operation Model

The reservoir operation models include the optimization model to develop the optimum releases from reservoir, simulation model to calculate the exact end storage based on optimum release policy, and real-time model that generalizes the release policy. In this study, real-time model is developed based on GP, MT, and MLR techniques.

### 3.1 Reservoir Optimization Model

#### 3.1.1 Objective Function

The objective function of the model involves maximizing total hydropower generated in a year. Mathematically the objective function can be expressed as:

$$\text{Max. } Z = \sum_{t=1}^N E_t \quad (3)$$

$$E_t = 0.278 \eta \gamma R_t H_t \text{ for all } t = 1, 2, \dots, 52 \quad (4)$$

where  $N$  is number of time periods (52 weeks),  $E_t$  is the generated hydropower energy in  $MWh$  during time period  $t$ ;  $R_t$  is the discharge through the turbine during time period  $t$  ( $Mm^3$ ),  $H_t$  is difference in elevation of water level and Tail water level



in  $m$ , ( $TWL$ ) ( $H_t = EL_t - TWL$ ),  $\gamma$  is unit weight of water ( $9.81 \text{ kN/m}^3$ ), and  $\eta$  is overall generation efficiency (which is taken as  $\eta = 0.86$ ).

The water available in the reservoir at the beginning of any time step is considered as the state of the system. The water releases from the reservoir over several time periods (weeks) in a year are taken as decision variables of the problem. The optimization involves maximization of hydropower generation subjected to constraints on storage volumes, releases, power generation, and mass balance of the reservoir system.

### 3.1.2 System Constraints

The objective function (Eq. 3) is subjected to the following system constraints:

*Storage Bounds* The reservoir storage for weekly periods has limits of minimum and maximum storages, which can be expressed as:

$$S_{\min} \leq S_t \leq S_{\max}, \text{ for all } t = 1, 2, \dots, 52 \quad (5)$$

where  $S_{\min}$  is allowable minimum storage volume;  $S_{\max}$  is allowable maximum storage volume; and  $S_t$  is storage volume at the beginning of time period  $t$  and all units are in  $\text{Mm}^3$ .

*Steady State Constraint* The reservoir storage volumes during starting of the initial time period and ending of the last time period in the operation horizon should be same.

$$S_1 = S_{T+1} \quad (6)$$

where  $S_1$  is storage volume at the beginning of first time period;  $S_{T+1}$  is storage volume at the end of last time period;

*Release Constraint* Water release from the reservoir can be expressed as follows:

$$R_{\min} \leq R_t \leq R_{\max}, \text{ for all } t = 1, 2, \dots, 52 \quad (7)$$

$$R_{\min} = 3.6 P_{\min} T_t / (\eta \gamma H_t), \text{ for all } t = 1, 2, \dots, 52 \quad (8)$$

where  $R_t$  is the water release at any time period  $t$ , ( $\text{Mm}^3$ );  $R_{\min}$  and  $R_{\max}$  are the minimum and maximum limits of water releases from the reservoir in a week;  $P_{\min}$  is the minimum power production limit.  $T_t$  is total number of hours the plant operating in a week.

**Environmental Flow Constraint** The minimum flow is maintained by providing the evaporation flow requirements as per reservoir release rules. As river flows are sufficient for JJAS months, no provision for environmental flows provided. For rest of the time periods (except JJAS months), the environmental flow can be expressed as:

$$DQ_t \geq DQ_{\min}, \text{ for all } t = 1, 2, \dots, 52 \quad (9)$$

where  $DQ_t$  is environmental flow provided in time period 't' (except JJAS) ( $\text{Mm}^3$ ), and  $DQ_{\min}$  is minimum flow required to meet environmental requirements in various time periods ( $\text{Mm}^3$ ).

**Evaporation Constraint** Reservoir evaporation in hot climate is serious effects in reservoir volumes. Normally, the evaporation loss is given by:

$$EV_t = A_t \times e_t, \text{ for all } t = 1, 2, \dots, 52 \quad (10)$$

where for given time periods:  $EV_t$  is the evaporation loss,  $A_t$  is reservoir surface water area corresponding to the average storage;  $e_t$  is the rate of evaporation.

**Power Production Constraint** The maximum and minimum power production can be expressed as follows:

$$P_{\min} \leq P_t \leq P_{\max}, \text{ for all } t = 1, 2, \dots, 52 \quad (11)$$

$$P_t = 0.278 \eta \gamma R_t H_t / T_t, \text{ for all } t = 1, 2, \dots, 52 \quad (12)$$

$$H_t = EL_t - \text{TWL}, \text{ for all } t = 1, 2, \dots, 52 \quad (13)$$

where  $P_{\min}$  and  $P_{\max}$  are minimum and maximum power production limits in MW and  $P_t$  is the power production rate in time period 't' (MW).

**Mass Balance Equation** Input and output system of a reservoir has to fulfill mass balance rules. This can be expressed as:

$$S_{t+1} = S_t + Q_t - R_t - DQ_t - EV_t - O_t, \text{ for all } t = 1, 2, \dots, 52 \quad (14)$$

where  $S_t$  and  $S_{t+1}$  represent the starting and ending reservoir storage volumes;  $Q_t$ ,  $R_t$ ,  $DQ_t$ ,  $EV_t$ , and  $O_t$  are the inflow, release, downstream environmental flow, evaporation loss, and overflow respectively during time period 't' ( $\text{Mm}^3$ ).

**Overflows** Excessive water spill out from reservoir is maintained by providing the overflow provisions in the system. It can be expressed as:

$$O_t = \text{Max}\{S_{t+1} - S_{\text{max}}, 0\}, \text{ for all } t = 1, 2, \dots, 52 \quad (15)$$

The reservoir operation problem is optimized by PSO algorithm. The sum of annual hydropower production is used as fitness function.

### 3.1.3 Solution Approach

The formulated model is solved by EMPSO technique. To handle the constraints of the problem, first as per EMPSO principle, generated random releases for different period are taken and simulation has been done inside the program. The policy is applied to get the energy. The calculated energy is accumulated to the stipulated time (for one year in this study) and energy is evaluated and compared. Simultaneously, the constrained criteria are checked and penalty is applied suitably for unfit conditions. Solution starts with the water available in the reservoir at the beginning of a time step. The water releases from the reservoir over several time periods (months, fortnights, or weeks) in a year are taken as decision variables of the problem. The optimization involves maximization of hydropower generation subjected to constraints on storage volumes, releases, power generation, and mass balance of the reservoir system.

## 3.2 Generalization of Release Policies

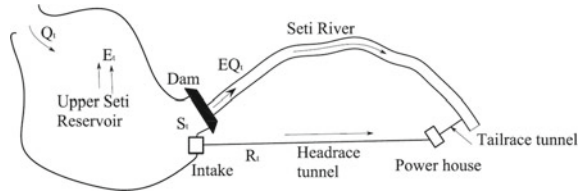
To generalize release policies based on optimal solutions obtained from reservoir operation model, the techniques MLR, GP, and MT are used and the best model is used for final implementation of real-time reservoir operation.

After computing release, evaporation loss, and other quantities, by using mass balance equation (Eq. 14) reservoir simulation is carried out.

## 4 Description of Case Study

The Tanahu Hydro Project (Formerly Upper Seti Hydropower Project) lies in the middle part of Nepal. The average annual power of the proposed project is 558 GWh. Based on the past flow records (from 2000 to 2006), the annual average inflow to the reservoir is 3536.52 Mm<sup>3</sup>. The dead storage capacity and gross storage capacity of reservoir are 63.51 and 333.71 Mm<sup>3</sup> respectively. Full Supply Level (FSL), Minimum Operation Level (MOL), Intake Invert Level (IIL), and Tail Water Level (TWL) are fixed as 425.0, 370.5, 360, and 308.25 m from mean sea level respectively. The minimum and maximum operation heads are fixed as 62.25 and 116.75 m, respectively. The overall efficiency ( $\eta$ ) of the plant is assumed as 86%. The maximum

**Fig. 1** Schematic diagram of Tanahu reservoir system



discharge capacity of the tunnel is 141 m<sup>3</sup>/s. The data are collected from Nepal Electricity Authority (NEA) and Department of Hydrology and Meteorology (DHM) of Nepal. The schematic diagram of Tanahu Reservoir system with hydropower components is shown in Fig. 1. The statistical properties of reservoir inflows: such as mean flow, minimum flow, maximum flow, and standard deviation are 68.01, 9.62, 265.08, and 71.58 Mm<sup>3</sup> respectively.

### 4.1 Data for Real-Time Release Model

The reservoir release data that obtained from optimization model in Ghimire and Reddy [11] are used in this study. The release data for all the years (from 2000 to 2006) are shown in Fig. 2. In the data set, first four year data are used for training purpose and next three years data are used for testing purpose. Reservoir releases statistics for training and testing period are given in Table 1.

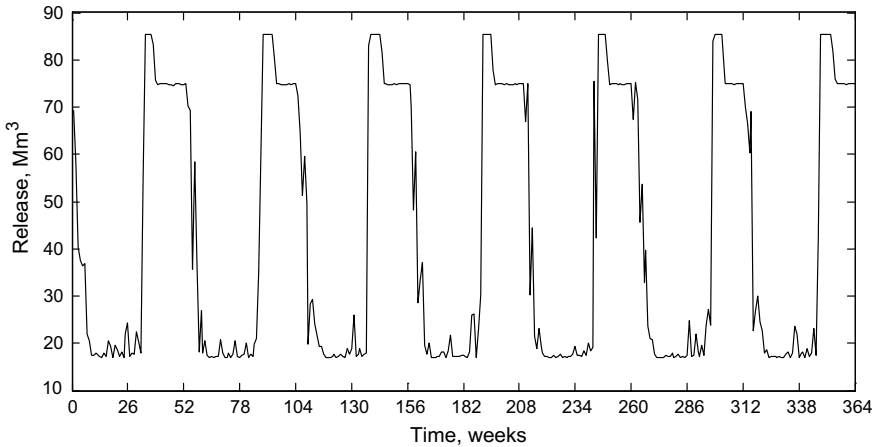


**Fig. 2** PSO release policy for weekly time period for Tanahu reservoir [11]

**Table 1** Reservoir release statistics for weekly time period

Statistical parameters	Training period 2000–2003	Testing period 2004–2006
Average release (Mm <sup>3</sup> )	43.767	42.007
Standard deviation (Mm <sup>3</sup> )	28.021	28.080
Maximum release (Mm <sup>3</sup> )	85.277	85.277
Minimum release (Mm <sup>3</sup> )	17.055	17.055

## 5 Discussion on Result

Modeling tools such as MLR, MT, and GP already introduced in earlier sections are used for the following six models. Each model has  $Q_t$  which is reservoir inflow in the present time stage  $t$  and can be obtained from inflow forecasting model. This variable is stochastic in nature and depends on the inflow forecasting model. The rest of the variables used in the model are deterministic variables. The following six set of models with several combination of variables are used for model development. They are:

- (1)  $R_t = f(Q_{t-1}, Q_t, S_t)$ ;
- (2)  $R_t = f(Q_t, R_{t-1}, S_t)$ ;
- (3)  $R_t = f(Q_{t-1}, Q_t, R_{t-1}, S_t)$ ;
- (4)  $R_t = f(Q_{t-2}, Q_{t-1}, Q_t, S_t)$ ;
- (5)  $R_t = f(Q_{t-2}, Q_{t-1}, Q_t, R_{t-1}, S_t)$ ; and
- (6)  $R_t = f(Q_{t-2}, Q_{t-1}, Q_t, R_{t-2}, R_{t-1}, S_t)$ .

Where  $R_t$  is the reservoir release at present time step  $t$ ;  $S_t$  is the reservoir storage volume at the beginning of present time step  $t$ ;  $Q_t$  is reservoir inflow at present time step  $t$ ;  $R_{t-1}$  is the reservoir release at one step past from present time step  $t$ ;  $R_{t-2}$  is the reservoir release at two step past from present time step  $t$ ;  $Q_{t-1}$  is reservoir inflow one step past from present time step  $t$ ;  $Q_{t-2}$  is reservoir inflow two step past from present time step  $t$ . In all cases,  $R_t$  is depended variable. The current inflow  $Q_t$  is the independent variable getting from reservoir inflow forecasting model.

### 5.1 Model Development

To develop all the models, initial four years data are taken for training purpose, immediate two years data are used for testing purpose, and remaining one year data is used for validation purpose. Each model is executed with modeling tools as discussed earlier.

Before fitting the data in the GP model, least mean square error is selected as the main criterion for model selection. The GP parameters set to the program are: Population size = 500; Program size = 80–512 (variable); Mutation frequency = 95%; Mutation rate = 0.01; Crossover frequency = 50%. In addition to that the

instructions such as: +, -, /, \*, power, sqrt, sin, cos, etc., are also considered. The MLR and MT are applied as usual principles.

To fit the data in model tree, setting of MT parameters to the program is: cross-validation fold = 10; min number of instances = 4, and disabled the pruning and smoothing criteria.

While applying the MLR, the developed matlab program is used and objective is set as minimization of RMSE value.

### 5.2 Model Performance

All six models (model no: 1–6) which also depends on inflow forecasting model, are executed by using modeling tools: MLR, MT, and GP. Their performances are measured by coefficient of determination and root mean square error. The performances  $R^2$  and RMSE for both training and testing data sets are given in Figs. 3 and 4, respectively.

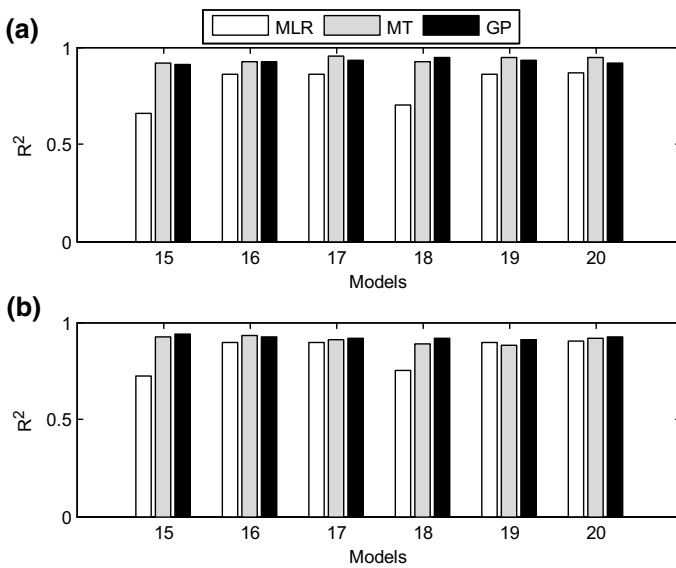
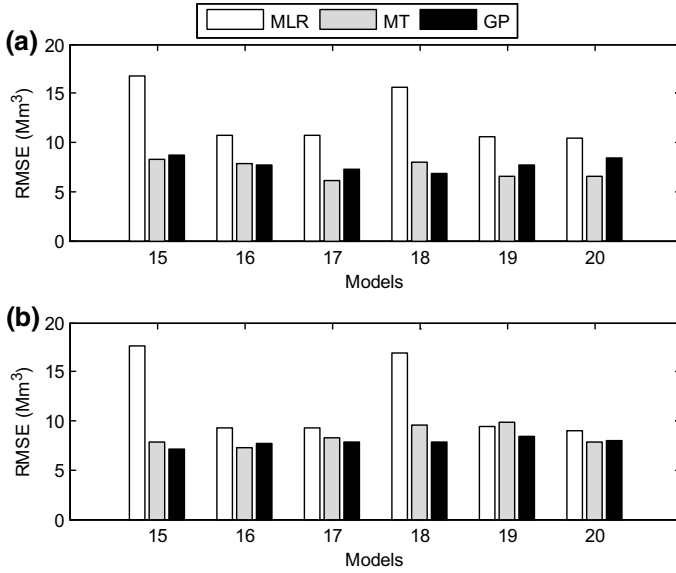


Fig. 3  $R^2$  plots for a Training and b Testing data sets for with inflow forecasting models





**Fig. 4** RMSE plots for **a** Training and **b** Testing data sets for with inflow forecasting models

**Table 2**  $R^2$  and RMSE for training and testing sets of selected models for weekly operation policies

Performance	Models	Training			Testing		
		MLR	MT	GP	MLR	MT	GP
$R^2$	$R_t = f(Q_{t-1}, Q_t, R_{t-1}, S_t)$	0.882	0.958	0.932	0.885	0.917	0.931
RMSE	$R_t = f(Q_{t-1}, Q_t, R_{t-1}, S_t)$	9.65	5.79	7.350	9.599	8.07	7.31

### 5.3 Model Selection

Selection of the model is based on the model performance criteria given in earlier section. Models giving the best performance values such as maximum coefficient of determination and minimum RMSE for both training and testing data sets are selected. The minimum difference of performance values between training and testing data sets are considered during the selection of the best models from each category. The selected model and their performances are shown in Table 2.

The performance values for selected models MLR, MT, and GP are presented in Table 2. While comparing the performances between MLR, MT, and GP models, it is found that MT and GP models are giving much better result than MLR models in both cases (independent on inflow forecasting model and dependent on inflow forecasting model). In between MT and GP models, GP model seems superior than MT model. Therefore, GP model having function set  $\{R_t = f(Q_{t-1}, Q_t, R_{t-1}, S_t)\}$  that



depends on inflow forecasting model is selected to develop the integrated model for further application.

## 6 Development of REAL-TIME Integrated Model

The reservoir release models discussed in earlier section are able to give the release decision for only one time step. While release decision is taken, in effects, the actual state of some parameters such as reservoir state, evaporation from reservoir, etc. is changed. These new parameters should apply to take the new release decision for the next time step. The actual state of those parameters can be obtained from reservoir simulation model. After getting the actual values of those parameters from reservoir model, the new release decision can be estimated from the release decision model. The block diagram of integrated real-time reservoir release model is shown in Fig. 5, where the integration of inflow forecasting model to the integrated model depends on the selection of release decision model.

A program is written in MATLAB 7.1 environment for real-time reservoir integrated model as shown in Fig. 5 and reservoir simulation model. In real-time reservoir integration model, both the reservoir release decision and reservoir inflow forecasting models which are developed in GP environment, are linked with each other. A program for reservoir simulation model is also written in MATLAB 7.1 environment and linked to real-time reservoir operation integrated model. While developing the reservoir simulation model, all the constrains associated with this model are incorporated to the model.

### 6.1 Model Application

The real-time model is applied to the validation period for year 2006 in the case study explained as earlier. The reservoir release model that depends on inflow forecasting

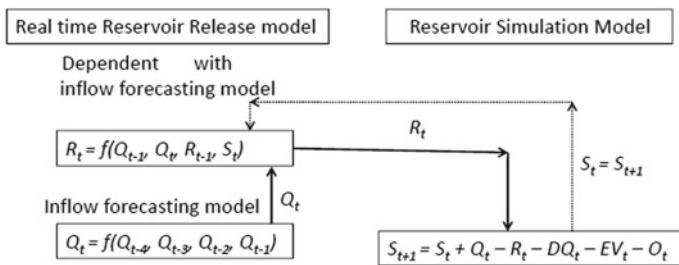


Fig. 5 Real-time reservoir release model integrated with reservoir simulation model





**Table 3** Annual power in GWh for validation year 2006 from different models

Year	PSO model	Project feasibility report [12]	GP model dependent with inflow forecasting model (Model-2)
2006	570.16	558.00	549.88

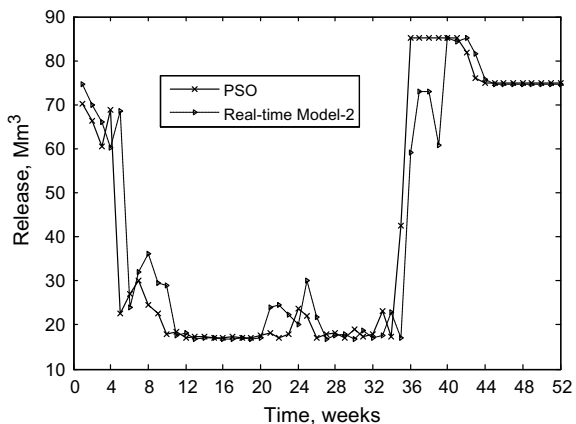
model, is applied with reservoir simulation model to develop the release policy for the year 2006. It should be noted that while applying the integrated model  $\{Q_t = f(Q_{t-4}, Q_{t-3}, Q_{t-2}, Q_{t-1})\}$ , it is seen that at least four step ahead inflow data are necessary.

During the application of reservoir release integrated model in the case study, following parameters are set in the model. They are: plant capacity ( $P_{max}$ ) = 122 MW; minimum plant operating limit ( $P_{min}$ ) = 14.81 MW; maximum tunnel capacity ( $R_{max}$ ) = 85.277 Mm<sup>3</sup>/week; minimum plant operating discharge ( $R_{min}$ ) = 10.314 Mm<sup>3</sup>/week; minimum environmental flow except JJAS periods ( $DQ_{min}$ ) = 1.8 m<sup>3</sup>/s (for JJAS periods,  $DQ_{min}$  = 0 m<sup>3</sup>/s); overall plant efficiency ( $\eta$ ) = 86%. All these data are taken from NEA [7].

### 6.2 Result and Discussion on Integrated Model

Annual powers that obtain from simulation model for the year 2006 using PSO release policy and real-time integrated models Model-2 are given in Table 3. The results show that the integrated real-time release model that has incorporated with reservoir inflow forecasting model gives annual power (549.88 GWh) and the annual power (570.16 GWh) gives by PSO model has the minimum difference. Here it is necessary to note that project report is indicated the annual power of 558 GWh could be generated.

**Fig. 6** Reservoir release for year 2006 from PSO and integrated real-time simulation model (Model-2)



From Table 3, it can be seen that PSO model-based operation policy gives more power than others. The real-time release policy is presented with PSO release policy to demonstrate the weekly release variation in Fig. 6. Figure 6 describes various level of power generation that using real-time operation policy, which could be reflect the real life problems that we may not get the expected real power. Hence GP model that incorporated to the inflow forecasting model giving better result is preferable for real-life operation purpose of Tanahu Hydropower Project.

## 7 Conclusions

In this study, real-time reservoir operation policy for Tanahu Hydropower Project is developed by using (i) MLR, (ii) MT, and (iii) GP techniques. The models are tested to the inflow forecasting value. Six set of models are tested that includes the current inflow. The optimum release policy obtained from PSO optimization model is used for generalization purpose. Based on performance analysis (RMSE and  $R^2$ ), the real-time operation rule having function set  $\{R_t = f(Q_{t-1}, Q_t, R_{t-1}, S_t)\}$  is found better than other models based on performance analysis.

The study is extended to develop the integrated real-time operation model. The annual energy for this validation year is compared with PSO optimization model. The result shows that the integrated GP model that incorporated the inflow forecasting model was giving reliable hydropower production. The release policy from this model showed that the model behaves less fluctuation with PSO optimization results. The difference in annual hydropower production PSO model and Real-time model becomes less than one percent.

## References

1. Kumar DN, Raju KS, Sathish T (2004) River flow forecasting using recurrent neural networks. *Water Resour Manag* 18:143–161
2. Mujumdar PP, Ramesh TSV (1997) Real-time reservoir operation for irrigation. *Water Resour Res* 33(5):1157–1164
3. Koza JR (1992) Genetic programming: on the programming of computers by means of natural selection. The MIT press, MA, Lomdon, Cambridge
4. Rabunal JR, Puertas J, Suarez J, Rivero D (2007) Determination of the unit hydrograph of a typical urban basin using genetic programming and artificial neural networks. *Hydrol Proc* 21:476–485
5. Reddy MJ, Ghimire BNS (2009) Use of model tree and gene expression programming to predict the suspended sediment load in rivers. *J Intell Syst* 18(3):211–227
6. Kisi O, Guven A (2010) Evapotranspiration modeling using linear genetic programming technique. *J Irri Drain Eng ASCE* 136(10):715–723
7. Azamathulla HM, Ghani AA (2011) Genetic programming for predicting longitudinal dispersion coefficients in streams. *Water Resour Manag* 25(6):1537–1544
8. Fallah-Mehdipour E, Bozorg HO, Marino MA (2012) Real-time operation of reservoir system by genetic programming. *Water Resour Manage* 26:4091–4103

9. Quinlan JR (1992) Learning with continuous classes. In: Proceedings Australian joint conference on artificial intelligence, World Scientific, Singapore, pp 343–348
10. Wang Y, Witten IH (1997) Introduction for model trees for predicting continuous classes. In: Proceedings of the European conference on machine Learning, University of Economics, Faculty of Informatics and Statistics, Prague
11. Ghimire BNS, Janga Reddy M (2013) Optimal reservoir operation for hydropower production using particle swarm optimization. ISH Journal of Hydraulic Engineering, Taylor and Francis. <https://doi.org/10.1080/09715010.2013.796691>
12. NEA (2001) Project feasibility report of upper seti hydropower project, NEA, Nepal

# Nexus of Water Footprint with Energy and GDP of Saudi Arabia and Solution for Sustainable Water Usage



Vineet Tirth

**Abstract** The Kingdom of Saudi Arabia (KSA) is the largest oil-producing country in the Arabian Peninsula and the Middle East. The country is fast developing under the dynamic leadership and undergoing a transition between modernization and tradition. On the one hand, KSA is among the most stressed regions of the world from the water resource point of view; on the other hand, it is a country with the highest oil reserves in the world. The water footprint (WFP) per capita of Saudi Arabia is among the top 10 countries, and the energy footprint is among the top 20 countries in the world. About 50% of the water in KSA is derived from the desalination, at a high cost, which is subsidized by the government. Hence, a large part of the economy is compromised to cater to this subsidy, adversely affecting the growth of the GDP of the country. In the present study, a state of art and most recent analysis has been done for nine years on the factors contributing to the development index of KSA. The focus is on per capita water footprint. About 70% of the electric power in the KSA is consumed for the purpose of air-conditioning, which generates condensate water as a by-product, often drained. A most effective measure to recycle wastewater is suggested by harnessing the condensate from the air-conditioning and using it for sanitation, without any purification or filtration. The proposed solution can cater to the daily water need of 0.4 million residents of KSA and can save more than 30 million USD per annum, almost 4.37% of the GDP of 2018.

**Keywords** Water footprint · Water resources · Wastewater recycling · GDP · Sustainable water usage · Energy footprint

---

V. Tirth (✉)

Mechanical Engineering Department, College of Engineering, King Khalid University, Abha, Asir 61411, Saudi Arabia  
e-mail: [v.tirth@gmail.com](mailto:v.tirth@gmail.com); [vtirth@kku.edu.sa](mailto:vtirth@kku.edu.sa)

© Springer Nature Singapore Pte Ltd. 2020  
R. AlKhaddar et al. (eds.), *Advances in Water Resources Engineering and Management*, Lecture Notes in Civil Engineering 39,  
[https://doi.org/10.1007/978-981-13-8181-2\\_4](https://doi.org/10.1007/978-981-13-8181-2_4)

43

## Abbreviations

KSA	Kingdom of Saudi Arabia
WFP	Water footprint
UG	Underground
GDP	Gross domestic product
pcpa	Per capita per annum
pcpd	Per capita per day
USD	United States Dollars
RO	Reverse osmosis
VAT	Value-added tax
TWh	Tera watt hours

## 1 Introduction

Water, air, food, and shelter are essential for life, among them water and air are critical life-support fluids. Although the earth has one-third part land and two-thirds part water, still that water being saline cannot be used by the man, animals, and plants for direct consumption. Based on the sources, types, and utility, water is classified into several types, represented in Fig. 1. The renewable water refers to the water from natural resources. The water generated from the resources and precipitation within the country is called internal renewable water and that obtained from the resources outside the countries viz. rivers, lakes, reservoirs, rainwater, shared, and/or flowing downstream from other countries is called external renewable water. Internal renewable water sources are rain, river, springs, groundwater, recharge from precipitation, etc. The nonrenewable water is exhausted over the period of time like groundwater, which cannot be reinstated by man. The virtual water is purchased or borrowed from the external sources directly or, in the form of food, i.e., the water equivalent to produce the food and agricultural products imported or borrowed. The nonrevenue water is unaccountable due to several reasons viz. unauthorized, unmetered consumption, loss of the transmission, leakage, etc. [1–3].

The status of water resource availability and consumption of water in different parts of the world is shown in Fig. 2. The region, shown in dark green color, about 20% of the area, mainly in central Africa, South America, and some parts of Europe has surplus renewable water resources. The main reason for sufficient and surplus water resources is the geopolitical location where the ground and natural renewable water assets are enough and either the population is less (as in Europe) or the WFP of the people is less (the case of central Africa). The color light green about 25% indicates a balance between the WFP and the resources. Beyond green color, the gray color indicates about 20% of the area, the depleting renewable and nonrenewable water resources. The pink color, about 20% area, indicates fast depleting water resources, falling groundwater levels, and water scarcity in the region. The red color about 15%

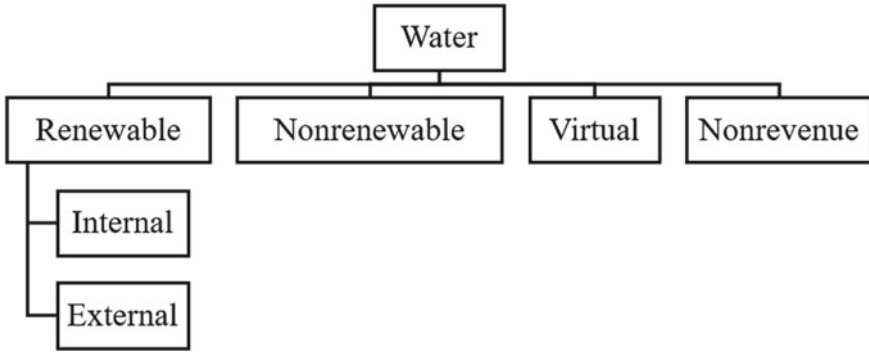


Fig. 1 Classification of types of water

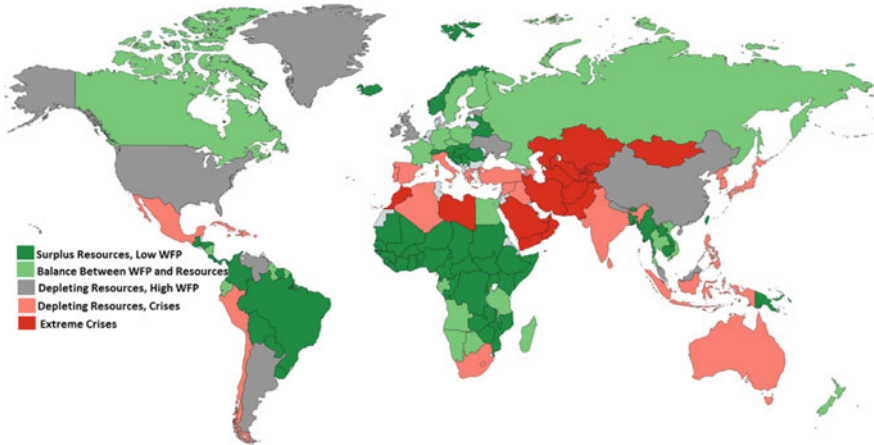


Fig. 2 Status of water resources in the world

area indicates regions of exhausted underground water, shortage of renewable water resources, extreme water shortage and scarcity. In the next two decades, the colors are expected to turn pinkish and reddish [4, 5].

This study is focused on KSA, by far the largest country in the Middle East and a region of the fastest depleting water resource and extreme crises of renewable water. The land area of KSA is about 2.15 Million Sq. km, which is the biggest in the Arabian Peninsula. The KSA is a desert country, yet it has a long coastline in the east with the Persian Gulf and in the west, along with the Red Sea. The total coastal area is about 2230 km. By far, KSA has diversified demography. The demography, provinces, and the natural nonrenewable surface water resources are shown in Fig. 3. It is inferred from the figure that the availability of rivers, springs, surface water is minimal compared with the geographical area of KSA [5–7].



Fig. 3 Map of KSA with demography and natural water resources [5]

## 2 Materials and Methods

The data given in the study has been taken from the up to date and recent sources, mostly the Web sites of the government of KSA, the UN, and the World Bank. The reports and the statistics published have been included in the study. The data for nine years from 2010 to 2018 has been analyzed, and the curves are plotted. The factors which influence directly or indirectly the growth index of the country viz. GDP, energy footprint, water footprint, population, etc. have been studied in relation to each other. The effect of the recession on oil prices on the economy, GDP, and socioeconomic status of the KSA has been discussed briefly and precisely. The study further converges to the WFP of Saudi citizens and its burden on the Saudi economy. A simple and effective solution to relieve the economy by 30 million USD by using the condensate water for the sanitary purposes has been proposed. Since, the year 2018 is still in progress, to make the study relevant and up to date, the data for 2018 has been taken up to June 2018 (half year). The projection in the growth rates of population, GDP, etc., for 2018, has been done using statistical tools for

the complete year. This study offers a green solution to water crises by suggesting recycling of water in KSA, which may be adopted for other Middle East countries.

### 3 Results and Discussion

The water for the domestic, agricultural, and industrial purpose is supplied by the municipal department (public works), the mobile water tankers which ply within the urban areas and supply the water, which is either desalinated or obtained from the reservoirs. A minimal quantity of water is supplied by the wells, mainly for agricultural purposes. Figure 4 shows the water supply methods being used in KSA [8–10].

The fraction of water obtained for the domestic, industrial, and agricultural purposes in KSA are derived mainly from three sources. The major part of the water (50%) is derived from about 30 desalination plants, established near the coastal belt of KSA. This is the water supplied to the households for domestic use. About 40% of water is extracted from deep underground (UG) aquifers. This water is mainly used for the agricultural purpose and the industries. Remaining about 10% of water is the surface water obtained from the rain, surface runoff, collected in water reservoirs or downstream flow mainly from the neighboring countries. The UG water is very deep, and the aquifers are fast depleting in KSA [9–12]. Figure 5 shows the water resources in KSA.

The population of KSA from 2010 to 2018 including the citizens and the expatriates is plotted in Fig. 6. The KSA has a total population of about 33.55 million in 2018 (up to June 2018) of which, about 35% are expatriates and the remaining are

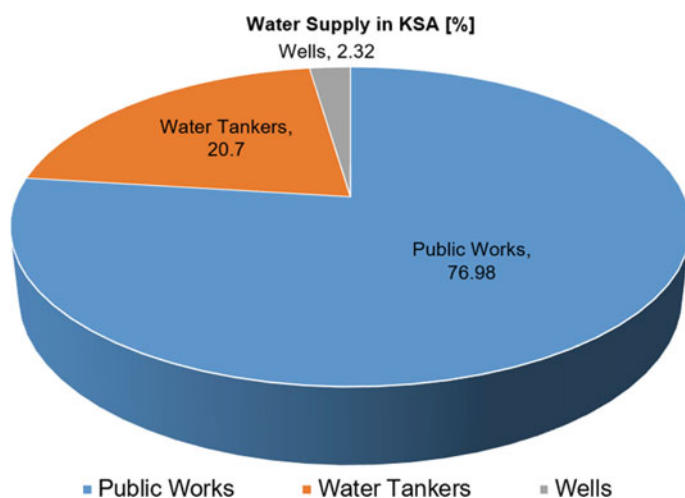


Fig. 4 Water supply methods in KSA



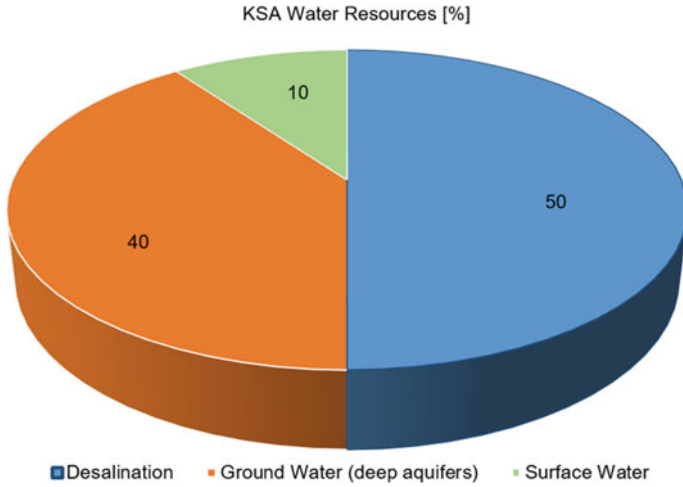


Fig. 5 Water resources in KSA

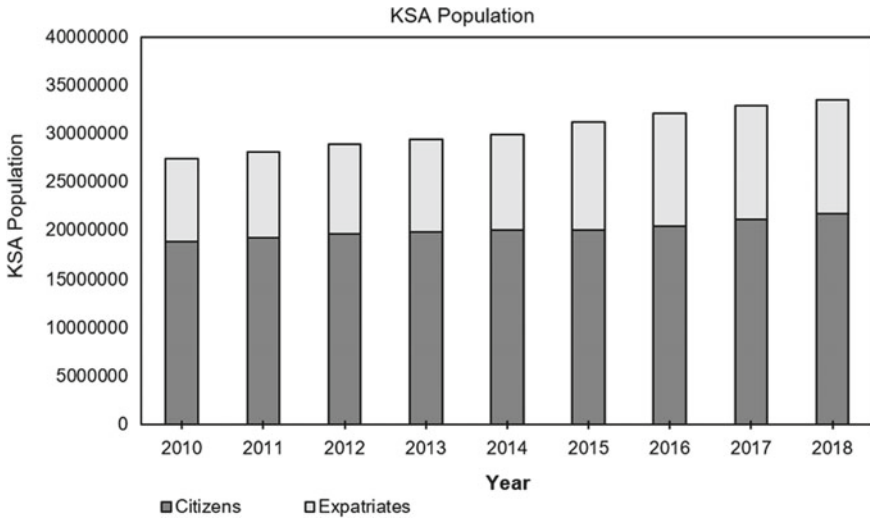


Fig. 6 Population of KSA

the citizens. The population density in 2018 is 15.6 people per sq. km, including the expatriates [8, 13].

The average growth in the population of KSA is 2.55% per year from 2010 to 2018. The growth rate of the population of KSA and the total population of KSA have been plotted against the year in Fig. 7. Though the growth in population is steady, almost linear, the population growth rate in KSA shows a strange variation. From 2010 to 2013, the rate of population growth declines, then it increases in 2014,



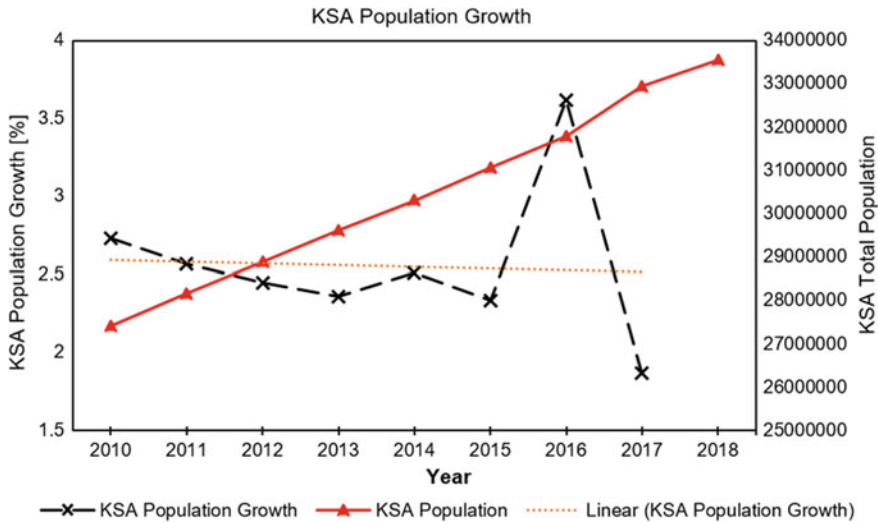


Fig. 7 Population growth in KSA

again declines in 2016, and then reaches a maximum to about 3.5% followed by a decline to the lowest rate in 2017. The growth rate of 2018 is not included since the year has not been completed yet. This variation in the growth of population is due to a large number of expatriates coming in the country and going out, resulting in a zigzag growth rate. The expatriate’s population in KSA is about 35% in 2018, hence any analysis without including them is irrelevant. In the year 2017, a large number of expatriate families have left the country due to several taxes applied by the government and so a decline in growth rate is observed.

Gross domestic product (GDP) is one of the most reliable indicators of growth of the economy of a nation and the human development index of the residents. The GDP of KSA and the GDP per capita are plotted over nine years from 2010 to 2018 [8–13] in Fig. 8. The economy of KSA is oil dependent, the revenue loss resulted in 2015-2017, due to the falling crude oil prices, almost by 80% and also to meet the additional expenditure on the country due to a war in Yemen [14]. It is observed from Fig. 8 that the GDP per capita rises steeply from 2010 to 2012, then it becomes saturated in 2013, rises again up to 2015, and then drops up to 2017. This drop in GDP is due to the taxation, an increase in the fuel prices, and the cut in the salary of the government employees in the year 2016 as a part of the austerity measures. Then, in 2017, the oil prices recovered and the effect of other austerity measures supported the government, as a result, the salary of all the government employees was reinstated, leading to a rise in GDP in 2018. Still, the level of GDP could not reach its peak as in 2015, due to the increased fuel prices and implementation of 5% value-added tax (VAT) across the Middle East countries. The GDP of the country increases from 2010 to 2014 and then declines in 2015 and 2016, due to the fall in the crude oil price in the international market and the war expenditure. The correction



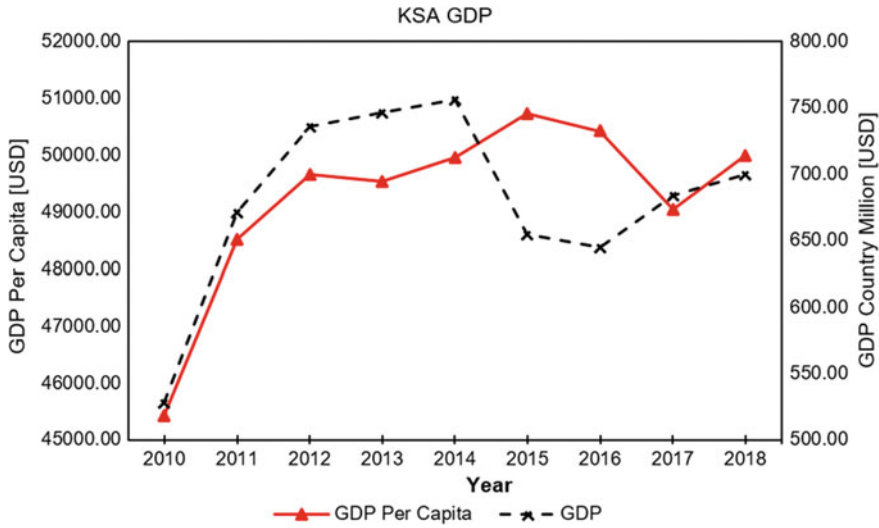


Fig. 8 GDP of KSA as a country and GDP per capita

in the GDP is observed from the year 2016 to 2017–2018 due to implementing the taxes and austerity measures, reducing the expenditure by a reduction in salary, etc. The complete data for 2018 was not available so the figures in the first two quarters of the year are considered as the GDP of the year 2018. The decline in GDP after 2015 and then its improvement, post 2016 may be attributed to the correction in the oil prices in international markets and the strengthening of United States Dollars (USD) respectively [8, 15].

The consumption of power mainly electricity is a universal indicator of energy and carbon footprint of the population of the country. The total electricity consumption of KSA and that consumed per capita over a period of nine years from 2010 to 2018 is revealed in Fig. 9. The trend of increase in energy consumption by the people and the country may be estimated by the polynomial equations of second order, given in Fig. 9. The increase in the energy footprint of the country saturates toward the top, mainly due to increased urbanization but the improvised policies of the government, as a part of Saudi Vision 2030 [15] to use the energy efficient appliances in both, the domestic and industrial applications. The increase in energy consumption is also due to the increase in population. On the other hand, the steep increase in the energy footprint per capita is due to the improvement in the quality and standard of living, increasing urbanization and use of more electric appliances by the people.

The department of statistics in KSA conducts a large number of studies and surveys. These studies and reports are often published in official news agencies, the most popular and prompt of them are the Arab News and the Saudi Gazette. The total energy consumption of KSA is mainly in three categories, as shown in Fig. 10. The largest fraction of electric energy is consumed in air-conditioning, in households, public places, government establishments, and industries. There is hardly any space

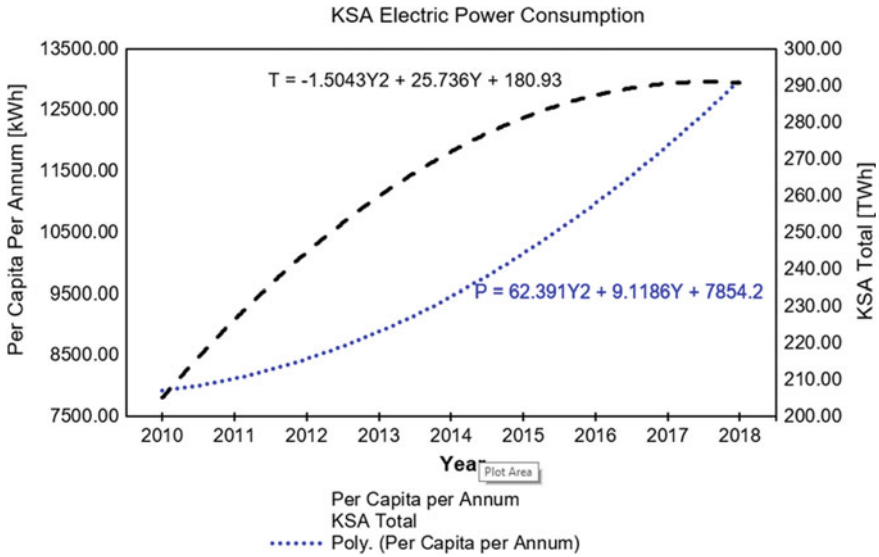


Fig. 9 Total and per capita consumption of electric power in KSA

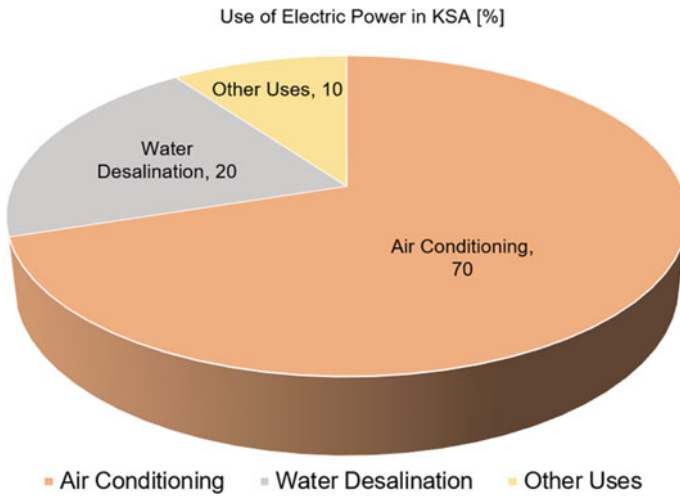


Fig. 10 Use of electric power in KSA

which is not air-conditioned in KSA. About 70% of electric power is consumed in air-conditioning [16–18], which amounts to 203 TWh in 2018. The demand for electric energy is expected to double by 2030 [8].

In Fig. 11, a comparative study of WFP per capita per day (pcpd) and that, for the country, per annum is made over the period of study. In 2018, the WFP reached 300 Lt. per capita per day, one of the highest in the world, in a country which is in extreme

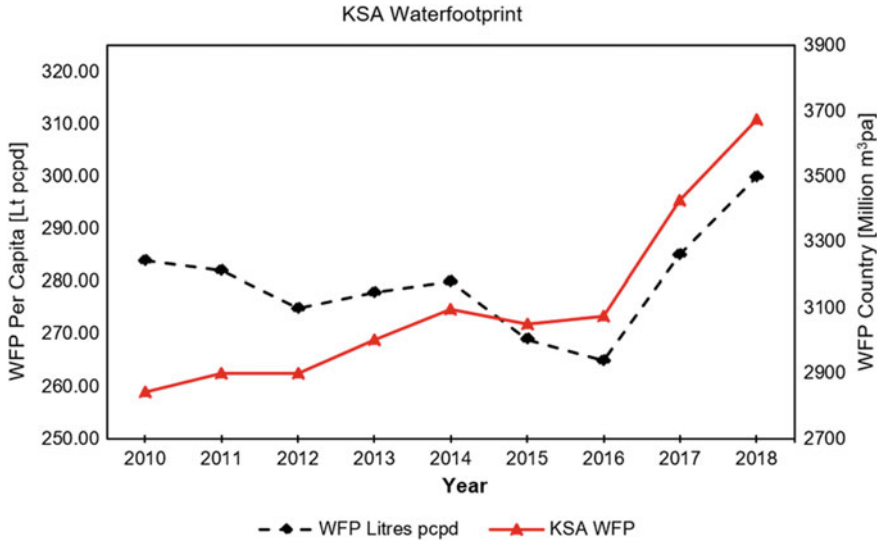


Fig. 11 WFP of KSA and per capita

shortage of renewable water resources. As per the united nations recommendation, 50 L of water is essential per day to maintain the necessary hygiene and for personal consumption [5, 7, 19–21]. KSA consumes six times more than that. The WFP of the country is also increasing, almost a similar trend is observed in the WFP of the country and WFP pcpd. The decline in the WFP in the year 2015 and 2016 is mainly due to the reduction in the population of the expatriates in this period and also a check on the construction activities as a part of the austerity measures.

An attempt has been made to study the WFP of KSA with other indicators of development. In Fig. 12, the WFP of KSA is studied with its GDP. Due to the variation of GDP, as a result of the oil prices, the relationship from 2014 to 2016 may not be established, otherwise, before 2014 and after 2016, both show an increasing trend.

In Fig. 13, the WFP per capita per day is studied with GDP per capita and it is interesting to note that in spite of the austerity measures and correction in the economy, the WFP declines without any trend, therefore it may be considered as piecewise linear. Then, after 2016, even in the recession and peak of the austerity period, the WFP increases and reaches its peak in 2018. The reason for this increase is attributed to the increased number of pilgrims to the country in this period. The variation in the GDP has been reported and discussed in Fig. 8. The variations in the WFP and the GDP are due to independent factors and may not be correlated to each other in the dynamic period of transformations in the economy between 2015 and 2018.

The WFP per capita per day when studied with the electric energy consumed per capita, represented in Fig. 14, indicates that the energy footprint increases steeply.



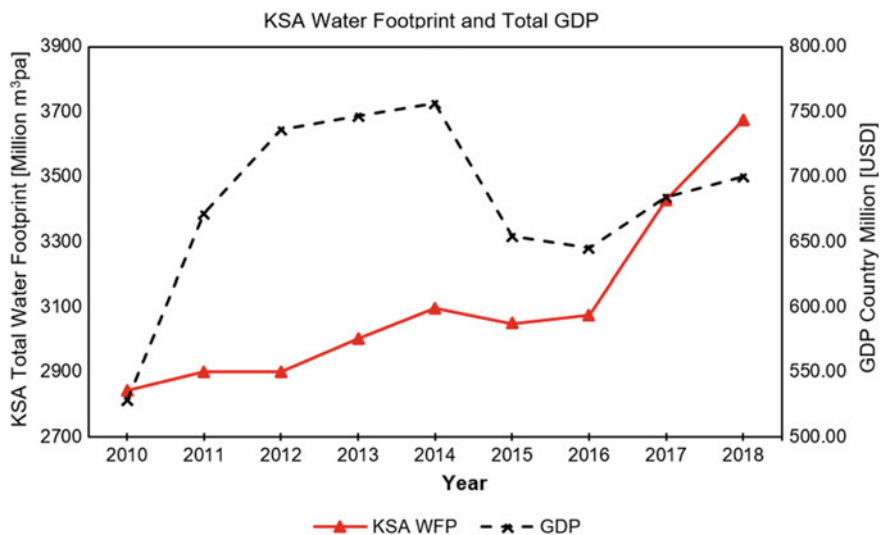


Fig. 12 WFP of KSA and GDP

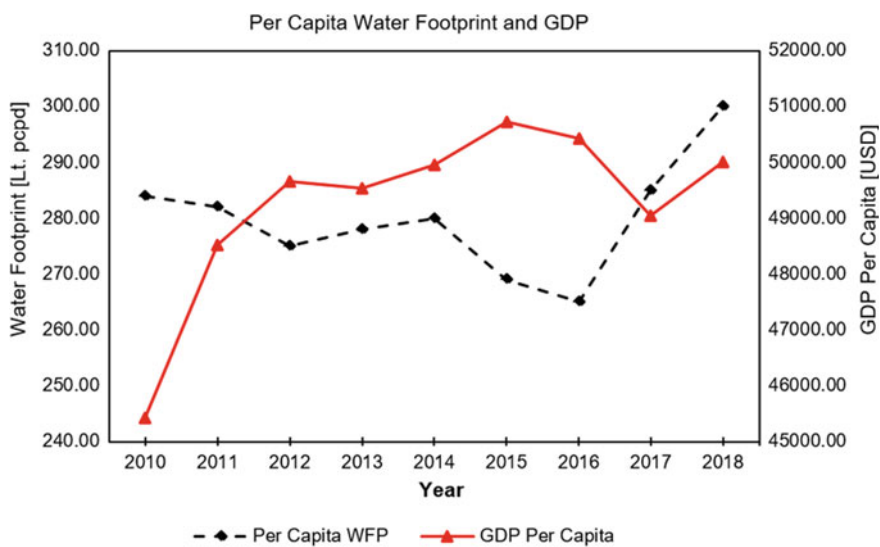


Fig. 13 Per capita WFP and GDP in KSA

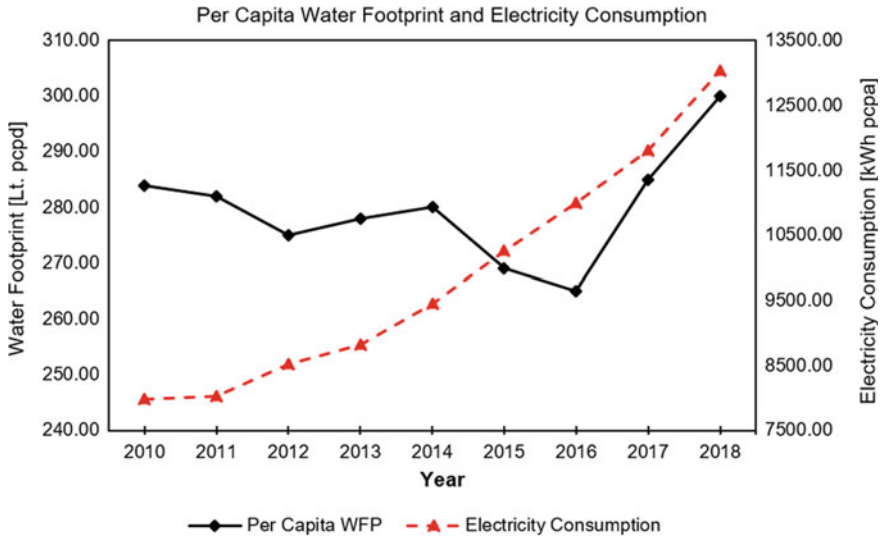


Fig. 14 WFP pcpd and the energy consumption pcpa in KSA

The WFP remains saturated from 2010 to 2014, declines in 2015 and 2016 due to reduced expatriate population, and then increases as soon as the development and urbanization regain momentum.

Based on the detailed analysis of the factors which define the development of a country and its residents, it is striking to reveal that the electric power consumed in air-conditioning in KSA is 70% of the total electric power consumption [16, 17]. Virtually all public space is air-conditioned in KSA. The electric power of 3.5 kW is equivalent to one ton of refrigeration and 70% of the total power consumed in KSA in 2018 results in 203 TWh of electric power used for space cooling, which is equal to 5783.48 Tons of refrigeration. One ton of refrigeration produces water condensate equivalent to 0.1–0.3 gallons, depending on the humidity in the air [22–25]. Now taking the mean on 0.2 gallons of water condensate produced from air-conditioning, per ton, 5783.48 Tons of refrigeration will produce 1156.7 Million gallons of condensate water. This amount is equivalent to 4378.56 Million liters or 4.378 Million m<sup>3</sup> of condensate water per annum, sufficient for 0.4 Million citizens of KSA for one year. It has been studied from Fig. 5 that in KSA, about 50% of water is obtained from the desalination plants across the country, which provides water at highly subsidized tariff to the residents [26]. The minimum cost of desalinated water with the highest efficient plant is 0.7–0.8 USD per m<sup>3</sup> [27–29], which does not include the cost of pumping, transportation, piping, losses, disposal of wastewater, etc.

It is proposed that the water condensate obtained from the air-conditioning units in all the public places should be used for the sanitary purpose in the toilets, which is possible at each and every public place including houses, hospitals, government establishments, malls, schools, airports, mosques, etc., without any treatment or



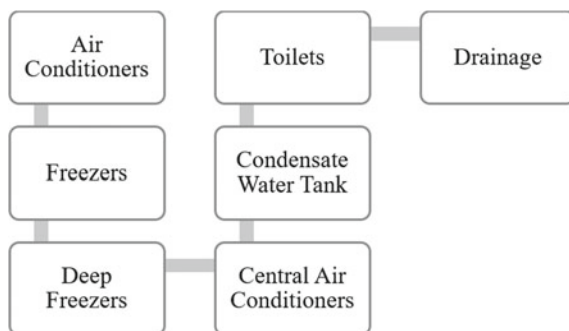


**Fig. 15** Condensate from the air-conditioning systems supplied to toilets

**Table 1** Calculation for recycling the condensate and its impact on the economy of KSA

Indicator	Value
Total electricity consumed in KSA (2018)	290 [TWh]
Used in air-conditioning (70%)	2.03 [TWh]
Equivalent Tonnage of Refrigeration (1TR = 3.51 kW)	57834757835 TR
Water Condensate produced @ 0.2 Gallon per TR	11566951567 Gallons
Water Condensate produced in Liters (1 Gallon = 3.78541 L)	43785654131 L
Water Condensate produced in m <sup>3</sup> (1 m <sup>3</sup> = 1000 L)	43785654.13 m <sup>3</sup>
This water can be sufficient for (WFP pcpd in KSA = 300 L in 2018)	399868.9875 Peoples
Cost of desalinated water saved (1 m <sup>3</sup> of desalinated water is produced @0.7 USD) without pumping, losses, piping cost	30649957.89 [USD]
Total saving in one year	30.64995789 [Million USD]
This is equal to [% of GDP 2018]	4.378565413% GDP in 2018

purification. Considering a minimum cost of 0.7 USD per m<sup>3</sup> of desalinated water and neglecting the distribution expenditures, this condensate water will directly save 30.64 Million USD per annum, equal to 4.37% of the GDP of KSA per annum in the year 2018. The condensate water used for sanitary and services purpose requires a little modification in the plumbing design of a building [22–25]. A proposed schematic diagram of such a system is given in Fig. 15, which also shows alternative uses of this water. Moreover, a properly collected, transferred, and stored condensate water is as good as the rainwater and with purification, it may be consumed for drinking and cooking purposes also. The calculations discussed in the preceding section are given in Table 1.



## 4 Conclusion

The economy of KSA and its GDP is amidst volatile transformation. The country lists among the highest WFP and EFP in the world. The major source of revenue is the oil exports but the KSA is moving aggressively toward the oil-independent economy. The EFP per capita is 13 MWh in 2018, about 70% of which is used in air-conditioning. The WFP pcpd for Saudi residents is 300 L. Almost 50% of the water is produced from desalination at a very high cost and is highly subsidized by the government, which has a huge burden on the economy. The condensate water obtained from air-conditioning units can generate enough water of 0.4 million residents in KSA and save 4.37% or 30.64 million USD. This water may be directly used for sanitation purposes and thus given a practical and simple cost-effective solution for sustainable water usage.

**Acknowledgements** The author thankfully acknowledges the facilities of Saudi Digital Library and computing resources provided by King Khalid University, Abha-Asir, Kingdom of Saudi Arabia to complete the work.

## References

1. <http://www.fao.org/nr/water/aquastat/tables/index.stm>. Accessed on 15 July 2018
2. Hoekstra AY, Hung PQ (2002) A quantification of virtual water flows between nations in relation to international crop trade. *Water Res* 49(11):203–209. Available at <http://waterfootprint.org/en/water-footprint/national-water-footprint/virtual-water-trade/>
3. Chapagain AK, Hoekstra AY (2008) The global component of freshwater demand and supply: an assessment of virtual water flows between nations as a result of trade in agricultural and industrial products. *Water Int* 33(1):19–32
4. <https://www.weforum.org/agenda/2017/01/water-water-everywhere-so-why-dont-we-pay-it-more-attention>. Accessed on 14 July 2018
5. [http://www.fao.org/nr/water/aquastat/countries\\_regions/SAU/index.stm](http://www.fao.org/nr/water/aquastat/countries_regions/SAU/index.stm). Accessed on 15 July 2018
6. Alsalah D et al (2015) Assessing the groundwater quality at a Saudi Arabian agricultural site and the occurrence of opportunistic pathogens on irrigated food produce. *Int J Environ Res Public Health* 12(10):12391–12411
7. World Bank (2007) Water resources data from making the most of scarcity, pp 143–148, 150,153–154, 182–183
8. [https://www.stats.gov.sa/sites/default/files/household\\_energy\\_survey\\_2017en.pdf](https://www.stats.gov.sa/sites/default/files/household_energy_survey_2017en.pdf). Accessed on 16 July 2018
9. Study WI (2014) CHAPTER 4 Water demand and supply in Saudi Arabia, pp 157–180. Available at [http://shodhganga.inflibnet.ac.in/bitstream/10603/110554/12/13\\_chapter4.pdf](http://shodhganga.inflibnet.ac.in/bitstream/10603/110554/12/13_chapter4.pdf)
10. Ouda OKM (2013) Saudi Arabia water resources, water shortage, public awareness water pricing system. *Resour Environ* 3(1):10–13
11. Chowdhury S, Al-Zahrani M (2012) Water resources and water consumption pattern In Saudi Arabia Shakhawat. In conference: the proceedings of the 10th gulf water conference, At Doha, Qatar
12. Droogers P, Immerzeel WW, Terink W, Hoogeveen J, Bierkens MFP, van Beek LPH, Debele B (2012) Water resources trends in Middle East and North Africa towards 2050. *Hydrol Earth Syst Sci* 16(9):3101–3114

13. [http://www.fao.org/nr/water/aquastat/countries\\_regions/SAU/index.stm](http://www.fao.org/nr/water/aquastat/countries_regions/SAU/index.stm). Accessed on 16 July 2018
14. Rambo KA, Warsinger DM, Shanbhogue SJ, Lienhard VJH, Ghoniem AF (2017) Water-energy nexus in Saudi Arabia. *Energy Procedia* 105:3837–3843. Available at <http://dx.doi.org/10.1016/j.egypro.2017.03.782>
15. Kingdom of Saudi Arabia Vision 2030 document. pp 49, 65
16. <http://saudigazette.com.sa/article/28266/ACs-use-70-of-electricity-consumption-in-Kingdom>. Accessed on 15 July 2018
17. <https://qz.com/1284239/70-of-saudi-arabias-electricity-is-used-for-air-conditioning/> Accessed on 15 July 2018
18. Alrashed F, Asif M (2014) Trends in residential energy consumption in Saudi Arabia with particular reference to the eastern province. *J Sust Dev Energy, Water Environ Syst* 2(4):376–387. Available at <http://www.sdwes.org/jsdwes/pi2014.02.0030>
19. Ercin AE, Hoekstra AY (2014) Water footprint scenarios for 2050: a global analysis. *Environ Int* 64:71–82. Available at <http://dx.doi.org/10.1016/j.envint.2013.11.019>
20. Dong H, Geng Y, Sarkis J, Fujita T, Okadera T, Xue B (2013) Regional water footprint evaluation in China: a case of Liaoning. *Sci Total Environ* 442:215–224. Available at <http://dx.doi.org/10.1016/j.scitotenv.2012.10.049>
21. Vanham D, Bidoglio G (2014) The water footprint of Milan. *Water Sci Technol* 69(4):789–795
22. <http://iopscience.iop.org/article/10.1088/1742-6596/953/1/012059/pdf> Accessed on 18 July 2018
23. <https://www.watertechonline.com/benefits-harvesting-hvac-condensate/> Accessed on 18 July 2018
24. Ardita IN, Subagia IWA (2018) The application of condensate water as an additional cooling media intermittently in condenser of a split air conditioning. *J Phys: Conf Series* 953(1):012059
25. [http://www.allianceforwaterefficiency.org/Condensate\\_Water\\_Introduction.aspx](http://www.allianceforwaterefficiency.org/Condensate_Water_Introduction.aspx) Accessed on 17 July 2018
26. Ouda OKM (2013) Review of Saudi Arabia municipal water tariff. *World Environ* 3(2):66–70
27. Almulla Y (2014) Gulf Cooperation Council (GCC) countries 2040 energy scenario for electricity generation and water desalination. pp 1–84
28. Ghaffour N, Missimer TM, Amy GL (2013) Technical review and evaluation of the economics of water desalination: current and future challenges for better water supply sustainability. *Desalination* 309(2013):197–207. Available at <http://dx.doi.org/10.1016/j.desal.2012.10.015>
29. [https://ac.els-cdn.com/S0011916412005723/1-s2.0-S0011916412005723-main.pdf?\\_tid=5709b854-516c-482d-8a3d-fdf451adb35f&acdnat=1532193501\\_d955ee2e725cbad53eb9768e73107f38](https://ac.els-cdn.com/S0011916412005723/1-s2.0-S0011916412005723-main.pdf?_tid=5709b854-516c-482d-8a3d-fdf451adb35f&acdnat=1532193501_d955ee2e725cbad53eb9768e73107f38). Accessed on 15 July 2018

# Statistical Parameters of Hydrometeorological Variables: Standard Deviation, SNR, Skewness and Kurtosis



Chetan Sharma and C. S. P. Ojha

**Abstract** Global spatial patterns of standard deviation, signal-to-noise ratio (SNR), skewness and kurtosis of eight hydrometeorological variables, i.e. potential evapotranspiration (PET), average temperature (Tavg), precipitation (Pre), maximum temperature (Tmax), minimum temperature (Tmin), wet day frequency (Wet), diurnal temperature range (DTR) and vapour pressure (Vap) are studied and discussed in this chapter. Global high resolution gridded hydrometeorological data provided by Climate Research Unit (CRU) is used. Not much variation is found in the annual values of Pre, DTR and Wet with respect to mean. High values of standard deviation in annual values of Tavg, Tmax and Tmin are found. It is found that higher variability in the dataset is generally associated with a lower mean value. Only a few regions of the world are found to be significantly skewed. About 3.5–9.5% regions of the world are found to be significantly leptokurtic for all variables except for PET for which almost all datasets are found significantly leptokurtic.

**Keywords** Standard deviation · SNR · Skewness · Kurtosis · Global patterns · Precipitation · Temperature · Vapour pressure

## 1 Introduction

The study of the climate using statistics is said climatology [24]. Historical behaviour/pattern of climatic variables may be helpful to ascertain their future behaviour. Different statistical parameters computed using historical data are often useful to check any significant change. Significant and persistent change in the mean value of climatological variables is often related to climate change [21].

---

C. Sharma (✉)  
Department of Civil Engineering, GBPIET, Pauri Garhwal, India  
e-mail: [chetan.cvl@gmail.com](mailto:chetan.cvl@gmail.com)

C. S. P. Ojha  
Department of Civil Engineering, Indian Institute of Technology Roorkee, Roorkee, India

Different tests are used to find the behaviour of time series, i.e. Mann-Kendall [9], Spearman's rho [20] and Theil-Sen slope estimator [17, 22], Mann-Whitney Pettit test [14], Cumulative-Deviation [3], etc. Trend estimation and to detect significant change in climatic variables are also done by different researchers [1, 4, 6, 7, 11, 12, 18, 19]. The researchers used synthetic series considering unit mean and standard deviation 0.1–1.0 to check the performance of different methods [2].

Studies to estimate trend and shifts in the time series are available but to find actual ranges of important statistical parameters, i.e. standard deviation, skewness and kurtosis are rare [4, 10, 23, 25, 27, 29].

The main objective of this chapter about the global patterns of important hydrometeorological variables, i.e. potential evapotranspiration (PET), average temperature (Tavg), precipitation (Pre), wet day frequency (Wet), maximum temperature (Tmax), minimum temperature (Tmin), vapour pressure (Vap) and diurnal temperature range (DTR), is to find actual values/ranges of statistical parameters, i.e. skewness and kurtosis from observed data and to find most likely values/ranges.

## 2 Study Area and Data

The study area, i.e. the world map with continents and other regions is shown in Fig. 1. Annual average/total data of eight hydrometeorological variables, i.e. potential evapotranspiration (PET), average temperature (Tavg), precipitation (Pre), wet day frequency (Wet), maximum temperature (Tmax), minimum temperature (Tmin), vapour pressure (Vap) and diurnal temperature range (DTR) for 115 years (year 1901–2015), is considered. High resolution monthly average global dataset at the grid interval of  $0.5^\circ \times 0.5^\circ$  provided by Climate Research Unit (CRU) is transformed to annual values (data available at <http://www.cru.uea.ac.uk/data>). Each dataset is pre-screened, i.e. grid points with erroneous/missing values for sufficiently longer length are not considered in the study.

## 3 Methodology

Monthly average global gridded dataset for eight hydrometeorological for 115 years (year 1901–2015) is converted to annual average values, so each grid point has 115 data points in the time series. Statistical parameter, i.e. standard deviation, SNR, skewness and kurtosis, is computed at each grid point as follows

$$\text{Standard Deviation } \sigma = \frac{1}{N} \sum_{i=1}^N (x_i - \mu)^2 \quad (1)$$



Fig. 1 World map. Source <https://www.worldatlas.com/aatlas/image.htm>

The reciprocal of coefficient of variation is called signal-to-noise ratio [16]. SNR shows how much data varies per unit standard deviation.

$$\text{Signal-to-noise ratio SNR} = \frac{1}{CV} = \frac{\mu}{\sigma} \tag{2}$$

Here,  $x_i, i = 1, 2 \dots N$  is the data values.  $\mu, CV$  are mean and coefficient of variation.

Skewness is the property which shows the symmetry of probability distribution and it is given as follows

$$\text{Skew} = \frac{N}{(N - 1)(N - 2)} \sum_{i=1}^N \left( \frac{x_i - \mu}{\sigma} \right)^3 \tag{3}$$

Skewness of normal distribution is 0, as it is symmetrical. Left (negative) skewness shows more data on left tail of the probability distribution, while right (positive) skewness shows more data on right side of the probability distribution.

Kurtosis is a measure to show the relative tailedness of the probability distribution than normal distribution. The kurtosis is given as

$$\text{Kurt} = \frac{N(N + 1)}{(N - 1)(N - 2)(N - 3)} \sum_{i=1}^n \left( \frac{x_i - \mu}{\sigma} \right)^4 - \frac{3(N - 1)^2}{(N - 2)(N - 3)} \tag{4}$$

The kurtosis of normal distribution is 0. A value less than zero is called platykurtic and shows that there are fewer and less extreme values. While the distribution having positive value of kurtosis is called leptokurtic and shows higher outliers than normal distribution.



## 4 Results and Discussions

### 4.1 *Spatial Patterns of Standard Deviation*

Global spatial patterns of standard deviation are shown in Fig. 2. There is not much variation found in the annual average PET across the globe. Almost 94% of regions show standard deviation up to 66 mm/annum. Similarly, not much variation is found in average temperature in all land areas. Around 88% dataset show 1.2 °C or lesser standard deviation. Northern hemisphere shows a little higher standard deviation than Southern hemisphere. Variation in precipitation shows similar patterns with the mean for most of the regions, i.e. regions which show higher precipitation have higher inter-annual variability and vice versa. Regions near Arctic Circle in Eastern South America and Some regions of South-East Asia show the highest variability in annual wet day frequency. Maximum and minimum temperature exhibits similar patterns of annual variability with average temperature. Mix pattern of annual variability of DTR is found on a global scale. Most of the regions of North America and Australia show the highest variability in DTR (0.85–1.71 °C). Some regions of India, South-East Asia and Eastern Africa show little variability in DTR. A small variation in spatial patterns of annual variation of vapour pressure is found. Madagascar (Africa) and Uruguay, Columbia and Venezuela (America) show highest ranges of standard deviation in Vap.

### 4.2 *Spatial Patterns of SNR*

SNR shows the variability of data around the mean, i.e. SNR values close to unity indicates that standard deviation is almost equal to mean value and SNR values significantly higher or lower than unity shows lesser variability with respect to mean.

Global spatial patterns of SNR for all variables are shown in Fig. 3. SNR pattern for PET shows that regions with lesser mean PET have higher variability with respect to mean than the region with higher average PET, for example, most of the regions North to Tropic of Cancer have relatively lower mean and SNR values are up to 10. Western coastal regions of India, Middle East, Western Africa and Eastern South America having a higher mean of PET and SNR values are also high, which show lesser variability with respect to mean. Average temperature showing similar patterns of SNR with PET that is higher mean is followed by lesser inter-annual variability and vice versa except for the regions of extremely low average temperatures, i.e. North to Arctic Circle, Higher Himalayas and Northern China. High variability is found in the precipitation data with respect to mean for most of the regions. Almost 96% data shows SNR value up to 10. SNR pattern for precipitation also shows higher variability with lower precipitation and vice versa. There is not much variability found in the wet day frequency data with respect to mean. Almost 77% regions show SNR value in the range of 6–15. It also shows higher variability associated with lower

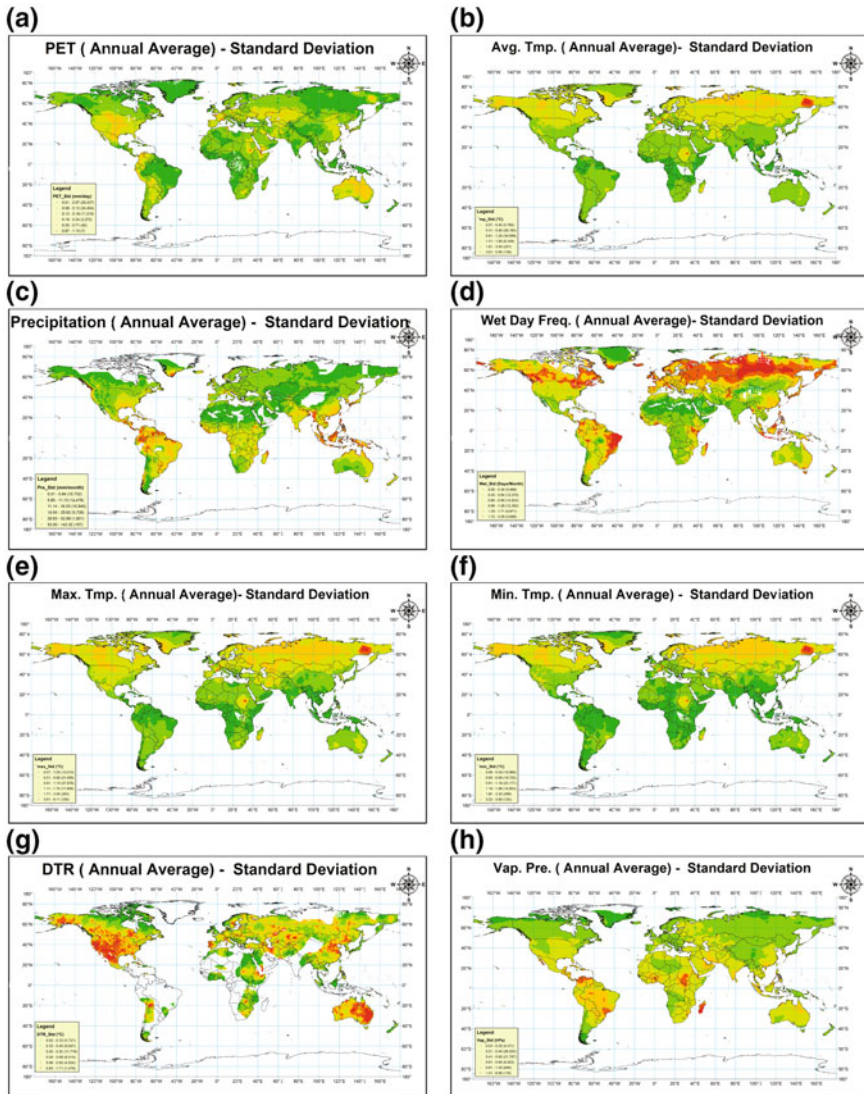


**Fig. 2** Global spatial patterns of standard deviation. Global spatial variation of the long-term annual average of: **a** potential evapotranspiration, **b** average temperature, **c** precipitation, **d** wet day frequency, **e** maximum temperature, **f** minimum temperature, **g** diurnal temperature range and **h** vapour pressure. Variation of lower to higher values is shown by variation from Green colour to Red colour. Unavailable or erroneous data is not used in the study and left blank on the map. A number of datasets in the corresponding range are given in bracket in legend

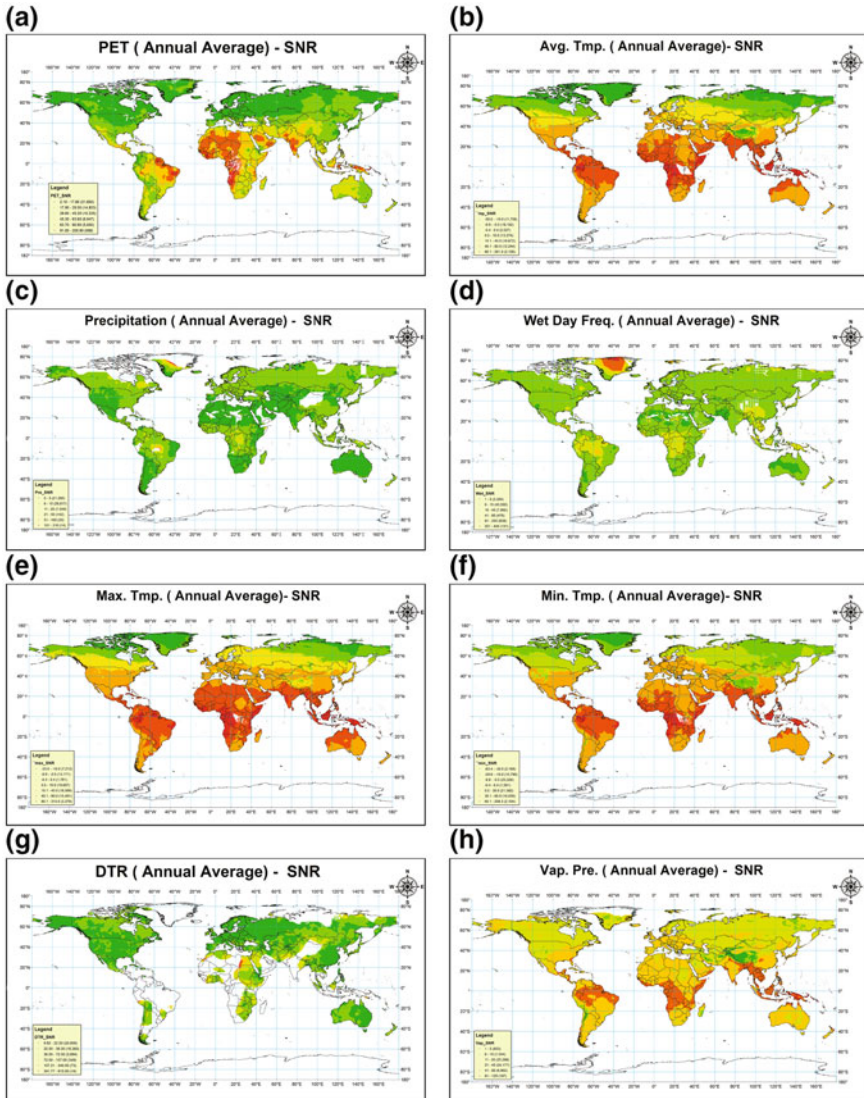


Fig. 3 Global spatial patterns of SNR. Figure labels and symbology are same as Fig. 2



mean and vice versa. SNR values of maximum and minimum temperature data show similar patterns with average temperature. There is not much variability associated with mean in DTR. All datasets showed SNR value more than 7. Mix patterns in the variability with mean in found in DTR, as for some regions SNR value is found to be low with lower mean and for some, it was found high. Low inter-annual variability with mean in vapour pressure data is found. Almost 98% region has SNR values more than 11. For most of the regions lower variability is found to be associated with higher average vapour pressure. For some regions, i.e. higher Himalaya and Southern China, high variability is found with low average vapour pressure.

### 4.3 Spatial Patterns of Skewness

Positive skewness shows a higher concentration of data towards lower values or left to the mean and negative skewness shows a higher concentration of data to the right. Skewness values in the range of  $-2$  to  $+2$  are generally acceptable [8]. The global spatial patterns of skewness for all variables are shown in Fig. 4.

PET datasets are found to be less skewed as more than 98% of dataset showed skewness in the range of  $-2$  to  $2$ . Higher positive skewness is found in some regions of Eastern Russia near Arctic Circle and Madagascar. Average temperature data is found to be less skewed for most of the world. The skewness for more than 99% dataset is found to be in the range of  $-2$  to  $2$ . Some regions of Eastern Russia and Madagascar are found to be having high positive skewness ( $>2$ ). More than 97% of precipitation datasets are found to be little skewed (skewness  $-2$  to  $2$ ). Some area of Myanmar shows high negative skewness ( $<-2$ ) which shows a higher frequency of small range of high annual precipitation. Some regions of Sahara (Africa) and Western South America showed higher positive skewness ( $>2$ ) which indicates higher frequency of low precipitation range. More than 99% dataset of wet day frequency is found to be insignificantly skewed (skewness  $-2$  to  $2$ ). Higher positive skewness ( $>2$ ) is found in some regions of Sahara (Africa). Similar patterns of skewness are found in maximum and minimum temperature with average temperature. All regions did not show significant skewness in DTR (skewness in the range of  $-2$  to  $2$ ). Most of the vapour pressure data ( $>98%$ ) are also found to be insignificantly skewed (skewness  $-2$  to  $2$ ). High positive skewness ( $>2$ ) is found in Madagascar. High negative skewness ( $<-2$ ) is found in some regions of north-eastern Russia.

### 4.4 Spatial Patterns of Kurtosis

Kurtosis defines the relative peakedness/flatness of the data relative to normal distribution. More precisely, it gets the idea of heaviness or lightness of tail. Kurtosis virtually does not say anything about the peak. Positive values of kurtosis (leptokurtic) show that the data is having heavier tails and negative values (platykurtic) show

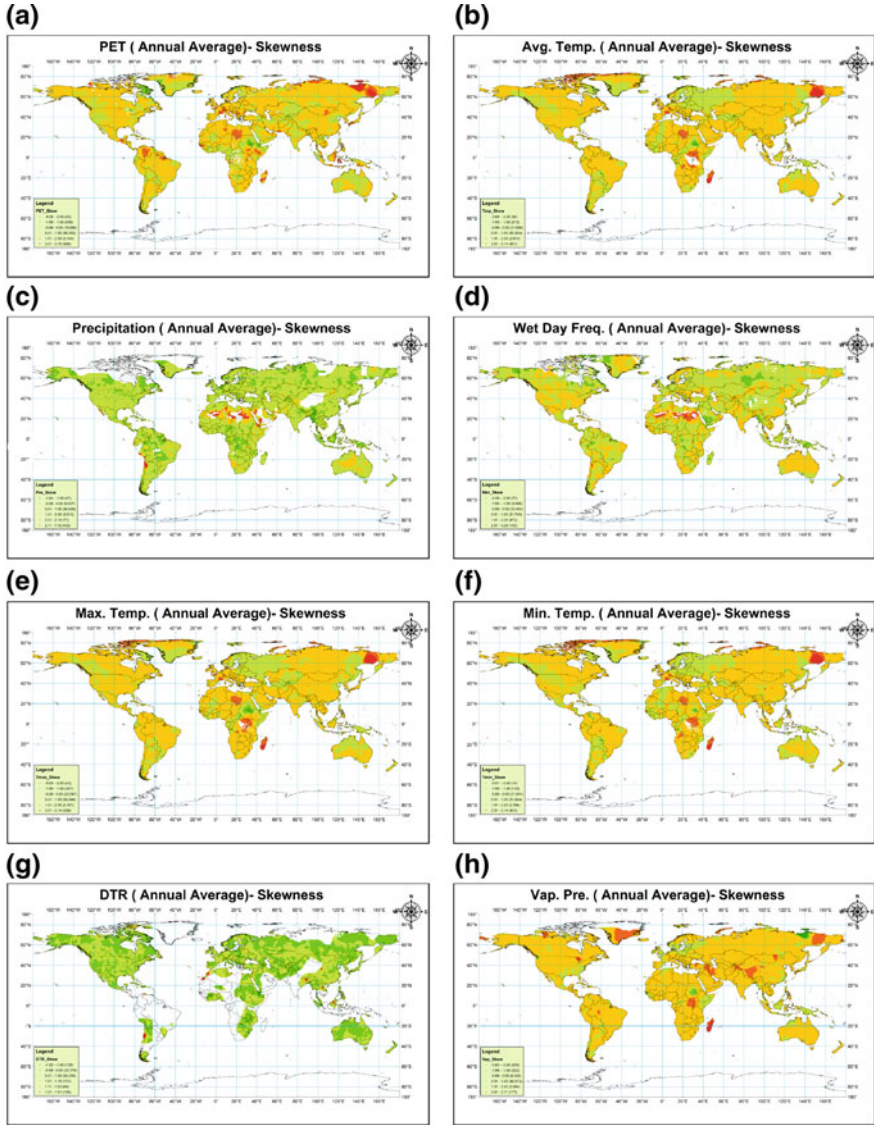
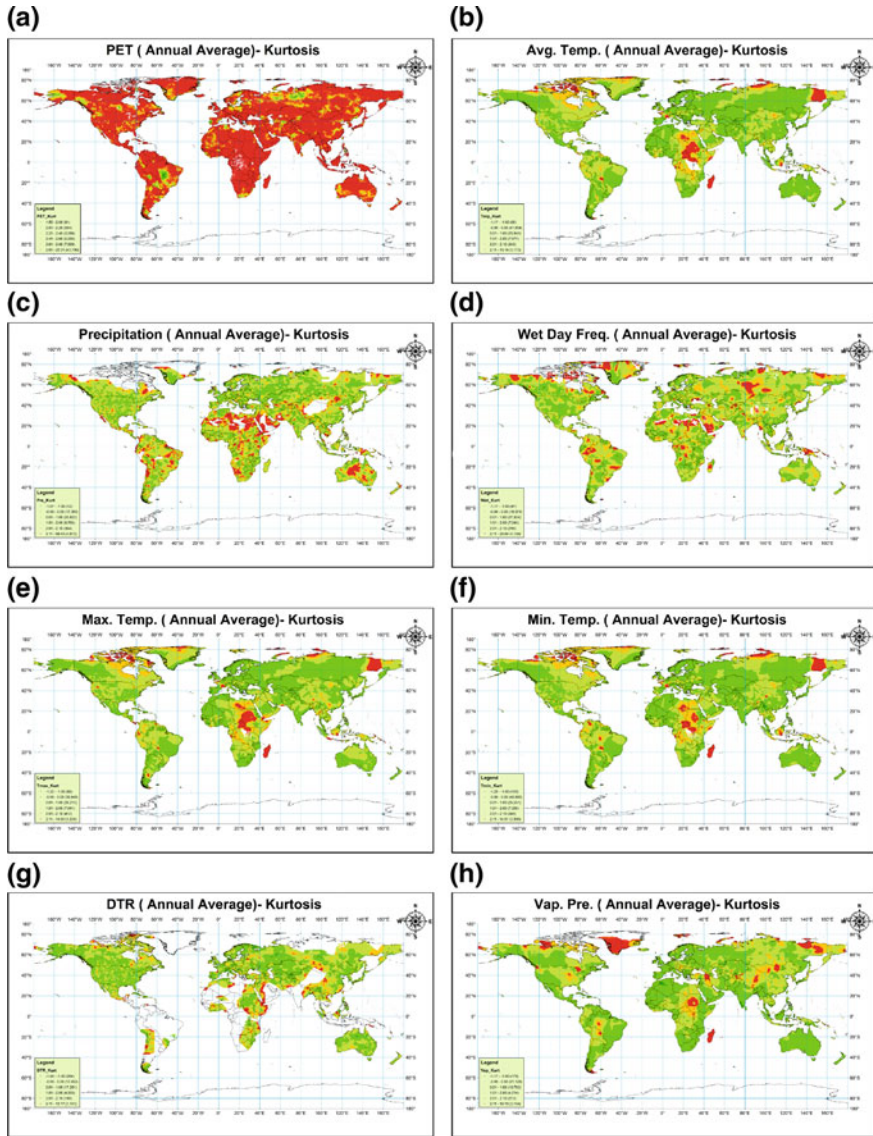


Fig. 4 Global spatial patterns of skewness. Figure labels and symbology are same as Fig. 2



**Fig. 5** Spatial patterns of kurtosis for different variables. Figure labels and symbology are same as Fig. 2

thinner tails. Kurtosis value in the range of  $-2$  to  $+2$  is generally acceptable to prove normal univariate distribution [8]. Global spatial patterns of kurtosis are shown in Fig. 5.

No negative kurtosis is found for PET. More than 99% of the dataset is having the kurtosis more than 2.0, which indicates high frequency of both low and high

PET in the whole world. More than 95% of average temperature data is found to be having insignificant kurtosis ( $-2$  to  $2$ ). Some regions of Northern and Eastern Russia, Madagascar and Middle Africa have kurtosis of more than  $2$ . Most of the ( $>90\%$ ) precipitation data is not found to be having significant kurtosis ( $<-2$  or  $>2$ ). Some regions of Sahara, Middle East and Middle Australia are found to be having higher positive kurtosis ( $>2$ ). For only 9% regions of the world, wet day frequency data shows significant positive kurtosis ( $>2$ ), for example, some regions of Southern Russia, Sahara (Africa), Southern Middle East and Middle South America. Maximum and minimum temperatures are found to be having a similar pattern with average temperature. Almost all regions are found to be in the range of  $-2$  to  $+2$  except for some regions of Eastern Africa and the Middle East, where it is found to be leptokurtic. Vapour pressure data for Madagascar, Middle Africa, Eastern Russia and Southern Greenland is found to be leptokurtic. Remaining regions of the world (around 94%) show kurtosis in the range of  $-2$  to  $+2$ .

## 5 Summary and Conclusions

Global spatial patterns of different statistical parameters, i.e. skewness and kurtosis for eight hydrometeorological variables, i.e. potential evapotranspiration (PET), average temperature (Tavg), precipitation (Pre), wet day frequency (Wet), maximum temperature (Tmax), minimum temperature (Tmin), vapour pressure (Vap) and diurnal temperature range (DTR), are presented in this chapter. Climate Research Unit (CRU) data for 115 years (1901–2015) is used for this purpose.

SNR data directly relates variation in data value with respect to mean. SNR results show that most of the PET, DTR and Vap data are found in the range of 15–120. SNR value of up to 15 is found for more than 99% Pre (precipitation) data. DTR data is also mostly found to have SNR value up to 15. It was seen that mostly higher variability is associated with datasets having lower means.

Only few of data is found to be significantly negatively skewed (skewness  $<-2$ ) and on an average 0.6% data is found to be significantly positively skewed (skewness  $>2$ ). Significant positive skewness for PET, Tavg, Tmax, Tmin and Vap is found in some regions of Eastern Russia and Madagascar, while for Pre-data and Wet data in some regions of Sahara (Africa) and Western North America.

None of the data is found to be significantly platykurtic (kurtosis  $<2$ ). PET is found to be significantly leptokurtic (kurtosis  $>2$ ) for almost whole world. About 5–6.5% datasets of other variables show leptokurtic nature. Tavg, Tmax, Tmin and Vap data in some regions of Eastern and Northern Russia, Madagascar, Central Africa, Northern Canada and Greenland are found to be significantly leptokurtic. Pre-data in some regions of Africa, Middle East, South America, Canada and Middle Australia, Wet data in some regions of Russia, Indonesia, Sahara, Madagascar, Middle East, South America, Canada and Greenland and DTR data in some regions of Middle East, East-

ern Africa, Mongolia, Central China and Eastern India are found to be significantly leptokurtic.

## References

1. Arora H, Sharma C, Ojha CSP et al (2015) Spatio-temporal trend analysis of hydro-meteorological variables over Ganga Basin: a comparison between CMIP3 and CMIP5 Data. In: Hydro-2015 International. Roorkee
2. Bayazit M, Onoz B (2008) To prewhiten or not to prewhiten in trend analysis? *Hydrol Sci J* 52:611–624. <https://doi.org/10.1623/hysj.53.3.669>
3. Buishand TA (1982) Some methods for testing the homogeneity of rainfall records. *J Hydrol* 58:11–27. [https://doi.org/10.1016/0022-1694\(82\)90066-X](https://doi.org/10.1016/0022-1694(82)90066-X)
4. Choi G, Collins D, Ren G et al (2009) Changes in means and extreme events of temperature and precipitation in the Asia-Pacific network region, 1955–2007. *Int J Climatol* 29:1906–1925. <https://doi.org/10.1002/joc.1979>
5. Donat MG, Alexander LV (2012) The shifting probability distribution of global daytime and night-time temperatures. *Geophys Res Lett* 39. <https://doi.org/10.1029/2012gl052459>
6. Duhan D, Pandey A (2013) Statistical analysis of long term spatial and temporal trends of precipitation during 1901–2002 at Madhya Pradesh, India. *Atmos Res* 122:136–149. <https://doi.org/10.1016/j.atmosres.2012.10.010>
7. Goswami BN, Venugopal V, Sengupta D et al (2006) Increasing trend of extreme rain events over India in a warming environment. *Science* 314:1442–1445. <https://doi.org/10.1126/science.1132027>
8. Gravetter FJ, Wallnau LB (2011) Essentials of statistics for the behavioral sciences. Wadsworth Cengage Learning
9. Kendall MG (1975) Rank correlation methods, 4th edn. Charles Griffin, London
10. Manatsa D, Morioka Y, Behera SK et al (2015) Linking the southern annular mode to the diurnal temperature range shifts over southern Africa. *Int J Climatol* 35:4220–4236. <https://doi.org/10.1002/joc.4281>
11. Milly PCD, Dunne KA, Vecchia AV (2005) Global pattern of trends in streamflow and water availability in a changing climate. *Nature* 438:347–350. <https://doi.org/10.1038/nature04312>
12. Modarres R, Sarhadi A (2009) Rainfall trends analysis of Iran in the last half of the twentieth century. *J Geophys Res Atmos* 114:1–9. <https://doi.org/10.1029/2008JD010707>
13. Onoz B, Bayazit M (2003) The power of statistical tests for trend detection. *Turkish J Eng Environ Sci* 27:247–251
14. Pettitt AN (1979) A non-parametric approach to the change-point problem. *J R Stat Soc Ser C (Appl Stat)* 28:126–135
15. Sang YF, Wang Z, Liu C (2014) Comparison of the MK test and EMD method for trend identification in hydrological time series. *J Hydrol* 510:293–298. <https://doi.org/10.1016/j.jhydrol.2013.12.039>
16. Schroeder DJ (2015) *Astronomical optics*. Academic Press
17. Sen PK (1968) Estimates of the regression coefficient based on Kendall's Tau. *J Am Stat Assoc* 57:269–306
18. Sharma C, Arora H, Ojha CSP (2015) Assessment of the effect of climate change on historical and future rainfall in Uttarakhand. In: Hydro-2015 International, Roorkee
19. Sharma C, Ojha CSP (2018) Climate change detection in Upper Ganga River Basin. In: International conference on sustainable technologies for intelligent water management, Roorkee
20. Sneyers R (1991) On the statistical analysis of series of observations. In: WMO Tech. Note. World Meteorological Organisation, Geneva, pp 143–145

21. Stocker TF, Qin D, Plattner GK et al (2013) IPCC, 2013: climate change 2013: the physical science basis. Contribution of working group I to the fifth assessment report of the intergovernmental panel on climate change. Cambridge University Press, Cambridge, United Kingdom and New York, NY, USA
22. Theil H (1950) A rank-invariant method of linear and polynomial regression analysis, I. In: Proceedings of the Koninklijke Nederlandse Academie van Wetenschappen. Springer Netherlands, pp 386–392
23. Van Der Schrier G, Barichivich J, Briffa KR, Jones PD (2013) A scPDSI-based global data set of dry and wet spells for 1901–2009. *J Geophys Res Atmos* 118:4025–4048. <https://doi.org/10.1002/jgrd.50355>
24. Von Storch H, Zwiers FW (2001) Statistical analysis in climate research. Cambridge University Press
25. Wang F, Zhang C, Peng Y, Zhou H (2014) Diurnal temperature range variation and its causes in a semiarid region from 1957 to 2006. *Int J Climatol* 34:343–354. <https://doi.org/10.1002/joc.3690>
26. Xie H, Li D, Xiong L (2014) Exploring the ability of the Pettitt method for detecting change point by Monte Carlo simulation. *Stoch Environ Res Risk Assess* 28:1643–1655. <https://doi.org/10.1007/s00477-013-0814-y>
27. Ye H, Fetzer EJ (2010) Atmospheric moisture content associated with surface air temperatures over northern Eurasia. *Int J Climatol* 30:1463–1471. <https://doi.org/10.1002/joc.1991>
28. Yue S, Pilon P, Cavadias G (2002) Power of the Mann-Kendall and Spearman's rho tests for detecting monotonic trends in hydrological series. *J Hydrol* 259:254–271. [https://doi.org/10.1016/S0022-1694\(01\)00594-7](https://doi.org/10.1016/S0022-1694(01)00594-7)
29. Zhou L, Dai A, Dai Y et al (2009) Spatial dependence of diurnal temperature range trends on precipitation from 1950 to 2004. *Clim Dyn* 32:429–440. <https://doi.org/10.1007/s00382-008-0387-5>

# A New Approach to Analyze the Water Surface Profile Over the Trench Weir



Swati Bhave and Sanjeev Kumar

**Abstract** To divert water from streams containing streams for its usage in different purposes like irrigation, hydropower, water supply, etc., the most appropriate kind of weir is trench weir. It involves a trench constructed transversely at the streams, underneath of its bed level. The uppermost level of this trench is roofed with bottom rack bars to avoid the incoming of sediment into the trench. Bottom rack is kept porous, so when water flows above it, a part of it moves into the trench and get collected to an intake well. This kind of weir has certain benefits as it does not disturb much the flow of the river. Because of the fact that it is constructed below the river bed, the sediment of size less than the spacing of the rack bars moves into the trench. As a result, post-monsoon cleaning of the trench is mandatory. Design of sidewalls and size of the trench requires water surface profiles over the bottom racks. This paper deals with a new approach to analyze the water surface profile over the bottom rack. The equation proposed has been and compared with the observed water surface profile. By using proposed equation, water surface profile was computed and it was found comparable to the observed ones and also the proposed equation is more suitable to compute water surface profile above the bottom rack for various slope of rack.

**Keywords** Boulder stream · Discharge · Rack · Trench weir · Water surface profile

## 1 Introduction

Normal kinds of elevated-crest weirs are unsuitable for Boulder Rivers. If raised-crest weir is built transversely the river, the increase in water level at the upstream side of the weir may create significant fluctuations in the flow of the stream. The residues get settled down at the upstream side of the crest as a consequence of this opening

---

S. Bhave (✉) · S. Kumar  
Department of Civil Engineering, Indian Institute of Technology, Roorkee, India  
e-mail: [swatibhave19@gmail.com](mailto:swatibhave19@gmail.com)

© Springer Nature Singapore Pte Ltd. 2020  
R. AlKhaddar et al. (eds.), *Advances in Water Resources Engineering and Management*, Lecture Notes in Civil Engineering 39,  
[https://doi.org/10.1007/978-981-13-8181-2\\_6](https://doi.org/10.1007/978-981-13-8181-2_6)

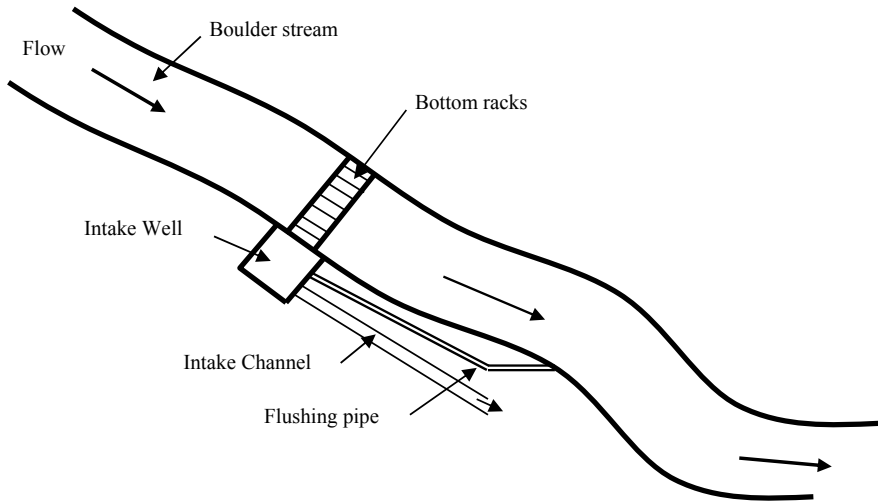


Fig. 1 Sketch of a trench weir

of the bottom racks and get certainly choked up. Erosion arises at the downstream side of weir, and as a result, cracks develop in the weir.

To deal with the problems linked with elevated-crest weirs, the utmost suitable weir implemented in Boulder Rivers for irrigation, hydropower generation, etc., is trench weir. Trench weir as in Fig. 1 shows the different entities of it, and photograph of a constructed trench weir is given in Fig. 2.

It is basically a ditch constructed transversely at the river underneath its bed or at the raised up bed. In ancient practices, the trench was constructed on the raised up

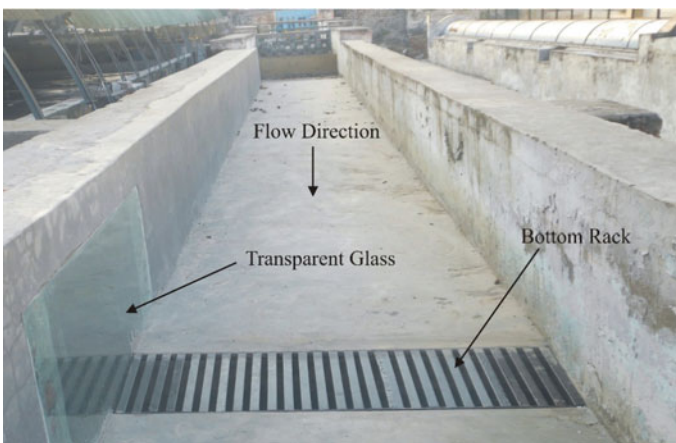


Fig. 2 Photograph of trench weir



bed. Such, elevated weir has similar difficulties, which are present in the raised-crest weir and therefore not practiced nowadays. On the basis of this observation and the knowledge obtained till now, the top of the trench is kept on the level of bed of stream.

The uppermost level of weir is covered using bottom rack. Since, bottom rack is porous entity, therefore, when water flows over the bottom rack, it moves in the trench and gets accumulated in an intake well, which is further connected to the trench. The bottom racks bars can be constructed using rounded steel bars or flats bars or T-shape bars and positioned lengthwise along the river flow at the bed level. The bottom racks are designed to transport heavy boulders that are possible to move down during the time of extreme flood. Trench weir gives a benefit that it does not disturb the bed level of the stream.

Water surface profile (WSP) is important and plays a vital role to design the sidewalls and size of trench. The type of flow above the trench weir is spatially varied flow (SVF) with decreasing discharge. Therefore, by solving the equation of spatially varied flow to obtained the WSP. Dimension of the adjacent walls of the trench weir is decided on the base of WSP. By assuming specific energy constant above the bottom rack, Mostkow [1] analyzed the flow above longitudinal bottom rack of circular bars and proposed a relationship for diverted discharge ( $Q_d$ ) into the trench is given below. Paudyala and Twatchai [2] suggested that any structural component that stand out of the bed of river damages easily by the rolling large sediment particles. Ahmad and Mittal [3] suggested that effective length of bottom rack can be obtained when diverted discharge is equal to incoming discharge. Brunella et al. [4] conducted experiments for rounded bars and proposed a relationship to calculate the discharge coefficient. Ghosh and Ahmad [5] found that the value of coefficient of discharge is lower for flat bars as compared to rounded bars. Kuntzman and Bouvard [6] on bottom rack intake. Kumar et al. [7] conducted experiments for flat bars and identified the effect of various parameters on coefficient of discharge. Naghavi and Maghrebi [8] proposed an empirical formulation to calculate coefficient of discharge. Nosed [9] by assuming critical approach flow condition, over longitudinal bars and suggested a design chart for diverted flow. Righetti and Lanzoni [10] conducted experiments for rectangular bar and found that diverted discharge decreases along longitudinal direction.

$$Q_d = C_d \varepsilon B L_w \sqrt{2gE} \quad (1)$$

where  $\varepsilon$  = porosity of rack;  $B$  = width of the rack (across the main channel);  $L_w$  = wetted length of bottom racks;  $g$  = acceleration due to gravity;  $E$  = specific energy at approach; and  $C_d$  = discharge coefficient.

## 2 Experimental Setup

Experimentations were conducted in a rectangular channel as shown in Fig. 3, of 1 m wide, 0.64 m deep and 17 m long. Water was supplied from an overhead tank

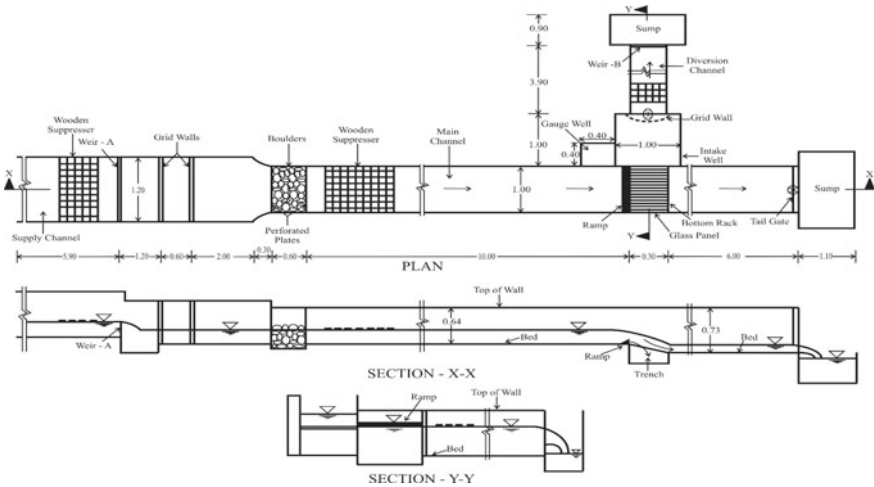


**Fig. 3** Layout of experimental setup

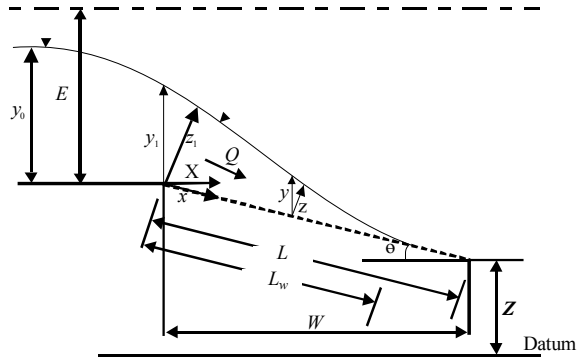
to the main channel fixed with sharp crested rectangular Weir-A, whose height was 10.5 cm and 75 cm in length provided in the channel of width 75 cm. A trench was built across the bed of the main channel 1 m wide, 0.3 m long and 0.43 m deep and a ramp was placed before the trench weir on the upstream side of the main channel; its corner was rounded to provide a smooth transition from the horizontal upstream to the sloping downstream. The trench at its left-hand side connected to a well which is used to store diverted water, whose length is 1 m, width is 1 m and depth is 0.9 m and intake well is further opened to a diversion channel of length = 3.9 m, width = 0.3 m and depth = 0.72 m. A weir (Weir-B) was constructed across the diversion channel, which is used to obtain the diverted discharge into the trench. Also, wooden suppressors were provided to minimize the surface disturbance in both main channel and diverted channel. Weir-A and Weir-B were calibrated by using a magnetic flow meter fitted in the main supply pipe and Pitot tube, respectively.

### 3 Present Approach for the Computation of Water Surface Profile

Flow above the bottom rack is spatially varied flow (SVF) with decreasing discharge. Therefore, equation of the SVF can be solved to obtain water surface profile above the rack. Dimensions of the sidewalls of the trench weir are decided according to water surface profile above the rack. The flow in a rectangular channel with a bottom rack is shown in Fig. 4.



**Fig. 4** Flow surface profile over a rack



Considering Fig. 5, specific energy equation at any section can be written as:

$$E = y \cos^2 \theta + \frac{Q^2}{A^2 \times 2g} \tag{2}$$

Here,  $y$  = depth of flow normal to the surface of datum at any section,  $\theta$  = slope of rack,  $V$  = velocity of flow at approach,  $Q$  = discharge at main channel and  $A$  = Flow area.

Now,  $y \cos \theta = z$

$z$  = depth of flow normal to the bottom rack at any section.

Differentiating both side w.r.t  $x$ , we get

$$\frac{dE}{dx} = \frac{d}{dx}(z \cos \theta) + \frac{d}{dx} \left( \frac{Q^2}{B^2 \times z^2 \times 2g} \right) \tag{3}$$

$$\frac{dE}{dx} = \cos \theta \frac{dz}{dx} + \frac{1}{B^2 \times 2g} \frac{d}{dx} \left( \frac{Q^2}{z^2} \right) \tag{4}$$

$$\frac{dE}{dx} = \cos \theta \frac{dz}{dx} + \frac{Q}{B^2 \times g \times z^2} \left( \frac{dQ}{dx} \right) - \frac{Q^2}{B^2 \times g \times z^3} \left( \frac{dz}{dx} \right) = 0 \tag{5}$$

$$\left( \cos \theta - \frac{Q^2}{B^2 g z^3} \right) \frac{dz}{dx} = \frac{Q}{B^2 z^2 g} \left( \frac{-dQ}{dx} \right) \tag{6}$$

From Mostkow equation (i.e., Eq. 1)

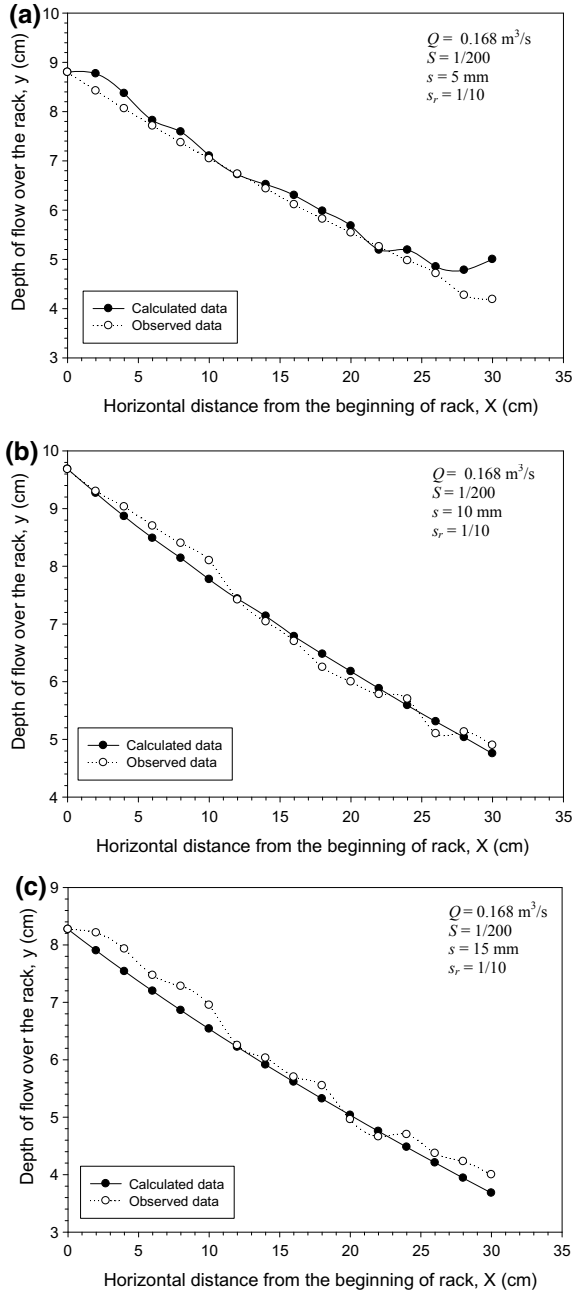
$$\left( \frac{-dQ}{dx} \right) = C_d \varepsilon B \sqrt{2gE}$$

and  $Q = By\sqrt{2g(E - y)}$

Putting values of  $-dQ/dx$  and  $Q$  in Eq. (6), we have



**Fig. 5** Comparison between observed and computed water surface profile using Eq. (20) for various spacing of rack **a**  $s = 5$  mm, **b**  $s = 10$  mm and **c**  $s = 15$  mm



$$\begin{aligned}
\left[ \cos \theta - \frac{B^2 z^2 \times 2g(E - z \cos \theta)}{B^2 g z^3} \right] \frac{dz}{dx} &= \frac{Bz \sqrt{2g(E - z \cos \theta)}}{g B^2 z^2} \times C_d \varepsilon B \sqrt{2gE} \\
\left[ \cos \theta - \frac{2(E - z \cos \theta)}{z} \right] \frac{dz}{dx} &= \frac{2\sqrt{E(E - z \cos \theta)}}{z} \times C_d \varepsilon \\
\frac{dz}{dx} &= \frac{2\sqrt{E(E - z \cos \theta)} \times C_d \varepsilon}{z \cos \theta - 2(E - z \cos \theta)} \\
\frac{dx}{dz} &= \frac{z \cos \theta - 2(E - z \cos \theta)}{2\sqrt{E(E - z \cos \theta)} \times C_d \varepsilon} \\
\int_0^x dx &= \frac{1}{2C_d \varepsilon} \int \frac{3z \cos \theta - 2E}{\sqrt{E(E - z \cos \theta)}} dz \\
x &= \frac{1}{2C_d \varepsilon} \left[ \int \frac{3z \cos \theta}{E \sqrt{1 - \frac{z \cos \theta}{E}}} dz - \int \frac{2}{E \sqrt{1 - \frac{z \cos \theta}{E}}} dz \right] \quad (7)
\end{aligned}$$

Let  $\frac{z \cos \theta}{E} = u$ , and hence,  $dz = E \frac{du}{\cos \theta}$ , so from Eq. (7)

$$x = \frac{1}{2C_d \varepsilon} \left[ 3 \int \frac{u}{\sqrt{1-u} \cos \theta} du - 2 \int \frac{1}{\sqrt{1-u} \cos \theta} du \right] \quad (8)$$

Let  $1-u = v$ . Hence,  $du = -dv$ , now from Eq. (8)

$$\begin{aligned}
x &= \frac{1}{2C_d \varepsilon} \left[ \frac{-3E}{\cos \theta} \int \frac{1-v}{\sqrt{v}} dv + \frac{2E}{\cos \theta} \int \frac{1}{\sqrt{v}} dv \right] \\
x &= \frac{1}{2C_d \varepsilon} \left[ \frac{-3E}{\cos \theta} \int \left( \frac{1}{\sqrt{v}} - \sqrt{v} \right) dv + \frac{2E}{\cos \theta} \int \frac{1}{\sqrt{v}} dv \right] \\
x &= \frac{1}{2C_d \varepsilon} \left[ \frac{-3E}{\cos \theta} \left( 2v^{1/2} - \frac{2v^{3/2}}{3} \right) + \frac{2E}{\cos \theta} \times 2v^{1/2} \right] \\
x &= \frac{2Ev^{1/2}}{\cos \theta} [-3 + v + 2] \times \frac{1}{2C_d \varepsilon} \\
x &= \frac{2E}{\cos \theta} (-u) \times (1-u)^{1/2} \times \frac{1}{2C_d \varepsilon} \\
x &= \frac{-E}{C_d \varepsilon \cos \theta} \left( 1 - \frac{z \cos \theta}{E} \right)^{1/2} \times \frac{z \cos \theta}{E} + C \quad (9)
\end{aligned}$$

At  $x = 0$ ,  $z = z_1$

$$\frac{-E}{C_d \varepsilon \cos \theta} \left[ 1 - \frac{z_1 \cos \theta}{E} \right]^{1/2} \times \frac{z_1 \cos \theta}{E} + C = 0$$

$$C = \frac{E}{C_d \varepsilon \cos \theta} \left[ 1 - \frac{z_1 \cos \theta}{E} \right]^{1/2} \times \frac{z_1 \cos \theta}{E} \quad (10)$$

Putting value of  $C$  from Eq. (9) in Eq. (10), we get

$$x = \frac{E}{c_d \varepsilon} \left[ \frac{z_1}{E} \times \left( 1 - \frac{z_1 \cos \theta}{E} \right)^{1/2} - \frac{z}{E} \times \left( 1 - \frac{z \cos \theta}{E} \right)^{1/2} \right] \quad (11)$$

Equation (11) can be used to obtain water surface profile over racks. Water surface profile computed using Eq. (11) for different sets of data is compared with the observed ones. Such computed and observed water surface profiles for five sets of data are shown in Fig. 5a–c for different spacing of racks.

Equation (11) These figures depict that the comparisons between computed and computed water surface profile give the satisfactory results. Thus, Eq. (11) can be used to obtain water surface profile above the bottom racks. Attempt has also been made to compare the proposed equation with an existing equation derived by using Mostkow equation.

## 4 Conclusion

The present study was aimed to develop a new approach intended for the computation of water surface profile above the bottom rack so that one can design the sidewalls of trench weir, because size of trench is fixed on the basis of water surface profile. Water surface profile is computed using proposed equation and compared with the observed one and found that computed water surface profile is comparable to the observed one.

## References

1. Mostkow MA (1957) A theoretical study of bottom type water intake. *La Houille Blanche* 4:570–580
2. Paudyal GN, Twachai T (1987) Design of a bottom intake structure for mountain streams. *International symposium on design of hydraulic structures*. Fort Collins, Colo., USA, pp 73–82
3. Ahmad Z, Mittal MK (2004) Hydraulic design of trench weir on Dabka River—a case study. *Water Energy Int CBI* 60(4):28–37
4. Brunella S, Hager WH, Minor HE (2003) Hydraulics of bottom rack intake. *ASCE J Hydraul Eng* 129(1):2–10
5. Ghosh S, Ahmad Z (2006) Characteristics of flow over bottom racks. *Water Energy Int CBIP* 63(2):47–55
6. Kuntzmann J, Bouvard M (1954) Theoretical studies of bottom type water intake grids. *La Houille Blanche* 9(9/10):569–574
7. Kumar S, Ahmad Z, Kotheyari UC, Mittal MK (2010) Discharge characteristics of a trench weir. *ELSEVIER J Flow Meas Instrum* 21:80–87

8. Naghavi B, Maghrebi MF (2010) Experimental study of sediment flow discharge in new system of bottom intakes with porous media. Springer J Transp Porous Media 85:867–884
9. Nosedá G (1956) Operation and design of bottom intake racks. In: Proceedings of 6th general meeting, IAHR, vol 3(17), pp 1–11
10. Righetti M, Lanzoni S (2008) Experimental study of the flow field over bottom intake racks. ASCE J Hydraul Eng 134(1):15–22
11. French RH (1994) Open-channel hydraulics. McGraw-Hill Publishing Company Limited, New Delhi

# Soil Loss Assessment in Imphal River Watershed, Manipur, North-East India: A Spatio-Temporal Approach



Loukrakpam Chandramani and Bakimchandra Oinam

**Abstract** Land and water resources are vital resources. Whenever these resources are under stress and pressure which may be natural or anthropogenic, heavy loss is incurred. Soil loss is one of such significant environmental problems. Various models such as USLE, RUSLE, USPED and LISEM are developed for rapid assessment of soil loss. Assessment of soil loss is considered as a significant, as it leads to loss of top layers of soil and thus reduces the fertility and quality of the soil, which eventually leads to soil degradation and thus affects the sustainability of the inhabitants. Soil loss in the Imphal River watershed, of Manipur, a north-eastern state of India, is assessed using RUSLE for the time period of 2006 and 2017. The rate of soil loss is classified on the basis of classification by NBSS&LUP, India. Positive changes in the spatial extent is observed in 'No Erosion' and 'Extreme' and Negative changes are observed in 'Slight'; 'Moderate' and 'High' class of erosions. The area under 'No Erosion' is increased by 13.64 and 5.57% in the 'Extreme' class of erosion from 2006 to 2017. Land use of the study area also significantly affects the rate of soil loss.

**Keywords** Soil loss/soil erosion · RUSLE · USPED · NBSS&LUP

## 1 Introduction

Out of the most vital natural resources which are present in our environment, land and water are the most significant resources. These resources are under tremendous stress due to ever-increasing human pressure. Sustainable development can be achieved only when available resource is managed optimally with minimum impact

---

L. Chandramani (✉) · B. Oinam  
Department of Civil Engineering, National Institute of Technology, Manipur,  
Imphal West 795001, Manipur, India  
e-mail: [chandramani106@gmail.com](mailto:chandramani106@gmail.com)

B. Oinam  
e-mail: [bakim143@gmail.com](mailto:bakim143@gmail.com)

© Springer Nature Singapore Pte Ltd. 2020  
R. AlKhaddar et al. (eds.), *Advances in Water Resources Engineering and Management*, Lecture Notes in Civil Engineering 39,  
[https://doi.org/10.1007/978-981-13-8181-2\\_7](https://doi.org/10.1007/978-981-13-8181-2_7)



on environment. Nearly 33% of the Himalayan region suffers from various forms of land degradation problems [15]. Land degradation is defined as the gradual decrease in the quality of soil and land, physically and chemically due to effect of certain factors causing particular phenomenon.

The ecosystem and landscapes of an environment are continuously in changing states. These are due to various drivers and factors which are both natural and anthropogenic. Degradation of the land or soil resource can occur at various spatial and temporal scales. The complexity of the spatial and temporal scale quantifies the degree or severity of the degradation [21]. Aridity, extreme climatic events over a long stress of duration and drought may be considered as the natural cause of land degradation while unchecked or unsustainable land use by the human such as deforestation, shifting cultivation, over-cultivation, overgrazing as well as the socio-economic drivers [5].

Land degradation or soil degradation monitoring and assessment are done at multi-spatial scale. Few of the assessments done at the global scale may be listed as LADA (Land Degradation Assessment In Dryland) project of FAO (Food And Agriculture Organization of the United Nation); UNCCD (United Nations Convention To Combat Desertification) and GLASOD (Global Assessment of Human-induced Soil Degradation). On the national level or country level, for India, the assessment of land degradation, mapping, monitoring and assessment are done mainly by Central Arid Zone Research Institute (CAZRI); All India Soil and Land Use Survey (AIS&LUS); National Bureau of Soil Survey and Land Use Planning (NBSS&LUP); and National Remote Sensing Centre (NRSC).

Space Application Centre (SAC), Indian Space Research Organisation (ISRO), Ahmadabad, India, published 'Desertification and Land Degradation Atlas of India' in 2016. According to the analysis, 96.40 mha area of India underwent degradation process during 2011–2013, nearly one-third of the total geographical area, the area under land degradation is 94.53 mha (28.76% of the TGA) during 2003–05. In 2011–13, states with larger areas like Jharkhand, Maharashtra, Jammu & Kashmir, Odisha, Rajasthan, Madhya Pradesh, Gujarat, Telangana and Karnataka contribute around 23.95% [14].

As for the state of Manipur, total percentage of area under desertification/land degradation for the period of 2011–13 is observed to be 26.96% of the total geographical area. Of all the degradation types, vegetation degradation is a most significant process of desertification/land degradation in the state which accounts about 25.78% in 2011–13 and followed by water erosion which accounts for about 0.36% of all the total geographical area of the state [14].

In this chapter, the water-based soil erosion assessment using the geo-spatial techniques is discussed.

## 2 Soil Erosion

Soil erosion is defined as a process in which topsoil on the soil surface is carried away from the land by water or wind and transported to other surfaces. It is considered as the second prevalent environmental problem the world faces after population growth [7]. The eroded soil during soil erosion transport pesticides, nutrients, and other harmful farm chemicals into streams, rivers and pollutes surface and groundwater resources, which in returns are the root cause of other environmental pollution [6].

Whenever soil is left exposed during the rain, the raindrops displace the topmost crust and thus wash away attributing to the soil erosion. Detachment of the soil layer, transportation of the loose particle and deposition in the low-lying area are the three stages involved in soil erosion [10]. The impact incurred by rainfall is more affected on sloping land where the surface soil is easily carried away as the water splashes downhill into valleys and waterways. The rate of erosion is also thus influenced by various physical factors such as the soil composition, slope of the land and extends of vegetative cover.

Remote sensing and GIS is one of the significant tools that can be used for studying the environmental phenomenon. This tool can integrate spatial and non-spatial data for solving many problems and answering many questions. Not only this, it also gives the synoptic view of the region which is very useful in environmental studies.

For that, we require timely and accurate estimation of soil erosion loss or evaluation of risk has for various region remote sensing and GIS techniques come in very handy. This technique can also be assessed and estimate how fast the soil is being eroded before affecting any conservation strategies. For evaluation of erosion process, understanding and knowledge of parameters such as terrain, soil and crop management of the region is required, which can be easily obtained by using the remote sensing and GIS techniques [7]. Various soil erosion models are developed to estimate rates of sediment and nutrient transport under different land-use and land-class systems. There are three categories of models: the empirical models, the conceptual models and physical-based models. Few of the GIS-based models listed are USLE (Universal Soil Loss Equation), USPED (Unit Stream Power-based Erosion Deposition), RUSLE (Revised Universal Soil Loss Equation), WEPP (Water Erosion Prediction Project), LISEM (Limburg Soil Erosion Model) and EUROSEM (European Soil Erosion Model). Even though these models are all GIS-based, there is a significant variation in their complexity, variable inputs, the processes, the representation, the scale of intended use and the types of output information they provide [10].

## 3 Methods and Technique

Universal Soil Loss Equation (USLE) model had emerged as a leading soil erosion model and it can be applied in varying landscapes with simplicity in input variables [22]. This model was first developed by Wischmeier and Smith [24]. This model

analysed various soil erosion factors and ultimately introduced water-based soil erosion assessment model. This model predicts the soil erosion on the basis of terrain parameters, soil, rainfall pattern and soil management practice.

The model was then improved and replaced by the Revised Universal Soil Loss Equation (RUSLE) by Renard et al. [13]. Soil erodibility, length-slope factor, rainfall erosivity factor, supporting conservation practices (*P*-factor) and crop management factor are used as variables. European Soil Erosion Model (EUROSEM) is developed to assess soil erosion models with varying and physical-based parameters.

Water Erosion Prediction Project (WEPP) is a physical model. Process-based models for run-off and soil erosion prediction attempts to assess and model soil loss in different landscapes. WEPP can assess soil loss in complex terrain profiles. This model computes rates of deposition and detachment. WEPP uses a steady-state erosion and deposition by static approach whose erosion is caused by dynamic flow [8].

The USPED is a tool efficient model to predict the deposition and erosion by integrating various inputs. It is assessed in the GIS environment.

The aim of this chapter was to review the current state of erosion assessment and GIS applications. This will include: (1) the traditional application of the RUSLE model in assessing erosion and (2) the geo-spatial application, the application in predicting and estimating magnitude and extent of erosion at watershed using RUSLE.

#### 4 Revised Universal Soil Loss Equation (RUSLE)

The empirical Revised Universal Soil Loss Equation (RUSLE) [13] estimates average loss of soil annually which is based on the intensity of the impact of raindrops and other factors. The model was originally used for the field size or the plot size study area, but it is often used for large spatial area study also. Soil loss is acquired by multiplying input variables, namely rainfall erosivity, slope-length, soil erodibility factor, supporting conservation practices and crop management factor [12].

$$A = LS * K * R * P * C \quad (1)$$

where *A* signifies area of soil loss (tons ha<sup>-1</sup> per year); *R* signifies rainfall erosivity factor (MJ mm ha<sup>-1</sup> h<sup>-1</sup> per year); *K* is the soil erodibility factor (tons MJ h<sup>-1</sup> mm<sup>-1</sup>); *LS* is the slope-length factor; *C* is the crop management factor; and *P* is the practice management factor.

## 5 Rainfall Erosivity Factor (*R*-Factor)

Rainfall erosivity signifies impact intensity of raindrops and requires details of variable like continuous precipitation [24]. The value of the rainfall erosivity signifies or quantifies the effects of raindrop impact and also rate of run-off which will be associated with the rainfall.

Few of the equations for calculating rainfall erosivity (*R*-factor) are given below [24]:

$$R = \sum_1^{12} 1.735 * 1010^{(1.5 \log_{10}(\frac{P_i}{P}) - 0.08188)} \quad (2)$$

where *R*—Rainfall erosivity factor (MJ mm ha<sup>-1</sup> h<sup>-1</sup> per year)  
*P<sub>i</sub>*—monthly rainfall (mm); *P*—annual rainfall [1]

$$R = a \cdot \text{MFI} + b \quad (3)$$

where *R*—Rainfall erosivity factor expressed in MJ mm ha<sup>-1</sup> h<sup>-1</sup> per year

$$\text{MFI} = \sum_1^{12} P_i^2 / P$$

*P<sub>i</sub>* = monthly rainfall in mm; *P* = total annual rainfall in mm [4]

$$R = 1/n \sum_{j=1}^n \sum_{k=1}^{mj} (\text{EI}_{30})_K \quad (4)$$

where *R* signifies average annual rainfall erosivity expressed in MJ mm ha<sup>-1</sup> h<sup>-1</sup> per year,

*n* is the number of years covered by the data records,

*m<sub>j</sub>* is the number of erosive events of a given year *j*,

and *EI<sub>30</sub>* is the rainfall erosivity index of a single event *k* [17].

$$R = 38.5 + 0.35 * P \quad (5)$$

where *P*—rainfall (mm).

## 6 Soil Erodibility Factor (*K*-Factor)

*K*-factor is the average soil erodibility factor expressed in tons MJ h<sup>-1</sup> mm<sup>-1</sup>, and it signifies resistance of the soil to both transport and detachment. As proposed by Wischmeier et al., biological factors like the organic matter content, permeability of the soil and structure are used in the estimation of *K*-factor [23]. Values of this factor are high in silt and fine sand as these types are unstable. If the organic matter content is high, the resistance decreases which attributes to the high rate of detachment of the soil [23].

Equations which are used to calculate the soil erodibility are as follows [24]:

$$K = 2.8 * 10^{-7} M^{1.14} (12 - a) 4.3 * 10^{-3} * (b - 2) * 3.3 * 10^{-3} (c - 3) \quad (6)$$

where *K* signifies soil erodibility factor in tons ha<sup>-1</sup> per unit *R*; *M* gives particle size parameter (% silt + % very fine sand) \* (100 - % clay); *a*, *b* and *c* signifies organic matter content (%), soil structure code and the soil permeability class [13].

$$K = 0.0034 + 0.0405 * \exp \left[ -0.5 \left( \frac{\log Dg + 1.659}{0.7101} \right)^2 \right] \quad (7)$$

where *Dg* signifies geometrical particle diameter (on the basis of fractions of the texture classes and arithmetic mean of the particle diameter of each texture class) [3].

$$K = \frac{SAN + SIL}{CLA} * \frac{1}{100} \quad (8)$$

where SAN, SIL and CLA are the percentages of sand, silt and clay, respectively [16].

$$K = A * B * C * D * 0.1317 \quad (9)$$

$$A = \left[ 0.2 + 0.3 \exp \left( -0.0256 SAN \left( \frac{1 - SAN}{100} \right) \right) \right] \quad (9.1)$$

$$B = \left[ \frac{SIL}{CLA + SIL} \right] \quad (9.2)$$

$$C = \left[ 1.0 - \frac{0.25 * c}{c + \exp(3.72 - 2.95 * c)} \right] \quad (9.3)$$

$$D = \left[ 1.0 - \frac{0.70 * SN1}{SN1 + \exp(-5.41 + 22.9 * SN1)} \right] \quad (9.4)$$

where  $C$ —organic carbon content; SIL, CLA and SAN are the percentages of silt, clay and sand, respectively, and  $SN1$ —sand content subtracted from 1 and divided by 100.

## 7 Length-Slope Factor (LS-Factor)

Slope-length factor ( $L$ ) and slope steepness factor ( $S$ ) are topographical factors which indicate the effect of topography on erosion horizontally. The distance from the point of origin of overland flow to the point where deposition begins, due to decrease in slope gradient, is known as slope length. Slope steepness also influences soil erosion and is signified by slope gradient. This factor attributes in higher overland flow velocities and correspondingly higher erosion [13, 24].

Equations for calculation of LS-factors are [19]:

$$LS = (65.4 * \sin(S) + 4.56 * \sin(S) + 0.065) * (L/72.6) \quad (10.1)$$

where  $L$  signifies slope length in m and  $S$  signifies steepness in percentage (up to 21%) [19]

$$LS = (6.432 * \sin(S0.79) * \cos(S)) * (L/22.1)0.7 \quad (10.2)$$

where  $L$  signifies slope length in m and  $S$  signifies steepness in percentage (greater than 21%) [9]

$$L = \left( \frac{\lambda}{22.1} \right)^m \quad (11.1)$$

where  $L$  signifies slope-length factor;  $\lambda$  gives field slope (m);  $m$ , the dimensionless exponent which depends on the slope.  $m$  is 0.5,  $\theta > 5\%$ ;  $m$  is 0.4,  $\theta = 4\%$ ;  $m$  is 0.3,  $\theta < 3\%$ ;  $\theta =$  slope in percentage [9]

$$S = 10.8 \sin \theta + 0.03, \quad \theta < 9\% \quad (11.2)$$

$$S = 16.8 \sin \theta - 0.05, \quad \theta \geq 9\% \quad (11.3)$$

where  $S =$  slope steepness factor and  $\theta =$  slope angle in percentage [11]

$$LS = (m + 1)[A/22.13_m_{\sin \theta}/0.09]n \quad (12)$$

where  $\theta =$  the land surface slope in degree;  $A =$  upslope area of the watershed;  $m$  and  $n$  are the constants equal to 0.6 and 1.3, respectively.

**Table 1** C-factor assigned for different land-use patterns

Land-use class	C-factor
Settlement/built-ups	1.0
Vacant land	1.0
Agricultural land	0.28
Fallow land/open land	1
Plantations area	0.28
Dense forested area	0.004

## 8 Crop Management Factor (C-Factor)

Land cover ‘vegetation’ is also an important factor which influences and monitors soil erosion. In RUSLE, vegetation cover has significant influence and the factor is known as C-factor. It is the ratio of soil loss from land cropped under specific condition to the corresponding loss clean tilled, continuous fallow [24]. This factor depends on vegetation cover and growth stage.

C-factor can be calculated with the use of the following equations.

The normalized difference vegetation index (NDVI) is widely used as an indicator for the vegetation growth. Hence, its values are scaled and used to estimate C-factor [20].

$$C = \exp \left[ -\alpha * \frac{\text{NDVI}}{(\beta - \text{NDVI})} \right] \quad (13)$$

where  $\alpha$ ,  $\beta$  are the parameters that determine the shape of the NDVI–C curve.

$$\text{NDVI} = \frac{\text{NIR} - \text{RED}}{\text{NIR} + \text{RED}} \quad (13.1)$$

where NIR is near infrared band and RED is the red band of the imageries used.

C-factor differs with differences in land-use pattern. C-factor corresponding to various land-use classes is shown (Table 1) [18].

## 9 Support Practice Factor (P-Factor)

P-factor defines ratio of soil loss with a specific support practice to the corresponding loss with upslope and downslope cultivation. Input layer for this factor is generated using the knowledge of the conservative practice and corresponding slope of the

**Table 2** *P*-factor assigned for different land-use patterns and slopes

Land-use class	Slope in %	<i>P</i> -factor
Agriculture	0–5	0.1
	5–10	0.12
	10–20	0.14
	20–30	0.19
	30–50	0.25
	50–100	0.33
Other land	All	1

study area. Impacts on drainage patterns, run-off concentration and velocity due to the control practice are considered in this factor. Wischmeier and Smith categorize that the land use into agricultural and other land types and the slopes of the study area is classified into six classes for slope, and thus, *P* values are assigned for separate classes. Wischmeier and Smith assigned the values considering management practices of the locals [24]. The assigned values of *P*-factor are given in Table 2.

## 10 USPED (Unit Stream Power-Based Erosion Deposition)

USPED (Unit Stream Power-based Erosion Deposition) predicts the spatial pattern rate of erosion and deposition. The model considers a steady-state overland flow and uniform rainfall condition.

$$\{qs(r)\} = Kt(r)\{q(r)\}m \sin b(r)n \quad (14)$$

where  $b(r)$  signifies slope in degree;  $q(r)$  gives the flow rate;  $Kt(r)$  gives transportability;  $m, n$  are the constants on the type of flow, usually  $m = 1.6$  and  $n = 1.3$ .

Steady state of flow can be expressed as the function of contributing as per unit contour width  $A(r)\{m\}$

$$\{q(r)\} = A(r)i \quad (15)$$

where  $i(m)$  signifies uniform rainfall.

For the uniform land cover and soil type,  $Kt$  is constant; the net deposition/erosion rate is estimated based on the divergence of the sediment flow.

$$\begin{aligned} ED(r) &= \text{div } qs(r) \\ &= Kt[(\text{grad } h(r)) \cdot s(r) \cdot \sin b(r) - h(r) \cdot \{kp(r) + kt(r)\}] \end{aligned} \quad (16)$$



where  $s(r)$  gives the unit vector for the steepest slope direction;  $h(r)$  [m] gives the depth of water estimated from the upslope area  $A(r)$ ;  $kp(r)$  depicts terrain curvature in the direction of the steepest slope and  $kt(r)$  signifies curvature in the direction tangential to a contour line projected to the normal plane.

While developing the USPED model, no experimental work was performed and thus USLE and RUSLE parameters are used as input in the model to assess the impact of soil and land cover on the net soil erosion and deposition.

$$T = R * K * C * P * Am(\sin b)n \quad (17)$$

where  $R \sim i m$ ;  $KCP \sim Kt$  and  $LS = Am(\sin b)n$   
 $m$  is 1.6 and  $n$  is 1.3 for area with prevailing rill erosion  
 $m$  and  $n$  are 1 if the type of erosion is sheet erosion.

Net estimated soil erosion and deposition

$$\begin{aligned} ED &= \text{div}(T \cdot s) \\ &= d(T * \cos a)/dx + d(T * \sin a)/dy \end{aligned} \quad (18)$$

where  $a$  signifies aspect of the terrain surface in degree [11].

## 11 Case Study on Imphal River Watershed, Manipur, India

A case study had been done using RUSLE model on the Imphal River watershed, Manipur, India, to assess the soil loss for the years 2006 and 2017. The spatial as well as the temporal aspect of the soil erosion/loss is discussed.

The study area (Fig. 1) extends from 24°41'49.143" N to 25°24'27.218" N latitude and 93°47'14.301" E to 94°18'8.596" E longitude, with total area coverage of 183,796.956 ha.

The case study is done using the precipitation data of the years 2006 and 2017 from Tropical Rainfall Measuring Mission (TRMM); also Landsat 5-TM and Landsat 8-OLI imageries of the time periods are used. For generating the soil erodibility layer, various soil datasets from the International Soil Reference Information System (ISRIC) are used and SRTM Digital Elevation Model dataset is used for generating various terrain parameters (Table 3).

For the assessment, the study area is divided into two terrain divisions, namely hilly division and valley division, on the basis of the administrative boundary of the districts of the state. Parts of Imphal East, Imphal West and Thoubal districts constitute the valley division and parts of Senapati, Tamenglong and Ukhrul districts constitute the hilly division as shown in Fig. 2. The spatial extents of valley division and hilly division are 411.06 and 1426.90 km<sup>2</sup>, respectively.

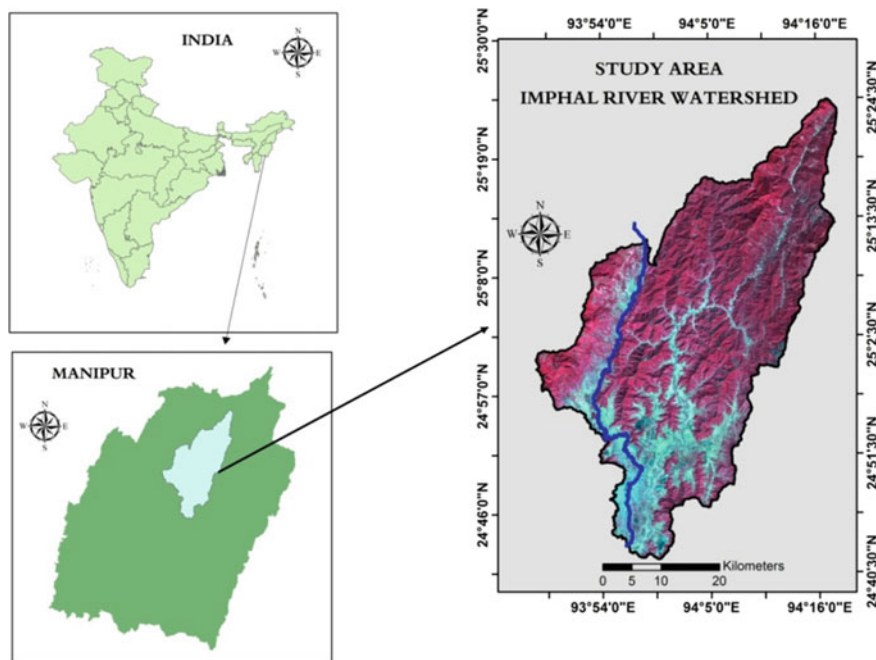


**Fig. 1** Study area (Imphal River watershed)

**Table 3** Dataset and sources

Dataset	Source
Precipitation	TRMM (2006 and 2017)
Satellite imagery	Landsat 5-TM (2006) and Landsat 8-OLI (2017)
DEM	SRTM-DEM
Soil data	ISRIC

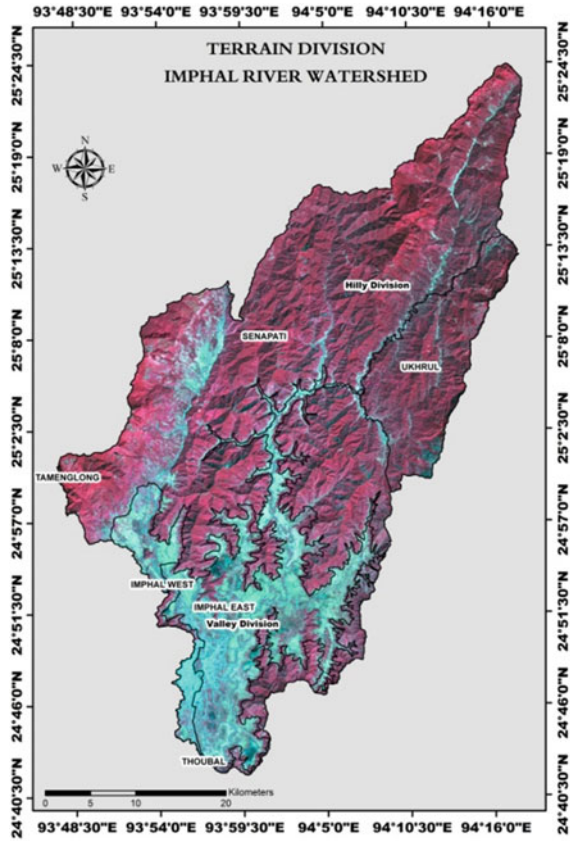
The soil loss of the study area is estimated using RUSLE and USPED. For estimation of soil loss using RUSLE, variables, namely  $R$ -factor,  $K$ -factor,  $LS$ -factor,  $C$ -factor and  $P$ -factor, are considered as the input variables.

$R$ -factor is generated using precipitation data, TRMM, for both the years and is resampled to 30 m spatial resolution. For the calculation of rainfall erosivity (Fig. 3a and b), the equation by Wischmeier and Smith [24] (Eq. 2) is adopted.

Soil erodibility factor ( $K$ -factor) (Fig. 4) is generated using the soil layer procured from ISRIC database. The equation by Sharpley and Williams [16] (Eq. 9) is used for calculation of this factor.

Slope-length factor (Fig. 5) is calculated using the equation given by [9] (Eqs. 11.1, 11.2 and 11.3). SRTM-DEM is employed to generate this factor.

Fig. 2 Study area (terrain division)



According to Van der Kniff et al., crop management factor (*C-factor*) (Fig. 6a and b) is generated using the equation by [20] (Eq. 13). NDVIs in equation are generated using the NIR and RED bands from Landsat imageries for both the time periods.

Support practice management (*P-factor*) (Fig. 7a and b) is established using the practice factor table given by Wischmeier and Smith [24] (Table 2). For this establishment, the slope and land-use layers are generated using the SRTM-DEM and Landsat 5-TM and Landsat 8-OLI imagery.

The total soil loss per year of the study area is estimated using equation given in Eq. (1). The generated soil erosion layer is reclassified into five classes on the basis of classification given by the National Bureau of Soil Science and Land Use Planning (NBSS&LUP). The classification is shown in Table 4.

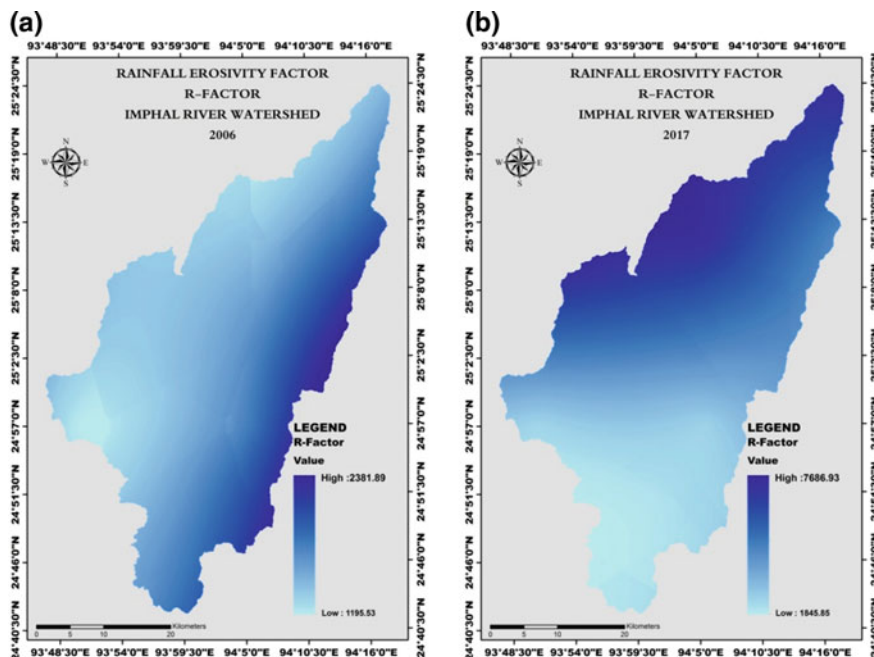


Fig. 3 a Rainfall erosivity (2006). b. Rainfall erosivity (2017)

Table 4 Soil loss classification (NBSS&LUP)

Soil loss rate (tons ha <sup>-1</sup> per year)	Class
Below 5	No erosion
5–10	Slight
10–30	Moderate
30–60	High
60–above	Extreme

## 12 Result and Discussion

In this case study, soil loss of the Imphal River watershed of the state of Manipur, one of the north-eastern states of India, is assessed for the years 2006 and 2017.

The classified soil loss layer generated using RUSLE model is shown in Fig. 8a and b. The figure depicts the spatial distribution of the rate of soil loss as well as the changes in erosion in temporal aspect. The areas under different classifications of soil loss classes (Table 5) clearly state that, in both the time periods, the area under ‘No Erosion’ is much higher compared to that of Extreme soil loss and other classes. Again, it is observed that ‘Extreme’ class has increased tremendously.

The soil loss is further assessed based on terrain division as mentioned earlier. From the assessment, it is observed that the valley division has higher rate of soil

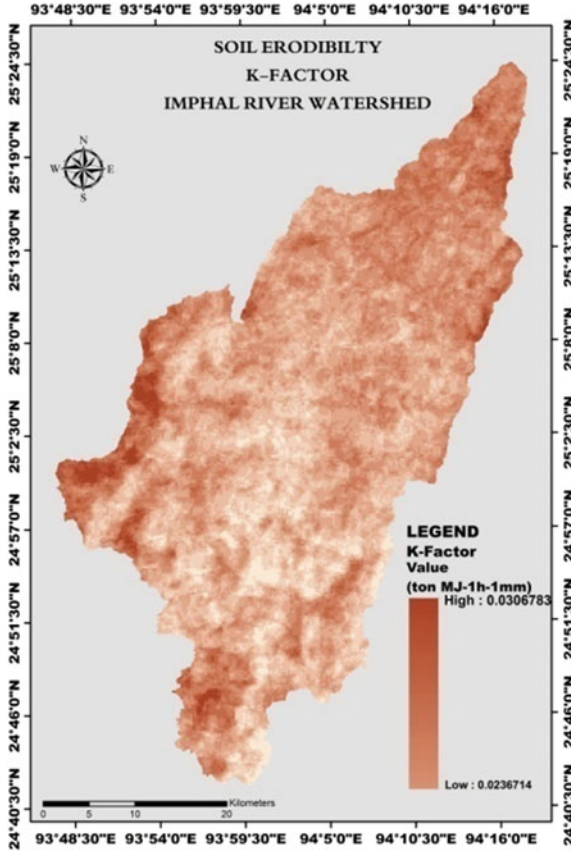


**Fig. 4** K-factor

**Table 5** Soil loss distribution (2006 and 2017)

Soil loss rate (tons ha <sup>-1</sup> per year)	Area (ha) 2006	Percentage of area under soil loss (2006)	Area (ha) 2017	% of area under soil loss (2017)	Class
Below 5	46,709.37	25.4256	71,810.64	39.07189	No erosion
5–10	30,528.99	16.61803	16,529.49	8.993631	Slight
10–30	42,840.45	23.31961	27,415.44	14.91663	Moderate
30–60	27,030.24	14.71354	21,174.39	11.5209	High
60–above	36,599.94	19.92267	46,861.11	25.49695	Extreme

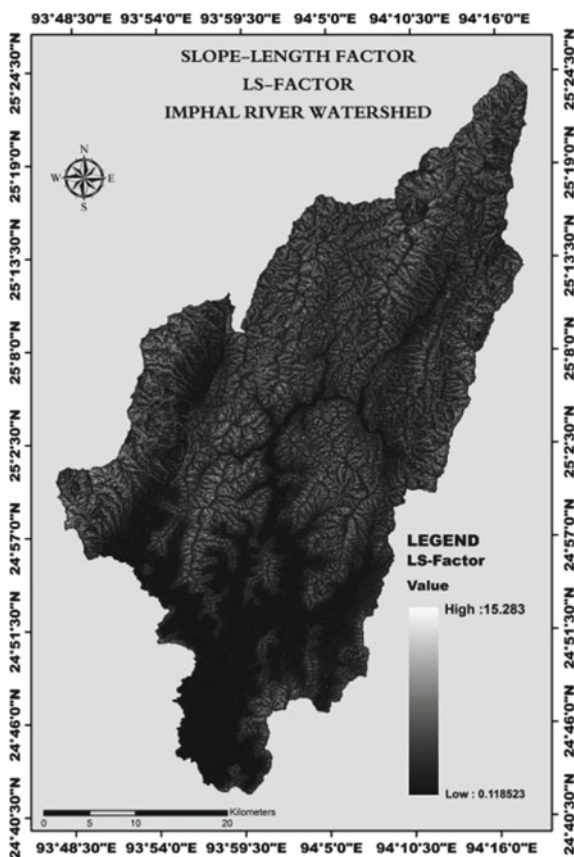


Fig. 5 LS-factor

Table 6 Distribution of soil loss, division wise (2006 and 2017)

Year	2006 (tons ha <sup>-1</sup> per year)			2017 (tons ha <sup>-1</sup> per year)		
	Min	Max	Mean	Min	Max	Mean
Valley division	0.5232	338.974	74.539	0.0016	639.7888	93.59326
Hilly division	0.011	338.974	30.167	7E-07	639.7888	44.15408

loss as compared to its counterpart, i.e. hilly division. The mean soil loss 19.054492 tons ha<sup>-1</sup> per year has been observed in valley division and 13.987253 tons ha<sup>-1</sup> per year in the hilly division (Table 6).

All the factors, namely LS-factor, *K*-factor, *C*-factor, *P*-factor and *R*-factor, are the significant parameters for soil loss assessment, but the latter three factors affect dominantly and attribute to higher soil loss rate in the valley division in both the time periods under study (Tables 7 and 8). The mean values of the mentioned dominant factors (Table 8) mainly attribute in the higher rate of soil loss in the valley division.

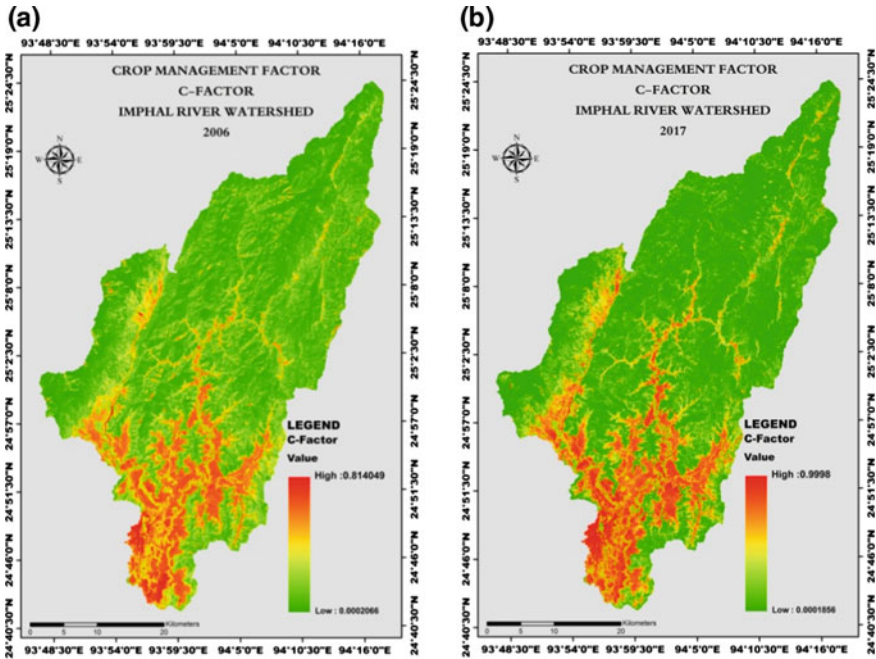


Fig. 6 a C-factor (2006). b C-factor (2017)

Table 7 Distribution of LS-factor and K-factor (division wise)

	Valley division		Hilly division	
	LS-factor	K-factor	LS-factor	K-factor
Min	0.118523255	0.023671415	0.118523255	0.023671415
Max	15.28302956	0.030678317	15.28302956	0.030678317
Mean	0.698170444	0.026712071	2.714741044	0.0268703

Land-use class of the study area also affects the soil loss. The valley division is mainly comprised of built-up and agricultural land uses. The mean value of the soil loss (Table 9) in the land-use classes in both the years 2006 and 2017 clearly depicts the observation of the higher soil loss rate in the valley division of the study area.

### 13 Conclusion

Soil erosion is one of the major factors that contribute to the degradation of land or soil, both physically and chemically. Assessment of soil loss or erosion has become an essential for the prevention and management of the resource. Geo-spatial techniques



**Table 8** Distribution of C-factor, P-factor and R-factor (division wise)

Division	Valley division						Hilly division					
	C-factor		P-factor		R-factor		C-factor		P-factor		R-factor	
Parameter	2006	2017	2006	2017	2006	2017	2006	2017	2006	2017	2006	2017
Year	2006	2017	2006	2017	2006	2017	2006	2017	2006	2017	2006	2017
Min	0.01	0.00	1.00	1.00	1195.53	1845.85	0.000	0.000	1.00	1.00	1202.25	1976.32
Max	0.81	1.00	12.00	12.00	2227.33	5472.12	0.814	1.000	13.00	13.00	2381.89	7686.93
Mean	0.46	0.36	8.04	8.52	1603.44	2366.44	0.115	0.060	2.72	3.41	1582.67	4895.26



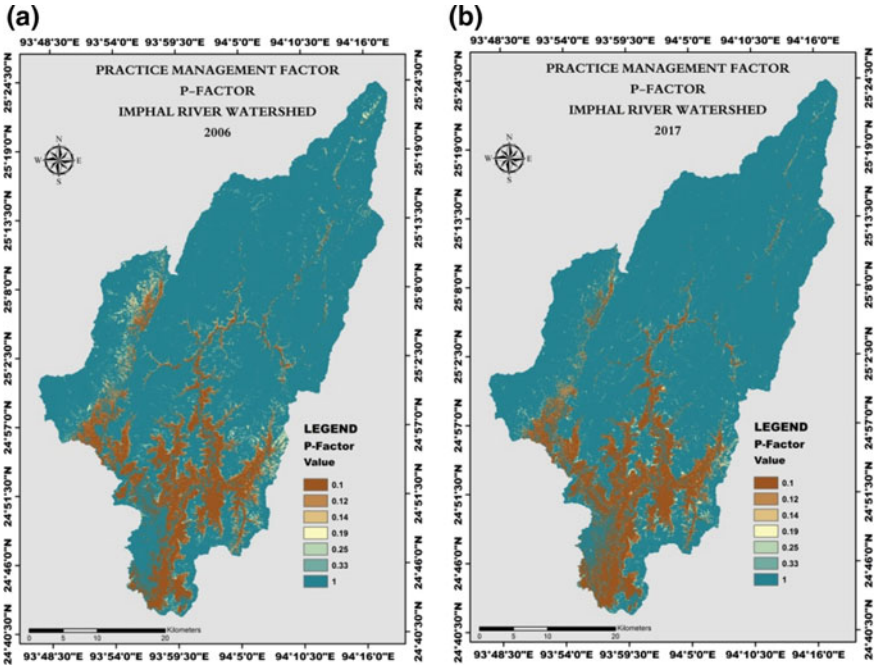


Fig. 7 a P-factor (2006). b P-factor (2017)

Table 9 Distribution of soil loss, land use wise (2006 and 2017)

Land use	2006 (tons ha <sup>-1</sup> per year)			2017 (tons ha <sup>-1</sup> per year)		
	Min	Max	Mean	Min	Max	Mean
Built-up	0.2173	338.9743	65.6936	0.0000	639.7888	107.2173
Agriculture	0.2153	338.9743	94.2424	0.0000	639.7888	159.3027
Barren soil	0.1050	338.9743	37.2754	0.0000	639.7888	60.9529
Vegetation	0.0110	338.9743	19.5197	0.0000	487.3350	5.8678
Water bodies	0.3003	338.9743	54.4516	13.6879	639.7888	144.0293

are widely implicated for assessing soil loss due to its capability to integrate various layers and parameters.

Among all the three types of model classes, empirical model is the most popular and widely used all over the world. The physical processes have capability of representing accurately more in the physical-based model. Both the spatial and temporal variabilities are involved in the assessment of natural erosion process. The necessity for a large amount of input data and parameter is the major drawback of such model. The empirical-based models such as USLE, RUSLE, MUSLE and USPED are widely applied for its limited data requirement and ease of applicability. These empirical models do not represent or depict the real erosion process and have major



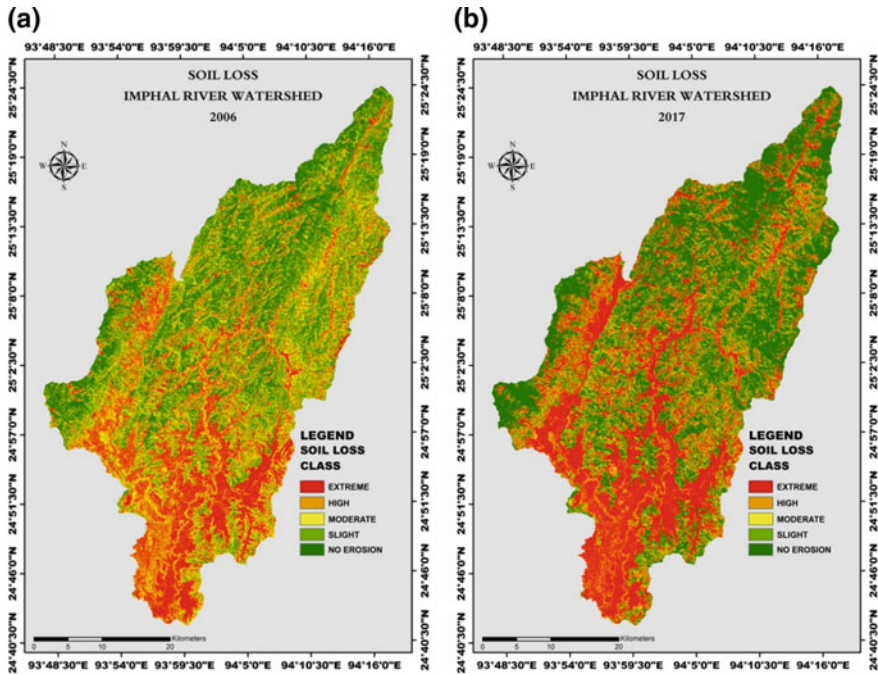


Fig. 8 a Soil loss (2006). b Soil loss (2017)

issues about the scale factor. In spite of its drawbacks, they are extensively used and preferred over the physical-based model, because of its limited data input, mostly in this data-scarce part of the world [2].

As a part of this chapter, a case study is performed using dataset for the time periods of 2006 and 2017, so as to assess the amount of soil loss in the Imphal River watershed of Manipur, using empirical-based model, RUSLE. Increased in the spatial extent are observed in ‘No Erosion’ and ‘Extreme’, and decreased inspatial extent are observed in ‘Slight’; ‘Moderate’ and ‘High’ class of erosions. The area under ‘No Erosion’ is increased by 13.64 and 5.57% in the ‘Extreme’ class of erosion.

Assessment in other approach is done by dividing the study area into two divisions, valley division and hilly division. It is observed that soil loss rate is more aggressive in valley division as compared to the hilly division in both the timelines.

Increase in population and corresponding increase in pressure on the natural resources also attribute for increase in soil loss. Soil loss is widely dependent on land use and land cover of the study area. The hilly division with thick vegetation cover is less susceptible to soil loss despite of its higher elevation and varying slopes. Land use such as built-ups and agriculture affects significantly in the soil loss as observed in this case study.

The LS-factor and the K-factor are considered to be equal in both the time periods, respectively, due to the data unavailability and scarcity of the field data which can

be used to incorporate the mentioned parameters. This is the major drawback of the case study performed.

Even though the result from this case study does not project the real-world erosion in the years 2006 and 2017, it still gives us the overview and potential site of the erosion in the watershed. The result from this case study is still considered to be satisfactory because the region is data scarce and the unavailability of the physical data persists.

**Acknowledgements** The authors gratefully acknowledge the ‘United States Geological Survey (USGS)’ for providing the remote sensing data, Landsat and SRTM, and also ‘the Tropical Rainfall Measuring Mission’ for precipitation dataset from their respective archive.

## References

1. Arnoldus HMJ (1980) An approximation of the rainfall factor in the universal soil loss equation. In: De Boodt M, Gabriels D (eds) *Assessment of erosion*. Wiley, Chichester, pp 127–132
2. Bakimchandra O (2011) *Integrated fuzzy-GIS approach for assessing regional soil erosion risks*. Ph.D. thesis, University of Stuttgart, Stuttgart, Germany, Aug 2011
3. Bouyoucos GJ (1935) The clay ratio as a criterion of susceptibility of soils to erosion. *J Am Soc Agron* 27:738–741
4. Brown LC, Foster GR (1987) Storm erosivity using idealized intensity distributions. *Trans ASAE* 30:c379–c386
5. Eckert S, Hüsler F, Liniger H, Hodel E (2015) Trend analysis of MODIS NDVI time series for detecting land degradation and regeneration in Mongolia. *J Arid Environ* 16–28
6. Gallaher RN, Hawf L (1997) Role of conservation tillage in production of a wholesome food supply. *PARTNERS FOR A 23*
7. Jahun BG, Ibrahim R, Dlamini NS, Musa SM (2015) Review of soil erosion assessment using RUSLE model and GIS. *J Biol Agric Healthc* 5(9)
8. Landi A, Barzegar AR, Sayadi J, Khademalrasoul A (2011) Assessment of soil loss using WEPP model and geographical information system. *J Spat Hydrol* 11:40–51
9. McCool DK, Foster GR, Mutchler CK, Meyer LD (1987) Revised slope steepness factor for the universal soil loss equation. *Trans ASAE* 30(5):1387–1396
10. Merritt WS, Letcher RA, Jakeman AJ (2003) A review of erosion and sediment transport models. *Environ Model Softw* 18(8):761–799
11. Mitasova H, Hofierka J, Zlocha M, Iverson LR (1996) Modelling topographic potential for erosion and deposition using GIS. *Int J Geogr Inf Syst* 10:629–641
12. Panagos P, Meusburger K, Ballabio C, Borrelli P, Alewell C (2014) Soil erodibility in Europe: a high-resolution dataset based on LUCAS. *Sci Total Environ* 479–480:189–200
13. Renard KG, Foster GR, Weessies GA, McCool DK (1997) Predicting soil erosion by water: a guide to conservation planning with the Revised Universal Soil Loss Equation (RUSLE). In: Yoder DC (ed) *Agriculture handbook 703*. U.S. Department of Agriculture
14. SAC, ISRO (2016) *Desertification and land degradation Atlas of India (based on IRS AWiFS data of 2011–13 and 2003–05)*. Space Applications Centre, ISRO, Ahmedabad, India, Ahmedabad
15. Sehgal J, Abrol IP (1994) *Soil degradation in India: status and impact*. Oxford and IBH Publishing Co., New Delhi, p 80
16. Sharpley AN, Williams JR (1990) EPIC—erosion/productivity impact calculator: 1. Model documentation, vol 1768. U.S. Department of Agriculture, Technical Bulletin, pp 235
17. Singh G, Rambabu, Chandra S (1981) Soil loss prediction research in India. *Bull. No. T-12/D-9, CSWCR & TI, Dehradun*

18. Tirkey AS, Pandey AC, Nathawat MS (2013) Use of satellite data, GIS and RUSLE for estimation of average annual soil loss in Daltonganj watershed of Jharkhand (India). *J Remote Sens Technol* 1(1):20–30
19. USDA (1978) Predicting rainfall erosion losses—a guide to conservation planning. Washington, DC
20. Van der Knijff JM, Jones RJA, Montanarella L (2000) Soil erosion risk assessment in Italy. European Soil Bureau, Joint Research Center of the European Commission
21. Waswa BS, Plek PLG, Lulseged T, Okoth P, Mbakaya D (2012) From space to plot: assessment of land degradation patterns in Kenya and its implication for sustainable land management. *Agro Environ*
22. Wilson JP, Lorang MS (1999) Spatial models of soil erosion and GIS. In: *Spatial models and GIS: new potential and new models*, pp 83–108
23. Wischmeier WH, Johnson CB, Cross BV (1971) A soil erodibility nomograph for farmland and construction sites. *J Soil Water Conserv* 26:189–193
24. Wischmeier WH, Smith DD (1978) Predicting rainfall erosion losses: a guide to conservation planning. In: *Agriculture handbook 282*. USDA-ARS, USA

# Analysis of the Extreme Rainfall Events Over Upper Catchment of Sabarmati River Basin in Western India Using Extreme Precipitation Indices



Shivam Gupta , Ankit Gupta , Sushil K. Himanshu  and Ronald Singh

**Abstract** Analysis of extreme rainfall events provide an idea of the probable occurrence of such events in future, and catchment response to such events can be utilized for assessing the flood characteristics of the river basins. This study focuses on the analysis of the extreme precipitation events in the upper catchment of Sabarmati River in western India. Extreme precipitation indices such as the number of rainy days, annual precipitation, daily intensity index, consecutive wet spells, one-day maximum rainfall were calculated as per the norms suggested by Expert Team on Climate Change Detection Monitoring and Indices (ETCCDMI) of Intergovernmental Panel on Climate Change (IPCC). These precipitation extremes were analysed using the IMD gridded precipitation datasets, and associated flood characteristics of the river basin were analysed with the available daily streamflow data for the period 1992–1994. This chapter explains the spatial variation in extreme rainfall events and its effect on the streamflow of the river. Finding of the study reveals no significant trend in the extreme rainfall events of the basin, but catchment response to the extreme rainfall events is evident which could be verified with longer period streamflow data analysis.

**Keywords** Precipitation indices · Extreme precipitation events · Trend analysis · ETCCDMI · Sabarmati river basin

---

S. Gupta · A. Gupta (✉) · S. K. Himanshu · R. Singh  
National Remote Sensing Centre, ISRO, Hyderabad, India  
e-mail: [ankitgupta.isro@gmail.com](mailto:ankitgupta.isro@gmail.com); [ankitgupta@nrs.c.gov.in](mailto:ankitgupta@nrs.c.gov.in)

S. Gupta  
Indian Institute of Technology, Guwahati, Assam, India

S. K. Himanshu  
Indian Institute of Technology, Roorkee, Uttarakhand, India

© Springer Nature Singapore Pte Ltd. 2020  
R. AlKhaddar et al. (eds.), *Advances in Water Resources Engineering and Management*, Lecture Notes in Civil Engineering 39,  
[https://doi.org/10.1007/978-981-13-8181-2\\_8](https://doi.org/10.1007/978-981-13-8181-2_8)

## 1 Introduction

Global warming and climate change phenomena are causing a paradigm shift in the climatic pattern which is resulting in unusual changes in the precipitation occurrence and distribution. In recent time, extreme precipitation events have been observed to be increased in terms of magnitude as well as in frequency worldwide [1]. Intergovernmental Panel on Climate Change (IPCC) [2] stated that the increased temperature would enhance the evaporation process from the large water bodies which could result in more intense precipitation events. Several contemporary studies on extreme events worldwide also provide testimony of the rising trends of such events [3–5].

Heavy precipitation in India causes massive damage to the life and properties. Recent heavy precipitation events in Mumbai, Chennai, Bangalore, Kashmir and Kedarnath are the prime evidences of increasing extreme precipitation events in India [6]. Daily rainfall data of Indian subcontinent have been used over the period 1951–2000 for analysing the trends in extreme events and found that the extreme precipitation events are rising significantly followed by significant decreasing trend in moderate events in central India [7]. Similarly, it used long-term (1901–2004) high-resolution gridded precipitation data for analysing extreme rainfall events in central India [8]. Extreme precipitation analysis on observed precipitation data series from 129 observed stations for the duration of 1910–2000 and observed that 61% of the total observed station is having the increasing trend of extreme events [9]. Similarly, a study carried out on extreme rainfall events analysis in the largest tributary of Brahmaputra River basin in north-east India and found that river catchment is likely to face severe extreme rainfall events because of the climate change [10]. Few studies comparing various salient techniques for analysing the trend in rainfall time series were also done, which shows that rainfall is increasing in the arid Kachchh region [11].

This study aims to analyse the extreme precipitation events in a river basin of western India which partially covers the states Gujarat and Rajasthan of India. Extreme precipitation events and its impact on the corresponding discharge of the river basin are also analysed using the observed streamflow data at the upper catchment of the Sabarmati River.

## 2 Study Area and Data Used

The study area lies in the upper catchment of Sabarmati River basin, up to Derol Bridge, which covers the total area of 6211.56 km<sup>2</sup>, and lies between the geographical extent of north 23.578°–24.917° latitude and east 72.698°–73.597° longitude, as shown in Fig. 1. The extent of the study area is elongated in shape; with a maximum length and width from north to south and west to east, it is 159.70 and 65.65 km, respectively. The study area has a nearly equal coverage in Rajasthan (upper portion) and Gujarat (lower portion) states of India, with 1173 m as highest elevation and

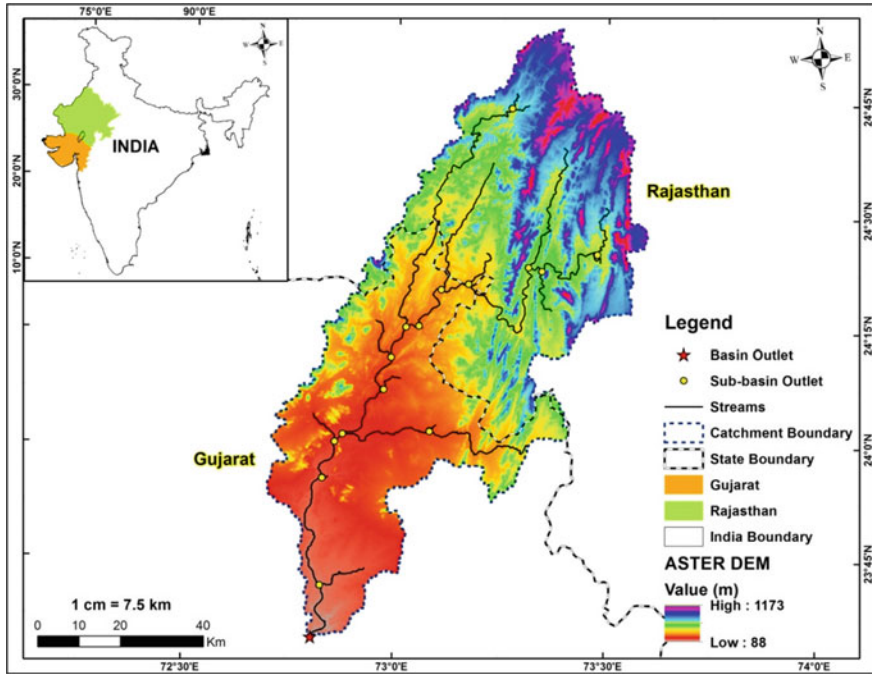


Fig. 1 Location map of the study area

88 m as lowest. Upper catchment up to Derol Bridge receives annual average rainfall of 790 mm.

In this study, the ASTER DEM of 30 m resolution (shown in Fig. 1 within the study area) has been used for catchment delineation up to Derol Bridge as an outlet in Gujarat state. Daily precipitation gridded data by Indian Meteorological Department (IMD) at 0.25° resolution and observed daily discharge data from India Water Resources Information System (WRIS) have also been used in this study. It has been concluded that Empirical Bayesian Kriging (EBK) technique is well suited for the generation of spatially distributed rainfall maps [12]. Therefore, for the generation of all spatial maps in this study, EBK technique has been used.

### 3 Methodology

#### 3.1 Precipitation Extreme Indices

Extreme precipitation events were analysed as per the norms defined by ETCCDMI [13] using the IMD gridded datasets. Five indices were selected for the analysis

which is Simple Daily Intensity Index (SDII), number of rainy days (wet days), annual precipitation (PCPTOT), consecutive wet days (CWD), consecutive dry days (CDD). The threshold for accounting a day as wet days was considered to be 1 mm of precipitation received on that particular day. Annual precipitation is the sum of everyday precipitation for a year, and SDII is defined as the annual precipitation divided by the number of days in a year which comes in unit of mm/day. SDII is an important index for assessing the severity of precipitation. Consecutive wet days (CWD) are the longest spell of days receiving precipitation more than 1 mm, whereas consecutive dry days (CDD) are considered as the longest spell of days without any rain. CD and CWD are very important indices for assessing the temporal distribution of precipitation within a year. Apart from the extreme analysis of precipitation, its impact on regional hydrology and discharge of the upper catchment of the Sabarmati River was also analysed using the observed streamflow data.

### 3.2 Trend Analysis

Trend analysis was performed using the Mann–Kendall nonparametric test, and magnitude of change was assessed using Sen's slope estimator [14].

#### 3.2.1 M–K Nonparametric Test

The M–K statistics ( $S$ ) are defined as

$$S = \sum_{i=1}^{N-1} \sum_{j=i+1}^N \text{sgn}(x_j - x_i) \quad (1)$$

where  $N$  is the number of observed data in time series. Assuming  $(x_j - x_i) = \theta$ , the value of  $\text{sgn}(\theta)$  is computed as follows:

$$\text{sgn}(\theta) = \begin{cases} 1 & \text{if } \theta > 1 \\ 0 & \text{if } \theta = 1 \\ -1 & \text{if } \theta < 1 \end{cases} \quad (2)$$

These statistics represent the number of positive differences minus the number of negative differences for all the differences considered. For large samples ( $N > 10$ ), the test is conducted using a normal distribution with the mean and the variance as follows:

$$\text{Var}(S) = \frac{N(N-1)(2N+5) - \sum_{k=1}^n t_k(t_k-1)(2t_k+5)}{18} \quad (3)$$



where  $n$  is the number of tied (zero difference between compared values) groups and  $t_k$  is the number of data points in the  $k$ th tied group.

$$Z = \begin{cases} \frac{S-1}{\sqrt{\text{Var}(S)}} & \text{if } S > 0 \\ 0 & \text{if } S = 0 \\ \frac{S+1}{\sqrt{\text{Var}(S)}} & \text{if } S < 0 \end{cases} \quad (4)$$

The value of  $Z$  is computed, and if the value lies within the limits  $\pm 1.96$ , the null hypothesis of having no trend in the series cannot be rejected at 95% level of confidence.

### 3.2.2 Sen's Slope Estimator

The magnitude of trend in a time series can be determined using nonparametric method known as Sen's estimator [15]. This method assumes a linear trend in the time series. In this method, the slopes ( $T_i$ ) of all data pairs are calculated first by

$$T_i = \frac{x_j - x_k}{j - k} \quad \text{For } i = 1, 2, \dots, N \quad (5)$$

where  $x_j$  and  $x_k$  are data values at time  $j$  and  $k$  ( $j > k$ ), respectively. The median of these  $N$  values of  $T_i$  gives Sen's estimator of slope ( $\beta$ ). A positive value of  $\beta$  indicates an upward trend and a negative value indicates a downward trend in the time series.

## 4 Results and Discussion

Precipitation data from the India Meteorological Department gridded data were taken for the grids falling inside the upper catchment of the river basin (Fig. 1), and the analysis was made according to the indices analysis of the selected gridded rainfall stations. Extreme indices signify the distribution of extreme events during a certain time period, and results will be discussed based on intensity-based indices and distribution-based indices in the following sections.

### 4.1 Analysis of Extreme Precipitation Indices

Indices such as annual precipitation, number of rainy days (wet days), consecutive wet days and consecutive dry days provide an estimate of rainfall occurrence and distribution in a particular year. Days receiving the rainfall more than or equal to

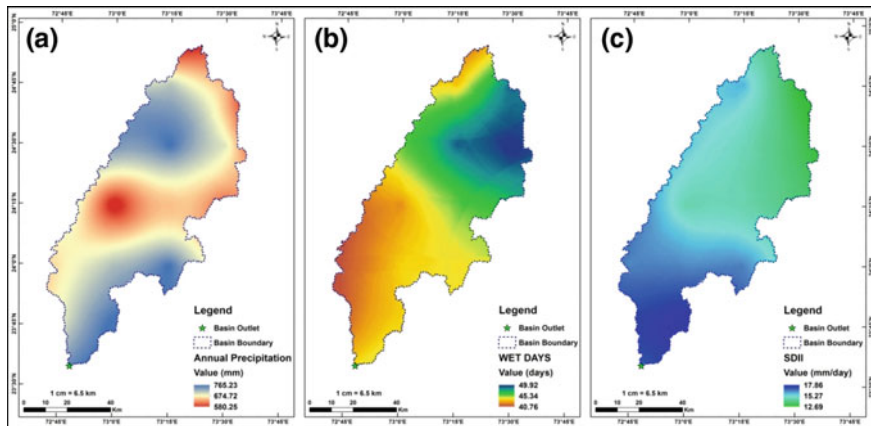


**Fig. 2** Spatial variation of **a** average annual precipitation, **b** wet days and **c** rainfall intensity

1 mm depth are considered as the rainy days; this value was adopted by following the norms of ETCCDMI report. Annual precipitation estimate is a reliable indicator of the year being a dry year or a wet year. Annual precipitation analysis of the catchment shows the annual precipitation varies from 580 to 765 mm in the basin (Fig. 2a). Wet day's distribution in the river basin shows variation from 40 days in a year to 49 days (Fig. 2b). Wet days are the indicators of the distribution of rainfall occurrence in a year; upper catchment of the river basin shares its parts with Rajasthan and Gujarat states and both the states come under arid region, and wet days analysis shows that the major rainfall occurs in the month of monsoon season. Figure 2c shows the precipitation intensity distribution in the catchment, and it varies from 12 to 17 mm/day from upper part of the catchment to the lower part. Lower part of the basin faces the higher intensity of precipitation as compared to the upper part because of the higher annual precipitation and lesser number of wet days in the region.

Figure 3 shows the consecutive wet days (CWD) and consecutive dry days (CDD) distribution in the basin. CWD and CDD are the indicators of the spells of rainy days and spells of dry days which are good indicators of the drought onset and end condition in a region. River basin comes in the arid region, and this is the region behind having low CWD values across the basin and very long dry spells. Figure 3a shows CWD variation from 8 to 13 days in a year whereas CDD spells last longer than 100 days in a year (Fig. 3b).

#### 4.2 Trend Analysis of Extreme Indices

Trend analysis of the precipitation indices was performed using Mann–Kendall non-parametric test as explained in Methodology Section. Trend analysis of the indices

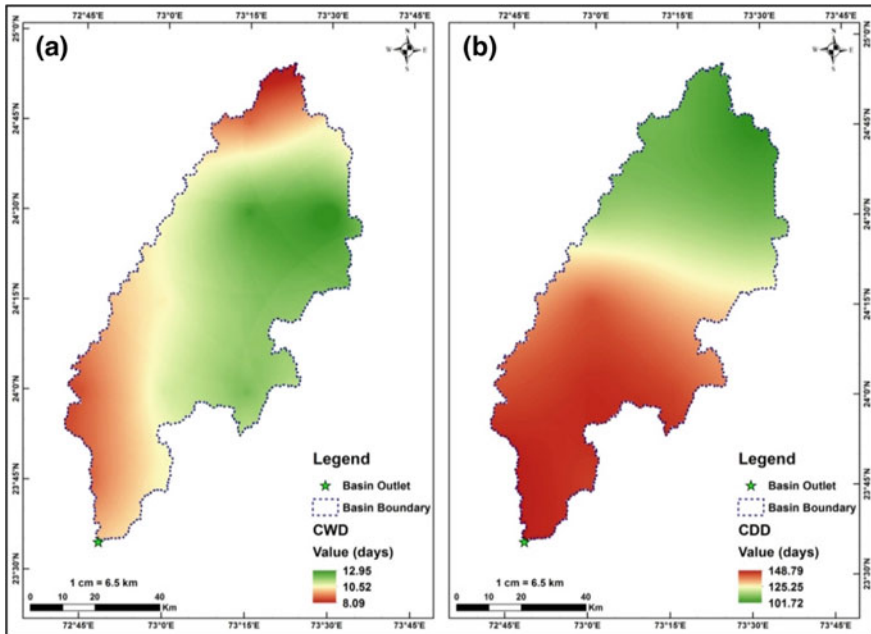


Fig. 3 Spatial variation of **a** consecutive wet days **b** consecutive dry days

shows no increasing trends in the annual precipitation, wet days and daily precipitation intensity. Annual precipitation shows insignificant decreasing trend with Z value  $-1.09$  with magnitude of  $0.27$  mm/yr; similarly daily precipitation intensity also follows decreasing but insignificant trend with Z value of  $-1.5$  and magnitude of  $0.12$  mm/day. Consecutive dry day spells tend to increase, but it was found insignificant.

Observed streamflow data from 1992 to 1994 for the upper catchment of Sabarmati River (Derol Bridge gauging site) were taken to analyse the catchment response for the extreme rainfall events (Fig. 4). It was observed that the catchment exhibits intermittent river characteristics with prompt response to the storm events in the monsoon season, and during rest of the season, the river runs almost dry or carries very less discharge.

### 5 Conclusion

Upper catchment of the Sabarmati River shares its boundaries with arid zone of Gujarat and Rajasthan states; extreme rainfall events were analysed in the catchment using IMD gridded datasets. Although trends in the major of the extreme indices were found insignificant at 95% confidence level, but the seasonal variation of the



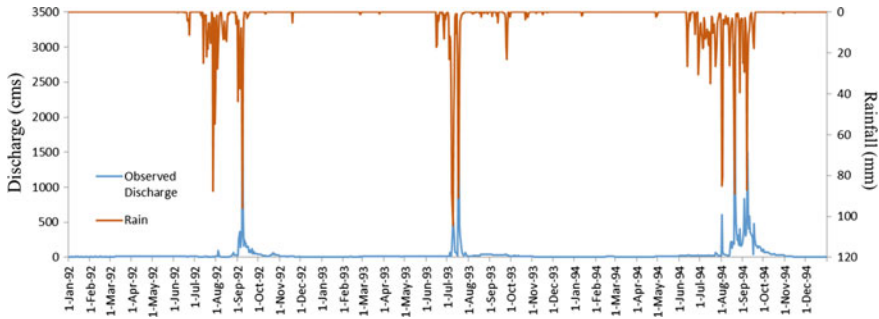


**Fig. 4** Rainfall and streamflow hydrograph for the upper catchment

precipitation indices could have significant effect on region hydrology. This study is significant for the region as the region has faced severe flood events in recent years, i.e. during Gujarat floods which covered several districts of Gujarat and Rajasthan and caused several deaths and loss of properties. The proposed methodology has a limitation of long-term observed streamflow data to analyse the extreme flood conditions, and short-term streamflow data analyses show that the catchment is very prone to the extreme rainfall events and show lean flow during the non-monsoon period which corresponds to low base flow contribution in the river. Long-term flood forecasting associated with extreme rainfall events for the river basin could be performed by return period and flood frequency analysis with longer period observed streamflow and rainfall data.


## References

1. Rajeevan M, Bhate J, Kale JD, Lal B (2006) High resolution daily networked precipitation data for the indian region: analysis of break and active monsoon spells. *Curr Sci* 91:296–306
2. Intergovernmental Panel on Climate Change (IPCC) (2007) Climate change 2007: the physical science basis. In: Solomon S et al (eds) Contribution of working group I to the fourth assessment report of the intergovernmental panel on climate change. Cambridge University Press, Cambridge, UK
3. Groisman PY, Knight RW, Karl TR (2001) Heavy precipitation and high stream flow in the contiguous United States: trends in the twentieth century, *Bull Am Meteorol Soc* 82:219–246. [https://doi.org/10.1175/1520-0477\(2001\)082%3c0219:hpahsi%3e2.3.co;2](https://doi.org/10.1175/1520-0477(2001)082%3c0219:hpahsi%3e2.3.co;2)
4. Alexander LV et al (2006) Global observed changes in daily climate extremes of temperature and precipitation. *J Geophys Res* 11:D05109. <https://doi.org/10.1029/2005JD006290>
5. Guhathakurta P, Rajeevan M (2007) Trends in the rainfall pattern over India. *Int J Climatol* 28:1453–1469. <https://doi.org/10.1002/joc.1640>
6. Guhathakurta P, Sreejith OP, Menon PA (2011) Impact of climate change on extreme rainfall events and flood risk in India. *J Earth Syst Sci* 120(3):359. <https://doi.org/10.1007/s12040-011-0082-5>
7. Goswami BN, Venugopal V, Sengupta D, Madhusoodanan MS, Xavier PK (2006) Increasing trend of extreme rain events over India in a warming environment. *Science* 314:1442–1444. <https://doi.org/10.1126/science.1132027>

8. Rajeevan M, Bhate J, Jaswal AK (2008) Analysis of variability and trends of extreme rainfall events over India using 104 years of gridded daily rainfall data. *Geophys Res Lett* 35(18). <https://doi.org/10.1029/2008gl035143>
9. Roy SS, Balling RC (2004) Trends in extreme daily precipitation indices in India. *Int J Climatol* 24(4):457–466. <https://doi.org/10.1002/joc.995>
10. Shivam G, Goyal MK, Sarma AK (2017) Index-based study of future precipitation changes over Subansiri river catchment under changing climate. *J Environ Inform*. <https://doi.org/10.3808/jei.201700376>
11. Machiwal D, Gupta A, Jha MK, Kamble T (2018) Analysis of trend in temperature and rainfall time series of an Indian arid region: comparative evaluation of salient techniques. *Theor Appl Climatol*. <https://doi.org/10.1007/s00704-018-2487-4>
12. Gupta A, Kamble T, Machiwal D (2017) Comparison of ordinary and Bayesian Kriging techniques in depicting rainfall variability in arid and semi-arid regions of Northwest India. *Environ Earth Sci* 76:512. <https://doi.org/10.1007/s12665-017-6814-3>
13. Donat MG, Alexander LV, Yang H, Durre I, Vose R, Caesar J (2003) Global land-based datasets for monitoring climatic extremes. <https://doi.org/10.1175/bams-d-12-00109.1>
14. Kendall MG (1975) Rank correlation methods, 4th edn. Charles Griffin, London
15. Sen PK (1968) Estimates of the regression coefficient based on Kendall's tau. *J Amer Stat Assoc* 63(324):1379–1389. <https://doi.org/10.1080/01621459.1968.10480934>

# Rainfall Runoff Modelling of Urban Area Using HEC-HMS: A Case Study of Hyderabad City



Vinay Ashok Rangari , V. Sridhar, N. V. Umamahesh and Ajey Kumar Patel

**Abstract** Uncontrolled urbanization and climate change play a significant role in urban flooding. The condition in which rainfall excess exceeds the drainage capacity of storm water drains is called urban flooding. Urbanization disrupts the natural water balance by increasing impervious areas and reduction in infiltration. This increases runoff from urban catchments and leads to higher flood peaks even for short-duration low-intensity rainfall. Such flash floods significantly increase the expenses on mitigation efforts owing to their destructive nature. Urban flood management is one of the important topics of concern as frequent disasters are happening in almost all the urban areas. This is the indication of poor storm water management in urban areas particularly in developing countries like India. Thus, to improve the situation proper storm water drains and sewage network need to be planned and installed considering present land use pattern and probable future development. Present study focuses on the simulation of critical storm event for analysing drainage capacity for part of Hyderabad city (Zone XII). This study area is the most flooded catchment in Hyderabad, and it is ranked as priority number 1 in urban flooding. The drainage network exists in certain parts of the study area. Rainfall data is collected from the Indian Meteorological Department (IMD), and extreme rainfall events are found out. The response of the catchment to the extreme rainfall is modelled using HEC-HMS and HEC-Geo HMS. The simulated model gives a peak discharge of 590.5 m<sup>3</sup>/s at the outlet (Hussain Sagar Lake) for the August 2008 rainfall event having 221.4 mm precipitation for the duration of 34 h.

**Keywords** HEC-HMS · ArcGIS · Flood · Zone XII · Model

---

V. A. Rangari (✉) · V. Sridhar · N. V. Umamahesh · A. K. Patel  
Department of Civil Engineering, National Institute of Technology Warangal, Warangal 506004,  
Telangana, India  
e-mail: [vinayrangari@gmail.com](mailto:vinayrangari@gmail.com)

© Springer Nature Singapore Pte Ltd. 2020  
R. AlKhaddar et al. (eds.), *Advances in Water Resources Engineering and Management*, Lecture Notes in Civil Engineering 39,  
[https://doi.org/10.1007/978-981-13-8181-2\\_9](https://doi.org/10.1007/978-981-13-8181-2_9)

113

## 1 Introduction

Urban flooding is in an increasing trend in the recent years. Much effort has been on the modelling of river flood researched over the years. The main focus on urban flooding is due to the presence of the abundant commercial and industrial settlements in urbanized areas. As per the WMO report [15], the total population in urban areas has been increased from 36 to 54% from 1961 to 2014 the high value of land. Uncontrolled urbanization alters the natural catchments leading to high impervious percentage which results in decreased infiltration. Hence, the rainfall to runoff conversion is very high which results in higher peaks and higher flood volumes when compared to rural catchments [11].

Storm water drains play an important role in conveying the rainfall from the urban areas to the outlet point mostly a water body like river or lake. Due to the unavailability of space and increased land value, storm water management is topic of concern in urban areas [16]. As a result of poor maintenance and uncontrolled urbanization, almost all the storm water drains do not have the capacity to take excess runoff due to extreme flooding events, and hence, flash floods occur almost in events of short-duration rainfall with high intensity [1].

The research in urban flooding has been carried out all over the world many years and has resulted in many useful mathematical modelling tools both freeware and proprietary software. With the advent of graphical user interface (GUI), software like SWMM, HEC-HMS, HEC-RAS, MIKE FLOOD modelling of the urban flood became easy and easily understandable outputs have been generated by these software. Geographical information system (GIS) software like ArcGIS, QGIS has made the work still simpler for extracting data for direct inputs to the model [5, 4]. A number of case studies show high efficiency of HEC-HMS and HEC-RAS models in the mapping of flood inundation for large watersheds [3, 10, 2, 6, 9]. The availability of DEM has made the simulation to more extensive simplification of reality when data availability is less [8]. The main aspect of flood modelling is to understand the characteristics of flood in the urban area and the impacts of heavy rainfall on the runoff of the urban catchments and the various socio-economic aspects of flood. In the following section, the response of the study area to some historical extreme rainfall events on the urban catchment is analysed using HEC-HMS which is the extensive part of this study. HEC-HMS is capable of solving the widest possible sort of problems including large river basins to small urban or natural watershed runoff. Moreover, the results of HEC-HMS model can directly be incorporated into flood routing and analysis.

## 2 Study Area and Data Collection

Hyderabad is divided into 16 storm water zones by Greater Hyderabad Municipal Corporation (GHMC). Out of these 16 zones, Zone XII-Kukatpally and Zone XIII-Alwal and Begumpet areas are major flood prone areas. The area chosen for the



**Fig. 1** Boundary map of the study area. *Source* GHMC

present study is Zone XII of Hyderabad city, Telangana (Fig. 1). It is most critical storm water zone of the Hyderabad city and is marked as priority number 1 for management by GHMC. It is situated in the latitude between  $17^{\circ}34'35.44''$  N and  $17^{\circ}24'34.03''$  N and longitude of  $78^{\circ}22'51.348''$  E and  $78^{\circ}28'40.397''$  E. Zone XII is most critical storm water zone of the Hyderabad city and Greater Hyderabad Municipal Corporation (GHMC) has marked it as priority number 1 for management. The average elevation present in this area is 489.5 m, and the municipal area covering an area of  $171.13 \text{ km}^2$  and the ultimate point of disposal is Hussain Sagar Lake.

The data used in present study is obtained from the different sources. Most of the data regarding digital elevation model (DEM) map, land use–land cover map were extracted from Cartosat 30 m DEM obtained from Bhuvan (Fig. 2). The sub-catchments, drains and junctions details are obtained from the Voyant's Solutions Pvt. Ltd [14]. The rainfall data is from the Indian Meteorological Department (IMD), Hyderabad.

### 3 Methodology

#### 3.1 The Problem Statement

Hyderabad is one of the fast growing metropolitan cities in India. Hyderabad is facing urban flooding problems particularly from the millennium, and the historical rainfall data is an evidence for the above statement. Hyderabad has been divided into 16 storm water zones by GHMC. The most critical storm water zone is Zone XII covering an area of  $171.13 \text{ km}^2$  and is marked first priority for urban flood management. Due to the insufficiency of drains, major flooding issues have been faced by this particular zone. In order to study the response of this particular zone to the given rainfall,



**Fig. 2** CartoSAT DEM of the study area Zone XII. *Source* Bhuvan

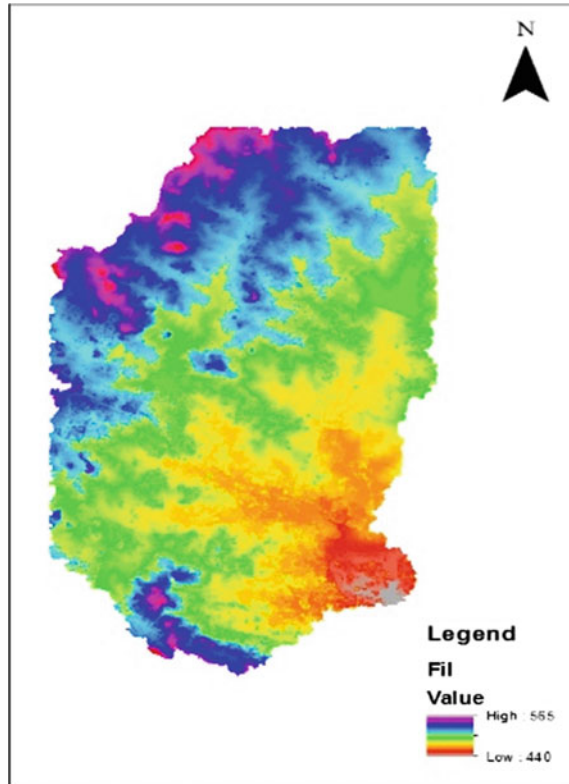
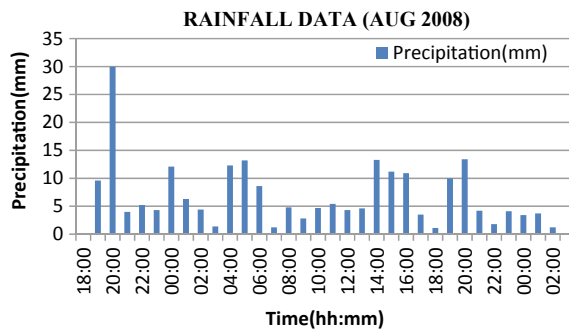


**Fig. 3** Rainfall data for August 2008. *Source* IMD



historical extreme flood events have been analysed and one such extreme rainfall event occurred in August 2008 having a total duration of 36 h and 221 mm rainfall depth is taken for the study purpose (Fig. 3).

**Table 1** Percentages' land use

Land use	Area in 2016 (%)
Built-up	66.02
Barren	25.70
Lake	3.05
Vegetation	5.23

### 3.2 Land Use Classification

Urbanization along with rapid population growth allows changes in land use and land cover (LULC) and thus alters the natural catchment and its properties. LULC is one of the important data required for the rainfall runoff modelling. Thus, to accurately simulate the critical events model parameters must be refined to suite present land use conditions. The land use map for the study area is prepared using the pixel-based image classification tool in ArcMap 10.3. Urban flood modelling requires high-resolution satellite images so that features can be identified properly. LISS III images have  $30\text{ m} \times 30\text{ m}$  resolution map which identifies very less features in urban areas. Google earth image for the study area is downloaded and pixel-based image classification done using maximum likelihood classification. The method uses training data to estimate probabilities of variances of defined classes assuming equal probabilities for all the classes. The main advantage of this technique is, based on the statistics, it provides an estimate of overlap areas. Figure 3 shows the land use map for study area divided into four classes as built-up area, barren land, lake and vegetation. Table 1 shows the area occupied by each class.

### 3.3 Heavy Rainfall History of Hyderabad City

Year-wise record of heavy rainfall events is given below:

- On 1 August 1954, the city had recorded a rainfall of 190.5 mm and severe devastation took place in the city.
- In 1970, recorded rainfall was 140 mm in 24 h.
- In year 2000, Hyderabad city experienced 240 mm of rainfall in just 24 h. Total rainfall in August was 468 mm, which is the worst calamity in almost 50 years.
- The city experienced heavy rainfall for 36 h recording 221 mm of rain in August 2008 (simulated rainfall event).

## 4 Rainfall–Runoff Modelling

The basin model of study area is developed using HEC-GeoHMS, a hydrological model based on remote sensing [12] and simulations run is performed using HEC-HMS [13] to analyse the runoff response of catchment for given extent an distribution of event rainfall. Valuable hydraulic or hydrologic information can be extracted from digital elevation model (DEM) in the absence of extensive field data. Cartosat 30 m  $\times$  30 m resolution DEM (Fig. 2) is processed in the HEC-GeoHMS, the GIS preprocessor for the HEC-HMS to delineate the drains and divide the catchment into a sequence of interconnected subbasins. The inputs to the model include land use information, hydrologic soil group and rainfall event. Percentage imperviousness for each and every subbasins is calculated (Table 2) by processing land use data in ArcGIS 10.1. Other input parameters to the model such as the stream length, slope, positioning of subbasin centroid and elevation, longest flow path for each subbasin, and the length along the stream path are also extracted. Figure 3 shows the basin model of the study area developed using the HEC-GeoHMS. SCS unit hydrograph method is used as a transform model to convert the rainfall to runoff. The only input required for the transform model is the lag time, and HEC-HMS technical reference manual suggests the usage of 0.6 times the time of concentration for ungauged watersheds. Time of concentration is calculated using the Kirpich formula, and then lag time is calculated based on the above statement. The advantage of SCS method is: (1) It works good in different environments, (2) it requires only a few variables (lag time, land use and slope) which makes the calculation part easy, and (3) despite its simplicity, it yields results that are as good as those of complex models [7]. In urban flood simulation, infiltration is one of the most important parameters, and hence, Green-Ampt infiltration technique was used to simulate the infiltration in each subbasin. Sandy loam soil is predominantly present in the study area, and hence, the inputs for the Green-Ampt infiltration model was taken from the HEC-HMS Technical reference manual, and the inputs taken are listed in Table 3. Thus, HEC-HMS model for the study area is formulated and simulated to reproduce past rainfall event of August 2008 (Fig. 3) over present land use conditions. Control specifications define the time range in which the model has to run the simulation. Entire rainfall duration (08-Aug-2008 18:00 h to 10-Aug-2008 03:00 h) is given as a control specification to run the simulation. The Muskingum-Cunge routing method is used to handle the movement of the water in the reach. Figure 5 shows the basin model developed for the study area.

**Table 2** Percentage imperviousness

HMS ID	Percentage imperviousness	HMS ID	Percentage imperviousness	HMS ID	Percentage imperviousness	HMS ID	Percentage imperviousness
W1020	0.86	W880	0.79	W750	0.98	W630	0.93
W1010	0.78	W870	0.83	W740	0.75	W620	0.7
W1000	0.86	W860	0.49	W730	0.84	W610	0.69
W980	0.8	W840	1	W720	0.9	W600	0.67
W960	0.81	W830	0.80	W710	0.77	W590	0.88
W950	0.85	W820	0.85	W700	0.94	W580	0.452
W940	0.86	W810	0.49	W690	0.94	W570	0
W930	0.75	W800	0.83	W680	0.66	W560	0.9
W920	0.79	W790	0.87	W670	0.98	W550	0.467
W910	0.80	W780	0.625	W660	0.92	W540	0.472
W900	0.85	W770	0.89	W650	0.99	W530	0.517
W890	0.81	W760	0.81	W640	0.833	W520	0.61

**Table 3** Green-Ampt infiltration parameters

Parameter	Assigned value
Suction head	8.27 mm
Conductivity	0.27 mm/h
Initial deficit	2.5 mm
Impervious percentage	0.7 (calculated individually for subbasins)

## 5 Results and Discussion

### 5.1 Land Use Classification

Google earth imagery of 2016 was used to classify the land use into four categories, namely Barren, built-up, lake and vegetation (Fig. 4), and the results are presented in Table 1. The results show that the area is completely urbanized with around 66% built-up area. This clearly shows there is high chance of conversion from rainfall to runoff with higher peaks and high flood volumes (Fig. 5).

### 5.2 Percentage Imperviousness

Percentage imperviousness is one of the important parameters for calculating the infiltration losses. Land use map created for the entire zone is subdivided into 50 sub-

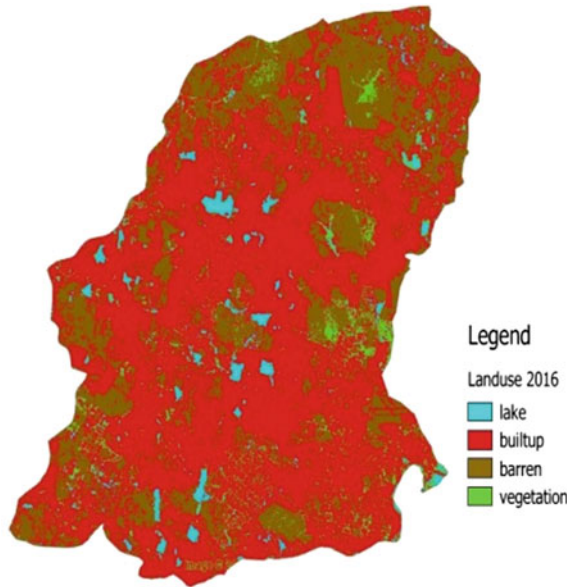


**Fig. 4** Land use classification

catchments, and the percentage of built-up area in each sub-catchment is calculated separately from the attribute table (Table 4).

### 5.3 *HEC-HMS Results*

HEC-HMS was run with real time rainfall event of August 2008. The subbasin parameters mainly required are the lag time, infiltration parameter and the transform parameters. The infiltration parameter values are given for the sandy loam soil as specified in HEC-HMS technical reference manual. Percentage imperviousness values for each sub-catchment are calculated as given in Table 4. The entire stream network is simplified into a series of drains. The drain routing parameter requires the length of the drain, slope of the basin, width of the drain and the shape of the drain. The drain size is taken as rectangular drain with 3 m width. Control specification is given to run the model for the specified period. The entire duration of rainfall that is 08-Aug-08 18:00 to 10-Aug-08 03:00 is given as control time, and model simulation run is performed. The simulation output is obtained in the form of hydrographs at outlet of every unit in the model (sub-catchment, junctions and reaches). The hydrographs showing the reaches with maximum peak discharge is presented in Fig. 6. Figure 7 shows the hydrograph at basin outlet. Table 4 shows the

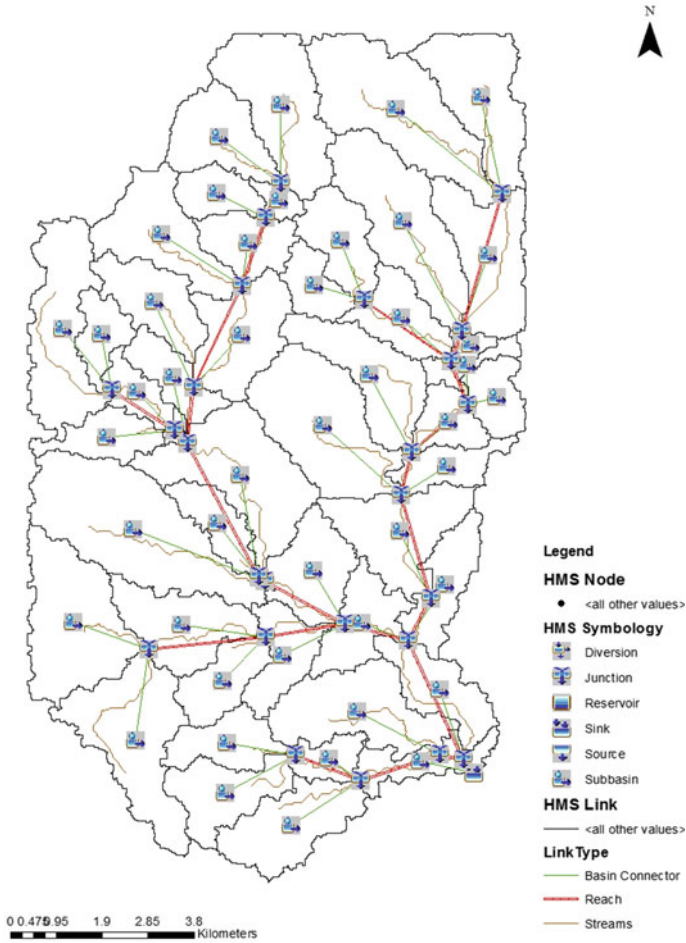


**Fig. 5** Basin model HEC-GeoHMS

output summary with the peak discharge at each junction, reach and sub-catchment, whereas summary of basin outlet is represented in Table 5. The results show that the outlet point that is the Hussain Sagar Lake is having a peak discharge of 590.6 m<sup>3</sup>/s during the event.

**Table 4** Junctions' summary table

Junction ID	Peak discharge (m <sup>3</sup> /s)	Reach ID	Peak discharge (m <sup>3</sup> /s)	Sub-catchment ID	Peak discharge (m <sup>3</sup> /s)	Sub-catchment ID	Peak discharge (m <sup>3</sup> /s)
J169	47.1	R60	38.8	W1020	18	W740	7.8
J176	24.8	R80	46.6	W1010	5.6	W730	7.2
J181	68	R120	46.8	W1000	8.9	W720	8.9
J184	54.9	R130	17.6	W980	14.1	W710	6.3
J187	583.9	R140	91.4	W960	10.7	W700	18.8
J190	78.4	R160	72.3	W950	23.1	W690	4
J193	520.9	R190	120.2	W940	27.4	W680	2.1
J196	313.6	R210	29.7	W930	12.7	W670	12
J207	222.8	R230	44.6	W920	10.3	W660	13.7
J210	183.6	R240	101.5	W910	12.2	W650	7.4
J215	196.8	R260	123.5	W900	10.8	W640	24.1
J218	184.3	R280	146.1	W890	17.7	W630	18.2
J223	156.2	R300	146.9	W880	27.5	W620	12.2
J226	45.2	R310	182.7	W870	14.9	W610	19.5
J231	149.8	R330	176.3	W860	11.6	W600	10.6
J234	132	R350	213.6	W840	0.1	W590	7.6
J237	31.4	R360	74.3	W830	8.6	W580	25.6
J248	123.1	R370	306.2	W820	40	W570	21.3
J253	104.2	R380	190.9	W810	20.5	W560	2.8
J256	19.6	R410	50.4	W800	8.2	W550	15.1
J265	76.6	R440	67.1	W790	28.1	W540	20.7
J270	49.2	R450	504.2	W780	1.2	W530	31.2
J273	93.6	R470	581.7	W770	9.1	W520	24.8
J280	39.9	R480	23.4	W760	30		
J283	51.9	R490	44.9	W750	7.5		

**Table 5** Basin outlet summary

HMS ID	Drainage area (km <sup>2</sup> )	Peak discharge (m <sup>3</sup> /s)	Time of peak
Outlet 1	143.415	590.5	08-Aug-2008, 20:00

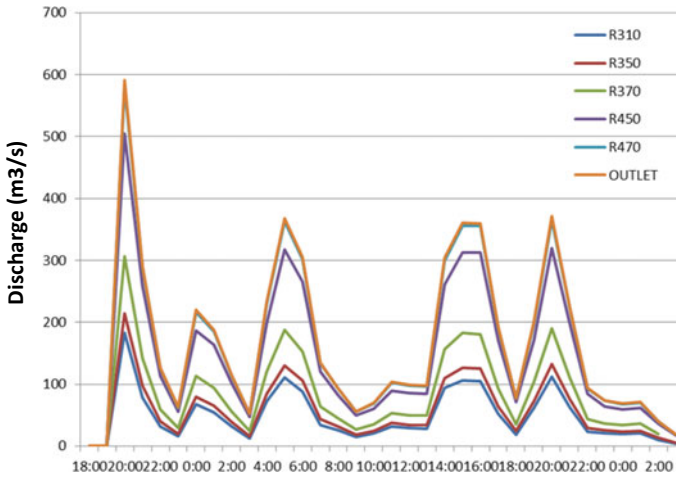


Fig. 6 Hydrographs of five reaches with maximum peaks

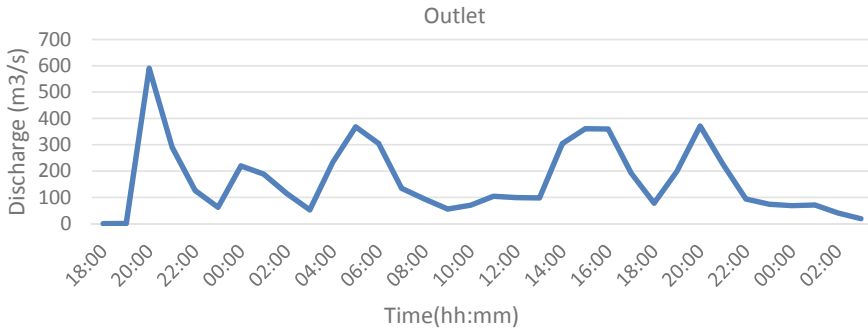


Fig. 7 Outlet hydrograph at basin outlet

## 6 Conclusion

With limited data availability, the runoff was quantified for the given rainfall event for the study area. Understanding the hydrological response of a watershed is one of the most important aspects in urban water management, and with the advent of hydrological models like HEC-HMS, it has become easier. Many researchers have successfully applied HEC-HSM model to produce rainfall–runoff hydrographs for large watersheds [3, 10, 2, 6, 9]. The literature shows that HEC-HMS model produces good results for event-based rainfall–runoff simulations and output can easily be incorporated into flood routing software for further processing [5, 11]. In this study, HEC-HMS model is used to produce runoff hydrographs for an urban catchment. Most of the parameters required for model simulation are extracted from digital elevation model (DEM) in ArcGIS 10.1. Model simulation results give the peak dis-



charges for each model unit which can be used to plan and design new developments in the area. The present study faces the limitation of measured data availability; thus, model results cannot be verified with real flow values. However, newspaper reports and information from interviews with local people suggest the model output discharges are approximate and thus can further be used in flood modelling as input parameters.

**Acknowledgements** This work is undertaken as a part of Information Technology Research Academy-Water, Media Lab Asia project entitled “Integrated Urban Flood Management in India: Technology Driven Solution.” We also thank Greater Hyderabad Municipal Corporation for sharing technical data. The Landsat satellite images are downloaded from the United States Geological Survey.

## References

1. Awakimjan I (2015) Urban flood modelling recommendations for Ciudad del Plata. Bachelor thesis, University of Twente, Netherland
2. Adnan NA, Atkinson PM (2012) Remote sensing of river bathymetry for use in hydraulic model prediction of flood inundation. In: IEEE 8th international colloquium on signal processing and its applications, pp. 159–163
3. Chang TJ, Wang CH, Chen AS (2015) A novel approach to model dynamic flow interactions between storm sewer system and overland surface for different land covers in urban areas. *J Hydrol* 524:662–679
4. Halwatura D, Najim MM (2013) Application of the HEC-HMS model for runoff simulation in a tropical catchment. *Environ Model Softw* 46:155–162
5. Hashemyan F, Khaleghi MR, Kamyar M (2015, August) Combination of HEC-HMS and HEC-RAS models in GIS in order to simulate flood (case study: Khoshke Rudan river in Fars province, Iran). *Res J Recent Sci* 4(8):122–127
6. Jinkang D, Li Q, Hanyi R, Tianhui Z, Dapeng Z, Youpeng X, Xu CY (2012) Assessing the effects of urbanization on annual runoff and flood events using an integrated hydrological modeling system for Qinhuai river basin, China. *J Hydrol* 464–465:127–139
7. Lastra J, Fernandez E, Diez-herrero A, Marquinez J (2008) Flood hazard delineation combining geomorphological and hydrological methods: an example in the Northern Iberian Peninsula. *Nat Hazards* 45:277–293
8. Magesh NS, Ch N (2012) A GIS based automated extraction tool for the analysis of basin morphometry. *Bonfring Int J Ind Eng Manag Sci* 2(Special issue special issue on geospatial technology development in natural resource and disaster management):32–35
9. Ranaee E, Mahmoodian M, Quchani SR (2009) The combination of HEC-Geo-HMS, HEC-HMS and MIKE11 software utilize in a two branches river flood routing modeling. In: Second international conference on environmental and computer science, IEEE, pp 317–321
10. Ray SM (2012) Simulation of runoff and flood inundation in Kosi river basin using hydrological models, ANN, remote sensing and GIS. M. Tech thesis, National Institute of Technology Rourkela
11. Suriya S, Mudgal BV (2012) Impact of urbanization on flooding: the Thirusoolam sub watershed—a case study. *J Hydrol* 412–413:210–219
12. U.S. Army Corps of Engineers Hydrologic Engineering Center (2013) HEC-GeoHMS user’s manual, Version 10.1, Davis, CA
13. U.S. Army Corps of Engineers Hydrologic Engineering Center (2010) Hydrologic modeling system HEC-HMS. User’s manual, Hydrologic Engineering Center
14. Voyant’s Solutions Pvt. Ltd. <http://www.voyants.in>. Hyderabad Zonal Office

15. WMO (World Meteorological Organization) (2009) Integrated flood management concept paper. WMO-No. 1047
16. Zameer A, Rao RM, Reddy K (2013) Urban flooding—case study of Hyderabad. Glob J Eng Des Technol 2(4):63–66

# Hydrodynamic Simulation of River Ambica for Riverbed Assessment: A Case Study of Navsari Region



Darshan Jayeshbhai Mehta and Sanjay Madhusudan Yadav

**Abstract** Physically based hydraulic or hydrological model will simulate the dynamics flow water of a river network against space and time with varying reach boundary conditions that may be enforced for the case of Ambica river stream. Such stream models refers to the physically based hydrologic or hydraulic models which usually helps in crucial part of flood prediction, flood forecasting and fluctuation of tidal that forecasts river levels in flood prone areas off the center stream of Ambica river. For the setting of a any river model, the measurements of river geometry, bed depth/slope, floodplain mapping and boundary condition flow are essential. The discharge and water level in the river reach of Ambika are controlled by Jhuj and Kelia dam which is 68.9 and 57.6 km away from Navsari city, respectively. Major flood events occurred in the years 1981, 1994, 1997, 2001, 2003, 2004, 2005, 2006, 2007, 2013 and 2014. Therefore, it becomes highly necessary that flood events are studied and analysed properly in order to propose adequate flood control and protection measures in time to come. At present, the carrying capacity of Ambica River is approximately around 2.5 lakhs cusecs ( $7079 \text{ m}^3/\text{s}$ ). In this paper, we used one-dimensional model which is released by US Army Corps of Engineers, i.e. HEC-RAS 5.0.4. over the river reach of Ambica, Navsari. In this paper, hydrodynamic simulation is performed to compute the water surface profiles for five-peak flood discharge of year 1981, 1994, 1997, 2004 and 2006. Thus, in this present paper from Ichhapore to Salej village which is approximately 1170 m long is selected for study purpose. The computed sections are then compared with existing sections on the river reach and are checked whether the sections are critical or not. Based on above study, it is recommended that the cross sections which the water is overtopped on the existing section, levees or retaining is to be constructed or need to be raised.

**Keywords** Ambica river · Floods · HEC-RAS · Hydrodynamic model

---

D. J. Mehta (✉)

Dr. S & S. S. Ghandhy Government Engineering College, Surat, India  
e-mail: [darshanmehta2490@gmail.com](mailto:darshanmehta2490@gmail.com)

S. M. Yadav

Sardar Vallabhbhai National Institute of Technology, Surat, India

## 1 Introduction

Flood occurs due to natural and also by precipitation, insufficient volume within banks of river or channels and silting of riverbeds. Furthermore, different variables like landslides leading the river course, unusual outlet, cyclone and dense rainstorms, snowmelt and glacial outbursts, and breaking of dam. For reducing such flood losses, many preventive steps are to be adopted [1]. The flood preventive or control measures can be termed as “flood management” which can be protected through structural as well as non-structural measures. The use of engineering challenges and real science has built up method of reducing the consequences because of floods and giving sensible protection in response to security to life as well as property [2]. For the analysis of floods, there are many software in field like RiverCad software which is given by the BOSS international, and RiverCad is the allowed to user to display HEC-RAS output in AutoCAD [3]. CAD gives good environment for visualization, and GIS provides tools for more complex problem, storage, flood mapping and visualization of temporal spatial data [4]. After running HEC-RAS, GIS stream pro can describe the floodplain in Arc View GIS [5]. In future, some climatic movements cause an extraordinary difference in the water which is available in various regions. As a result, face of human life which includes production of agricultural, environment, nature and management of fish, use of energy, industrialized, domestic and urban water supply, and control of flood would be influenced. There are various other software like TUT FLOW, Mike-11, River Tool, River Flow 2D are utilized for the river modelling, flood analysis, etc. [6, 7]. Now, river reach can be created from terrain model which contains adequate determination for hydraulic modelling in HEC-RAS [8, 9]. Due to heavy rainfall on the upstream side Ambica River is flooded, therefore it is necessary to predict the flood and prepare flood mitigation plan [10]. Now, urgent requirement of various hydrodynamic model, which is used to carry out analysis as well as predict the flood water level on the any part of the Ambica basin. For assessment of flood, selected study area Ambica river basin, Navsari, in there are 39 cross sections in length of study reach is 1.17 kilometres long. This sub-catchment is situated in the plain and hilly region of Gujarat, and Maharashtra depleted by Kapri, Wallan, Kaveri and Kharera. In perspective of the over, the present examination endeavours to build up a hydrodynamic model to propose appropriate measures by method for channel or dike changes by utilizing hydrodynamic model for the Ambica basin, Navsari, Gujarat, for different flood events.

## 2 Objective of Study

The objective of the study is to analyse the portion or segment of lower Ambica river basin of Navsari region by assessing its river capacity of storage in response to flood magnitude of a particular year as well as slope.

### 3 Study Area

Navsari district is situated in the southern part of Gujarat State. It is one of the most important districts in Gujarat State bifurcated from Valsad district. It lies between Latitude 20°32' and 21°05' North and Longitude 72°42' and 73°30' East and falls in Survey of India Toposheet No's 46C, 46D, 46G and 46H. It is bounded by Surat district in the north, Dangs district in the east, Valsad district in the South and Arabian Sea in the west. Navsari district has a geographical area of about 2210.97 km<sup>2</sup>.

In Ambica basin, the information accessible at Kudkas G&D site located across Khapri River just upstream of proposed Dabdar dam site has been utilized for hydrological analysis at proposed Dabdar and Chikkar dam sites. The observed discharge data at Kudkas G&D site has been utilize to develop yield series for proposed Dabdar dam site from the year 1980 to 2006. The proposed Chikkar and Dabdar dam sites are located very close to each other and have same hydrometeorological characteristics. Hence, the G&D data available at Kudkas G&D site has been used for hydrological study of Chikkar dam also.

Figure 1 shows the study area of Ambica River from Ichhapore to Salej village, and Fig. 2 shows the location of rain gauges. Following are the details of the study area:

- Total number of the cross section are 39 (CS-1680 to CS-2820).
- River reach length is 1170 m (1.17 km).
- Red line indicates cross section in river reach.
- Yellow line indicates centreline of river.
- Average interval between one cross section to another is 30 metres.
- Upstream—Ichhapore.
- Downstream—Salej Bridge.

Figures 3, 4, 5, 6, 7, and 8 are the images of study area.

Ambica River is one of the flowing rivers from South of Tapi adjoining catchment in Gujarat as well as Maharashtra. Heavy rainfall occurred in the basin from the S-W monsoon season in the month of June to September. Flood occurs at Ambica basin frequently due to excess rainfall. Thus, the reason for selecting this area was the frequent flooding events occurring in Ambica basin. Due to floods in Ambica River, Devdha village and nearby regions and areas are affected. Since long back from past, the study region has been facing numerous flood events. These floods occurred in the year 1981, 1984, 1994, 1997, 2004 and 2006. The Devdha village and nearby areas and region are part improper drainage of flood of Ambica River. It has been observed that the either banks of the river have lower or broken levees. Present study aims to identify such sections from where water may enter in the study region.

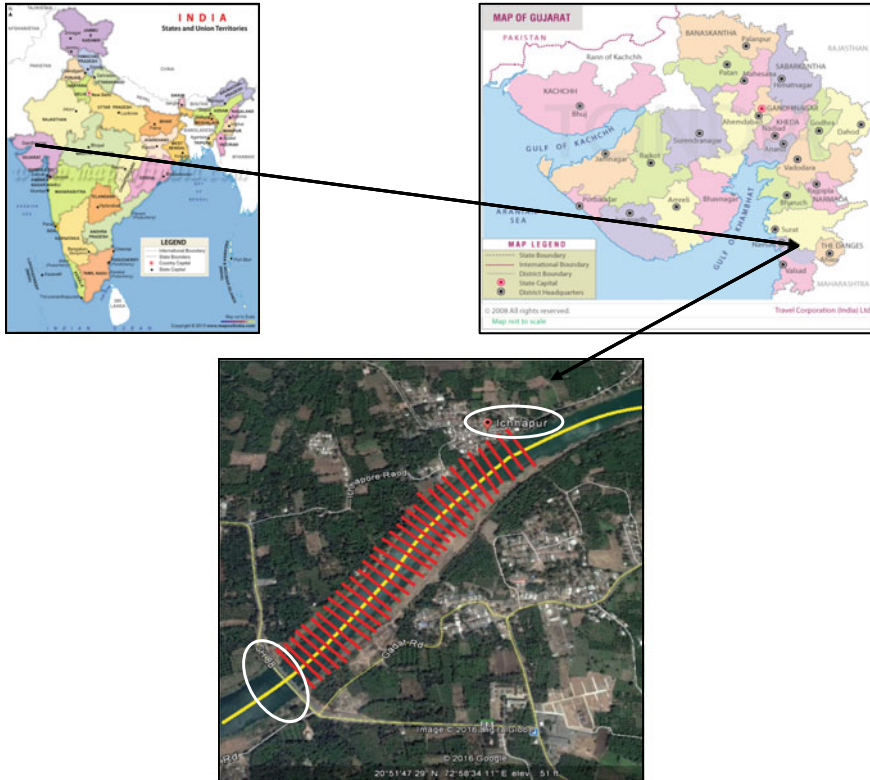


Fig. 1 Study area with cross-sectional details

#### 4 Overview of HEC-RAS Software

HEC-RAS was first published/ released in 1995 by US army with version of 4.0.1 and further latest with modified feature version was released in 2010. In our study, HEC-RAS 5.0.4 hydraulic design function was used for flood analysis. The new features in the software were added by the Hydrologic Engineering Centre (HEC), Institute for Water Resources (IWR), US Army Corps of Engineers. HEC-RAS is “programming that enables users to carry out steady and unsteady flow analysis as well as river hydraulics, i.e. computation of uniform flow, estimation of sediment transport capacity, design of stable channel and analysis of water quality.”

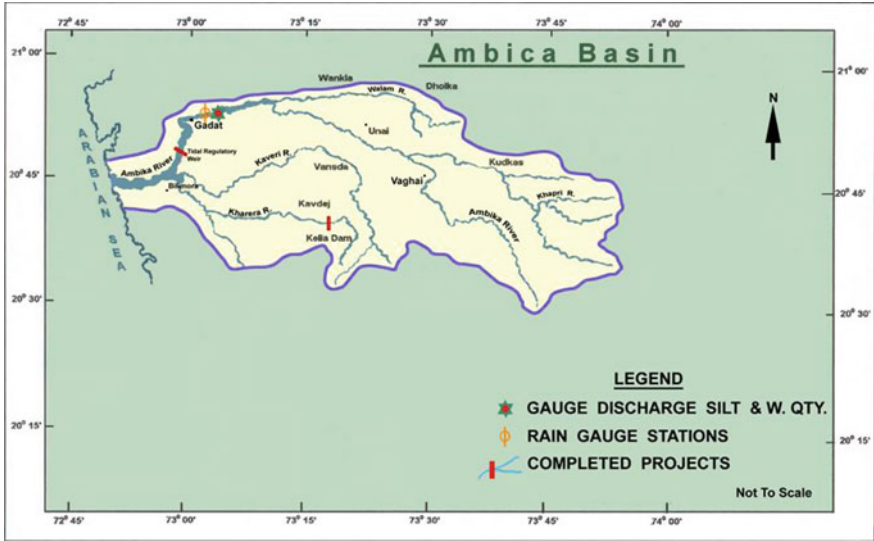


Fig. 2 Location of rain guages

Fig. 3 U/S side of Ambica river



### 4.1 HEC-RAS Input Parameters for Steady Flow Analysis

Figure 9 represents a definition sketch for the stream. In this, the stream width is divided into three segments as main channel, left bank flood way and right bank flood way. The location of left bank station and right bank station is also marked in the definition sketch. The typical water surface and flood water surface are shown in Fig. 9.

**Fig. 4** D/S side of Ambica river



**Fig. 5** Water level measuring scale



**Fig. 6** Flood level indicator







**Fig. 7** Ambica river, Study area



**Fig. 8** Ambica river, Study area

## **4.2 Geometric Data**

The geometric data of study reach collected from the field is the contribution for the development of cross segment geometry in HEC-RAS. The fundamental geometric data comprises cross-sectional data; reach lengths; creating in what way the different stream reaches is joined and stream junction information. The study reach consists of 39 cross sections. The detailed cross sections of river Ambica showing bed and bank level at an average interval of 30 m were collected from Irrigation Colony, Navsari.

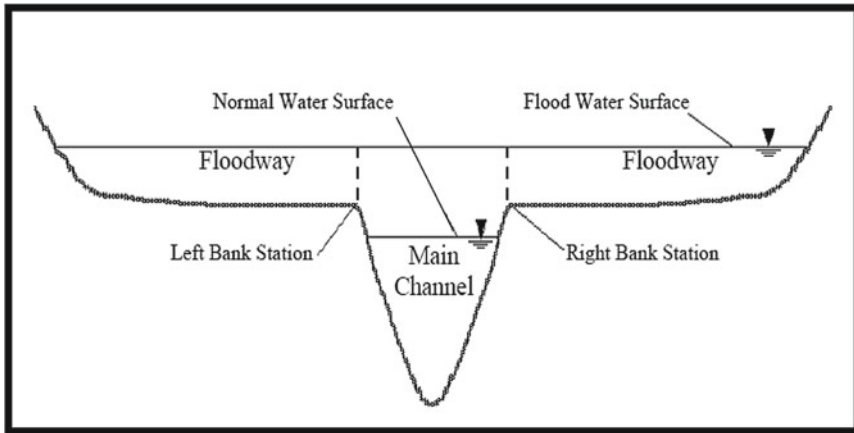


Fig. 9 Stream Schematic diagram

### 4.3 Cross-Sectional Geometry

For assessment of the any profile flow in river reach, the geometry is to be created or prepared with the help of cross-sectional data which is collected from hydraulic department. Distance between any two consecutive cross sections is referred to as length of reach. Cross sections were constructed to be perpendicular to the foreseen flow lines. The river section is represented by giving input as stations on x-axis and their elevations on y-axis.

### 4.4 Steady Flow Data

To execute any surface profile of water or level of water, flow profile is required to be entered. Discharge profile is comprised of flow regime, boundary conditions, discharge. These data comprise of:

- Cross sections are from u/s to d/s to be computed;
- the peak flood discharge of any year;
- And the boundary conditions (normal depth as bed slope is taken in our study).

Enter one peak discharge for every river cross section. Flow can be changed additionally as per the flood events within the river system.

**Table 1** Navsari region flood events

Sr. No.	Year	Discharge (cumecs)	Discharge (cusecs)	Velocity (m/s)
1	1981	11,000	388,163	3.47
2	1994	6500	229,369	3.33
3	1997	3200	112,920	3.03
4	2004	5000	176,437	3.28
5	2006	2750	97,040	2.93

Source Drainage Division Navsari/SWDC, Gandhinagar

## 5 Flood Conveyance Performance

For evaluating flood performance, past flood data from Drainage Division, Navsari and SWDC, Gandhinagar were collected and used. Flood frequency analysis results were based on simulation which corresponds within the u/s limit of the river reach which is selected for study purpose. Heavy rainfall results in flood which took place in 1981, 1994 and 2004. Table 1 shows the summary of flood event in Navsari City.

## 6 Methodology

For steady flow analysis and uniform flow computations, following steps are to be carried out using HEC-RAS hydraulic design functions:

**Step 1:** Create a new project from HEC-RAS software main window.

**Step 2:** Now, from edit option go to geometry editor to create a new river and reach. Name of River: Ambica

Reach Name: Ichhapore to Salej Bridge

**Step 3:** Enter the geometric data, i.e. cross-sectional data of river

**Step 4:** After adding 39 cross sections of study area, HEC-RAS software will draw the same cross section of Ambica River which is collected from Hydraulic Department of Navsari division.

**Step 5:** Enter the value “ $n$ ” for upstream reach. The “ $n$ ” value depends on bed material and can be selected as per the river reach bed material. For present study, value of ‘ $n$ ’ is taken as 0.035 for banks and 0.050 for channel (bed).

**Step 6:** Steady flow data is required to be entered in this step for different flood peak discharges.

**Step 7:** Go to run functions, select hydraulic design function in main window and then uniform flow computation in hydraulic design function.

**Step 8:** In this step, discharge of one flood event of specific year is to be entered for first cross section, in uniform flow window in hydraulic design. Repeat the procedure for remaining 38 cross sections.

**Step 9:** When the discharge of one flood event is entered, select compute in the same window.

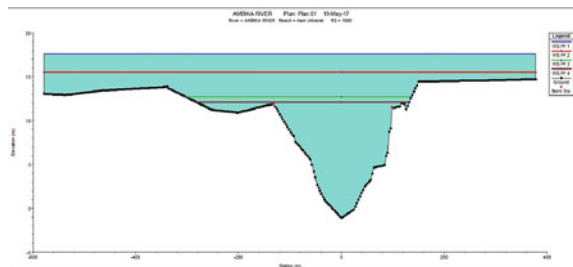
**Step 10:** After computation, HEC-RAS software shows whether a particular section is overtopped or not for given flood discharge. If the section is overtopped with given flood discharge, software will suggest to construct levees in that particular section. Same process will be carried out for all the 39 cross sections for the river reach of Ambica basin.

## 7 Findings and Discussion

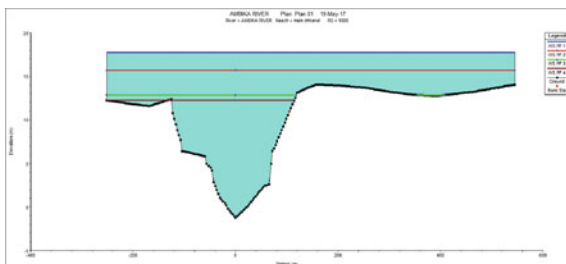
Analysis of steady flow using HEC-RAS (5.0.4) is carried out for 1.17 km span of Ambica river basin from d/s Salej Bridge to Ichhapore taking 39 cross sections. The simulation was also carried out for historical floods of 1981, 1994, 1997 and 2006 years. For this purpose, analysis of software is developed for Ambica river basin. A study meted out on management of disaster recommends that there is a necessity of an early warning system along with some protective measure as well as mitigation plan to minimize those area due to Ambica River flood. When all the data are entered and software has finished, the steady flow simulations to view the output are in a graphical and tabular format. The study deals with the assessment of urban flood area i.e. Ambica river basin of Navsari city using the significant historical flood events. From the above analysis, results show that the computed surface water profile at 1.17 km for 1981, 1994, 1997 and 2006 years magnitude of flood, respectively. Accordingly, the surface profile of water relating to other sections of the river may also be computed. The sections are delegated as highly critical (when the water profile is above existing bank, i.e.  $>0.7$  m), moderately critical (when the water profile above existing bank, i.e.  $0.4\text{--}0.7$  m) and critical (when the water profile above existing bank, i.e.  $0.4$  m). Figure 10, 11, 12, 13, 14, 15, 16 and 17 presents computed section using HEC-RAS software and past flood events.

The flow profile in the channel as, 11,000, 6500, 3200 and 2750 cumecs, has been considered for analysis of steady flow as well as for computation of uniform flow. When the values of flood magnitude are used as input at all the 39 sections of river

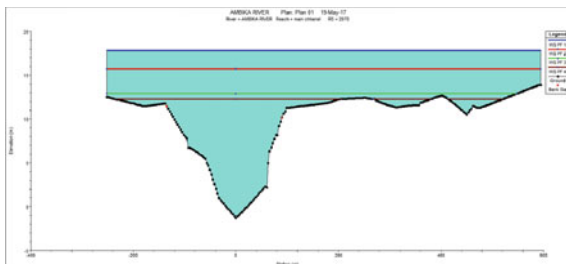
**Fig. 10** Computed CS-1680



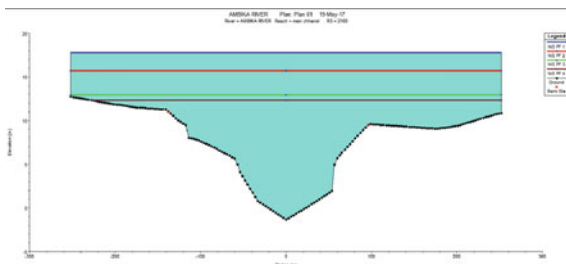
**Fig. 11** Computed CS-1980



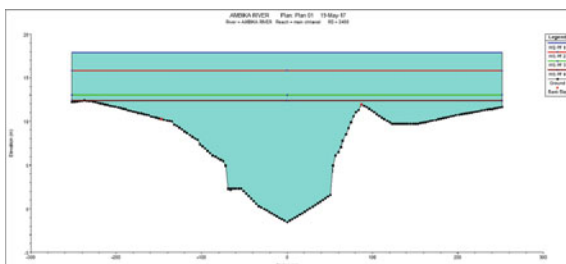
**Fig. 12** Computed CS-2070

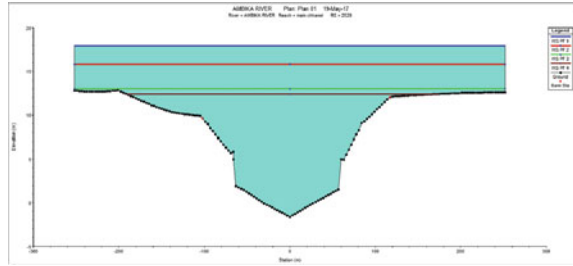
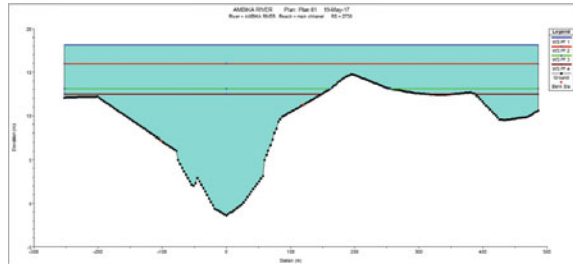
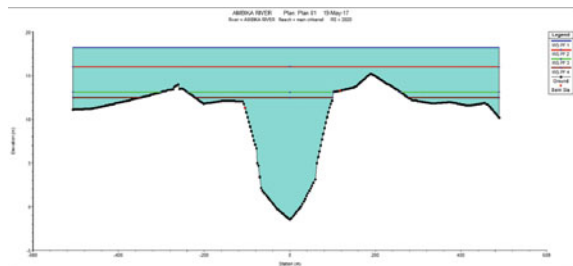


**Fig. 13** Computed CS-2160



**Fig. 14** Computed CS-2400



**Fig. 15** Computed CS-2520**Fig. 16** Computed CS-2730**Fig. 17** Computed CS-2820

reach, the result obtained from analysis is described in Figs. 10, 11, 12, 13, 14, 15, 16 and 17.

Following are the findings from the above analysis:

1. **At cross-section 1680**, for the release of 11,000 and 6500 cumecs discharge the sections are not adequate to carry the flow; however for the release of 3200 and 2750 cumecs discharge, the section is adequate.
2. **At cross-section 1980**, for the release of 11,000 and 6500 cumecs discharge, the section is not adequate to carry the flow; however for the release of 3200 and 2750 cumecs discharge, the section is adequate.
3. **At cross-section 2070**, for the release of 11,000 and 6500 cumecs discharge, the section is not adequate to carry the flow; however for the release of 3200 and 2750 cumecs discharge, the section is adequate.
4. **At cross-section 2160**, for the release of 11,000 and 6500 cumecs discharge the section is not adequate to carry the flow; however for the release of 3200 and

- 2750 cumecs discharge, the section is adequate to carry the flow on left bank only, as the right bank is not adequate.
5. **At cross-section 2400**, for the release of 11,000, 6500 and 3200 cumecs discharge the section is not adequate to carry the flow; however for the release of 2750 cumecs discharge, the section is not adequate to carry the flow on left bank only, as the right bank is not adequate.
  6. **At cross-section 2520**, for the release of 11,000 and 6500 cumecs discharge the section is not sufficient to carry the flow; however for the release of 3200 and 2750 cumecs discharge, the cross section is adequate.
  7. **At cross-section 2730**, for the release of 11,000 and 6500 cumecs discharge the section is not adequate to carry the flow; however for the release of 3200 and 2750 cumecs discharge, the cross section is adequate.
  8. **At cross-section 2820**, for the release of 11,000 and 6500 cumecs discharge the section is not adequate to carry the flow; however for the release of 3200 and 2750 cumecs discharge, the cross section is adequate.

As we can see from all the figures that maximum flooded area or overtopped cross sections are from CS-1680 to CS-2820 except 3200 and 2750 cumecs discharge. It has been observed that, due to encroachment on flood plain areas by agricultural activity the width of Ambica river in between these cross-sections is very small which restrict the natural flow of river in this reach. Thus, the effective cross section of the river has changed resulting in the less carrying capacity of the flood discharge causing flooding of surrounding area or region in the downstream part of the river. Construction of embankment, stone pitching, bunds and protection retaining walls along the side of river banks is to be recommended for the area which affected by flood. In addition, the people in the flood influenced regions found the easy system of warning or awareness to understand and utilize because they only need to observe or notice the water level in the river at u/s and d/s areas of the study reach.

## 8 Conclusions and Recommendations

In the above study, hydraulic or hydrodynamic software generated to assess the levels of water surface along the river from Salej Bridge to Ichhapore for flood magnitude. The river cross-sectional details at 39 locations along the Ambica River obtained from hydraulic department of Navsari division and the chainage read from 1:10,000 topo sheets. Flood study of year 1981, 1994 and 2004 has been done to assess inundation of the area downstream of the dam with the help of these models. It has been observed that flood would be occurred when the discharge from the dam would be generated than 3200 cumecs. With this discharge, surrounding region as well as villages and farms have been inundated. From the past flood magnitude, it is recommended to increase the capacity of Ambica basin, so as to reduce flood effects in and around surrounding region of Navsari City. Based on above study, sections which overtops over the existing water surface profile levees or flood protection walls need to be

raised. As an alternative option to alleviate flood, station and elevation clearance may possibly be kept high to diminish the devastation of floods in the flood prone locales of Ambica River.

**Acknowledgements** The authors are grateful to all the staff members of Navsari Irrigation Circle, State Water Data Center, Gandhinagar, for providing necessary data for this research work. The authors are thankful to Prof. B. M. Vadher, Dr. S. & S. S. Ghandhy Government Engineering College, Surat, for granting the permission to carry out the research work jointly.

## References

1. Shelly J, Parr David A (2009) Hydraulic design functions for Geomorphic channel design and analysis using HEC-RAS. *J World Environ Water Resour Congr* 2(3):41–50
2. Mondal I, Bandhyopadhyay J, Paul AK (2016) Estimation of hydrodynamic pattern change of Ichamati river using HEC-RAS model, West Bengal, India. *J Model Earth Syst Environ* 125(2):1–13
3. Yadav SM, Mehta DJ, Waikhom S (2013) Analysis of flood using HEC-RAS: a case study of Surat city. In: *Proceedings of international conference (HYDRO–2013)*, Chennai, Madras
4. Mehta DJ, Ramani MM, Joshi MM (2013) Application of 1-D HEC-RAS model in design of channels. *Methodology* 1(7):4–62
5. Salajegheh A (2010) Floodplain mapping using HEC-RAS and GIS in semi-arid regions of Iran. *Desert* 14(1):83–93
6. Agnihotri PG, Patel JN (2011) Improving carrying capacity of River Tapi (Surat, India) by channel modification. *Int J Adv Eng Technol* 2(5):231–238
7. Parhi P (2018) Flood management in Mahanadi Basin using HEC-RAS and Gumbel's extreme value distribution. Springer, *J. Inst. Eng. India Ser. A*
8. Mehta D, Yadav SM, Waikhom S (2013) Geomorphic Channel Design and Analysis using HEC-RAS hydraulic design functions. *Paripex Int J Glob Res Anal* 2(4):90–93
9. Patel A, Patel D, Prakash I (2016) Flood modelling using HEC-RAS and geo-informatics technology in lower reaches of Shetrunji River, Gujarat, India. In: *Proceedings of national conference on water resources & flood management with special reference to flood modeling*, Oct 14–15, 2016, Surat
10. Mansoor CN (2014). Flood hazard zonation mapping using geoinformatics technology; Benihalla Basin, Gadag and Dharwad District, Karnataka, India. *Int J Eng Res Technol* 3(9). ESRSA Publications



# Evaluation of the SWAT Model for Analysing the Water Balance Components for the Upper Sabarmati Basin



Ankit Gupta , Sushil K. Himanshu , Shivam Gupta  and Ronald Singh

**Abstract** Evaluation of various components of hydrologic cycle is necessary for planning and management of a river basin/watershed. The present study evaluated the water balance components in parts of upper Sabarmati basin (6211.56 km<sup>2</sup>) of central India using the soil and water assessment tool (SWAT) hydrologic model. The river basin was delineated to 31 sub-basins encompassing 116 hydrologic response units (HRUs). Monthly calibration (1992–1999) and validation (2000–2005) of the SWAT model were carried out using observed discharge data at Derol Bridge, Gujarat, India. Trend analysis results over the period of 1992–2005 for run-off and evapotranspiration shows an insignificant decreasing trend, along with decrease in precipitation with a magnitude of 21 mm/year. The model simulation results indicated a reduction in surface run-off (323.49–232.14 mm) and potential evapotranspiration (1935.71–1875.71 mm) between years 1992 and 2005. The present study also revealed a considerable decrease in water yield (493.2–317.6 mm) for same duration.

**Keywords** Soil and Water Assessment Tool · Water balance study · Trend analysis · Upper Sabarmati Basin · Hydrologic modelling

## 1 Introduction

The demographic changes, land and water use policies, climate change along with irregular frequency and intensity of rainfall influence the water resources which are crucial for growth and sustainable development. It is necessary to evaluate the changes in hydrological processes running in a watershed, at various spatio-temporal

---

A. Gupta (✉) · S. K. Himanshu · S. Gupta · R. Singh  
National Remote Sensing Centre, ISRO, Hyderabad, India  
e-mail: [ankitgupta.isro@gmail.com](mailto:ankitgupta.isro@gmail.com); [ankitgupta@nrsdc.gov.in](mailto:ankitgupta@nrsdc.gov.in)

S. K. Himanshu  
Indian Institute of Technology, Roorkee, India

S. Gupta  
Indian Institute of Technology, Guwahati, India

© Springer Nature Singapore Pte Ltd. 2020  
R. AlKhaddar et al. (eds.), *Advances in Water Resources Engineering and Management*, Lecture Notes in Civil Engineering 39,  
[https://doi.org/10.1007/978-981-13-8181-2\\_11](https://doi.org/10.1007/978-981-13-8181-2_11)

scales for reliable watershed management, as it serves as hydrological unit [1]. The present research implies applications of integrated remote sensing derived products within a geographic information system (GIS) modelling framework for hydrological investigation and assessment of water resources [2]. Availability of powerful computing tools including geographic information system (GIS) helps to overcome limitations and difficulties to develop continuous distributed models, based on available regional information [3–6].

Models are categorized into three classes, viz., empirical, conceptual and physically based, on the basis of model algorithm, data dependency of models and their applicability in simulation of physical processes [2]. Physically based modelling has always been the primary choice of researchers when dealing with complex problems like evaluation of water balance components [7]. These models use various empirical and complex physical-based mathematical formulae to represent major components of hydrological cycle. Models are also categorized to lumped, semi-distributed and distributed, based on degree to which spatial parameters affect the hydrological modelling processes [8, 9].

Limitations of hydro-meteorological datasets and decision support tools largely affect the research activities in the field of water resources. In the present study, the semi-distributed soil and water assessment tool (SWAT) hydrologic model was used for assessment of water balance components. The SWAT model has been proven as an effective model to study hydrological impacts around the world which can be used for understanding the effects of future development and management activities [10–13]. Various other methods were also used previously to simulate hydrology and soils, water balance components, land use and management [14]. Continuous models were also developed but commonly lacked adequate spatial detail [15, 16]. Whereas, in different spatial horizons, analysing rainfall variability and pattern of trends in water balance components in arid and semi-arid regions, have been vital aspect in hydrological studies [17–19].

The present study was carried out primarily to assess the water balance components over the upper Sabarmati basin using the SWAT model on monthly basis. Further, monthly average water balance over the entire basin was estimated. Observed hydro-meteorological dataset availability, heterogeneous land use and absence of any large storage structures make the basin favourable for present research work.

## 2 Study Area and Data Used

The study extent is parts of upper Sabarmati basin up to Derol Bridge as an outlet in Gujarat state, extends over an area of 6211.56 km<sup>2</sup> and lies between the geographical extent of north 23.578° to 24.917° latitude and east 72.698° to 73.597° longitude (Fig. 1). Study area extent has an elongated shape with a maximum length of 159.70 km from north to south and maximum width of 65.65 km from west to east. Nearly equal upper and lower portion of the study area is in two states viz., Gujarat and Rajasthan. Highest elevation in the area is 1173 m and lowest is 88 m.

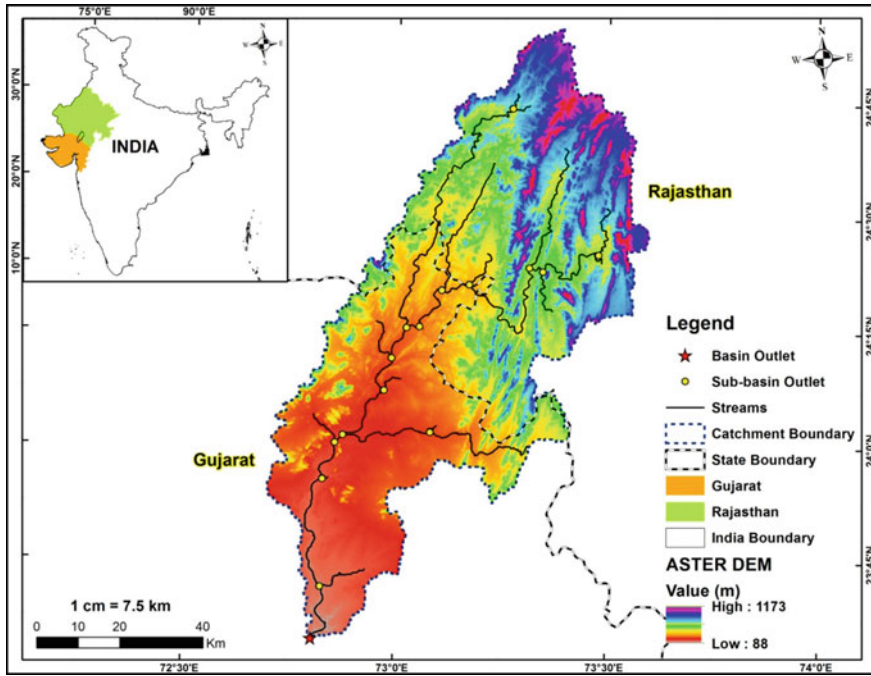


Fig. 1 Location map of the study area

Basin portion up to Derol Bridge receives annual average rainfall of 790 mm while it is higher in upper portion.

In the present study, the ASTER DEM with resolution of 30 m has been used for topographic database generation along with land use layer prepared from AWiFS remote sensing satellite data procured from National Remote Sensing Centre (NRSC) for year 2010–11 and soil data from National Bureau of Soil Survey and Land Use Planning (NBSSLUP) (both in Fig. 2, along with slope derived from DEM). The daily precipitation and temperature data were procured from Indian Meteorological Department (IMD). For calibration and validation of the hydrological model, observed daily discharge data from India—Water Resources Information System (WRIS) has been used.

### 3 Methodology

The SWAT hydrologic model is a semi-distributed, continuous timescale model, to estimate the impacts of different management practices on water resources and non-point source effluence [20]. Its expanding global use as well as several subsequent releases including its 2005 version was also described in detail [21, 22].

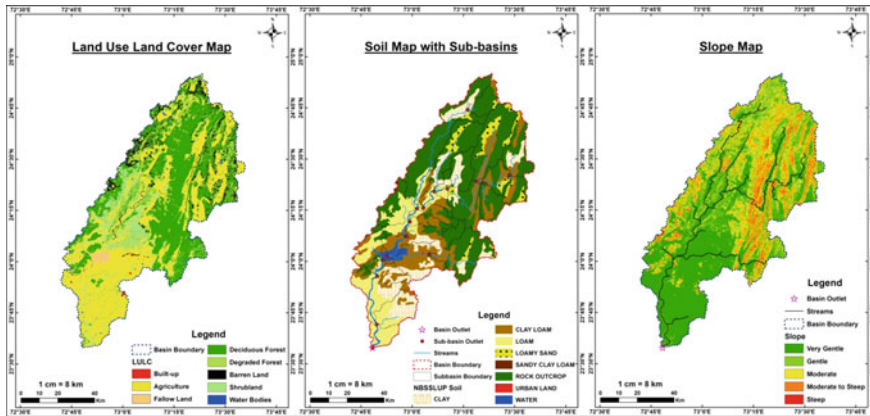


**Fig. 2** Land use and land cover, soil, slope map of the study area

SWAT uses the soil conservation service curve number (SCS-CN) technique to estimate surface run-off which narrates run-off to soil type, land use and management practices and is computationally efficient [23]. It has been used extensively worldwide for run-off simulation and sediment simulations for non-point source pollution estimation. It has also been used widely for simulation of streamflow at ungauged river basins and climate change impact assessment [24–26]. Numerous supplementary technical details about the model were also given [27]. In this study, we focus on in assessing the hydrologic components for water balance study using this efficient model in the parts of upper Sabarmati river basin also to predict the streamflow in the different sub-basins.

Model calibration was done within suggested range to enhance the model output so that it matches with the observed dataset and before that sensitivity analysis has also performed to identify the most sensitive parameters [28, 29]. The time series data of discharge were available for the Derol Bridge gauging station which was used to calibrate the discharge and to evaluate the model parameters.

### 3.1 Trend Analysis

Trend analysis was carried out using the Mann-Kendall (M-K) non-parametric test, and magnitudes of change were assessed using the Sen's slope estimator [30].

### 3.1.1 M-K Non-parametric Test

The M-K statistics ( $S$ ) is defined as

$$S = \sum_{i=1}^{N-1} \sum_{j=i+1}^N \text{sgn}(x_j - x_i) \quad (1)$$

where  $N$  = number of observed data in time series. Assuming  $(x_j - x_i) = \theta$ , the  $\text{sgn}(\theta)$  is calculated as

$$\text{sgn}(\theta) = \begin{cases} 1 & \text{if } \theta > 0 \\ 0 & \text{if } \theta = 0 \\ -1 & \text{if } \theta < 0 \end{cases} \quad (2)$$

This statistic indicates number of positive differences minus the number of negative differences for all the differences considered. For larger sample ( $N > 10$ ), the test is carried out using normal distribution

$$\text{Var}(S) = \frac{N(N-1)(2N+5) - \sum_{k=1}^n t_k(t_k-1)(2t_k+5)}{18} \quad (3)$$

where  $t_k$  = number of data points in the  $k$ th tied group and  $n$  = number of tied (zero difference between compared values) groups.

$$Z = \begin{cases} \frac{S-1}{\sqrt{\text{Var}(S)}} & \text{if } S > 0 \\ 0 & \text{if } S = 0 \\ \frac{S+1}{\sqrt{\text{Var}(S)}} & \text{if } S < 0 \end{cases} \quad (4)$$

Value of  $Z$  was estimated and if the value of  $Z$  lies within the limit of  $\pm 1.96$ , the null hypothesis of having no trend in the series cannot be rejected at 95% level of confidence.

### 3.1.2 Sen's Slope Estimator

Sen's estimator, a non-parametric method was used to determine the magnitude of trend in a time series [31]. In this method, the slopes ( $T_i$ ) of all data pairs are calculated first by

$$T_i = \frac{x_j - x_k}{j - k} \quad \text{For } i = 1, 2, \dots, N \quad (5)$$

where  $x_j$  and  $x_k$  are data values at time  $j$  and  $k$  ( $j > k$ ), respectively. The median of these  $N$  values of  $T_i$  gives the Sen's estimator of slope ( $\beta$ ). A negative value of  $\beta$  indicates a downward trend, and a positive value indicates an upward trend.

## 4 Results and Discussion

### 4.1 Model Setup

SWAT addresses the spatial variability of land use, soil and climatic variables through sub-basin and hydrological response unit (HRU) approach. The study area has been divided into 31 sub-basins and 116 Hydrological Response Unit's (HRUs). The HRUs of this catchment have been categorized into different classes mainly on the basis of uniformity in land use, soil and slope. Study area is deciduous forested area with larger extent followed by generic agricultural land and agricultural land of row crops, also catchment area has 61% gentle slope and 8.9% of steep rise in upper portion (Fig. 2). The higher altitude area contributes high run-off and significant amount of soil erosion, especially during monsoon periods may be partly due to inadequate management practices. Table 1 shows the distribution of different land use land cover, soils and slope classes distribution over the river basin.

### 4.2 Sensitivity and Uncertainty Analysis

In the present study, sensitivity and uncertainty analysis was carried out using the SUFI-2 algorithm of the SWAT-CUP program. Total 17 parameters were considered, most sensitive parameters based on ranking were considered for model calibration. The sensitivity analysis revealed that discharge is most sensitive to CH\_N2 (Manning's 'n' value for the main channel) followed by CH\_K2 (Effective hydraulic conductivity in main channel alluvium).

### 4.3 Calibration and Validation

Physical-based hydrological model considers large number of parameters for simulation of the output variables such as streamflow and evapotranspiration, which makes calibration a rigorous process. SWAT model accounts land use parameters such as curve number, soil parameters such as hydraulic conductivity, basin parameters such as slope, surface lag and channel parameters, e.g. manning coefficient of the channel.

**Table 1** Detailed land use, soils and slope distribution over Derol watershed

Land use/soil/slope distribution		Area (ha)	% watershed area
Land use	Built-up	660.94	0.11
	Agriculture	226,575.80	36.48
	Fallow land	22,761.6	3.66
	Deciduous forest	210,925	33.96
	Degraded forest	69,215.98	11.14
	Barren land	40,541.77	6.53
	Shrub land	45,541.11	7.33
	Water bodies	4933.417	0.79
Soils	Clay	82,337.03	13.26
	Clay loam	119,079.2	19.17
	Loam	92,150.15	14.84
	Loamy sand	28,842.71	4.64
	Rock outcrop	282,736.7	45.52
	Sandy clay loam	549.4236	0.09
	Urban land	230.3509	0.04
	Water	15,230.02	2.44
Slope	0–3%	199,594.6	32.13
	3–8%	145,888.7	23.49
	8–15%	97,368.45	15.68
	15–35%	134,441.9	21.64
	>35%	43,861.91	7.06

SWAT model for the upper Sabarmati river catchment (up to Derol Bridge) was calibrated using the observed streamflow for the period of 1992–1999. Based on the calibrated values of parameters, model was validated for the period of 2000–2005. Two performance metrics, i.e. coefficient of determination ( $R^2$ ) and Nash Sutcliff coefficient (N-S) were used for evaluating the model performance. Values of  $R^2$  and NS obtained after validation are 0.81 and 0.80, respectively. Figure 3 illustrates the observed and model generated-streamflow for the calibration (1999–1999) and validation period (2000–2005).

#### 4.4 Water Balance Analysis of the Basin

Validated model was further employed for water balance study of the river basin. Sabarmati river comes under the arid climate zone of Rajasthan and Gujarat state where annual average evapotranspiration exceeds the annual average precipitation.

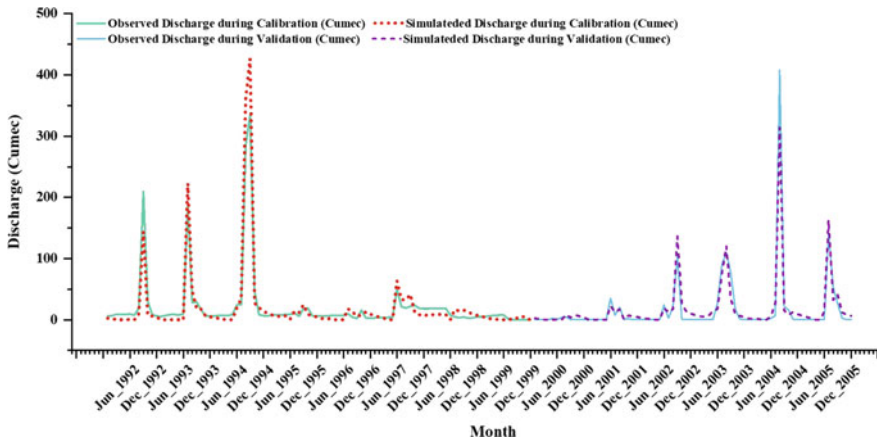


**Fig. 3** Comparison of the observed and SWAT simulated discharge for monthly calibration (1992–1999) and validation (2000–2005)

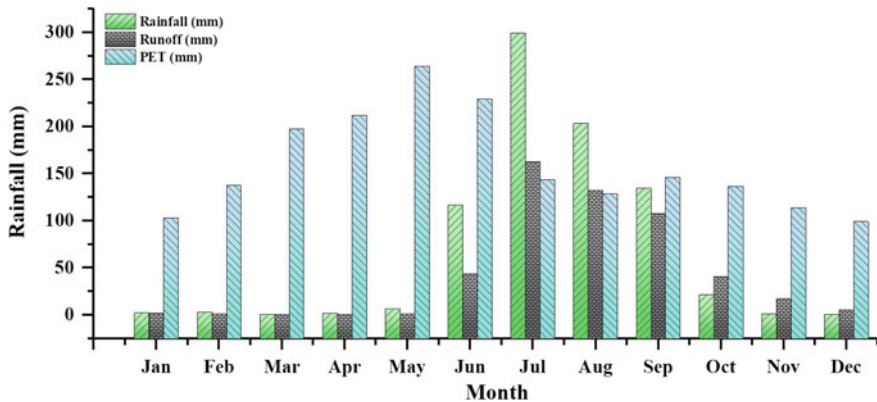


**Fig. 4** Monthly average values of water balance components

Analysis of the water balance component would provide an estimate of the water distribution and which could further be utilized for the better water management plans. Monthly water balance analysis was performed over the period of 1992–2005. Figure 4 represents the monthly distribution of the three water balance components, i.e. rainfall, run-off and evapotranspiration, indicates that major portion of rainfall occurs mostly in the monsoon months and rainfall exceeds the evapotranspiration, in rest of the months evapotranspiration exceeds the rainfall.

Trend analysis of the precipitation, run-off and evapotranspiration was carried out using M-K non-parametric test. Z statistics of MK test represents the significance/non-significance of existing trend at the confidence level of 95%. Trend analysis of the monthly precipitation over the period of 1992–2005 shows an insignificant decreasing trend with a magnitude of 21 mm/year, whereas trend analysis



results of the run-off and evapotranspiration also show insignificant decreasing trend. The final simulation results indicated an insignificant reduction in surface run-off (323.49–232.14 mm) and potential evapotranspiration (1935.71–1875.71 mm) between years 1992 and 2005, along with the considerable decrease in water yield (493.2–317.6 mm) for same duration.

## 5 Conclusion

In this study, streamflow of the Sabarmati river basin (up to Derol Bridge) was simulated using physical-based hydrological modelling which was further utilized for the water balance analysis of the river basin. Model performance was found to be satisfactory for simulating the streamflow of the basin. It has been observed that rainfall of high intensity for short duration may have occurred in the region. Therefore, soil and water conservation measures in this region are highly required which can help in controlling sediment loss and may increase efficient to water storage in the area. SWAT is a powerful tool which has evaluated hydrologic components for water balance study, water flows and productivity of different land uses in these types of catchments very efficiently. An improved conservation measures will prove highly effective in the area. The work presented here desires further evaluation of studies, examination of data, practised knowledge and experimental work.

## References

1. Singh P, Gupta A, Singh M (2014) Hydrological inferences from watershed analysis for water resource management using remote sensing and GIS techniques. *Egypt J Remote Sens Space Sci* 17(2):111–121. <https://doi.org/10.1016/j.ejrs.2014.09.003>
2. Pandey A, Himanshu SK, Mishra SK, Singh VP (2016) Physically based soil erosion and sediment yield models revisited. *CATENA* 147:595–620. <https://doi.org/10.1016/j.catena.2016.08.002>
3. Sahoo S (2013) Assessing hydrological modeling of Bandu River Basin, West Bengal (India). *Int J Remote Sens Geosci* 2(5)
4. Gupta A, Thakur PK, Nikam BR, Chouksey A (2014) Hydrological modelling of upper and middle Narmada Basin using geospatial tools. In: Tiwari HL, Suresh S, Jaiswal RK, Tiwari HL, Suresh S, Jaiswal RK (eds) *Hydraulics, water resources, coastal and environmental engineering* (pp 663–675). Excellent Publishing House, New Delhi, India. <https://doi.org/10.13140/rg.2.1.1065.3688>
5. Himanshu SK, Pandey A, Shrestha P (2017) Application of SWAT in an Indian River basin for modeling runoff, sediment and water balance. *Environ Earth Sci* 76(1):3. <https://doi.org/10.1007/s12665-016-6316-8>
6. Abbaspour KC, Rouholahnejad E, Vaghefi S, Srinivasan R, Yang H, Kløve B (2015) A continental-scale hydrology and water quality model for Europe: calibration and uncertainty of a high-resolution large-scale SWAT model. *J Hydrol* 524:733–752. <https://doi.org/10.1016/j.jhydrol.2015.03.027>

7. Himanshu SK, Pandey A, Patil A (2018) Hydrologic evaluation of the TMPA-3B42V7 precipitation data set over an agricultural watershed using the SWAT model. *J Hydrol Eng* 23(4):05018003. [https://doi.org/10.1061/\(ASCE\)HE.1943-5584.0001629](https://doi.org/10.1061/(ASCE)HE.1943-5584.0001629)
8. Krysanova V, Bronstert A, Müller-Wohlfeil DI (1999) Modelling river discharge for large drainage basins: from lumped to distributed approach. *Hydrol Sci J* 44(2):313–331. <https://doi.org/10.1080/02626669909492224>
9. Singh VP, Frevert DK (2006) *Watershed models* (2005 edn). CRC Press
10. Ficklin DL, Stewart IT, Maurer EP (2013) Effects of projected climate change on the hydrology in the Mono Lake Basin, California. *Clim Change* 116(1):111–131. <https://doi.org/10.1007/s10584-012-0566-6>
11. Tan ML, Ibrahim AL, Yusop Z, Duan Z, Ling L (2015) Impacts of land-use and climate variability on hydrological components in the Johor River basin, Malaysia. *Hydrol Sci J* 60(5):873–889. <https://doi.org/10.1080/02626667.2014.967246>
12. Thampi SG, Raneesh KY, Surya TV (2010) Influence of scale on SWAT model calibration for streamflow in a River Basin in the Humid Tropics. *Water Resour Manage* 24(15):4567–4578. <https://doi.org/10.1007/s11269-010-9676-y>
13. Dhami B, Himanshu SK, Pandey A, Gautam AK (2018) Evaluation of the SWAT model for water balance study of a mountainous snowfed river basin of Nepal. *Environ Earth Sci* 77(1):21. <https://doi.org/10.1007/s12665-017-7210-8>
14. Beasley AP, Huggins LF, Monke EJ (1980) ANSWERS: a model for watershed planning. *Trans ASAE* 23(4):938–944. <https://doi.org/10.13031/2013.34692>
15. Johansen NB, Imhoof JC, Kittle JL, Donigian AS (1984) *Hydrological Simulation Program-Fortran (HSPF): user's manual*. U.S. EPA, Athens, Georgia
16. Arnold JG, Williams JR, Nicks AD, Sammons NB (1990) *SWRRB: a basin scale simulation model for soil and water resources management*. Texas A&M University Press, Texas
17. Gupta A, Kumari M, Rao BK (2017) Spatial and temporal variability analysis using modelled precipitation data in upper catchment of Chambal Basin. In: Abdalla O, Kacimov A, Chen M, Al-Maktoumi A, Al-Hosni T, Clark I (eds) *Water resources in arid areas: the way forward*. Springer Water. Springer, Cham. [https://doi.org/10.1007/978-3-319-51856-5\\_5](https://doi.org/10.1007/978-3-319-51856-5_5)
18. Machiwal D, Gupta A, Jha MK, Kamble T (2018) Analysis of trend in temperature and rainfall time series of an Indian arid region: comparative evaluation of salient techniques. *Theor Appl Climatol*. <https://doi.org/10.1007/s00704-018-2487-4>
19. Gupta A, Kamble T, Machiwal D (2017) Comparison of ordinary and Bayesian kriging techniques in depicting rainfall variability in arid and semi-arid regions of north-west India. *Environ Earth Sci* 76:512. <https://doi.org/10.1007/s12665-017-6814-3>
20. Arnold JG, Moriasi DN, Gassman PW, Abbaspour KC, White MJ, Srinivasan R, Santhi C, Harmel RD, Van Griensven A, Van Liew MW, Kannan N, Jha MK (2012) SWAT: model use, calibration, and validation. *Trans ASABE* 55(4):1491–1508. <https://doi.org/10.13031/2013.42256>
21. Arnold JG, Fohrer N (2005) SWAT2000: current capabilities and research opportunities in applied watershed modeling. *Hydrol Process* 19(3):563–572. <https://doi.org/10.1002/hyp.5611>
22. Gassman PW, Reyes M, Green CH, Arnold JG (2007) The soil and water assessment tool: historical development, applications, and future directions. *Trans ASABE* 50(4):1211–1250. <https://doi.org/10.13031/2013.23637>
23. Arnold JG, Williams JR, Maidment DR (1995) Continuous-time water and sediment routing model for large basins. *J Hydraul Eng* 121(2):171–183. [https://doi.org/10.1061/\(ASCE\)0733-9429\(1995\)121:2\(171\)](https://doi.org/10.1061/(ASCE)0733-9429(1995)121:2(171))
24. Griensven AV, Meixner T (2007) A global and efficient multi-objective auto-calibration and uncertainty estimation method for water quality catchment models. *J Hydroinf* 9(4):277–291. <https://doi.org/10.2166/hydro.2007.104>
25. Maalim FK, Melesse AM (2013) Modelling the impacts of subsurface drainage on surface runoff and sediment yield in the Le Sueur Watershed, Minnesota, USA. *Hydrol Sci J* 58(3):570–586. <https://doi.org/10.1080/02626667.2013.774088>

26. Narasimhan B, Srinivasan R, Bednarz ST, Ernst MR, Allen PM (2010) A comprehensive modeling approach for reservoir water quality assessment and management due to point and nonpoint source pollution. *Trans ASABE* 53(5):1605–1617. <https://doi.org/10.13031/2013.34908>
27. Neitsch SL, Arnold JG, Kiniry JR, Williams JR (2005) Soil and water assessment tool theoretical documentation version 2005. Grassland, Soil and Water Research Laboratory, US Department of Agriculture - Agricultural Research Service, Blackland Research Center, Texas Agricultural Experiment Station, Temple, TX. Retrieved May 10, 2014, from <http://swat.tamu.edu/media/1292/swat2005theory.pdf>
28. Khare D, Singh R, Shukla R (2014) Hydrological modelling of Barinallah watershed using arc-swat model. *Int J Geol Earth Environ Sci* 4(1):224–235
29. Vandenberghe V, Van Griensven A, Bauwens W (2002) Detection of the most optimal measuring points for water quality variables: application to the river water quality model of the river Dender in ESWAT. *Water Sci Technol* 46(3):1–7
30. Kendall MG (1975) Rank correlation methods, 4th edn. Charles Griffin, London
31. Sen PK (1968) Estimates of the regression coefficient based on Kendall's tau. *J Amer Stat Assoc* 63(324):1379–1389. <https://doi.org/10.1080/01621459.1968.10480934>

# Rainfall-Runoff Modelling and Simulation Using Remote Sensing and Hydrological Model for Banas River, Gujarat, India



Anant Patel

**Abstract** This research developed a small-scale flood model that integrates Geographic Information and hydrological models. HEC-RAS model helped in simulation and to develop a relationship between runoff and rainfall in Banas River, Gujarat, India. Banas River has been taken as the study area because it is a region which was mostly flooded and having a severe effect on the Gujarat 2017 flood. This model comprises two models, a rainfall-runoff model that converts rainfall excess to surface flow and river runoff, and a second model as a hydraulic model that covers unsteady state flow through the river channel network. In HEC-RAS model, new GIS tool RAS Mapper has been used which is compatible with GIS facilities and modelling has been done with this tool. Results are also available in different parameters such as flood inundation depth, flood water velocity and time. Validation of the model is important, the results at the end of the simulation were compared with the previous observed flood water level data from past flood events in a particular fixed location. The results of this research will benefit in flood management and also used in future modelling for flood disaster forecasts.

**Keywords** Rainfall-runoff simulation · Remote sensing and GIS · HEC-RAS · Hydrological modelling · Banas River

## 1 Introduction

Rainfall is one of the most common forms of precipitation. The intensity of rainfall varies with place and time. The variation in the intensity of rainfall is responsible for many water problems like flood and drought. Flood events are defined as the occurrence of severe storms. With increasing in the average global temperature trend, which results into increase in exacerbate climate events [1]. So it is important to do river flood modelling for proper management of water and also to protect

---

A. Patel (✉)  
Nirma University, Ahmedabad, Gujarat, India  
e-mail: [anant.patel14@gmail.com](mailto:anant.patel14@gmail.com)

life, property and the environment. In developing countries such as India, hydrological balance is disrupted by many factors which results in major flood disaster, and it causes large economical and many life losses [2]. GIS modelling for floods or delimiting some flood-prone areas is very advanced, and numerous methods for calculating the extent of river have been developed [3]. However, earlier methods required lot of river cross-section data for river flood analysis and modelling. While in this current method, only DEM image is required for any type of flood modelling, so this method requires less data as well as modelling can be done in short time duration. Determining the flood extent is a most important duty of the whole community of hydrological research as it would be helpful for planners and engineers in their professional field. It is also realizing the importance of non-structural mitigation measures, which includes flood management and forecasting and early warning system. Flood forecasting system would be helpful to enhance the effectiveness by providing proper time for perfect actions as compared to all other mitigation measures. It will result into increase the importance of flood modelling for forecast to issue advance warning in severe flood situations to reduce loss of lives and property damages [4–6]. For flood forecasting, flood plain mapping and flood volume estimation, various hydrodynamic models, based on hydraulic routing, have been developed and applied to different rivers in the past using computer technology and numerical techniques [7]. The flood warning systems may help in the removal of population using rain forecasting, river stage monitoring and hydrological simulation using rainfall as input in the rainfall-runoff model [8]. In this research, HEC-RAS software with GIS technology has been used for rainfall-runoff modelling and simulation in which unsteady flow simulation was carried out for Banas River basin for the flood event of July 2017, Gujarat Flood-2017.

## 2 Study Area

The Banas River basin is taken as a study for rainfall-runoff simulation by using GIS and hydrological models. The Banas basin has a total catchment area of 8674 km<sup>2</sup>. In which, 3269 km<sup>2</sup> lies in Rajasthan State while the remaining 5405 km<sup>2</sup> lies in Gujarat. In this paper, analysis is done only for basin area falling Gujarat state which covers 5405 km<sup>2</sup> of catchment area [9].

Banas River originates from Aravalli hills which is in Rajasthan and it flows gradually in a South-West direction. Total length of Banas River is 266 km from which 78 km is in Rajasthan and remaining 188 km is in Gujarat state. Figure 1 shows location map of Banas River basin, which shows 62.3% of total basin area falls in Gujarat state and mostly in Banaskantha district.

There is Sipu River, which is the only right bank main tributary of Banas River while another six tributaries are on the left bank of Banas River, which are mainly the Khari, Suket, Baaram, Sukli, Batria and Sewaran which finally drain into the main channel.

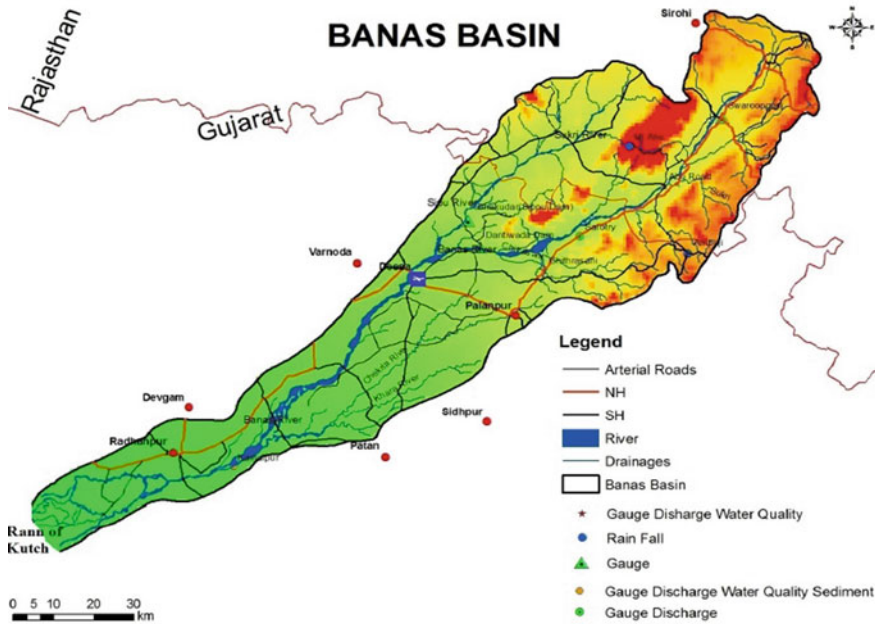


Fig. 1 Location map of Banas River basin (Source <http://cgwb.gov.in/watershed/>)

### 3 Methodology

The rainfall-runoff model is a combination of HEC-RAS and remote sensing technology in a GIS environment. A number of flood-related studies have shown that these models provide accurate and useful results [10]. In the current study, the main objective is to determine water levels and submerged areas or inundation area by using GIS-based hydrological model in Banas River basin.

#### 3.1 Rainfall-Runoff Modelling

In this study, HEC-RAS 5.0.3 has been used for rainfall-runoff modelling, which was developed and prepared by the US Army Corps of Engineers, is basically used for two-dimensional hydraulic and hydrological modelling for a full network of constructed and natural channels. HEC-RAS model gives water surface profiles for unsteady and steady gradually varied flow. The detailed flowchart for rainfall-runoff modelling in HEC-RAS software is given in Fig. 2.



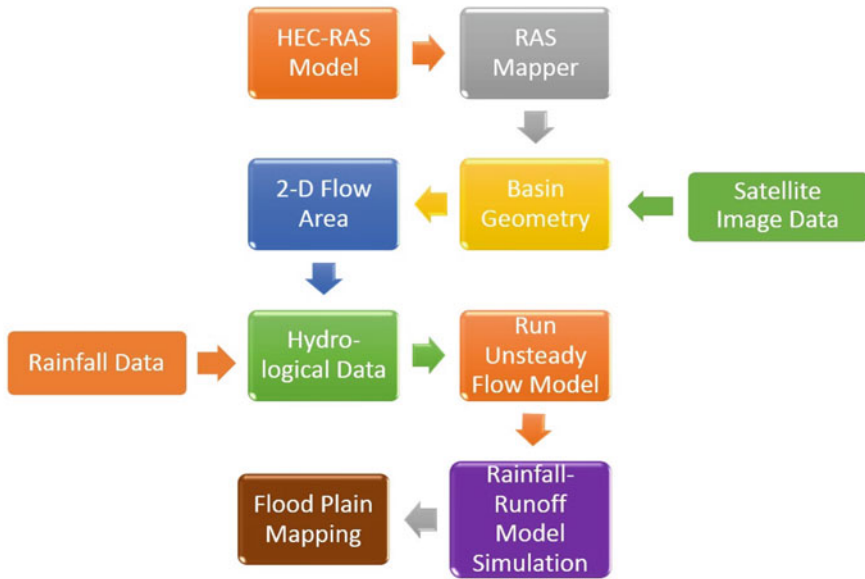


Fig. 2 Flowchart for rainfall-runoff modelling

### 3.2 GIS-Based Hydrological Model

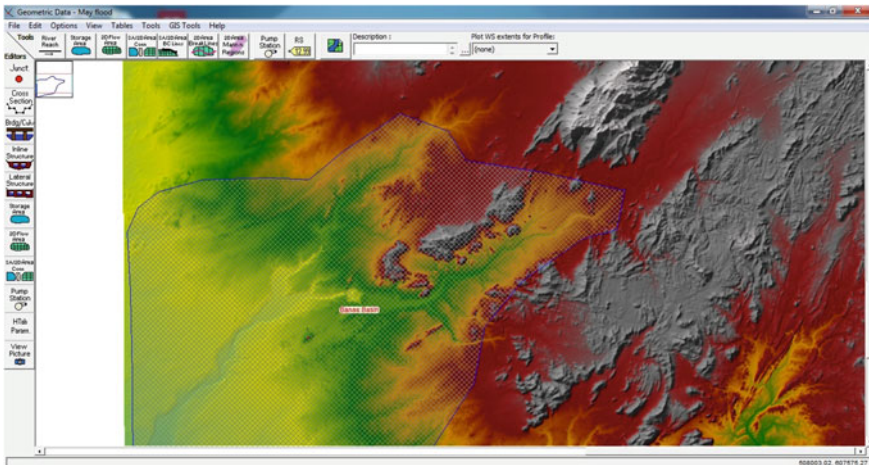


Fig. 3 Banas basin DEM terrain model from RAS Mapper (Source DEM image from <http://bhuvan.nrcs.gov.in/data/download/index.php>)



Remote sensing and GIS is a crucial decision support system in numerous field as well as water resources branch for collection, storage, compilation, selection by location, spatial analyses and presentation processes of data [1]. HEC-RAS software is a hydraulic modelling software that can perform flood mapping, 1D-2D analyses, rainfall-runoff simulations, and visualization operations by integrating interfaces [11].

Inside HEC-RAS software, RAS Mapper is a tool which is used for preparation of basin terrain by using GIS technology. Once terrain layer of the basin is generated in RAS Mapper, it is directly correlated with HEC-RAS geometry tool. In geometric data editor, 2D flow area is a tool in which 2D flow area polygon can be drawn to represent the boundary of the river basin [12]. A computational mesh or computational grid is created within the boundary of 2D flow area. In this grid, each cell having three properties cell centre, cell faces and cell points as shown in Fig. 3.

Hydrological data are required to run the unsteady flow simulation. Precipitation data are entered as a hydrological data as this study is related to rainfall-runoff modelling. So rainfall data are collected from State Water Data Centre—Gandhinagar for flood event occur during Gujarat-2017 flood in July month. Rainfall data are also collected from Gujarat State Disaster Management for particular event starting from 21 July to 31 July 2017. Rainfall of Banas basin for 2017 flood is given in Table 1.

In the month of July 2017, over the Arabian Sea and also over the Bay of Bengal a low-pressure system activated simultaneously, which results in heavy to very heavy rainfall in Gujarat state. Banaskantha district received 267% of the average rainfall in July 2017. Dhanera and Dantiwada recorded 231 and 342 mm of rainfall in 24 h on 24th July 2017 and 275 and 463 mm rainfall on 25th July 2017 respectively, which resulting in severe flooding in city area as well as villages and agricultural farms has been also flooded. In the history of 112 years, it was the heaviest rainfall in the affected area of Banaskantha and Sabarkantha district. Figure 4 shows rainfall analysis for Banas River basin.

All this rainfall data of Banas River basin have been entered into HEC-RAS software through unsteady flow data editor option. Rainfall data from 21 July to 31 July have been taken as a flood event 2017. All rain-gauge station data are collected and average rainfall is carried out based on arithmetic average rainfall method for a particular date.

Once precipitation data are entered in HEC-RAS, unsteady flow rainfall-runoff simulation can be started in model run option. Figure 5 shows unsteady flow rainfall-runoff simulation for Banas River basin.



**Table 1** Rainfall data for Bamas River basin—2017 flood (Rainfall in mm)

Region	Date										
	21-07-2017	22-07-2017	23-07-2017	24-07-2017	25-07-2017	26-07-2017	27-07-2017	28-07-2017	29-07-2017	30-07-2017	31-07-2017
Amirgadh	9	0	50	246	337	150	55	8	82	4	5
Bhabhar	4	44	108	92	174	28	8	54	48	13	3
Danta	0	14	29	179	167	104	70	43	34	21	15
Dantiwada	6	17	44	342	463	21	21	41	18	10	4
Deesa	13	15	86	212	210	119	19	8	16	15	15
Deodar	73	15	204	172	284	106	0	30	5	55	12
Dhanera	7	31	18	231	275	139	10	0	12	10	8
Kankrej	40	63	67	120	154	39	3	14	5	8	0
Lakhani	14	30	99	221	305	51	9	11	7	39	20
Palampur	7	51	30	255	380	62	46	23	25	49	7
Suigam	7	29	25	72	122	19	8	32	115	50	19
Tharad	20	40	40	119	180	59	6	12	4	39	8
Vadgam	70	40	17	200	357	60	28	19	13	29	14
Wav	2	15	15	82	187	46	8	10	10	45	10
<b>Average rainfall</b>	<b>20</b>	<b>29</b>	<b>60</b>	<b>182</b>	<b>257</b>	<b>72</b>	<b>21</b>	<b>22</b>	<b>29</b>	<b>28</b>	<b>10</b>

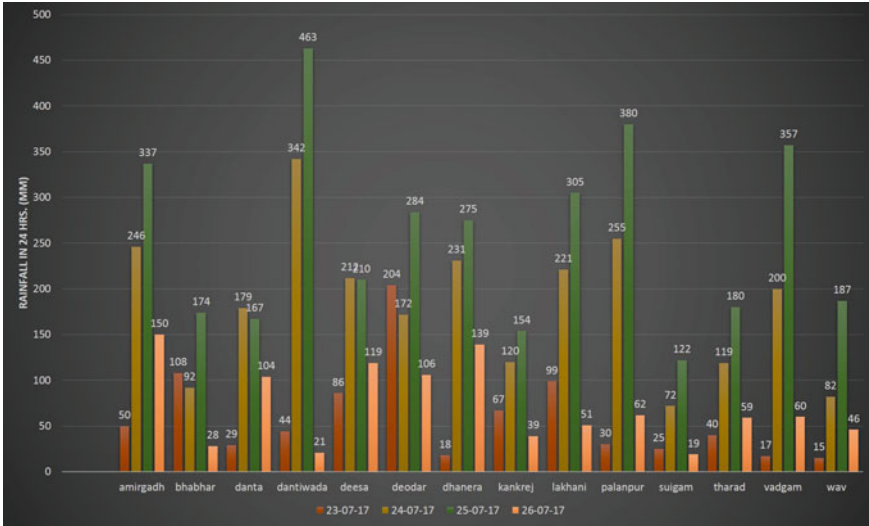


Fig. 4 Rainfall data analysis for Banas basin during flood-2017 (Source Rainfall data collected from State Water Data Centre—Gandhinagar)

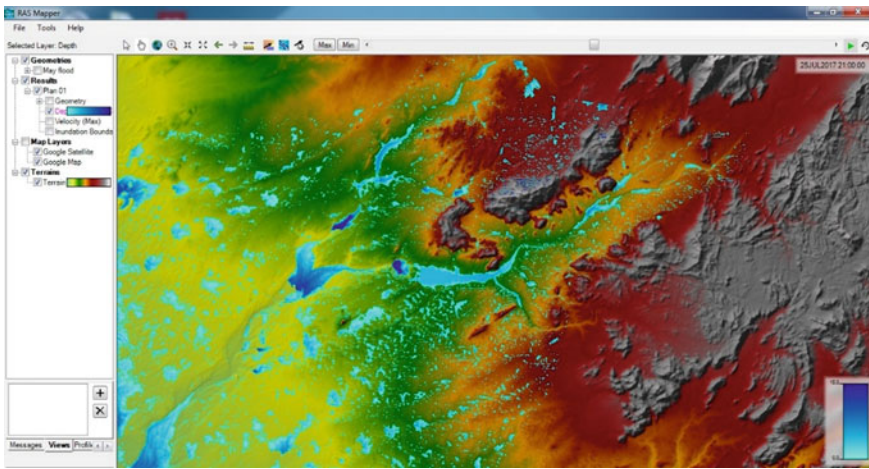
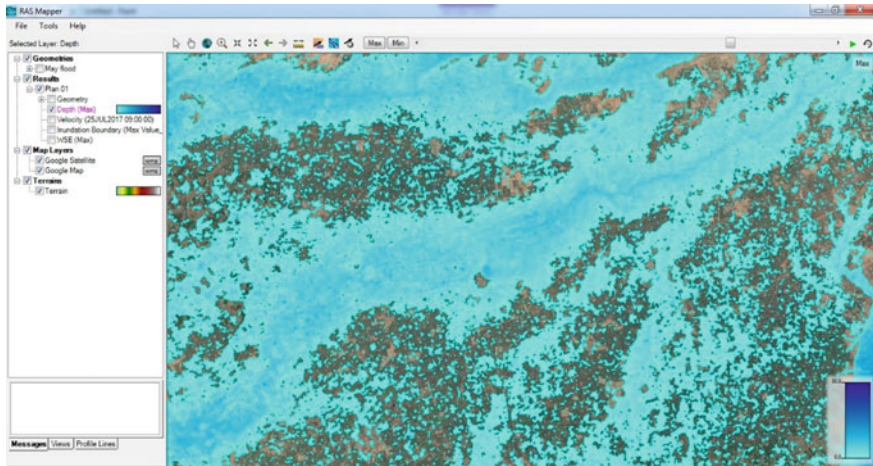


Fig. 5 Rainfall-runoff simulation in RAS Mapper (Source DEM image from <http://bhuvan.nrsc.gov.in/data/download/index.php>)



**Fig. 6** Flood inundation mapping for Dhanera Taluka (Source DEM image from <http://bhuvan.nrsc.gov.in/data/download/index.php>)

## 4 Results and Discussions

### 4.1 Hydrological Model Simulation

Hydrological simulation for rainfall-runoff and flood plain mapping will be beneficiary in many points of view for land and water resources management and also helpful in engineering purposes. This can be also applied in the study of flood-prone areas and for flood insurance studies.

In Fig. 6, it shows flood water depth after heavy precipitation on 24 and 25 July 2017. Rainfall in Banas river basin was very high during these two days and Dhanera Taluka was severely affected during this flood. Flood inundation map in Fig. 6 shows that different flood water depth for different area in Dhanera Taluka.

Once flood inundation map is prepared, flood inundation boundary line is also generated in RAS Mapper by using GIS technology. It is seen from Fig. 6 that most of the agricultural area, villages, towns, some parts of the roads and highways and railway tracks are flooded during this Flood 2017 event.

It has been seen in rainfall-runoff simulation that whole basin is flooded during maximum rainfall data is applied, which was taken as a case of 2017 flood. In this worst case, the most affected district is Banaskantha and Dhanera Taluka is severely affected. In Dhanera Taluka, mostly all the villages are flooded due to heavy precipitation and also release from the dam. From the Fig. 7, it is examined that Tharad, Dhanera, Kankrej, Lakhani, Suigam and Deesa Taluka of Banaskantha and Santalpur, Sami and Harij Taluka of Patan district got heavily flooded if rainfall intensity is above 300 mm in 24 h.

**Rainfall Simulation link:-** [https://www.youtube.com/watch?v=HzvsCC\\_Dan0](https://www.youtube.com/watch?v=HzvsCC_Dan0).

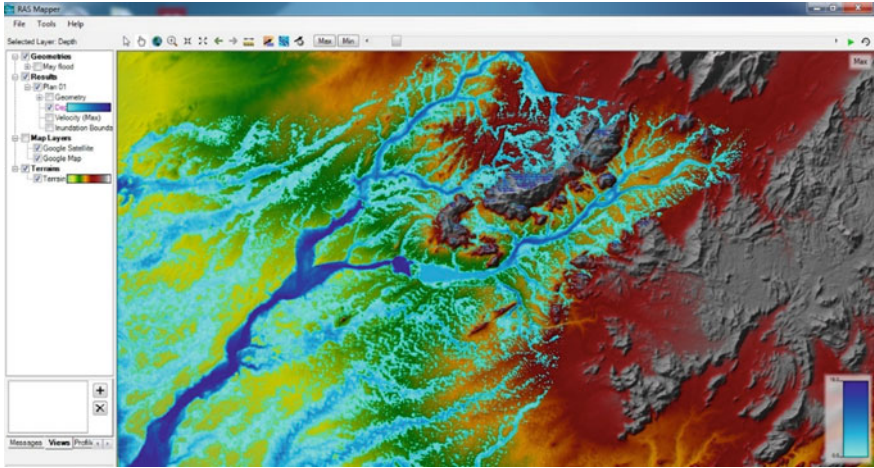


Fig. 7 Maximum rainfall-runoff simulation in Banas River basin (Source DEM image from <http://bhuvan.nrsc.gov.in/data/download/index.php>)

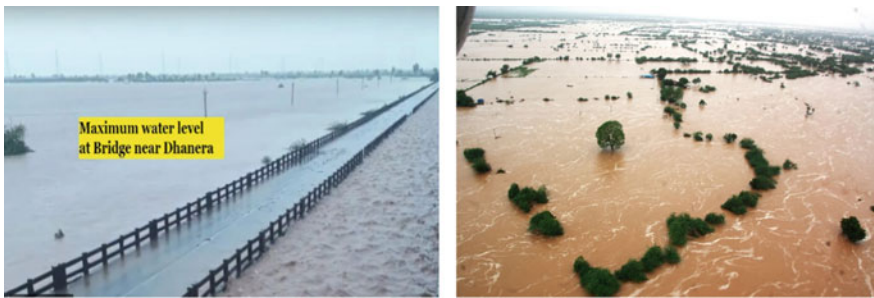


Fig. 8 Flooded area in Banas River basin (Source <http://india.com/news/india/gujarat> flood 2017)

### 4.2 Validation of Results

Validation of model is the most important in flood modelling study. For this study, it is done based on the comparison of modelled flood depths with observed flood depths based on floodmarks at specific location Fig. 8 and also from the Govt. of Gujarat Flood 2017 Report which says that Dhanera Taluka of Banaskantha district was flooded up to 10 feet of flood water, and other surrounding areas were also inundated for long time during this flood event [9]. So it has been seen in results that most of the Banas River basin area is flooded up to depth of 10 ft.

## 5 Conclusion

It is concluded from the paper that by combination of GIS technology with Hydrological model, it is very easy for decision support systems in preparation of flood management plans. It is also helpful in before, during and after floods, remote sensing and GIS are helped to decision makers for different analyses such as flood inundation mapping, flood risk and hazard analysis, flood damage analysis and also in flood mitigation management. Flood inundation depth, velocity and time maps can be derived and overlaid to obtain flood risk (hazard) map.

**Acknowledgements** Author is thankful to Civil Engineering Department, Nirma University to carry out this study. Author is also thankful to State Water Data Centre, Gandhinagar and Gujarat State Disaster Management Institute, Gandhinagar for providing necessary data to carry out this study. Special thanks to Vaibhav Patel, Priyank Patel, Miraj Patel students of Under Graduate, B.Tech in Civil Engineering, Nirma University for their help in this study.

## References

1. Hadi T, Feyzolahpour M, Mumipour M, Zakerhoseini F (2012) Rainfall-runoff simulation and modeling of Karun river using hec-ras and hec-hms models, Izeh district, Iran. *J Appl Sci* 12(18):1900–1908. <https://doi.org/10.3923/jas.2012.1900.1908>
2. İcaga Y, Tas E, Kilit M (2016) Flood inundation mapping by GIS and a hydraulic model (hec ras): a case study of Akarcaı Bolvadin subbasin, in Turkey. *Acta Geobalcanica* 2:111–118. <https://doi.org/10.18509/AGB.2016.12>
3. Iosub M, Minea I, Hapciuc O, Romanescu G (2015) The use of HEC-RAS modelling in flood risk analysis. *Air Water Compon Environ* 315–322. <https://doi.org/10.17378/AWC2015>
4. Kaffle T, Hazarika M (2007) Basin scale rainfall-runoff modeling for flood forecasts. In: 5th annual conference Mekong
5. Ling L, Yusop Z (2015) The calibration of a rainfall-runoff model. In: International conference on advances in civil and environmental engineering, University Teknologi MARA Pulau Pinang
6. Jarosińska E, Pierzga K (2015) Estimating flood quantiles on the basis of multi-event rainfall simulation—case study. *Acta Geophys* 63:1639–1663. <https://doi.org/10.1515/acgeo-2015-0046>
7. Parhi K (2013) HEC-RAS model for mannig’s roughness: a case study. *Open J Mod Hydrol* 3:97–101. <https://doi.org/10.4236/ojmh.2013.33013>
8. Neto R (2014) Assessment of rainfall-runoff models for flood river extreme event simulations. In: 6th international conference on flood management, Sau Paulo, Brazil, pp 1–10
9. Gujarat Floods (2017) Immediate relief report. Government of Gujarat. [http://gujaratinformation.net/downloads/book\\_eng\\_23082017.pdf](http://gujaratinformation.net/downloads/book_eng_23082017.pdf)
10. Polyakov V, Stone J, Collins H, Nearing A, Paige G, Buono J, Gomez-Pond L (2018) Rainfall simulation experiments in the southwestern USA using the Walnut Gulch rainfall simulator. *Earth Syst Sci Data* 10:19–26. <https://doi.org/10.5194/essd-10-19-2018>
11. Prajapati P, Bansal N (2017) Banaskantha flood 2017: flood risk assessment. *Int J Trend Sci Res Dev* 825–828
12. Sharma S (2015) Tutorial on HEC-GeoRAS and HEC-RAS modeling. <https://doi.org/10.13140/rg.2.1.2805.8329>

# GIS-Based Morphometric Analysis and Prioritization of Upper Ravi Catchment, Himachal Pradesh, India



D. Khurana, S. S. Rawat, G. Raina, R. Sharma and P. G. Jose

**Abstract** Morphological parameters have been recurrently used to assess the hydrological response of a watershed. Due to a strong mutual correlation between the runoff characteristics and the terrain of a watershed, the method is significantly popular, especially in an un-gauged catchment. In the present study, the hydrologic response of a Himalayan watershed and its sub-watersheds is discussed using various morphological parameters, and accordingly, the sub-watershed prioritization has been done. Morphological parameters have been extracted from digital elevation model (SRTM-DEM) in conjunction with Survey of India toposheets (1:50000 scale). Arc Hydro tools have been used for the preparation of watershed and sub-watershed boundaries, to calculate flow directions, flow accumulation and for stream ordering. Morphometric parameters categorized under linear, aerial and relief aspects are calculated for the entire catchment and also for its eight sub-watersheds separately. The drainage pattern is mostly sub-dendritic to dendritic in nature. The studied catchment has been categorized as an eighth order drainage catchment with a drainage density of 3.15 km/km<sup>2</sup>. The progressive increase in stream length ratio is a depiction of the attained geomorphic maturity of the basin. Considerable conformity between the sub-watersheds and their major catchment characteristics has been established. However, two sub-watersheds have been observed to behave in a different manner. In order to prioritize the catchment, a compound index was calculated by considering the individual rank assigned to all eight sub-watersheds based on 11 morphological parameters. The study reveals that SW6 sub-watershed has the highest priority and SW2 watershed has the least priority. Such maps have immense significance for field engineers for prioritizing the watershed management activities within the watershed especially in un-gauged condition.

**Keywords** Morphometry · DEM · GIS · Upper Ravi catchment · Drainage · Prioritization

D. Khurana (✉) · S. S. Rawat · P. G. Jose

Western Himalayan Regional Centre, National Institute of Hydrology, Roorkee, India  
e-mail: [dkhurana.nihr@gov.in](mailto:dkhurana.nihr@gov.in)

G. Raina · R. Sharma

University of Jammu, Jammu, Jammu and Kashmir, India

## 1 Introduction

Morphometry is the measurement of earth's configuration pertaining to various features such as surface, shape and dimension of its landforms in a way that they can be interpreted mathematically for further deliberation [1, 3, 18]. Linear, aerial, gradient and relief of channel network and contributing ground slope are measured for morphometric analysis [16, 17]. In recent years, the geographical information system (GIS) and remote sensing (RS) have proven to be very effective and time-saving in analysing any basin due to its ease of availability through open-source imagery programmes such as SRTM and ASTER. This data in conjunction with well-defined surveyed sheets such as geo-referenced Survey of India (SOI) toposheets can prove to be a very effective and frugal method of accurate watershed response assessment.

Since most of the morphometric parameters are in the form of ratios, the scale does not limit their applicability while comparing for different watersheds. Due to the lack of observed data, these simple morphometrical-based approaches are still popular in the characterization of sub-watersheds in reference to their susceptibility towards hydrological response behaviour. Estimating the geomorphologic parameters has always been challenging for field engineers. Regional methodologies have seldom been developed for the analysis of hydrological problems where sufficient data is unavailable and gauging is absent. With the advancement in the field of geospatial technologies like GIS and RS, geomorphological parameters can be easily extracted from the digitalized toposheets. It has been accepted widely that morphological parameters of the drainage basin are a clear reflection of geological and geomorphological evolution of an area over time, as substantiated in various morphological studies [5, 11, 14, 15, 23, 27]. Drainage lines of an area give an insight into the three-dimensional geometry of the region and are a clear manifestation of the evolution process [24]. Besides, it is important to analyse a watershed quantitatively to highlight its important hydrological aspects and their impact. Morphometric analysis based on observation of hydrologic and geomorphic processes at watershed scale reveals information regarding the formation and development of land surface processes [4, 25]. It has been concluded widely that crucial drainage system parameters such as flow intensity and surface run-off can be estimated on the basis of geomorphic features associated with morphometric parameters [19].

In the present study, various morphological parameters representing one-dimensional view via linear, two-dimensional view via aerial and three-dimensional view via relief aspect of the catchment have been extracted in GIS environment by dividing the complete upper Ravi catchment into eight sub-watersheds to calculate the selected morphometric parameters viz. stream order, stream length, bifurcation ratio, stream frequency, stream length ratio, form factor, drainage density, drainage texture, elongation ratio, circulatory ratio, infiltration number, relief ratio, relative relief, etc.

## 2 Study Area

River Ravi, one of the six rivers of the Indus basin system, originates from the Bharabhangal glacier in the hill state of Himachal Pradesh and has a total length of about 720 km and a catchment area of about 14,442 km<sup>2</sup> before joining the River Chenab in Pakistan. Ravi River has been allocated to India under the Indus water treaty (IWT). The upper catchment of the Ravi River (up to Chamba town of Himachal Pradesh) with its mountainous terrain having steep to very steep slopes has been taken as the study area (Fig. 1). The area of upper Ravi catchment is 3093 km<sup>2</sup> (up to Chamba town), and the perimeter is about 334 km. It is situated between 32°10'37.2" N–32°41'16.8" N latitude and 76°2'2.4" E–77°4'37.2" E longitudes. The study area encompasses a significant part of district Chamba and a small part of district Kangra of Himachal Pradesh. The upper Ravi has some major left bank tributaries such as Budhil Nullah, Tundah Nullah and Reshai Nullah. Its right bank has fewer tributaries such as Salun Nullah and Balani Nullah which are either having low discharge or are seasonal.

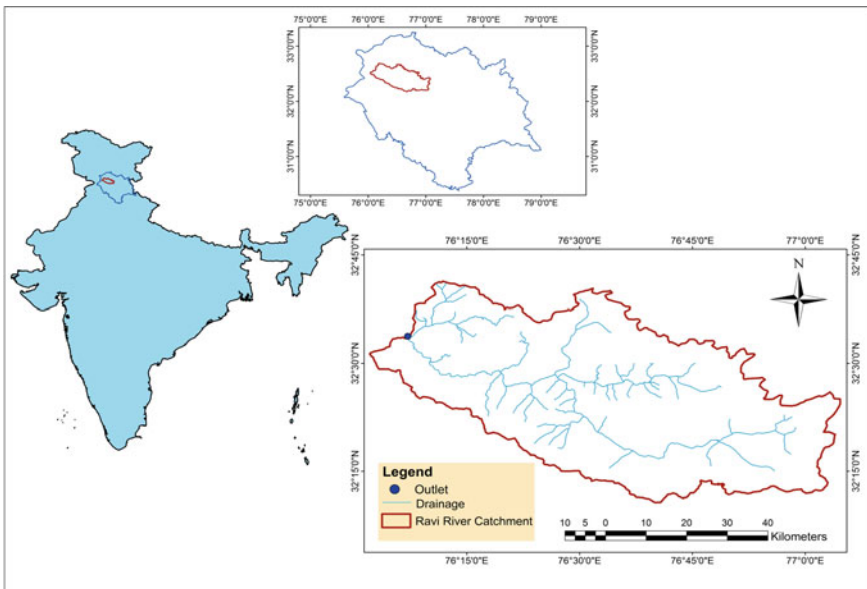


**Fig. 1** Location map of upper Ravi catchment (up to Chamba town), Himachal Pradesh, India



### 3 Methodology

#### 3.1 Extraction of Drainage Network

The manual stream order extraction of drainage network from SOI toposheets is a cumbersome exercise. However, it was observed that the accuracy of drainage network extracted from DEMs is entirely dependent on the threshold value provided by the user, and hence, the user must be well acquainted with the study area. It has been observed that any reduction in threshold value to match the drainage network of one part of the catchment (particularly for first-order streams) leads to the generation of virtual drainage lines in the other part of the catchment. Therefore, to overcome this problem, drainage lines of the study area were digitized in ArcGIS by using ten geo-referenced SOI toposheets (52D16, 52D10, 52D11, 52D12, 52D15, 52D23, 52D6, 52D7, 52H3 and 52H2) having 1:50000 scale and stored in shapefile format and were used for the calculation of morphometric parameters of the study area. SRTM-DEM of the study area is depicted in Fig. 2 showing the altitude ranges from 785 to 6148 m from msl which is used to ascertain the relief aspects of the study area. Corresponding stream orders of the digitized drainage network are depicted in Fig. 3.

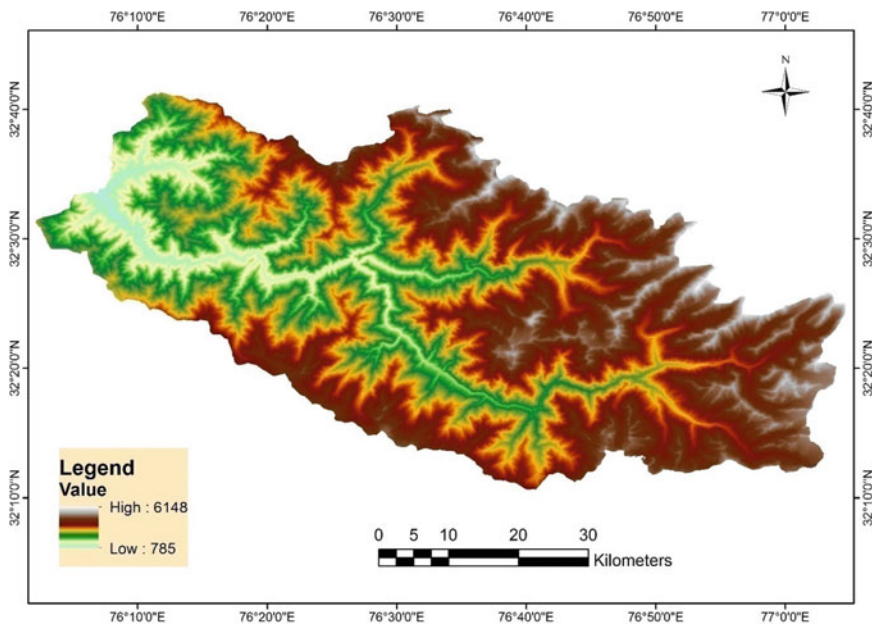


Fig. 2 Digital elevation model (SRTM) of upper Ravi catchment, Himachal Pradesh, India

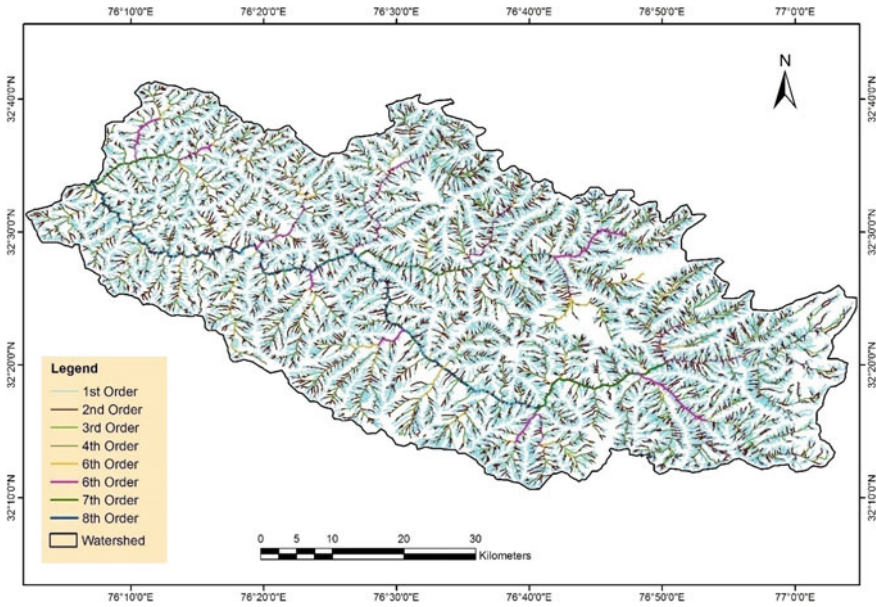


Fig. 3 Stream ordering of upper Ravi catchment, Himachal Pradesh, India

### 3.2 Morphometric Parameter Calculations

To evaluate the drainage basin morphometry, an analysis of various parameters has been done on the basis of standard well-established mathematical formulae given in Table 1.

## 4 Results and Discussions

In the present study, the morphological parameters have been extracted for entire upper Ravi River catchment and the same has been extracted separately for its eight sub-watersheds, namely SW1–SW8. Total drainage area of upper Ravi catchment is found to be 3093 km<sup>2</sup>. The drainage pattern is dominantly dendritic in nature and is influenced by topographical and geological conditions prevailing in the area. Based on the stream ordering on the basis of Strahler's system, the basin is found to be of the 8th order. Different sub-watersheds are shown in Fig. 4.

**Table 1** Linear, aerial and relief morphometric parameters used in the study and their standard formulae

S. No.		Parameter	Formula	References
1	Linear	Stream order ( $U$ )	Hierarchical rank	Strahler [29]
2		Stream length ( $L_u$ )	Length of the stream	Horton [11]
3		Mean stream length ( $L_{sm}$ )	$L_{sm} = L_u/N_u$	Strahler [29]
4		Stream length ratio ( $R_l$ )	$R_l = L_u/(L_u - 1)$	Horton [11]
5		Bifurcation ratio ( $R_b$ )	$R_b = N_u/N_u + 1$	Schumm [21]
6		Mean bifurcation ratio ( $R_{bm}$ )	$R_{bm} =$ average of $R_b$ of all orders	Strahler [28]
7	Aerial	Drainage density ( $D_d$ )	$D_d = L_u/A$	Horton [11]
8		Drainage texture ( $T$ )	$T = D_d * F_s$	Horton [11]
9		Stream frequency	$F_s = N_u/A$	Horton [11]
10		Elongation ratio ( $R_e$ )	$R_e = D/L$	Schumm [21]
11		Circulatory ratio	$R_c = 4\pi A/P^2$	Strahler [29]
12		Form factor ( $F_f$ )	$F_f = A/L^2$	Horton [11]
13		Perimeter	Length of catchment boundary	
14		Basin area	Area of catchment boundary	
15	Compactness coefficient	$0.2841 * P/A^{0.5}$	Gravelius [9]	
16	Infiltration number	$I_f = F_s * D_d$	Faniran [6]	
17	Relief	Total relief ( $H$ )	$H =$ Difference between maximum and minimum elevation of the watershed	Schumm [21]
18		Relative relief ( $R_r$ )	$R_r = H/L_p$ where, $H =$ total relief, $L_p =$ basin perimeter	Schumm [21]
19		Relief ratio ( $R_o$ )	$R_o = H/L$ where, $H =$ total relief, $L =$ basin length	Schumm [21]

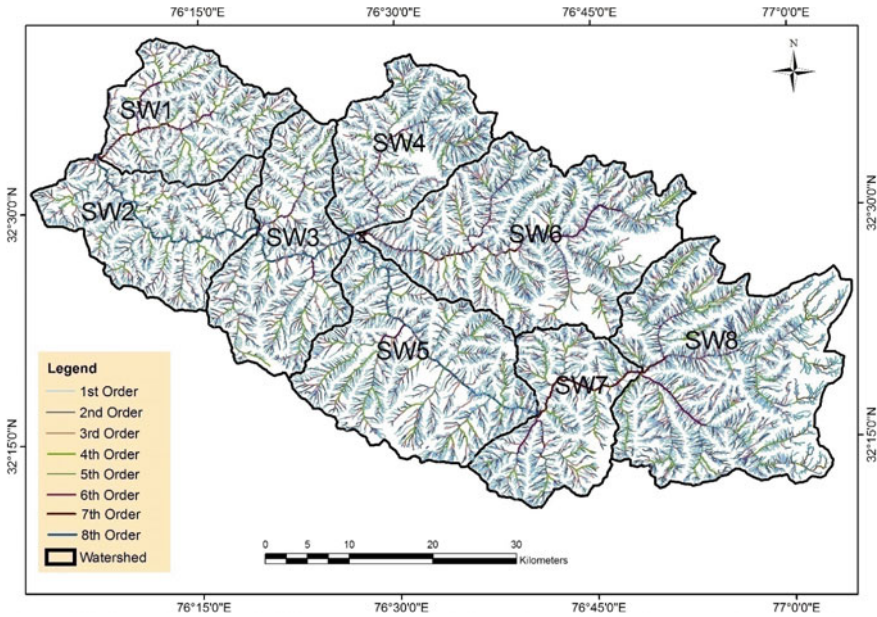


Fig. 4 Sub-watersheds of upper Ravi River catchment

#### 4.1 Aspect

Aspect broadly refers to the direction in which a mountain slope faces. The aspect influences the local climate significantly because during the time of prevailing heat, i.e. afternoon, the effect of the sun is majorly on the west facing slopes compared to the relatively sheltered east-facing slopes. The aspect map of the upper Ravi catchment is shown in Fig. 5. The slopes of the upper Ravi catchment are predominantly south facing. As the south-facing slope in the northern hemisphere is more open to sunlight and warm winds, the rate of evapotranspiration is much higher compared to a north-facing slope. In the Himalayas, south-facing slopes are warm, wet and forested compared to north-facing slopes which are cold, dry and heavily glaciated.

#### 4.2 Slope

Slope analysis is significantly important in geomorphologic studies for the development of watershed and morphometric analysis. The slope features are governed by climatic and morphogenic processes in regions of varying rock resistance [7, 13]. A slope map of upper Ravi catchment has been made using the generated DEM and spatial analysis tool in GIS and depicted in Fig. 6. Terrain slope classification has

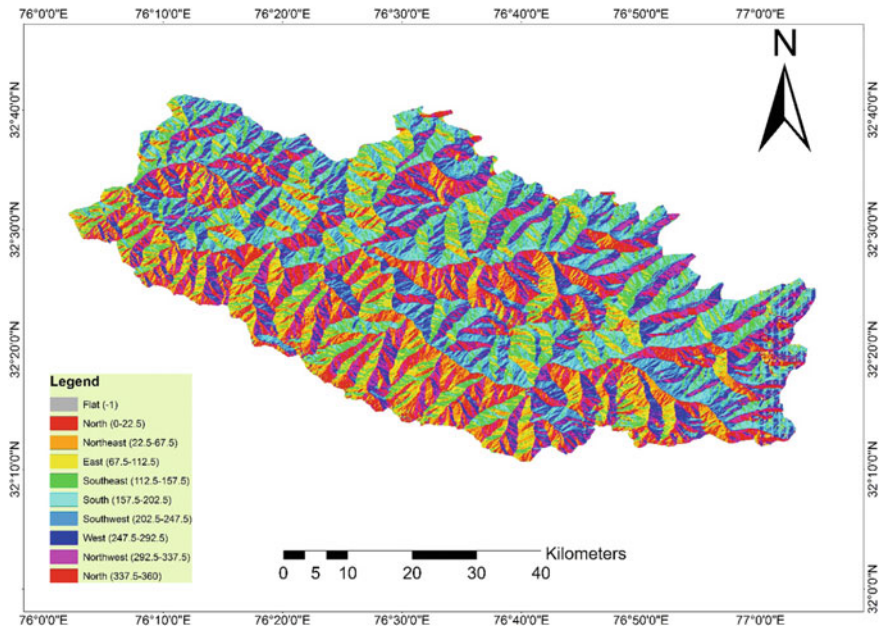


**Fig. 5** Aspect map of upper Ravi catchment (SRTM DEM)

been done which exhibits that 3.7% of study area lies between 0 and 15% slope value, 7.72% area lies between 15 and 30% slope value, 17.30% area lies between 30 and 50% slope value, 24.19% area lies between 50 and 70% slope value, 29.03% area lies between 70 and 100% slope value and 18.06% of area lies above 100% slope value. These values are a clear indication that the major part of the terrain has steep to very steep slopes. A higher value of slope has a direct relationship with run-off and has an increased erosion rate potential with less groundwater recharge. 18.06% area of the catchment is primarily vulnerable to rapid run-off and heavy erosion and sediment load as it is steeper than the stable slope value.

### 4.3 Linear Aspects

#### 4.3.1 Stream Order ( $U$ )

The ranking of streams in the upper Ravi basin has been done on the basis of Strahler's system which was proposed in 1964. Eight orders have been calculated for classification of the watershed, the highest being of the central stream, i.e. Ravi River (Table 2). Sub-watershed stream ordering has also been computed and is presented in Table 3. The basin is designated as an 8th order basin. The maximum stream

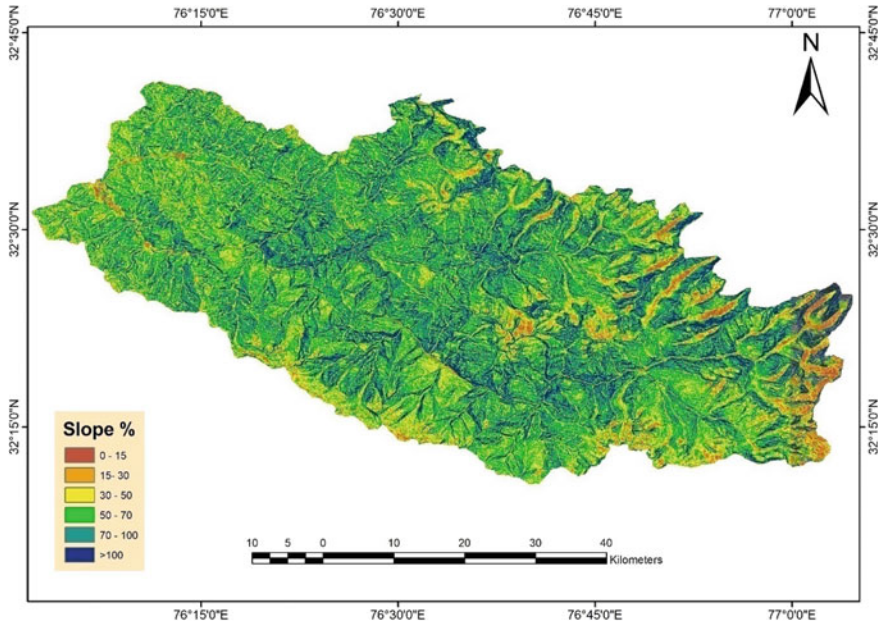


**Fig. 6** Slope map of upper Ravi River catchment (SRTM DEM)

number has been observed in the first order, and then, a declining trend has been observed order wise. In general, the stream order and stream frequency are found to be inversely proportional.

### 4.3.2 Stream Number ( $N_u$ )

Stream number has been defined as the number of stream channels belonging to each particular order. As per Horton's law [11], "the number of streams of different orders in a given drainage basin tends closely to approximate an inverse geometric series of which the first term is unity and the ratio is the bifurcation ratio".

A more crude form of this law simply states that the number of streams order wise gradually decreases as the order increases. This variation in any basin largely depends upon the physiographical, geomorphological and geological conditions of the region. A total of 21,047 streamlines are recognized in the upper Ravi catchment on the basis of SOI toposheets over which the drainage lines have been digitized to create a drainage shapefile. Out of these 21,047, 70.12% (14,757) is first order, 23.12% (4865) is second order, 5.24% (1101) is third order, 1.16% (244) is fourth order, 0.30% (61) is fifth order, 0.067% (14) is sixth order, 0.019% (4) is seventh order, and 0.005% (1) comprises the eighth order stream.

**Table 2** Linear aspects of morphometric analysis of upper Ravi catchment

S. No.	Parameters	Stream orders							
		I	II	III	IV	V	VI	VII	VIII
1	Stream number ( $U$ )	14,757	4865	1101	244	61	14	4	1
2	Stream length (km) ( $L_u$ )	5477.42	2276.52	965.38	480.17	277.54	117.42	61.47	83.01
3	Mean stream length (km) ( $L_{sm}$ )	0.37	0.47	0.88	1.97	4.55	8.38	15.36	83.01
4	Stream length ratio ( $R_l$ )	0.42	0.42	0.5	0.58	0.42	0.52	1.35	-
5	Bifurcation ratio ( $R_b$ )	-	3.03	4.42	4.51	4.00	4.36	3.5	4.0
6	Weighted mean bifurcation ratio	3.35							

**Table 3** Comparison of linear aspects of different sub-watersheds of upper Ravi catchment

Sub-watershed	Parameter	Stream order								Mean $R_b$
		I	II	III	IV	V	VI	VII		
SW1	Stream number	1089	401	105	25	6	2	1		3.32
	Stream length	400.8	163.99	96.16	53.26	16.88	13.13	12.31		
	Bifurcation ratio	2.72	3.82	4.2	4	3	2	-		
	Stream length ratio	-	0.41	0.59	0.55	0.32	0.78	0.94		
SW2	Stream number	1133	443	83	23	7	1	-		4.36
	Stream length	445.59	199.02	95.15	43.69	32.91	29.60	-		
	Bifurcation ratio	2.56	5.34	3.61	3.29	7.00	-	-		
	Stream length ratio	-	0.45	0.48	0.46	0.75	0.90	-		
SW3	Stream number	1385	527	115	24	6	2	1		3.5
	Stream length	537.69	244.20	100.35	49.16	34.53	13.22	15.52		
	Bifurcation ratio	2.63	4.58	4.79	4.00	3.00	2.00	-		
	Stream length ratio	-	0.45	0.41	0.49	0.70	0.38	1.17		
SW4	Stream number	1449	421	124	17	4	1	-		4.48
	Stream length	544.22	222.34	85.79	42.27	17.54	20.21	-		
	Bifurcation ratio	3.44	3.40	7.29	4.25	4.00	-	-		
	Stream length ratio	-	0.41	0.39	0.49	0.41	1.15	-		

(continued)



Table 3 (continued)

SW5	Stream number	1919	654	152	30	6	2	1	3.72
	Stream length	792.61	324.55	133.37	71.25	37.40	4.16	0.99	
	Bifurcation ratio	2.93	4.30	5.07	5.00	3.00	2.00	–	
	Stream length ratio	–	0.41	0.41	0.53	0.52	0.11	0.24	
SW6	Stream number	3098	1030	239	45	15	3	1	3.94
	Stream length	1083.06	463.75	192.96	78.04	65.78	28.49	26.95	
	Bifurcation ratio	3.01	4.31	5.31	3.00	5.00	3.00	3.01	
	Stream length ratio	–	0.43	0.42	0.40	0.84	0.43	0.95	
SW7	Stream number	1215	394	94	20	6	4	2	3.13
	Stream length	472.80	189.69	74.84	40.92	18.98	10.47	17.38	
	Bifurcation ratio	3.08	4.19	4.70	3.33	1.50	2.00	–	
	Stream length ratio	–	0.40	0.39	0.55	0.46	0.55	1.66	
SW8	Stream number	3469	985	198	60	11	3	1	3.99
	Stream length	1202.05	469.00	186.75	101.57	53.49	27.13	3.53	
	Bifurcation ratio	3.52	4.97	3.30	5.45	3.67	3.00	–	
	Stream length ratio	–	0.39	0.40	0.54	0.53	0.51	0.13	

### 4.3.3 Stream Length ( $L_n$ )

According to Horton [11], stream length of a watershed is the total length combined of all the stream segments in each respective stream order in a basin. A general trend has been observed that these stream lengths in almost any watershed follow a direct geometric series with the first one being of the lowest order and next one of the subsequent higher order and so on. Bedrock's hydrological characteristics and extent of a drainage area can be related to the stream length of any watershed. It has been observed that a permeable stratum is susceptible to more seepage and in turn results in smaller stream lengths whereas hard rocky strata prone to less seepage bear more significant number of stream lengths [22].

The result of order-wise stream length in upper Ravi catchment is shown in Table 2. It is evident that the stream length of the lower orders is much greater in magnitude than the stream lengths of higher orders, i.e. eighth order in the case of the above catchment. A critical comparison has also been done for eight sub-watersheds of the catchment the results of which have been shown in Table 3.

### 4.3.4 Mean Stream Length ( $L_{sm}$ )

The characteristic size of various components in a drainage network and its contributing area is exhibited by the mean stream length of that watershed Strahler [29]. Total stream length in each order when divided by the respective stream segments in that order yields the value of mean stream length. The mean stream length for the upper Ravi catchment varies from 0.371 to 83.01 (in km) (Table 2) with a mean  $L_{sm}$  value of 14.37 (in km). It has been observed that  $L_{sm}$  values for a specific order rise with the rise in order. Strahler [29] indicated that the mean stream length is a characteristic property of the drainage network which is related to its size and the size of its associated surfaces.

### 4.3.5 Stream Length Ratio ( $R_1$ )

The stream length ratio of upper Ravi catchment showed an increasing trend up to fourth order and then showed a decline in the fifth order. A sudden increase in the ratio is observed in the seventh order as shown in Table 2. This variation from the geometric trend in this catchment can be attributed to the lower number of high order stream segments which primarily exhibits that the catchment is well drained with lower order streams directly draining in highest order streams within a short span of time. Therefore, it can be concluded that drainage is considerably simpler and not much complex.

### 4.3.6 Bifurcation Ratio ( $R_b$ )

Bifurcation ratio has been broadly classified as an index of relief and dissection by Horton [11], whereas Strahler [28] opined that there is minimal variation in the trend of  $R_b$  across varied regions with varied environmental conditions only exception being the regions with powerful geological control. Bifurcation ratio has been defined by Schumm [21] as the ratio of the stream segments in one order divided by the stream segments of subsequent higher order. It is a dimensionless parameter which exhibits the degree of prevailing interrelationship between streams of various orders in a basin. The  $R_b$  for upper Ravi catchment varies from 3.03 to 4.0 (Table 2).

According to Strahler [29], in regions where the effect of geological structures on the drainage pattern is minimal, there the value of this parameter generally ranges between 3.0 and 5.0. The higher values of the ratio indicate a high level of structural control in the pattern of drainage network, whereas the lower values indicate that the sub-basins are less affected by structural disturbances [2, 29].

The bifurcation ratios have also been computed for all the sub-watersheds which have been shown in Table 3.

### 4.3.7 Weighted Mean Bifurcation Ratio ( $R_{bm}$ )

Strahler [27] used another representative number called weighted mean bifurcation ratio. Mathematically, it is calculated by multiplying the  $R_b$  value of every order with the total number of streams and taking an average of all the values. The weighted mean bifurcation ratio gives a clear picture of the watershed in terms of structural control. This parameter has also been calculated for all the sub-watersheds. It was observed that two watersheds, SW2 and SW4, have higher values of weighted mean bifurcation ratio compared to other sub-watersheds. It is interesting to note here that only these two sub-watersheds are sixth order sub-watersheds which clearly substantiate the fact that the weighted mean bifurcation ratio is a clear representation of structural control.

## 4.4 Aerial Aspects

### 4.4.1 Elongation Ratio ( $R_e$ )

The ratio of the diameter of a circle having the same area as of the basin to the maximum basin length is defined as elongation ratio ( $R_e$ ) Schumm [21]. Strahler has characterized a range of values for this ratio after assessing it for a variety of geological and climatic zones. This ranges between 0.6 and 1.0. Index of elongation ratio can be used to classify watersheds with varying slopes, i.e. more elongated (less than 0.5), elongated (0.5–0.7), less elongated (0.7–0.8), oval (0.8–0.9) and circular

**Table 4** Aerial aspects of morphometric analysis of upper Ravi catchment

S. No.	Parameters	Value
1	Perimeter (in km)	334.81
2	Length of basin ( $L_b$ ) (in km)	91.56
3	Basin area (in sq. km)	3093
4	Elongation ratio ( $R_e$ )	0.69
5	Drainage density ( $D_d$ ) (km/km <sup>2</sup> )	3.15
6	Stream frequency ( $S_f$ )	6.8
7	Circulatory ratio ( $R_c$ )	4.634
8	Form factor ( $R_f$ )	0.368
9	Drainage texture ( $D_t$ )	21.43
10	Compactness coefficient ( $C_c$ )	1.71
11	Infiltration number ( $I_f$ )	21.43

(0.9–0.10). The elongation ratio of upper Ravi catchment is calculated as 0.69 which indicates the catchment is elongated (Table 4).

#### 4.4.2 Drainage Density ( $D_d$ )

Strahler [29] has described drainage density as a ratio of total stream length and basin area. Its value is greatly influenced by the factors governing the characteristic length of a basin. Various geographical and landscape features are related to the drainage density value of a particular watershed, namely rock and soil properties, climate, relief, valley density, channel head and source area and the process of landscape evolution. The drainage density for upper Ravi catchment is calculated to be 3.15 km/km<sup>2</sup> (Table 4) which is moderate in nature. Moderate drainage density is an indication of a thick vegetative cover and a moderately permeable sub-soil.

#### 4.4.3 Stream Frequency ( $S_f$ )

Stream frequency ( $S_f$ ) is a ratio of all stream segments in a watershed to the area of the watershed [10]. It has also been stated that basins with lower values of  $S_f$  are a clear indication of low relief with a permeable sub-surface material [20]. The stream frequency value for upper Ravi catchment has been calculated as 6.80 (Table 4). Sub-watershed wise stream frequency has also been calculated which is shown in Table 5.

**Table 5** Aerial aspect of the sub-watersheds of upper Ravi catchment

Sub-watersheds	$L_b$ (in km)	$A$ (in $\text{km}^2$ )	$P$ (in km)	$R_e$	$D_d$	$S_f$	$R_c$	$R_f$	$D_t$	$C_c$
SW1	24.5	265.62	77.45	0.75	2.85	6.13	0.56	0.44	17.47	1.34
SW2	22.78	303.14	105.89	0.86	2.79	5.57	0.34	0.58	15.56	1.73
SW3	11	334.35	121.28	0.59	2.97	6.16	0.29	0.27	18.33	1.88
SW4	22.7	266.23	87.29	0.81	3.5	7.57	0.44	0.52	26.52	1.51
SW5	31	465.27	133.93	0.79	2.93	5.94	0.33	0.48	17.42	1.76
SW6	38.7	565.38	154.54	0.69	3.43	7.84	0.3	0.38	26.88	1.84
SW7	13.41	256.25	102.51	1.03	3.22	6.77	0.31	0.42	21.8	1.81
SW8	27.5	619.92	152.68	1.02	3.3	7.63	0.33	0.72	25.14	1.74

#### 4.4.4 Circulatory Ratio ( $R_c$ )

Circulatory ratio is a ratio of basin area to the area of a circle with the same circumferential length as that of the perimeter of the basin.  $R_c$  is a significant ratio that indicates the dendritic stage of a watershed. Circulatory ratio pertains to the basin geometry it depends on the geology, land use/land cover, relief, slope and climate [12]. A range has also been prescribed for different values of  $R_c$ , low values relate to the young stage of a watershed, medium values relate to the mature stage of a watershed, and higher values indicate the old stages of the life cycle of a watershed.  $R_c$  value of various sub-watersheds of upper Ravi catchment is in the range of 0.29–0.56 (Table 5).

#### 4.4.5 Form Factor ( $R_f$ )

It has been defined that form factor is a ratio between the basin area and square of basin length [10]. For a perfectly circular watershed, the value of form factor will be less than 0.754 always. The elongation characteristic of a watershed increases with a reduction in its value. It has been noticed that higher peak flows with considerably shorter duration arise in watersheds that have high form factors. Form factors have been computed for all the sub-watersheds of upper Ravi catchment for which the values range from 0.27 to 0.72 (Table 5). The form factor for the complete catchment has come out to be 0.368 (Table 4).

#### 4.4.6 Drainage Texture ( $D_t$ )

Drainage texture is a depiction of the relative spacing of drainage lines; it acts as a significant geomorphologic parameter of a watershed which underlines features such as lithology, infiltration capacity and relief aspects of the watershed terrain.

Drainage texture is the ratio of the total number of stream segments of all orders to the perimeter of that area [11]. Smith (1939) classified five different categories of  $D_t$ , namely very coarse (<2), coarse (2–4), moderate (4–6), fine (6–8) and very fine (>8) [26]. Drainage texture of upper Ravi catchment is found to be 21.43 (Table 4). It indicates that the watershed is of very fine drainage texture. Drainage factors have also been calculated for all the sub-watersheds of upper Ravi catchment (Table 5)

#### 4.4.7 Compactness Coefficient ( $C_c$ )

According to researcher compactness, the coefficient of a watershed is the ratio of the perimeter of watershed and circumference of the circular area, which equals the area of the watershed [9]. The  $C_c$  is a slope-dependent entity and is entirely independent of the watershed size. The value of compactness coefficient of upper Ravi catchment is found to be 1.71 (Table 4). The value of  $C_c$  in the eight sub-watersheds of upper Ravi catchment varies from 1.34 to 1.88. It can be seen from Fig. 4 that SW1 which has the closest value to unity has the most circular structure compared to SW3 which is elongated in shape.

#### 4.4.8 Length of Basin ( $L_b$ )

Basin length has been defined in a variety of ways by different people. Schumm [21] has defined the basin length as the longest dimension of the basin parallel to the principal drainage line. Gardiner [8] defined the basin length as the length of the line from a basin mouth to a point on the perimeter equidistant from the basin mouth in either direction around the perimeter. Using GIS capabilities, the basin length for upper Ravi basins and its various sub-watersheds have been determined and are depicted in Tables 4 and 5, respectively. The basin length for entire upper Ravi catchment has come out to be 91.56 km.

### 4.5 Relief Aspect

#### 4.5.1 Total Relief ( $H$ )

Generally termed as watershed relief, this parameter can be defined mathematically as the vertical distance/level difference between the highest and the lowest point of a watershed. Watershed relief controls the gradient of drainage lines within the watershed and hence significantly influences the soil erosion of the watershed [19]. The upper Ravi basin is characterized as a high relief basin with a relief value of 5363 m. SW 1 to SW 8 are also characterized as high relief sub-watersheds and hence are severely prone to generation of significant run-off and consequent soil erosion.

**Table 6** Relief aspects of upper Ravi catchment and its sub-watersheds

Sub-watershed	$H$ (m)	$R_h$ (m/km)	$R_r$ (m/km)
Upper Ravi catchment	5363	58.57	16.01
SW1	3744	152.81	48.34
SW2	3360	147.49	31.73
SW3	3622	329.27	29.86
SW4	3412	150.30	39.08
SW5	3887	125.33	29.02
SW6	4591	118.63	29.70
SW7	3243	241.83	31.63
SW8	3691	134.21	24.17

#### 4.5.2 Relief Ratio ( $R_h$ )

Relief ratio is defined as a ratio of the total relief of a basin to the length of basin [21]. The advantage of relief ratio over the total watershed relief is that it removes the size effect by dividing the total relief by the basin length. In upper Ravi basin, relief ratio varies from 118.63 m/km (SW6) to 329.27 m/km (SW3) (Table 6). Significantly, high relief ratio especially in SW3 indicates the steepness of the principal flow path, which eventually leads to bank erosions and heavy sediment load transport.

#### 4.5.3 Relative Relief ( $R_r$ )

Ratio of maximum watershed relief to the watershed perimeter is defined as  $R_r$ . It means that the steeper the slope, the higher is the surface above its base. The values of the relative reliefs for eight sub-watersheds of upper Ravi basin vary from 24.17 to 48.34 m/km, indicating high degree of variation in terrain structure of the catchment. Very high values of  $R_r$  for SW1 sub-watershed indicate that it is highly susceptible to soil erosion.

### 4.6 Prioritization of Sub-watersheds Using Morphological Parameters

Morphological parameters (linear, aerial and relief) for all sub-watersheds were calculated separately. For prioritization, all eight sub-watersheds are ranked based on their corresponding values of morphological parameters. Morphological parameters like drainage density, stream frequency, bifurcation ratio and drainage texture have a direct relationship with run-off. Therefore, the sub-watershed having the highest numerical value of these individual parameters was ranked first and next higher sub-watershed was ranked second and so on. Similarly, aerial parameters like elongation

ratio, circularity ratio, form factor and compactness coefficient have an inverse relationship with run-off. Therefore, the sub-watershed having the lowest value for these individual parameters was assigned the first rank and next lower was second and so on. Similarly, sub-watersheds are ranked according to relief aspect as it has a direct relationship with the erosivity. Finally, based on all individual ranking, a compound rank value was calculated for each sub-watershed and is depicted in Table 7. It is evident from Table 7 that SW6 has the highest priority (lowest value of compound rank value, i.e. 3.27) and SW2 has the least priority (highest value of compound rank value, i.e. 5.64). The highest priority indicates the greater degree of run-off in the particular sub-watershed. Thus keeping in mind the nature of each sub-watershed with respect to their susceptibility to massive run-off and low time of concentration, SW6 shall be counted as the highest priority watershed. It can also be assumed as a highly erosive sub-watershed. It implies that watershed management activities should be started from sub-watershed SW6 and should proceed subsequently according to the ranking (Fig. 7).

## 5 Conclusion

Morphometric analysis of any drainage system is a prerequisite to any hydrological study. Thus, this research is aimed at developing an insight into the interrelation of stream network behaviour of upper Ravi River catchment. The uses of remote sensing and GIS tools and techniques have proven to be a very effective and frugal tool for basin drainage analysis. This remote sensing data in conjunction with the old ground survey data such as SOI toposheet brings an unambiguous picture, which enables any geomorphologist or hydrologist to arrive at a concrete and holistic conclusion about the behaviour of a catchment. The study also substantiates that GIS-based approach is more appropriate than the conventional methods to analyse drainage basin and the effect of various parameters on landforms, soils and erosion characteristics. The morphometric parameter calculations using these techniques have a high degree of accuracy and can be even better with high-resolution satellite imagery. The morphometric analysis was carried out using SRTM DEM for relief aspects and SOI surveyed drainage for linear and areal aspects so that a holistic picture of the basin can be obtained combining both the satellite data and the ground survey data. The analysis shows the drainage network is dominantly dendritic in nature with a high value of drainage texture and very fine drainage. The sub-watersheds have also been demarcated, and morphometric analysis for each sub-watershed has been done to realize their conformity to the nature of their major catchment and to identify any exceptions exhibited in their drainage patterns.

The stream length ratio is almost constant up to fifth order, but a sudden rise after that clearly indicates a reduction in the number of higher order streams. This variation from the geometric trend in this sub-basin can be attributed to the lower number of high order stream segments which suggest that the basin is well drained with lower order streams directly draining in highest order streams within a short span of time;



**Table 7** Prioritization of sub-watersheds of upper Ravi River catchment

Sub-watershed	Ranking based on individual morphological parameter											Compo-und rank value	Final ranking
	$D_d$	$F_s$	$R_c$	$R_f$	$R_e$	$R_b$	$H$	$R_h$	$R_r$	$D_t$	$C_c$		
SW1	7	6	8	3	3	7	3	3	1	6	1	4.36	4
SW2	8	8	6	6	6	2	7	5	3	8	3	5.64	8
SW3	5	5	1	1	1	6	5	1	5	5	8	3.91	3
SW4	1	3	7	5	5	1	6	4	2	2	2	3.45	2
SW5	6	7	5	4	4	5	2	7	7	7	5	5.37	7
SW6	2	1	2	2	2	4	1	8	6	1	7	3.27	1
SW7	4	4	3	8	8	8	8	2	4	4	6	5.36	6
SW8	3	2	4	7	7	3	4	6	8	3	8	4.64	5

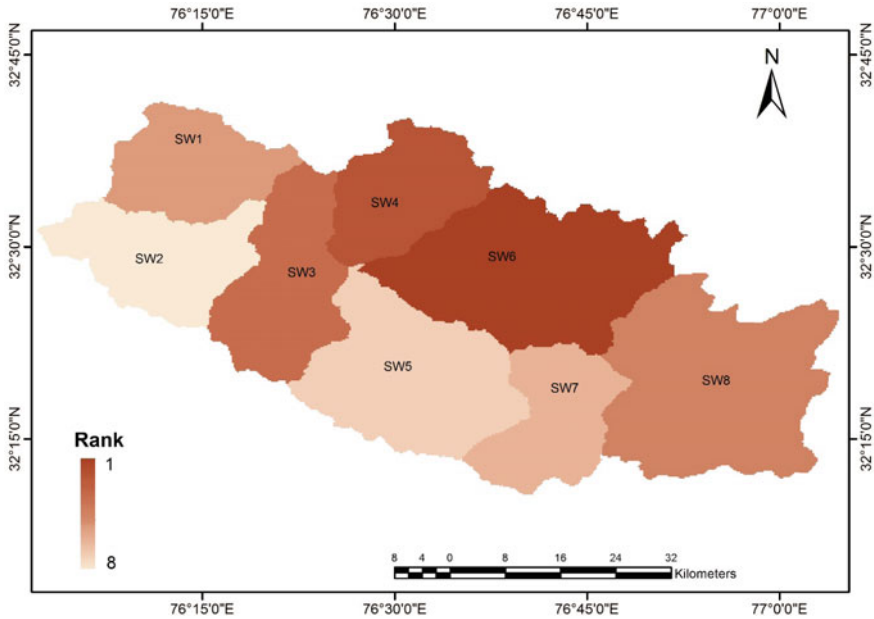


**Fig. 7** Sub-watershed-wise priority map of upper Ravi River catchment

the bifurcation ratio indicates that the watershed under consideration is of normal category with a moderate drainage density ( $<5$ ) which is also an indication of a permeable sub-soil structure. A moderate to high value of drainage density indicates moderate to steep slopes in the catchment. Elongation ratio for upper Ravi basin is 0.69 which indicates the elongated structure of the basin as is evident from the imagery as well. A higher elongation ratio value shows high infiltration capacity and low run-offs. Prioritization of sub-watersheds has been done according to rankings assigned on the basis of morphometric parameters. SW6 has the highest priority and SW2 has the least priority. Prioritization is the first and primary step for any watershed management and planning projects, and its accuracy plays a vital role in the eventual success of such projects. The database obtained through the morphometric analysis of upper Ravi basin can form a basis for further deliberations and studies pertaining to the integrated watershed management of the basin.

**Acknowledgements** The authors are grateful to the Director, National Institute of Hydrology, Roorkee, India, for providing all the necessary facilities required for this study. The work has been done under the aegis of Purpose Driven Study (PDS) of Western Himalayan Regional Centre, Jammu under the National Hydrology Project (NHP). The authors are also grateful to the Nodal Officer (NHP) for his constant support.

## References

1. Agarwal CS (1998) Study of drainage pattern through aerial data in Naugarh area of Varanasi district, U.P. *J Indian Soc Remote Sens* 26:169–175
2. Chopra R, Raman DD, Sharma PK (2005) Morphometric analysis of sub-watersheds in Gurdaspur district, Punjab using remote sensing and GIS techniques. *J Indian Soc Remote Sens* 33(4):531–539
3. Clarke JI (1996) *Morphometry from maps. Essays in geomorphology*. Elsevier Publication Co., New York, pp 235–274
4. Dar RA, Chandra R, Romshoo SA (2013) Morphotectonic and lithostratigraphic analysis of intermontane Karewa basin of Kashmir Himalayas, India. *J Mt Sci* 10(1):731–741
5. Evans IS (1972) General geomorphometry, derivatives of altitude, and descriptive statistics. In: Chorley RJ (ed) *Spatial analysis in geomorphology*. Harper and Row, New York, pp 17–90
6. Faniran A (1968) The index of drainage intensity—a provisional new drainage factor. *Aust J Sci* 31:328–330
7. Gayen S, Bhunia GS, Shi PK (2013) Morphometric analysis of Kangshabati-Darkeswar interfluves area in West Bengal, India using ASTER DEM and GIS techniques. *Geol Geosci* 2(4):1–10
8. Gardiner V (1975) Drainage basin morphometry, British geomorphological group. *Tech Bull* 14:48
9. Gravelius H (1914) *Grundrifi der gesamten Gewisserkunde. Band I: Flufikunde (Compendium of hydrology, vol I. Rivers, in German)*. Goschen, Berlin
10. Horton RE (1932) Drainage basin characteristics. *Am Geophys Union Trans* 13:348–352
11. Horton RE (1945) Erosional development of streams and their drainage basins; hydrophysical approach to quantitative morphology. *Bull Geol Soc Am* 56:275–370
12. John Wilson JS, Chandrasekar N, Magesh NS (2012) Morphometrical analysis of major sub watersheds in Aiyar & Karai Pottanar Basin, Central Tamil Nadu, India using remote sensing & GIS techniques. *Bonfring Int J Ind Eng Manag Sci* 2(special issue1):8–15
13. Magesh NS, Chandrasekar N, Kaliraj S (2012) A GIS based automated extraction tool for the analysis of basin morphometry. *Bonfring Int J Ind Eng Manag Sci* 2(1):32–35
14. Merritts D, Vincent KR (1989) Geomorphic response of coastal streams to low, intermediate, and high rates of uplift, Mendocino junction region, northern California. *Geol Soc Am Bull* 101:1373–1388
15. Muller JE (1968) An introduction to the hydraulic and topographic sinuosity indexes. *Ann Assoc Am Geogr* 58:371–385
16. Nag SK, Chakraborty S (2003) Influence of rock types and structures in the development of drainage network in hard rock area. *J Indian Soc Remote Sens* 31(1):25–35
17. Nautiyal MD (1994) Morphometric analysis of a drainage basin, district Dehradun, Uttar Pradesh. *J Indian Soc Remote Sens* 22(4):251–261
18. Obi Reddy GE, Maji AK, Gajbhiye KS (2002) GIS for morphometric analysis of drainage basins. *GIS India* 4(11):9–14
19. Ozdemir H, Bird D (2009) Evaluation of morphometric parameters of drainage networks derived from topographic maps and DEM in point floods. *Environ Geol* 56:1405–1415
20. Reddy GPO, Maji AK, Gajbhiye KS, (2004) Drainage morphometry and its influence on land-form characteristics in a basaltic terrain, Central India—a remote sensing and GIS approach. *Int J Appl Earth Obs Geoinformation* 6(1):1–16
21. Schumm SA (1956) *Evolution of drainage systems and slopes in bad lands at Perth Amboy, New Jersey*. *Geol Soc Am Bull* 67:597–646
22. Sethupathi AS, Lakshmi Narasimhan C, Vasanthamohan V, Mohan SP (2011) Prioritization of mini watersheds based on morphometric analysis using remote sensing and GIS in a drought prone Bargur Mathur sub-watersheds, Ponnaiyar River basin, India. *Int J Geomat-Geosci* 2(2):403–414
23. Shreve RW (1969) Stream lengths and basin areas in topologically random channel networks. *J Geol* 77:397–414

24. Singh KN (1980) Quantitative analysis of landforms and settlement distribution in southern uplands of eastern Uttar Pradesh (India). Vimal Prakashan, Varanasi
25. Singh S (1992) Quantitative geomorphology of the drainage basin. In: Chouhan TS, Joshi KN (eds) Readings on remote sensing applications. Scientific Publishers, Jodhpur
26. Smith GH (1939) The morphometry of Ohio: the average slope of the land (abstract). Ann Assoc Am Geogr 29:94
27. Strahler AN (1952) Dynamic basis of geomorphology. Geol Soc Am Bull 63:923–938
28. Strahler AN (1957) Quantitative analysis of watershed geomorphology. Trans Am Geophys Union 38:913–920
29. Strahler AN (1964) Quantitative geomorphology of drainage basins and channel networks. In: Chow VT (ed) Handbook of applied hydrology. McGraw-Hill, New York, pp 439–476

# Estimation of Domestic Water Demand and Supply Using System Dynamics Approach



Bharti Chawre

**Abstract** Water is a basic need for survival and well-being of all, and therefore, it is required to provide adequate quantity and potable quality of water to all. Water is used for all purposes such as domestic, agriculture and industrial needs, navigational, recreational, and power generation. In this study, water demands and supply for domestic sector have been presented. Based on various factors, e.g., the level of economy, technological advancement, and pricing policy, level of urbanization, ratio of private to public water supply, and population coverage under public water supply, the unit water demand and supply at the user end for domestic sector is calculated and discussed. With the help of Vensim simulation software, a system dynamics-based simulation model (domestic water sector model) for estimating the domestic water demand and supply has been developed. Domestic water sector model is validated on the available data, and the simulated results showed good agreement. Study showed that the water supply is meeting the projected water demand of 87.35 BCM in the year 2050 (for a projected population of 1.645 billions) because the highest priority is given to meet the domestic water demand as per National Water Policy of India, GOI.

**Keywords** Domestic water demand and supply · System dynamics · Vensim

## 1 Introduction

India is a land which has been blessed with large numbers of big and small rivers, the sweet water of which can be put to many uses such as drinking, other domestic needs, agriculture and industrial uses, navigational, recreational, and power generation. But due to various misuses and abuses, the quality of the existing water resources is degrading day by day and is becoming less usable and water scarcity is increasing. In a developing country like India, many factors are responsible for this situation.

---

B. Chawre (✉)

Scientist-C, Central Soil and Materials Research Station, New Delhi 110016, India  
e-mail: [bharti.bhanu.2005@gmail.com](mailto:bharti.bhanu.2005@gmail.com)

Rapid growth in water demand due to increase in population, increasing droughts in various states of India, declining surface water and groundwater quality, and unabated flooding, interstate river disputes, growing financial crunch, inadequate institutional reforms and enforcement are some of the crucial problems faced by the country's water sectors.

Water is a basic need for survival and well-being of all, and therefore, it is required to provide adequate quantity and potable quality of water to all. The provision of clean drinking water has been given priority in the Constitution of India, with Article 47 conferring the duty of providing clean drinking water and improving public health standards of the state. Agenda 21 and the fourth and final principle of Dublin [1] also says "water should be considered an economic good, adding that it is vital to recognize first of all the basic right of all human beings to have access to clean water and sanitation at an affordable price".

Different aspects of domestic demand have been studied by various researchers. According to Shiklomanov [2] worldwide, about 70% of the water used is for irrigation, 20% for industrial purposes, and 10% for domestic purpose. Lehman [3] investigated water demand reduction by implementing an inclining rate structure. The second phase of his study is to determine the elasticity of the rate, segmented by customer type, which can be used for rate forecasting and water demand management. Arrus and Garadi [4] observed that present forecasting methods arrive at the estimates of demand which lack sound foundations are difficult to control. Demand does not exist as such, since it is always determined by choices of economic development, which in turn involves specifying economic policy criteria, technical criteria, and social criteria. Baumli [5] presents information on current and projected urban demands, demand reduction measures, why water transfers are necessary, conditions for water transfers, and examples of water transfers for California. Spain is on the verge of introducing its National Hydrological Plan, a decree aimed at rescuing the country from serious drought. Weber [6] briefly discusses the major methods of demand forecasting and then concentrates on measuring conservation performance and integrating conservation targets into long-run demand projections. Biswas [7] discussed that with increasing population, water demand will increase while water availability is unlikely to increase creating conflict among different water sectors. Armal [8] discussed the aspects of the demand on one side and the planning of the resources on the other of Maharashtra, the most industrious state of India. Seckler [9] developed a simulation model which is based on a conceptual and methodological structure that mixes various strategies from earlier assessments. In that simulation model, projections are made for three important sectors: agriculture, domestic and industrial water use. In many large equipped cities of the world, the water withdrawal for domestic uses is 300–600 lpcd. On the other hand in developing agricultural countries of Asia, Africa, and Latin America, the domestic water withdrawal is 50–80 lpcd. In individual regions with insufficient water resources, it is not more than 10–40 lpcd [10]. A stochastic end-use model for the simulation of residential water demand has been developed by Blokker et al. [11]. The end-use model is based on statistical information of water-using appliances and residential users instead of water demand measurements. Blokker et al. [11] study shows that the simulation results are in

good agreement with measured water demand patterns. Nezhad et al. [12] studied the effect of price elasticity on domestic water demand for Ahvaz city of south of Iran. Study says that the increment of price of domestic water is low elastic because of being essential and non-substitutable.

Above studies say unit water demands are considered to be dynamic, depending upon above various factors. Therefore, in this study a system dynamics-based simulation model (domestic water sector model) for estimating the domestic water demand and supply has been developed. Based on the level of economy, technological advancement, pricing policy, and supply efficiency, the unit water demand at the source end for domestic sector is calculated. The level of urbanization, ratio of private to public water supply, and population coverage under public water supply are used in the estimation of domestic water supply.

## 2 Various Norms for Domestic Water Demand and Supply

Water required for drinking, cooking, washing, and cleaning (utensils, clothes, and house), water coolers and for other purposes such as watering plants/garden and washing personal vehicle, etc., is known as domestic water demand. Various standards have been suggested for estimating water requirements for human use. Glick [13] has estimated 50 L per capita per day (lpcd) as the basic human need. The world health organization [14] has suggested a target of 200 lpcd water supply in urban areas. A variety of factors affects water use in rural and urban areas, e.g., size of population, economic condition, commercial and manufacturing activities and other factors like climate quality, technology, costs, and conservation needs. Desirable and feasible norms can be established by reviewing past performance and modifying these on the basis of feasible resources. Water supply norms of urban population listed by Zakaria Committee [15] varied between 67.5 and 270 lpcd.

### 2.1 CPHEEO Norms

Norms for water supply suggested by the Central Public Health and Environmental Engineering Organisation [16] are given in Table 1.

The rural water supply norms recommended by CPHEEO and the National Technology Mission ranged between 40 and 70 lpcd. Reviewing the water supply and sanitation in urban areas, the National Commission on Urbanization [17] argued for more realistic targets and recommended 110–120 lpcd. Central Water Commission [18] assumed a unit figure of 140 lpcd for urban and 70 lpcd for rural population for the estimation of domestic water requirement. The National Water Development Agency (NWDA) in 1991 assumed a uniform rate of water supply of 200 lpcd for urban population for water balance studies of basins.

**Table 1** Recommended per capita water supply levels for designing schemes

Sl. No.	Classification of towns/cities	Recommended maximum water supply levels (lpcd)
1.	Towns provided with piped water supply but without sewerage system	70
2.	Cities provided with piped water supply where sewerage system is existing/contemplated	135
3.	Metropolitan and mega cities provided with piped water supply where sewerage system is existing/contemplated	150

*Note i.* Figures exclude “Unaccounted for Water (UFW)” which should be limited to 15%

In urban areas, where water is provided through public stand posts, 40 lpcd should be considered. Figures include the requirements of water for commercial, institutional and minor industries. However, for bulk supply such establishments should be assessed separately with proper justification. *Source* Ministry of Urban Development, Central Public Health and Environmental Engineering Organisation Manual on Water Supply and Treatment, Third Edition—Revised and Updated (May 1999), New Delhi [16]

### 3 Model Conceptualization and Formulation

Generally, there are overall two basic forecasting techniques used by water demand analysis. The first technique is based upon trend or extrapolative forecasting, where projections of future water consumption are based on past consumption data. The second technique is analytical technique, in which water consumption is disaggregated into major components [19]. Future changes in each component are predicted separately and aggregated. Most of the studies on the water demand projections also reflect a strong relationship between per capita GDP and withdrawal. As the GDP of a country increases, the water demand also increases in various sectors to support a better quality of life. Past trends can also give an indication about the likely projected trend of water withdrawal depending upon population and various socioeconomic-technological factors.

Based on the above study, unit water demands are considered to be dynamic, depending upon the above-mentioned factors. In the present study, an attempt is made to give a system dynamics-based simulation model (domestic water sector model) for estimating the domestic water. Vensim (Ventana **simulation**) simulation software [20] is used for this study to create system dynamics model incorporating dynamics feedbacks and simulations. Based on the level of economy, technological advancement, and pricing policy, the unit water demand at the user end is calculated for domestic sector. The unit water demand at the source is calculated after taking into account the water supply system efficiency.



In the model, the population is classified into two categories—urban and rural. The urbanization denotes the fraction of total population residing in urban areas. The water demand for rural and urban population is calculated separately and added to get the total domestic water demand. The level of urbanization, ratio of private to public water supply, and population coverage under public water supply are used in the estimation of domestic water supply.

### 3.1 Population and Economic Module

Population and economic module (View 1) calculates total, urban, rural populations and GDP. Although population dynamics can be quite complicated, the population rates are assumed from the census data for a large scale at the country level. Populations and GDP have been taken as LEVEL and are calculated from the respective RATE equations. Population and GDP growth rates are taken as exogenous variables, and the values are assumed as per the census, economic data, and projections.

### 3.2 Unit Water Demand

The unit water demand is defined as the water required at source per unit in different sectors. Accordingly, unit water demand for domestic sector is taken as the volume of water needed per capita per annum. The unit water demands depend on key factors like level of economy, pricing policy, technological advancements, and efficiency of supply systems besides the factors like social development, people's lifestyle, awareness, and attitude of the people toward water use. Therefore, unit water demands are considered to be dynamic, depending upon above-mentioned factors, and it is very difficult to quantify and find out a relationship between unit water demands and the factors on which it is dependent.

The unit water demands for the domestic sector are expressed as the function of a unit water demand at the user end ( $WD'_{\text{domestic\_sector,unit}}$ ) of that sector. It can be reduced by pricing mechanism that helps in awareness generation and attitudinal change toward water uses. Technological advancement levels will reduce the  $WD'_{\text{domestic\_sector,unit}}$ , say  $WD''_{\text{domestic\_sector,unit}}$ . Technological advancement refers to the use of technology at the user end, which reduces the wastage of water and thus helps in reducing the unit water demand at the user end. The actual unit water demands ( $WD''_{\text{domestic\_sector,unit}}$ ) at source are obtained by dividing the modified water demand ( $WD''_{\text{domestic\_sector,unit}}$ ) by the water supply system efficiency of domestic sector.

In general, the price elasticity ( $El_{p,\text{domestic\_sector}}$ ) of unit water demand at the user end is defined as the percentage change in the  $WD'_{\text{domestic\_sector,unit}}$  divided by the percentage change in water pricing ( $WP_{\text{domestic\_sector}}$ ) and can be expressed as:

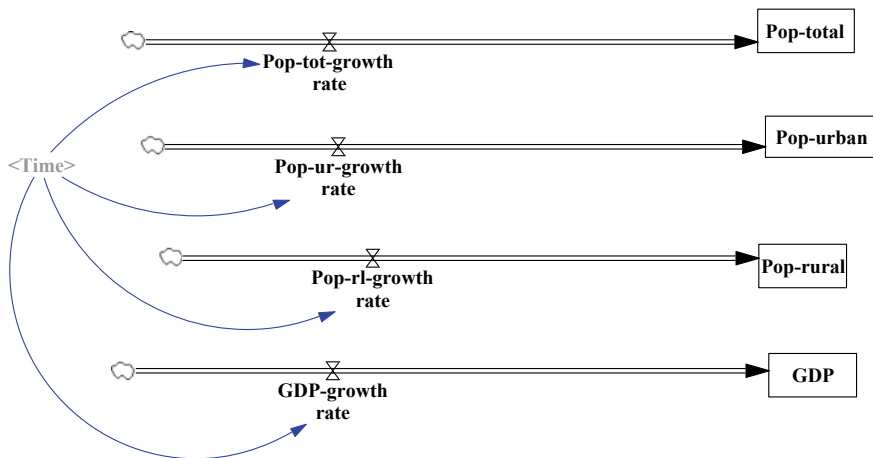


Fig. 1 View 1: Population and economic model

$$El_{p,domestic\_sector} = \frac{\frac{dWD'_{domestic\_sector,unit}(t)}{WD'_{domestic\_sector,unit}(t)}}{\frac{dWP_{domestic\_sector}(t)}{WP_{domestic\_sector}(t)}} \tag{1}$$

Therefore, the change in the unit water demand at the user end because of price elasticity may be expressed as:

$$\frac{dWD'_{domestic\_sector,unit}(t)}{dt} = WD'_{domestic\_sector,unit}(t) \left[ El_{p,domestic\_sector} \frac{dWP_{domestic\_sector}(t)/dt}{WP_{domestic\_sector}(t)} \right] \tag{2}$$

The technological advancement and its implementation will lead to reduction in this unit water demand. The reduced water demand  $WD''_{domestic\_sector,unit}(t)$  is calculated as:

$$WD''_{domestic\_sector,unit}(t) = WD'_{domestic\_sector,unit}(t) \times \eta_{tech,domestic\_sector}(t) \tag{3}$$

where  $\eta_{tech,domestic\_sector}(t)$  represents a demand reduction factor due to technological improvement. The value of  $\eta_{tech,domestic\_sector}(t)$  is taken as 1.0 at the initial stage which would keep on reducing and would be finally attaining a minimum value asymptotically corresponding to a maximum technological advancement level.

The actual unit water demand for domestic sector at source will depend upon the water supply system efficiency ( $\eta_{eff,domestic\_sector}(t)$ ) and is finally expressed as:

$$WD''_{domestic\_sector,unit}(t) = \frac{WD''_{domestic\_sector,unit}(t)}{\eta_{eff,domestic\_sector}(t)} \tag{4}$$

Domestic water sector model is described in views from 1 to 4 (Fig. 1, 2, 3 and 4).

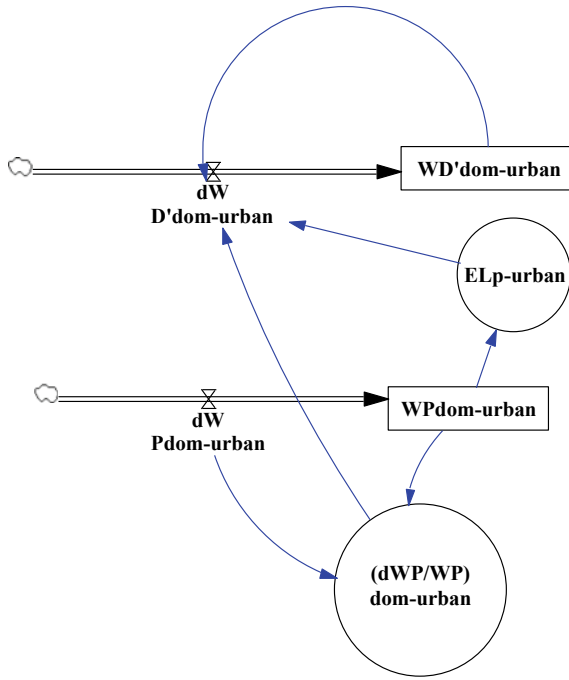


Fig. 2 View 2: Effect of price elasticity on urban domestic unit water demand at user end

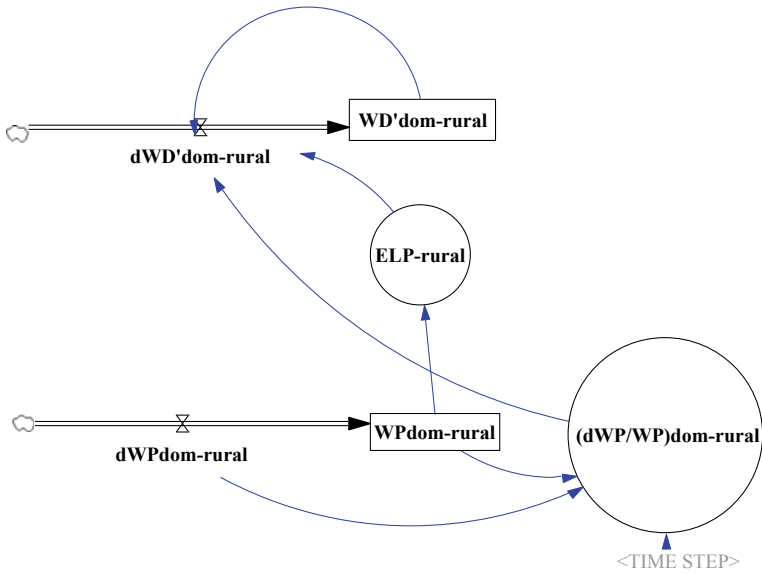


Fig. 3 View 3: Effect of price elasticity on rural domestic unit water demand at user end

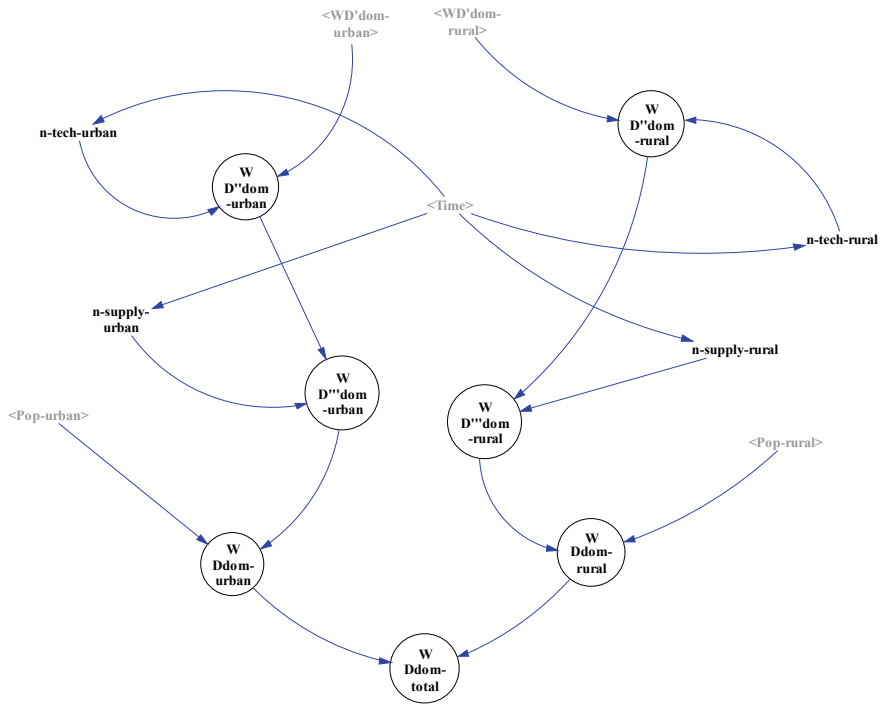


Fig. 4 View 4: Total domestic water demand at source

Domestic water demands are met either through public water supply or private water supply. Public water supply in general implies larger demand per capita, and its coverage of population is also an index-related with human well-being and health. Public water supply system includes water supply through house taps. People relying on self-supply obtain their water via dug wells, tube wells, or from other sources. The ratio of private to public unit water demand depends upon the government policy to allow the private sector participation in domestic water supply sector. It is generally perceived that as socioeconomic development takes place, the public water supply coverage also improves and is a prerequisite for improved health, social, and economic development. For countries with the high-income group, the coverage is somewhere total.

### 3.3 Unit Water Supply

Water supplies for domestic sector for rural and urban population are estimated by using Eq. (5). Water supply for urban and rural populations depends upon water demand and allocation factors. Allocation factor will be varying between 0 and 1



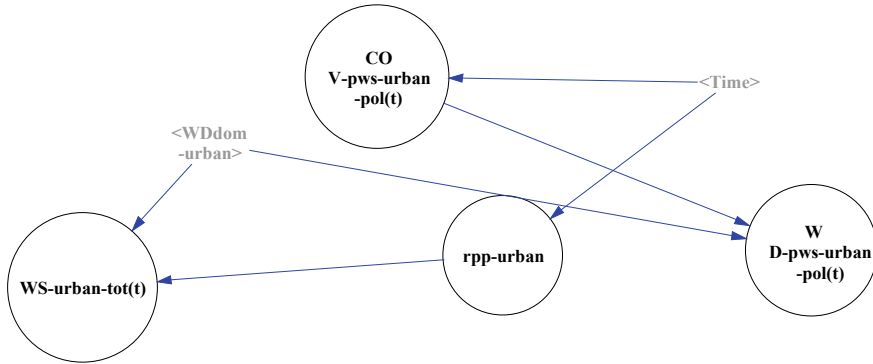


Fig. 5 View 5: Urban water supply

depending upon partial or full funds availability for the required urban and rural water supply. Allocation factor for urban and rural water supply is calculated as the ratio of the actual expenditure in a particular sector and the demanded expenditure in that sector as given in Eq. (6). Actual expenditure in a particular sector is taken as the minimum of the demanded expenditure and the maximum expenditure available in that sector. Model for domestic water supply is described in views from 5 to 7 (Figs. 5, 6 and 7). Equations from (1) to (5) are generalized equations for domestic water sector model; in this study, these equations applied for urban and rural sectors.

$$WS_{\text{domestic\_sector}}(t) = (rpp + (1 - rpp) \times AF_{\text{domestic\_sector}} \times COV_{\text{domestic\_sector}}(t)) \times WD_{\text{domestic\_sector}}(t) \quad (5)$$

$$AF(t) = \frac{EXP_{act}(t)}{EXP_{dem}(t)} \quad (6)$$

#### 4 Input Parameters

The year 1990 is chosen as the base year in the present study when major economic reforms in India were initiated. The total population of India in the year 1990–91 has been taken as 846.43 million according to the census of India. The initial value of population for the urban and rural has been taken as 217.61 million and 628.69 million, respectively, which is also based on the population census of India [21]. The average exponential population growth rates are taken from the projects based on United Nations Projections [22]. In the present study, the GDP growth rate of India is assumed as 7%. The initial value of GDP in 1990–91 of India at constant (1993–94 Prices, Factor Cost) prices was 6930108.7 million Indian rupees. Following the general norm of Central Water Commission [18] and NCIWRDP [23], the targeted unit water demand for domestic is taken as 140 lpcd for public water supply; 70

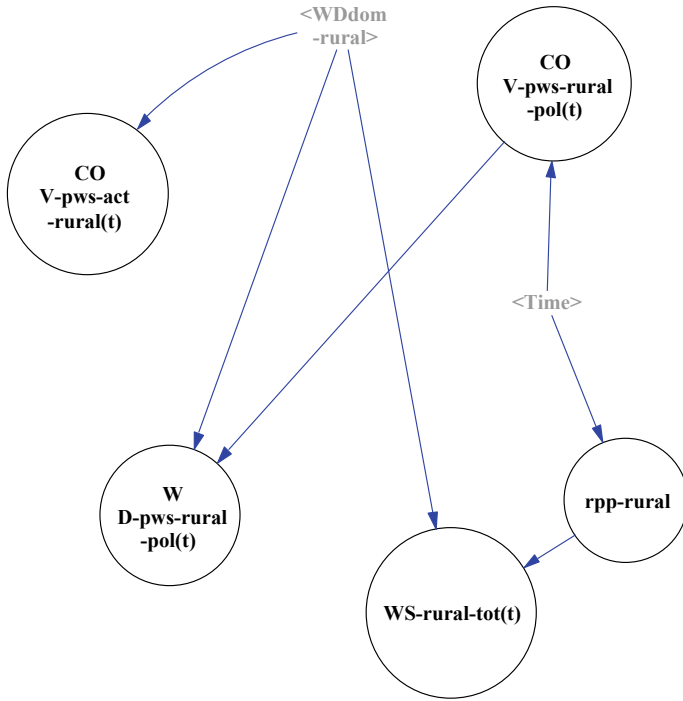


Fig. 6 View 6: Rural water supply

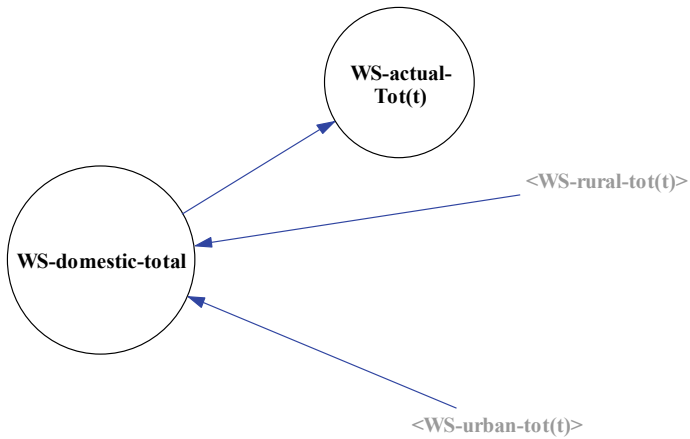


Fig. 7 View 7: Total water supply for domestic sector

lpcd for private water supply in urban areas corresponding to GDP growth rate, respectively; and 70 lpcd for both public and private water supply in rural areas in the present study. This gives the ratio of private to public water supply as 0.5 for urban and 1.0 for rural areas. The average water supply system efficiency for domestic sector is assumed as 70% in the present study and expected to be improved to about 90% by the year 2050.

Water demand in the residential sector is sensitive to price, but the magnitude of the sensitivity depends upon many variables that influence consumption including water prices. The city norms in India are based on the water demands of the city and on the availability of water there. No consideration of price elasticity is taken into account while fixing the water tariff norms in India as water supply is perceived to be a “public service” and the norms are considered to be minimum to maintain a reasonable standard of living. Therefore, in the present study, it is assumed that the domestic water tariffs are fixed to recover the supply costs and the price elasticity is considered to be zero in this range for water supply norms in India as many Indian cities with even surplus revenue receipts were having higher supplies as compared to deficit revenue receipts as per NIUA [24].

## 5 Results and Discussion

The system dynamics-based simulation model (domestic water sector model) encompassing various linkages and feedback to evolve water demand and supply for domestic sector has been formulated in the previous section. In this section, results are presented depending upon the population and economy, supply efficiencies, and technological reduction factor to ascertain the sustainability of the water resources to meet domestic water demand. The validation of the model is not as easy as the data is scattered and to be collected from various reports; therefore, the data lacks the uniformity of assumptions. The data for the year 1990 is fed as input to the proposed model. The model is run for the existing level of urbanisation, water requirement per capita, population, water supply efficiencies, etc., as given in the previous section. Comparison of model results and the available data from various reports are given in Table 2, and the summary of results of domestic water sector model is given in Table 3. It can be seen from Table 2 total population estimated from proposed model is 736.366 million, whereas from the data of Census of India [21] it is found to be 742.49 millions for the year 1999–2000. Similarly, total water supply from the proposed model is 22.4 BCM, whereas from the data of Planning Commission [25] it is found to be 23.3 BCM for the year 2001. It can be seen also from Table 3 that domestic water demands for urban and rural population are increased from 10.32 to 9.17 in 1990 to 61.57 to 25.6 BCM in 2050, respectively. Table 3 shows that the water supply is meeting the projected water demand of 87.35 BCM in the year 2050 because the highest priority is given to meet the domestic water demand as per National Water Policy of India, MoWR [26].

**Table 2** Comparison of model domestic water sector model results and the available data from various reports

Year	<i>Population</i>					
	Proposed model domestic sector			Census of India [21]		
	Total	Urban (M)	Rural (M)	Total	Urban (M)	Rural M
1990–1991	846.43 M	217.61	628.69	846.43 M	217.61	628.69
1999–2000	1.020 B	284.20	736.66	1.028 B	286.14	742.49
2010–2011	1.216 B	379.10	826.07	1.210 B	377.11	833.09
Year	<i>Domestic water supply in BCM</i>					
	Proposed model for domestic sector			Planning Commission [25]		
	Urban	Rural	Total	Urban	Rural	Total
1991	9.98	6.37	16.35	9.98	6.37	16.35
2001	13.69	8.71	22.4	13.89	9.41	23.3

**Table 3** Summary of domestic water sector model results

Year	Domestic water demand in BCM			Domestic water supply in BCM		
	Urban	Rural	Total	Urban	Rural	Total
1990	10.32	9.17	19.50	10.32	9.17	19.50
2050	61.75	25.6	87.35	61.75	25.6	87.35
Year	<i>Population in billion</i>					
	Urban		Rural	Total		
1990	0.217		0.628	0.845		
2050	0.853		0.792	1.645		

## 6 Conclusion

A system dynamics-based model to simulate and estimate the water demand and supply has been developed in the present study. Technological development, price elasticity, and supply efficiencies have been considered in estimating the water demand. The projected total water demand has been worked out to be 87.35 BCM in the year 2050. Population coverage under public water supply has been taken as 100% by the year 2050 and has been simulated accordingly. The model is validated on the available data, and it can be seen from Tables 2 and 3 that the model results are in good agreement with the available data.

Therefore, this approach can also be used for estimating the water demands and supplies for various sectors like irrigation, industrial, and power generation.



## References

1. Summit E (1992) Agenda 2. The United Nations programme of action from Rio. Final text of agreements negotiated at the United Nations Conference of Environmental and Development (UNCED)
2. Shiklomanov IA (1993) World water resources. Water in Crisis, New York, Oxford
3. Lehman PJ (1991) Water demand management through rate structure. In: American Water Works Association, Proceedings, Annual Conference, pp 497–505
4. Arrus R, Garadi A (1991) Intelligent system of computer-aided long-term water demand forecasting, Application in Algeria. Computational Mechanics Publ, Southampton, (Engl), pp 159–171
5. Baumli GR (1993) Without water transfers, cities will thirst. Management of Irrigation and Drainage Systems Integrated Perspectives, pp 85–92
6. Weber JA (1993) Integrating conservation targets into water demand projections. J-Am Water Works Assoc 85(8):63–70
7. Biswas AK (1994) Sustainable water resources development: some personal thoughts. Int J Water Resour Dev 10(2):109–116
8. Armal S (1997) Water resources for urban areas in Maharashtra State. Water Supply 15(1)
9. Seckler DW (1998) World water demand and supply, 1990 to 2025: scenarios and issues. Iwmi
10. Shiklomanov IA (1999) World Water Resources and their use. Joint SHI/NESCO. Product, St Petersburg-end-use model. J Water Res Plann Manage 136(1):19–26
11. Blokker E, Vreeburg J, van Dijk J (2009) Simulating residential water demand with a stochastic end-use model. J Water Res Plann Manage 136(1):19–26
12. Mansour Z-N, Belghis B, Lida Z (2013) Estimation of domestic water demand function in Ahvaz Iran. Herald J Econ Finance 1:15–20
13. Gliick P, (1997) Human population and water: meeting basic needs in the 21st century. Popul Environ Dev pp 105–121
14. World Health Organization (1998) The world health report 1998: life in the 21st century. A vision for all. World Health Organization
15. Zonal Committee (1963) Financial resources of urban local bodies. Committee report. Government of India, New Delhi
16. Committees of Ministry of Urban Development, Central Public Health and Environmental Engineering Organisation (1999) Manual on water supply and treatment. Central Public Health and Environmental Engineering Organisation, Ministry of Urban Development
17. Correa C (1988) Report of the National Commission on Urbanisation. New Delhi
18. CWC (1988) Water resources of India. Central Water Commission, Ministry of Water Resources, Government of India
19. Chawre B (2015) Domestic demands: issues and sustainability. J Sci Technol 1(4):85–193. ISSN 2394-375, EISSN 2394-3769
20. Eberlein R (2007) Vensim user guide (version 5). Ventana Systems, Harvard, MA
21. Registrar General (2010) Census of India. Census Commissioner, Office of the Registrar General, New Delhi
22. The Department of Economic and Social Affairs of the United Nations (2009) World population prospects: the 2008 revision. New York: Department for Economic and Social Affairs
23. NCIWRDP (1999) Integrated water resources development: a plan for action. Report of the National Commission for Integrated Water Resources Development Plan, Ministry of Water Resources, GOI, New Delhi
24. Urban Population of India and Expansion (1999) Solid waste management: improvement initiatives in selected cities of India. Nationa Institute of Urban Affairs
25. Planning Commission (2008) Eleventh five year plan, 2007–2012. Government of India
26. MoWR (2002) National Water Policy—2002. Ministry of Water Resources, Government of India, New Delhi

# Sustainable Development and Management of Groundwater in Varanasi, India



Padam Jee Omar, S. B. Dwivedi and P. K. S. Dikshit

**Abstract** Groundwater is the main source of drinking water for half of the world's population. Therefore, it is very important to conserve and manage this resource. Sustainable development and management of groundwater resource mean to the efficient management of the existing groundwater resources to meet the requirement of the present and future demand without affecting the risk associated with the damage to aquifer physical characteristics. In this paper, Varanasi was taken for the study of groundwater and its sustainable development. Varanasi is the oldest living city, situated on the bank of the holy river Ganga. Varanasi is the third most congested city of the Uttar Pradesh as per census 2011. Due to its religious importance, groundwater extraction is increasing day by day. A steady state of groundwater model was developed for the study area using groundwater flow modelling programme. This model was built in three layers to simulate the different type of soil layers. For conceptualization of the model, different layers and maps were prepared in GIS environment. Data collection was done in the field, and aquifer data was provided by different government organizations. For preparing maps, Landsat 8 satellite imagery was used and for DEM SRTM data was used. Modelling results were also calibrated and validated with the field data. Results reveal that Kashi Vidya Peeth block of the Varanasi is the most groundwater vulnerable regions. Results of this study are very helpful in applying sustainable development and management strategies for the groundwater.

**Keywords** MODFLOW · Sustainable development · GIS · Groundwater · Varanasi

---

P. J. Omar (✉) · S. B. Dwivedi · P. K. S. Dikshit  
IIT (BHU), Varanasi, India  
e-mail: [sss.padam.omar@gmail.com](mailto:sss.padam.omar@gmail.com)

© Springer Nature Singapore Pte Ltd. 2020  
R. AlKhaddar et al. (eds.), *Advances in Water Resources Engineering and Management*, Lecture Notes in Civil Engineering 39,  
[https://doi.org/10.1007/978-981-13-8181-2\\_15](https://doi.org/10.1007/978-981-13-8181-2_15)

201

## 1 Introduction

Groundwater is the main source of water for drinking and other daily use purposes. It is locked up in the ground and extracted with the help of pumping techniques. It becomes extremely significant due to its good quality and easily availability. But in recent years, it is getting depleted as extraction of groundwater increases. Groundwater model can simulate the real field condition of the system which can help in the understanding the behaviour and performance of the groundwater system. This can be done using mathematical equations. Groundwater model estimates the changes in the water balance due to pumping and other modes. Various researchers worked on the groundwater modelling. A dynamic steady-state groundwater model was developed by Graffi et al. [3], in which specific yield was estimated considering one unconfined layer. Capillary rise of water table was ignored in this study which can affect the soil moisture and evapotranspiration. A groundwater fluctuation study was done by Zare and Koch [11] from 2007 to 2009. They simulated a groundwater model using MODFLOW and results revealed that after 10 years of pumping and irrigation action in the study area groundwater table keep on rising, and it will lead to water logging in the 50% of the plain area. Some studies were also done on the interaction of surface and groundwater [2, 4, 5, 8, 9]. Singhal and Goyal [7] conceptualized a three-dimensional flow model using MODFLOW. In this model, random distributed recharge values were used as an average of recharge that is in general find by method of water budgeting. Groundwater flow model can be further used in transport modelling [6]. Zheng and Wang [12] developed three-dimensional transport model, Wels [10] done study on flow model and reviewed benefits of modelling and its application mainly in transport modelling, Anderson [1] described the difficulties involved in the groundwater flow modelling and mass transport modelling. He explains the behaviour of movement of flow in advection and dispersion medium.

In this study, groundwater flow model was developed for Varanasi district using MODFLOW, and the regions are identified which is susceptible for the groundwater vulnerable. This model was used to predict the corrective measures for enhancing the groundwater resources and safe groundwater abstraction.

## 2 Area of Study

The area selected for this study is Varanasi district of Uttar Pradesh, India. Study area is situated on a bank of river Ganga, a sacred river for Hindus. Varanasi is a holy city with minimum elevation of 43 m above mean sea level (msl) and maximum elevation of 99 m above msl. City had population of 1,201,815, according to 2011 census, and in 2018, estimated population is 4.1 million. Varanasi district consists of eight blocks and 1329 villages. Varanasi district stretched between latitudes  $25^{\circ} 09'N$ – $25^{\circ} 35'N$  and longitude  $82^{\circ} 40'E$ – $83^{\circ} 11'E$  which covers an area of 1535.28 km<sup>2</sup>. Location map of the study area is shown in Fig. 1. The average annual rainfall over the Varanasi

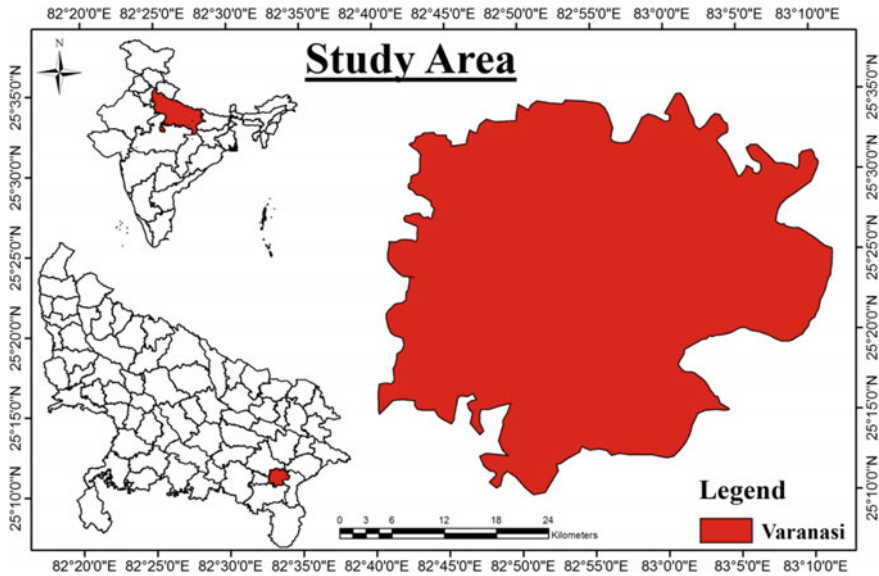


**Fig. 1** Location map of the study area

is 1200 mm. There is large variation between summer and winter temperature. In the summer, temperature variation is 22–46 °C, and in the winter variation is 7–17 °C. The monthly rainfall variation is 96–290 mm in rainy seasons. Between the driest and wettest months, the difference in the precipitation is 296 mm. Crops of Rabi and Kharif are main crops in the study area. As study area lies in the gangetic plain, the soil of this area is very fertile. In recent years, the water head of the river Ganga has decreased significantly. This may happen due to construction of unregulated water extraction, upstream dams and dwindling glacial sources.

### 3 Data Used and Model Development

Groundwater flow model requires various types of data for conceptualization of the MODFLOW. For this, required data was type of soil strata, topography of the area, river stage, groundwater initial head, precipitation, infiltration rate of the soil, climate data, land use and land cover, water demand. Table 1 shows the data used in this study and from where it was collected.

**Table 1** Data used in the study

Data	Type of data	Organization
Climate data	Rainfall, temperature and humidity	India Meteorological Department (IMD) Pune
Digital elevation model (DEM)	Shuttle Radar Topography Mission (SRTM) data of 90 m resolution	United States Geological Survey (USGS)
Satellite imagery	LANDSAT 8	United States Geological Survey (USGS)
Groundwater head and river stage	Groundwater level and top level of river	Field Survey
Census data	Population and livestock population	Office of the Registrar General & Census
Soil data	Soil type and vertical soil strata detail	National Bureau of Soil Survey and Land Utilisation Planning (NBSS & LUP), Nagpur

### 3.1 DEM and LULC Map Preparation

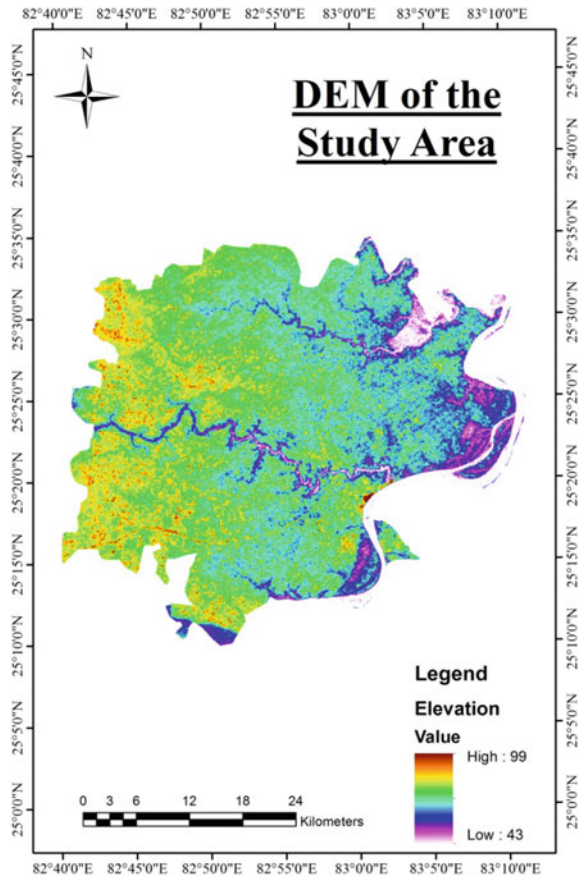
For this study, Shuttle Radar Topography Mission (SRTM) data of Varanasi district was used as a DEM. DEM data contains elevation data on a near-global scale at 90 m resolution. For the present analysis, DEM data was projected to WGS\_1984 and UTM\_Zone\_44 N coordinate system was used. Figure 2 shows the DEM of the study area.

The term land use can be explained as use of land by people habitually with importance upon the functional role of land in economic activities and land cover can be explained as the vegetative and non-vegetative blanket, either natural or man-made of the earth's surface. In the present study, land use and land cover map was prepared using image classification. For this purpose, three bands of LANDSAT 8 imagery were used. Band 5, band 4 and Band 3 were stacked using image processing software, and region of interest (ROI) was delineated. After that, using supervised classification algorithm final map was prepared.

### 3.2 Model Development

A simplified model of the groundwater flow of Varanasi district was developed. To process the GIS-based data such as river digitization, pumping well location, DEM of Varanasi district, and recharge rate map, ArcGIS was used. In the study area, groundwater recharge occurs due to precipitation and some water inflow from the Ganga River. Actual estimation of groundwater recharge rate is very tedious and time taking task, so 30–40% of the precipitation was taken as the recharge rate for

**Fig. 2** Digital elevation model of the study area



the study area. The rainfall is a major aspect for the estimating recharge rate in the area. For assigning the pumping wells, water demand was calculated for the whole study area. This water demand decides the number of pumping wells and location was decided by the field survey. Water from the wells is extracted throughout the year, and the extraction rate of the pumping well was taken  $600 \text{ m}^3/\text{day}$  based on the aquifer capacity. Initial groundwater head level data and observation head data were collected from the CGWB Varanasi.

For the hydraulic property, results of the aquifer pumping test were used in this study. Hydraulic parameters play a very important role in the movement of the groundwater flow. Hydraulic conductivity ( $K$ ) and transmissivity ( $T$ ) are not uniform over the study area. The variation in the hydraulic property is due to the heterogeneity nature of the soil. To avoid the complexity in the model hydraulic property was taken as constant in one strata of the soil. In the first layer of the soil, horizontal hydraulic conductivity ( $K_x$  and  $K_y$ ) in x and y direction are taken as same and equal to  $2.17 \times 10^{-5} \text{ m/s}$ , and vertical hydraulic conductivity ( $K_z$ ) is taken as  $2.17 \times 10^{-6}$

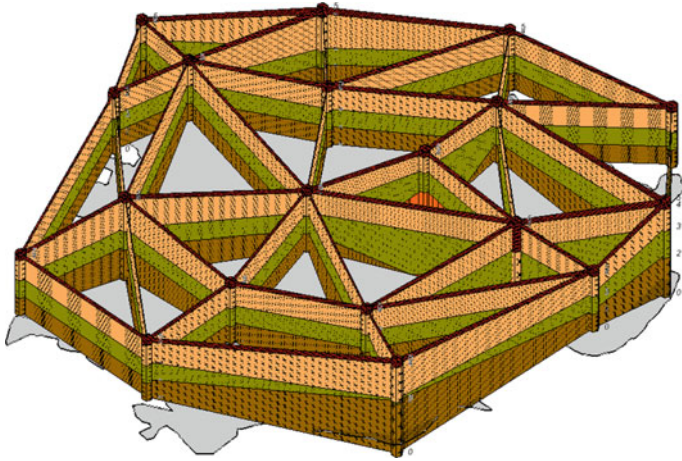


**Fig. 3** Fence diagram of the study area

m/s. Porosity and specific yield ( $S_y$ ) of the soil are taken as 0.30 and 0.11, respectively. Initial groundwater head for the Varanasi district approximately ranges from 6 to 30 m below ground level (bgl). Model was build up in three layers of uniform thickness of 40 m.

To know the vertical soil profile and characteristics of the soil strata, fence diagram was prepared. Fence diagram, as shown in Fig. 3, was prepared using the lithology data. Fence diagram reveals the vertical and lateral disposition of aquifers in the study area down to depth of 120 m below groundwater level. Top layer of the study area consists of surface clay with variation in depth of 3–8 m. Second layer made of fine sand and vary spatially in the nature. Below this layer clayey soil and sandy clay layer were found. Underneath, a relatively hard and impervious bed is encountered. Study area is spread over  $53.45 \text{ km} \times 47.56 \text{ km}$ , and this area is discretized into a three-dimensional grid with a single grid cell size of  $500 \text{ m} \times 500 \text{ m}$ . This grid cell size was selected to maintain a balance between the accuracy of the model and the computational time taken by the model to run. For the model, the boundary condition was taken as specified flow boundary.

### 3.3 Calibration and Validation of the Model

Calibration of the model was carried out by providing the approx values of the model parameters in such a way that it behaves like a real field condition. To minimize the error in the model PEST tool was used. Parameter estimation tool provides the most accurate values of the model parameters. After the model calibration, validation of model was done. For validation, three years of data was taken. Figure 4 given below explains briefly the methodology and steps followed in this study.

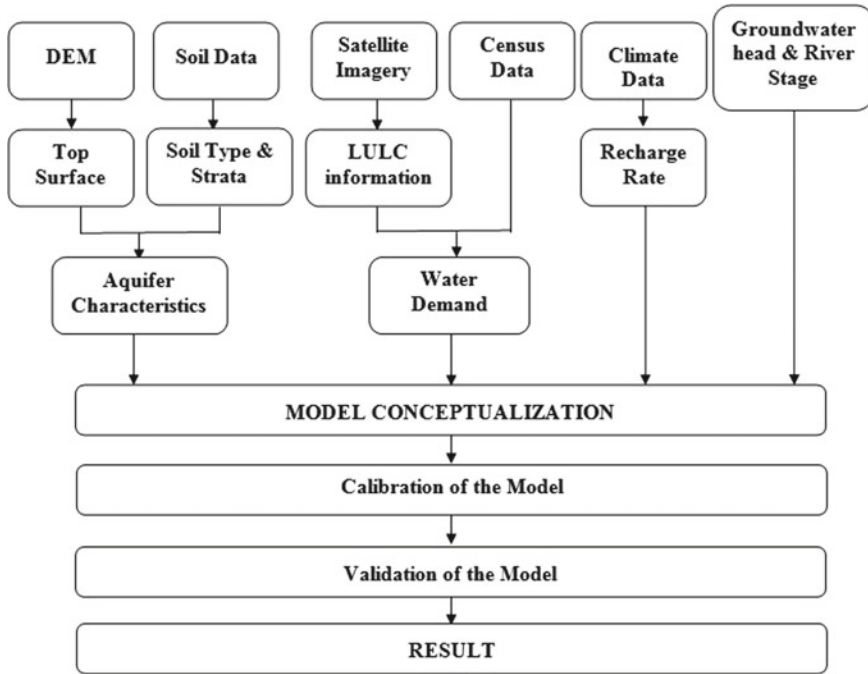
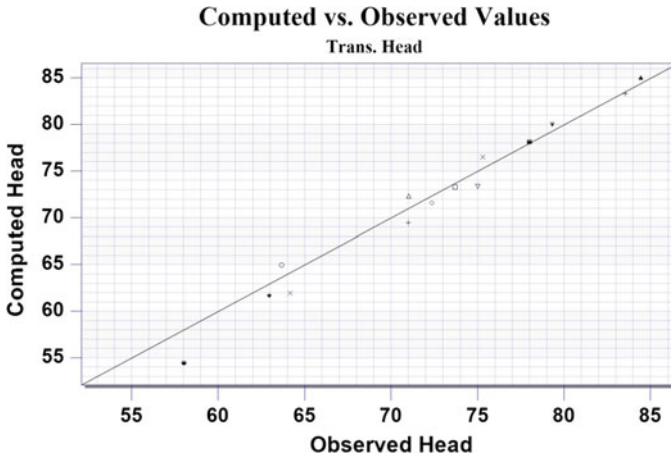


Fig. 4 Flow chart of methodology

## 4 Results and Discussion

The computed groundwater head in Varanasi district has shown the satisfactory results. The water level accuracy was judged by comparing the mean error, mean absolute and root mean square error calculated by the model. Root mean square (RMS) error is the square root of the sum of the square of the differences between calculated and observed heads, divided by the number of observation wells. Groundwater flow pattern obtained from the model represented almost accurate movement of the groundwater. But at some places, groundwater flow pattern was poorly represented by the model. It may be due to some pumping wells, small drainages and lake were not incorporated in the model and might have influenced the pattern of groundwater flow. In the calibration of the model, it was kept in the mind that model water level reasonably matches with the observed water level. Result of groundwater model for Varanasi district reveals that the computed groundwater level shows a decreasing trend of water level in Kashi Vidya Peeth block and near surrounding area, while the other blocks are shown the increasing trend of the water level. This result came may be due to the rapid increase in the population of the Kashi Vidya Peeth block and careless use of the water resource. Figure 5 shows the graph between the observed head and the head computed by the model. This result shows that the





**Fig. 5** Graph between computed head by the model and observed head

computed values of the water head are in good-fitness of the measured data, which indicate that the model is reliable.

## 5 Conclusion

Anthropogenic activities and natural processes affect the groundwater systems. This requires sustainable development and management strategies to keep groundwater resource in good condition. For this, groundwater flow modelling has become more popular and useful among researchers for various purposes. Due to overexploitation of the groundwater, it becomes essential to locate the groundwater scare regions and apply a strategic management plan to conserve this resource for future water demand. For this reason, a groundwater flow model was developed for the Varanasi district with known boundary conditions and known field observation values. This model was very helpful to estimate the groundwater level and the direction of the groundwater flow for the Varanasi district. GIS tools were used for pre-processing of the data such as geological data, climate data and hydrological data. Methodology presented here can be proved superior tools for a conceptual model development to deal with the groundwater modelling problems. Results of this study show large fluctuation in the groundwater head, and in Kashi Vidya Peeth block, there is huge water depletion. This fluctuation may be due to rising agricultural and domestic water demand. The maximum groundwater in the study area is exploited for agricultural purposes. To conserve this natural resource, more water conservation techniques are needed to keep the sustainable groundwater in the study area. Hence, this study can be very helpful in application and the management strategies for the sustainable development of the groundwater.

**Acknowledgements** Authors are grateful to IMD Pune, CWC Varanasi, CGWB and USGS for their support. Authors are also grateful to the department of civil engineering, IIT (BHU) Varanasi, India for financial and infrastructure support during the study.

## References

1. Anderson MP (1984) Movement of contaminants in groundwater: groundwater transport–advection and dispersion. *Groundwater Contam*, 37–45
2. Brunner P, Simmons CT, Cook PG, Therrien R (2010) Modeling surface water-groundwater interaction with MODFLOW: some considerations. *Groundwater* 48(2):174–180
3. Graafi I et al (2015) A high-resolution global-scale groundwater model. *J Hydrol Earth Syst Sci* 19:823–837
4. Maxwell R et al (2015) A high-resolution simulation of groundwater and surface water over most of the continental US with the integrated hydrologic model ParFlow v3. *J Geosci Model Dev* 8:923–937
5. Nield SP, Townley LR, Barr AD (1994) A framework for quantitative analysis of surface water-groundwater interaction: flow geometry in a vertical section. *Water Resour Res* 30(8):2461–2475
6. Omar PJ, Shivhare N, Shishir G, Dwivedi SB, Dikshit PKS (2018) Assessment of the impact of Landfill Leachate on the quality of Groundwater in Varanasi District, India. In: International conference on geomatics in civil engineering (ICGCE-2018).
7. Singhal V, Goyal R (2011) Development of conceptual groundwater flow model for Pali Area, India. *Afr J Environ Sci Technol* 5(12):1085–1092
8. Tian Y, Zheng Y, Wu B, Wu X, Liu J, Zheng C (2015) Modeling surface water-groundwater interaction in arid and semi-arid regions with intensive agriculture. *Environ Model Softw* 63:170–184
9. Townley LR, Trefry MG (2000) Surface water-groundwater interaction near shallow circular lakes: flow geometry in three dimensions. *Water Resour Res* 36(4):935–948
10. Wels C (2012) Guidelines for groundwater modelling to assess impacts of proposed natural resource development activities. British Columbia Ministry of Environment, pp 2–289
11. Zare M, Koch M (2014) 3D-groundwater flow modelling of the effects of the construction of an irrigation/drainage network on possible water logging in the Miandarband plain, Iran. *Basic Res J Soil Environ Sci* 2(2):29–39. ISSN 2345-4090
12. Zheng C, Wang PP (1999) MT3DMS: a modular three-dimensional multispecies transport model for simulation of advection, dispersion, and chemical reactions of contaminants in groundwater systems; documentation and user's guide. Alabama University

# Applications of GIS in Management of Water Resources to Attain Zero Hunger



Ashita Sharma, Manish Kumar and Nitasha Hasteer

**Abstract** The sustainable development goals as proposed by United Nations give huge importance to ending hunger and attaining food security for all by 2030. According to World Health Organization (WHO), food security can be achieved if everyone has access to sufficient, safe and nutritious food throughout the year. Every one in nine persons is deprived of sufficient and safe food. To meet the growing population demand, United Nations aims to double the productivity in agriculture by 2030. Though, by 2015 there is around 10% reduction in critically hungry population of world, yet, the food security for all is a far-sighted dream. Crunch of land and water resources is posing the biggest threat in meeting this target. Per capita availability of land has been decreased with the increase in population, and the water resources are either unavailable or polluted. For sustainable agriculture, there is a need to identify and map locations having adequate water and land resources. GIS models help in analyzing ground profiles, soil water content, rainfall patterns, and geographical terrain and crop conditions. Thus, GIS technologies can help in developing models for water resource management. Continuous monitoring and assessment of natural water resources can help in capacity building, mapping and/or monitoring of cultivable land. Advances in GIS technologies could be an efficient tool to achieve the “zero hunger” goal. The present chapter covers various developments in GIS for water resource modeling across the globe.

---

Authors have contributed equally to the chapter.

---

A. Sharma

Department of Civil Engineering, Chandigarh University, Gharuan, Mohali, Punjab, India  
e-mail: [ashu.asr.sharma@gmail.com](mailto:ashu.asr.sharma@gmail.com)

M. Kumar

Department of Biology, SD College Barnala, Barnala, Punjab, India  
e-mail: [kumarmanish639@gmail.com](mailto:kumarmanish639@gmail.com)

N. Hasteer (✉)

Amity University, Noida, Uttar Pradesh, India  
e-mail: [nhaster@amity.edu](mailto:nhaster@amity.edu)

**Keywords** Resource management · Water resource · Food security · Remote sensing · Hydrology

## 1 Introduction

Resource crunch is the fundamental issue that is cropping up due to population growth, ill-planned urbanization and changes in social behavior. The natural resources seem to have lost the renewability due to accelerated usage. The consumption rate is much higher than the production rate leading to serious shortage of resources. The biggest challenge in front of us these days is to attain food security. The world population is expected to reach 9.8 billion by 2050; India and China being the biggest contributors are the worst hit. To produce sufficient, safe and nutritious food for the growing population is need of the hour. United Nations estimates that 815 million people, i.e., 11% of the population of the earth do not get enough food. India being the densely populated nation, in spite of rich natural resource reservoirs, ranks 100 out of 119 countries in Global Hunger Index. The country with variety of ecosystems, large annual rivers, and rich biodiversity is currently lagging behind Bangladesh and North Korea too in terms of hunger conditions. Situation in Africa is getting worsened day by day. Considering the state of global hunger, United Nations in its millennium development goals aims to reduce it by 2020 and attain zero hunger.

Food production is dependent mainly on land and water resources. The per capita availability of land is less than 0.25 ha [1]. The decline in availability of freshwater resources due to climate change and overexploitation is very evident. Apart from population growth, mismanagement of resources poses another threat to global food security. It is documented that 70% of freshwater is used in agriculture. According to World Bank, per capita availability of freshwater resources has decreased by 70% from 1962 to 2014 in most of the nations [22]. Changes in climatic patterns have further affected the hydrological cycle, thus leading to change in rainfall patterns and initiating drought and flood conditions. Decrease in groundwater level has affected the soil moisture and has further affected the crop production. Resource crunch is expected to increase in future too, so for sustainable development and to attain the goal of zero hunger there is a need to formulate policies and framework for the efficient management of resources.

Resources can be efficiently and diligently managed if we have clear and crisp data of resource availability and utilization. Mapping of resources, models for utilization and recharge, identification of crucial areas is required to be achieved. Geographical Information Systems (GIS) is a tool that can capture spatial data, create estimates, analyze data, formulate models, and help in decision-making. Applications of GIS have been explored in management of land and water resources. Mapping of freshwater resources, understanding hydrological patterns, continuous monitoring of resource utilization, analyzing the water content in soil, predictions and modeling of resource help in decision-making while formulating strategies for attaining zero hunger.

## 2 GIS: A Tool to Manage Resources

GIS, an information system designed for storing, analyzing and displaying spatial data enables better decision-making and improved communication through systematic management of geographic information. It is a tool that links the geographic information about the features on the earth such as buildings, roads, rivers to the descriptive information and helps to streamline information collection, dissemination, maintenance and use. The term can relate to a complete system of hardware and software designed to work with spatial data or a software tool that has been designed to handle geographic information; thereby enabling us to answer questions about where things are and what is located at a given location. There are many fields that have contributed toward the foundation of GIS and computer science being one of them that provides the framework for storage and management of geographic information. The system acquires data through multiple sources. It may be acquired through satellites by way of active or passive remote sensing. The acquired data is then processed through a GIS software package that encompasses databases, imaging and statistic tools.

With rapid development in the field, GIS has emerged as an integral tool for resource planning and management. Last decade has witnessed proliferation of GIS applications for surveying, planning, analyzing, assessing and managing landscapes, environment, agriculture, transportation, banking among many other diverse sectors for better decision-making. In the field of agriculture, it has been successfully used to design effective farming techniques and plays an important role in promoting high impact agricultural practices for better crop yield and thus making sure that people have sufficient access to nutritious food all throughout the year. Application of GIS to manage water resources increases agriculture productivity and helps to eliminate hunger and also all forms of malnutrition.

## 3 Water Resource Management

Though approximately 75% of earth's surface is water but only 0.0067% of total water can be used as other resources are either not fit for human usage or is not available to us easily. Thus, recognizing the importance of water resource, United Nations has incorporated the management of water resources too as one of the millennium development goals, and their aim is to attain sustainable development and water for life by 2030 [5]. Per inhabitant freshwater availability is maximum in America and least is in Asia. Thus, sustainable development and food security cannot be achieved without considerable management of water resources. The distribution of water resources varies due to geographical location, topography, terrain and climatic conditions making it difficult to get the information about various resources. The challenges faced during management of water resources include inability of getting information about topographically remote and inaccessible area, modeling on basis

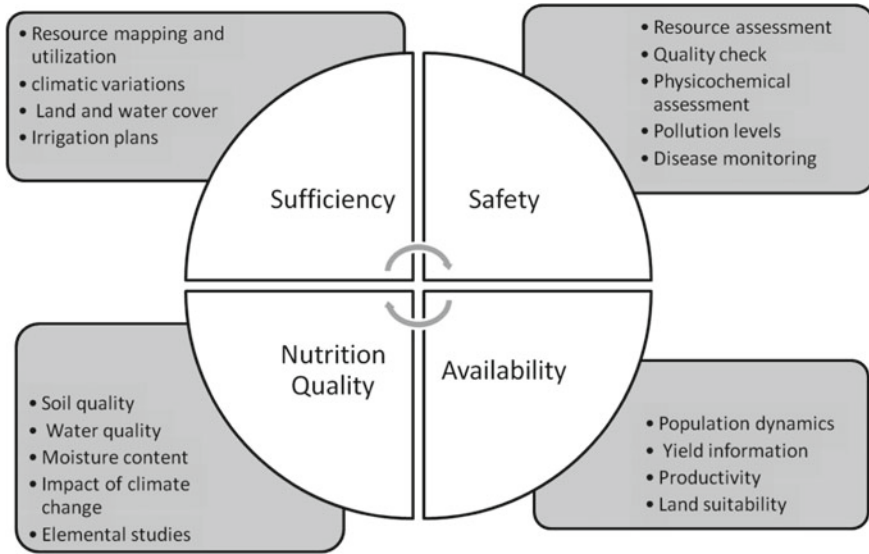


**Fig. 1** Applications of GIS in various aspects of food security

of terrain, analyzing spatial and temporal variations, modeling of hydrological factors for qualitative and quantitative estimates. Integrating remote sensing and GIS can provide analytical and descriptive information about spatial and temporal status of resources. The main knowledge gaps in planning for agricultural policies and analyzing the hydrological aspects are lack of real-time data of water and land use, insufficient information on groundwater profile and lack of analytical tools. These gaps can be filled by remote sensing and GIS. The data obtained through satellites can be both spatial and temporal which can help in keeping surface water accounts, making groundwater restoration plans, irrigation management, estimating hydrological profiles, impact of climate change, drought and information related to precipitation. This data can help in formulating policies and framework. Figure 1 represents use of GIS in attaining various aspects of food security.

- Surface water estimates

Advances in remote sensing and availability of high-resolution data now help in even analyzing the smallest of surface water bodies. GIS aids in proving high-resolution data of surface water imageries, and it has been suggested that the data obtained through GIS is much more reliant than secondary data. For example, Gediz river basin in Western Turkey appeared about 60% larger in remote sensing data than that of in government records. Similarly, the spatial information of Amazon river basin which is spread across wide region and various states helped in the legal framework for water use policies [4]. GIS not only provides information about quantity of surface water bodies but also recent advances in technology have made it

possible for the policy makers to get an idea of salinity and pollution levels. Studies are also being carried out to analyze risk of exposure of agrochemicals [21]. Applications of remote sensing have also been observed in estimating change in surface water quality by the change in land use (Yong 2002). GIS had been an efficient tool in modeling the relationship between land use and surface water flows [10]. Contamination of surface water bodies with pesticides, heavy metals and other toxins has posed serious threat to civilization. Irrigation of agricultural land with contaminated water hampers the “security” aspect of food security. GIS models have been successful in estimating contamination of surface water bodies with agrochemicals and industrial pollutants both qualitative and quantitative [18]. In India, the satellite data from IRS-IC and LISS-III is being used to provide watershed information along with land cover and water profiles in soil. This information is a prerequisite for water resource management [3].

- Groundwater hydrology

Groundwater is the only source of freshwater in many of the developing nations in tropical areas. The groundwater reservoirs account for 30% of freshwater reservoirs on the earth but due to variability in terrain and geographical conditions assessment of reservoir capacity, and recharge rate is difficult without specific technologies and analytical tools. Use of high-resolution imagery and GIS can help in getting exact information about the groundwater sources, usage, contamination and recharge rate. The increased availability of 3-D data have made it possible for the volumetric analysis of groundwater data. It has been well documented that human activities are causing overextraction of groundwater resources. Due to injudicious use, numerous groundwater reservoirs across the globe have reached and/or exceeded their renewable capacity, i.e., water drawn is much more than recharge rate (Plessis 2017). It is important to identify the areas where groundwater recharge is low so as to minimize the extraction and look for ways to recharge.

GIS technologies have also been successful in providing information about soil moisture. Soil moisture is an important physicochemical parameter in agriculture soil. Information about soil quality and its water content can help in planning for agricultural policies and framework. Several experiments have been carried out to get operational data for the soil moisture. It has been documented that use of algorithms can help in converting radiometer data to moisture maps. Gamma rays remote sensors are known to measure the soil moisture of linear maps. Also, the impact of climatic factors on groundwater recharge can be analyzed and modeled. Studies have been made by installing weather stations near the recharge point of well to model and analyze the relationship [2, 20].

Number of characteristics such as lithology, lineament, landform, environmental gradient, vegetal cover, groundwater recharge and flow are taken into consideration while evaluating the groundwater resources in the areas containing stiff rocks. The spatial information collected by the use of GIS is very precise and correct as compared to the conventional approaches of hydrological studies. Further, GIS is cost-effective, when compared with conventional approaches. On the one side, GIS

methods help in analyzing large amount of data while on the other side, field studies aid to authenticate results. Both GIS and conventional approaches provide an improved and better picture of features regulating existence of groundwater in hard rock aquifers.

These thematic maps are then unified employing tool named “Spatial Analyst.” Further, this tool along with mathematical and Boolean operators finds its application in designing models based on the concepts of the problem as delineation of groundwater potential zones. Several literature reports have emphasized the use of remote sensing and GIS for exploring groundwater and identification of non-natural recharge site [3, 15]. In one of the literature report, Jaiswal et al. [6] employed GIS technique for generation of groundwater prospect zones toward rural growth. Many other workers employed GIS to demarcate groundwater potential zone [9, 10, 12, 13, 16]. Some have used GIS for processing and clarification of groundwater quality information [14].

- Rainfall predictions

The hydrological cycle is an important biogeochemical cycle which helps in circulation of water on planet earth. Prediction of precipitation in a particular area not only helps in managing water resources but can also aid in planning the agriculture strategies and time of sowing. The human activities have accelerated the change in rainfall patterns; hence, the ancient knowledge in this case needs to be reviewed to understand the recent rainfall patterns in various areas [8]. The satellite data not only help in prediction of occurrence of rainfall but it also provides the information of quantity of precipitation. Modeling of all precipitation data with surface and groundwater data can significantly help in analyzing the yield/output or problems in agricultural land. Software and models have been developed to evaluate the land for suitability for particular kind of crop based on water resources available [7]. The GIS had been used in mapping of recharge zones based on precipitation [17]. Food security had been severely affected by the change in climatic conditions and rainfall patterns and quality, use of GIS and related technologies have been helpful in understanding the variability in patterns and quality.

## 4 Future Perspectives

Recent advances have enabled the extensive use of GIS in water resource management, especially in the mapping of resources. The focus now needs to shift to development of models to predict the water use and possible contamination. Also, there is a need to extend the use in all possible areas so as to assess the global resources and make the policies and framework to meet food security at the global level. Another important aspect that has to be focused is the estimation of quality of resources. Recent trends have been paving way for the assessment of physicochemical aspects of water used in irrigation. Quantitative assessment of groundwater and surface water resources needs to be evaluated for their accuracy. The comparative



studies for evaluation of GIS as a suitable technique for various parameters also need to be focused. Modeling of water availability and use can prove to be an important aspect of sustainable agriculture and thus attaining food security for all.

## References

1. Bruinsma J (2009) The Freshwater outlook: by how much do land, water and crop yields need to increase by 2050? In: Looking ahead in world food and agriculture: perspectives to 2050. FAO, Rome, pp 233–278. Retrieved from <http://www.fao.org/docrep/014/i2280e/i2280e06.pdf>
2. Chen Z, Grasby S, Osadetz MK (2002) Prediction of average annual groundwater levels from climate variables: an empirical model. *J Hydrol* 260:102–117
3. Chowdary VM, Ramakrishnan D, Srivastava YK, Chandran V, Jeyaram A (2009) Integrated water resource development plan for sustainable management of Mayurakshi watershed, India using remote sensing and GIS. *Water Resour Manage* 23(8):1581–1602
4. de Deus LAB, de Britto FGA, dos Santos CSM, de Melo França CASS, Andrade CD, Ferreira VJRP, de Berrêdo Viana D, de Freitas MAV (2016) GeoAmazonas—GIS for water resources management. *J Geogr Inf Syst* 8:558–577
5. du Plessis Anja (2017) Freshwater challenges of south africa and its upper vaal river: current state and outlook. Springer
6. Jaiswal RK, Mukherjee S, Krishnamurthy J, Saxena R (2003) Role of remote sensing and GIS techniques for generation of groundwater prospect zones towards rural development-an approach. *Int J Remote Sens* 24(5):993–1008
7. Kalogirou S (2002) Expert systems and GIS: an application of land suitability evaluation. *Comput Environ Urban Syst* 26(2–3):89–112
8. Kløve B, Ala-Aho P, Bertrand G, Gurdak JJ, Kupfersberger H, Kværner J, Muotka T, Mykrä H, Preda E, Rossi P, Uvo CB, Velasco E, Pulido-Velazquez, M (2014) Climate change impacts on groundwater and dependent ecosystems. *J Hydrol* 518:250–266
9. Lokesh N, Gopalakrishna GS, Mahesh MJ (2007) Hydrogeomorphological studies in Kallambella watershed, Tumkur district, Karnataka State, India using remote sensing techniques and GIS. *J Indian Soc Remote Sens* 35(1):97–105
10. Mattikalli NM, Richards KS (1996) Estimation of surface water quality changes in response to land use change: application of the export coefficient model using remote sensing and geographical information system. *J Environ Manage* 48(3):263–282
11. Murthy KSR (2000) Groundwater potential in a semi-arid region of Andhra Pradesh: a geographical information system approach. *Int J Remote Sens* 21(9):1867–1884
12. Obi Reddy GP, Chandra Mouli K, Srivastav SK, Srinivas CV, Maji AK (2000) Evaluation of groundwater potential zones using remote sensing data—a case study of Gaimukh watershed, Bhandara district, Maharashtra. *J Indian Soc Remote Sens* 28(1):19–32
13. Pratap K, Ravindran KV, Prabakaran B (2000) Groundwater prospect zoning using remote sensing and geographical information system: a case study in Dala-Renukoot area, Sonbhadra district Uttar Pradesh. *J Indian Soc Remote Sens* 28(4):249–263
14. Rao YS, Jugran DK (2003) Delineation of groundwater potential zones and zones of groundwater quality suitable for domestic purposes using remote sensing and GIS. *Hydrol Sci J* 48(5):821–833
15. Saraf AK, Choudhury PR (1998) Integrated remote sensing and GIS for groundwater exploration and identification of artificial recharge sites. *Int J Remote Sens* 19(10):1825–1841
16. Singh AK, Prakash SR (2003) An integrated approach of remote sensing, geophysics and GIS to evaluation of groundwater potentiality of Ojhala sub watershed, Mirzapur District, U. P. India. <http://www.GISdevelopment.net>
17. Singh AK, Panda SN, Kumar KS (2013) Artificial groundwater recharge zones mapping using remote sensing and GIS: a case study in Indian Punjab. *Environ Earth Sci* 62(4):871–881

18. Tiwari AK, De Maio M, Singh PK, Mahato MK (2015) Evaluation of surface water quality by using GIS and a heavy metal pollution index (HPI) model in a coal mining area, India. *Bull Environ Contam Toxicol* 95(3):304–310
19. Tong ST, Chen W (2002) Modeling the relationship between land use and surface water quality. *J Environ Manage* 66(4):377–393
20. Van der Kamp G, Maathuis H (1991) Annual fluctuations of groundwater levels as a result of loading by surface moisture. *J Hydrol* 127:137–152
21. Verro R, Calliera M, Maffioli G, Auteri D, Sala S, Finizio A, Vighi, M (2002) GIS-based system for surface water risk assessment of agricultural chemicals. 1. Methodological approach. *Environ Sci Technol* 36(7):1532–1538
22. World Bank (2018) Renewable internal freshwater resources per capita (cubic meters), FAO AQUASTAT DATA. Retrieved from: <https://data.worldbank.org/indicator/ER.H2O.INTR.PC>

# Electrocoagulation as an Eco-Friendly River Water Treatment Method



Khalid S. Hashim, Rafid AlKhaddar, Andy Shaw, P. Kot, Dhiya Al-Jumeily, Reham Alwash and Mohammed Hashim Aljefery

**Abstract** Electrocoagulation (EC) is an effective water and wastewater treatment technology, where the coagulants are produced in situ by electrolytic oxidation of a sacrificial anode. In this technique, pollutant removal is done without adding chemicals; therefore, it remarkably reduces the sludge produced and consequently reduces the cost of sludge handling. This method has been efficiently used to remove, up to 99%, of a wide range of pollutants such as heavy metals, oil, dyes, and fluoride. Therefore, the EC method could be the cost-effective, safe, and reliable option to face the growing water scarcity. However, like any other treatment method, the EC technology still has some drawbacks that could limit its applications. This chapter has been therefore devoted to present the principles, history, applications, limitations, advantages and disadvantages of the electrocoagulation technology, the role of key operating parameters on the performance of the EC reactors, and highlight the differences between the traditional coagulation process and EC technology. More importantly, this chapter will highlight the defects of EC technology that need to be enhanced.

**Keywords** Electrocoagulation · Phosphate and nitrate · Heavy metals · Advantages and disadvantages

---

K. S. Hashim (✉) · R. AlKhaddar · A. Shaw · P. Kot · D. Al-Jumeily  
Department of Civil Engineering, Liverpool John Moores University, Liverpool, UK  
e-mail: [k.s.hashim@ljmu.ac.uk](mailto:k.s.hashim@ljmu.ac.uk); [Khalid\\_alhilli@yahoo.com](mailto:Khalid_alhilli@yahoo.com)

R. Alwash  
Department of Environment Engineering, University of Babylon, Babylon, Iraq

M. H. Aljefery  
Merjan Teaching Hospital, Babylon, Iraq

© Springer Nature Singapore Pte Ltd. 2020  
R. AlKhaddar et al. (eds.), *Advances in Water Resources Engineering and Management*, Lecture Notes in Civil Engineering 39,  
[https://doi.org/10.1007/978-981-13-8181-2\\_17](https://doi.org/10.1007/978-981-13-8181-2_17)

219

## 1 Introduction

Water is the most essential element to ensure the reliability and sustainability of the ecosystem of our planet. Although 1400 million cubic kilometres of water covers 71% of the earth surface, less than 2.5% of this huge amount is freshwater [35]. A vast amount of this freshwater is captured in glaciers, snowy mountain ranges, and groundwater, which leaves less than 1% safe for drinking purposes [35, 63]. Moreover, with the increasing population and industrial growth that generate billions of litres of polluted wastewater every day, freshwater resources are becoming limited and/or contaminated [51, 66]. According to the WHO/UNICEF [106], at the turn of the last century, about 1.1 billion people were without access to a safe drinking water source. Furthermore, some forecasting studies confirm that by 2050 the world's population will experience severe drinking water scarcity [32, 35]. It is believed that by 2050 more than 50% of the world's population will not have an access to safe drinking water sources [35].

To reverse this downward trend, a board range of treatment technologies have been developed and applied to treat water and wastewater such as chemical precipitation, biological treatment, electrocoagulation, ion exchange, ultrasound, photo-degradation, and membrane filtration [6, 7, 31, 56, 94]. Amongst these methods, the electrocoagulation (EC) method has recently gained increasing popularity as a promising alternative to treat polluted water and wastewater because it bears many environmentally and economically attractive merits [45, 63].

## 2 Definition of EC Process

Electrocoagulation is a process of in situ production of coagulants by applying an electric current through metallic electrodes to remove suspended pollutants in liquors [47, 50, 92]. This method consists of three main stages: generation of coagulant agents (destabilising agents), destabilisation of pollutants, and flocs formation [50]. Initially, the destabilising agents (such Al and Fe) are electrochemically generated from the sacrificial electrodes, and these agents destabilise pollutants due to providing an opposite electrostatic charge. Once charged, the pollutants start the bridging process forming flocs that can easily be separated from the solution [32, 50]. Therefore, it can be said that the EC method utilises the advantages of three traditional treatment methods: traditional chemical coagulation, flotation, and electrochemistry [63].

## 3 Principles of the EC Process

The principle of the EC process is the application of an electrical current to the solution being treated through sacrificial metallic electrodes to form in situ coagulating ions [19, 46, 50]. Selection of the material of the metallic electrodes is dependent

on several key parameters such as material availability, cost-effectiveness, oxidation potential, toxicity, and the properties of the targeted pollutant [18, 63]. The literature shows that several materials, such as stainless steel [3], diamond [16], iron [67], zinc [102], graphite [86], and aluminium [44, 48, 103], were used as electrodes in EC units. However, it is well documented that aluminium is a very effective and efficient, as an electrode material, to remove different pollutants at suitable operating conditions [18, 32, 33, 50].

As the electrical current starts to flow through the immersed electrodes, the anode starts to dissolve forming coagulating ions, while the cathode generates hydroxide ( $\text{OH}^-$ ) ions and hydrogen ( $\text{H}_2$ ) gas [20, 33, 50, 72]. The EC reactions are determined by several operating parameters such as the initial pH, applied current, electrolysis time, solution conductivity, and electrode material [12, 32, 59].

In the case of using aluminium (Al) as an electrode material, the anode liberates  $\text{Al}_{(\text{aq})}^{3+}$  ions, while the cathode produces  $\text{H}_2$  gas [19, 33]; these reactions are represented in the following equations [20, 33, 50]:

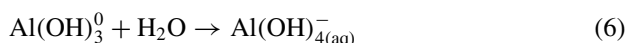
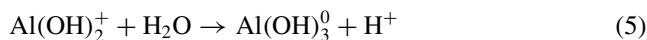
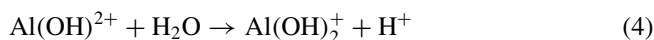
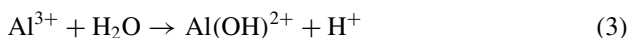
**At the anode:**



**At the cathode:**



After dissolution, the  $\text{Al}_{(\text{aq})}^{3+}$  ions undergo several reactions to yield different monomeric and polymeric substances such as  $\text{Al}(\text{OH})^{2+}$  and  $\text{Al}_{13}\text{O}_4(\text{OH})_{24}^{7+}$ , which in turn readily coagulate pollutants forming flocs [5, 33, 50]. In fact, speciation of aluminium (hydrolysis of dissolved ions) is highly governed by the pH of the solution being treated, where  $\text{Al}(\text{OH})^{2+}$  is the prevailing species of aluminium for pH range of 5–6,  $\text{Al}(\text{OH})_4^-$  is the predominant species for pH above 9, while  $\text{Al}(\text{OH})_3$  is predominant in neutral or slightly alkaline pH [50, 100]. Generally, aluminium speciation is modelled as follows [50, 52]:



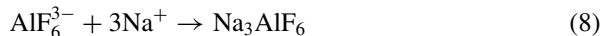
#### 4 Pollutants Adsorption and Precipitation in EC Method

Since the electrolysis process started, an electrophoretic immigration of negatively charged ions started towards the anode and positive ions move towards the cathode. This electrophoretic movement works to concentrate the negatively charged colloids near to the anode, which in turn greatly increases their collision rate with the coagulant species, and aggregates formation consequently [19, 26, 93]. Colloids in the EC method are aggregated by adsorbing them into the freshly formed flocs, and/or chemical transforming [33, 99, 110]. Aluminium and iron hydroxides have a high affinity for dispersed negatively charged colloids, especially metallic ones, that lead them to coagulate forming large aggregates [34, 41, 50]. Positively charged metallic ions can bond themselves to  $\text{OH}^-$ , such as  $\text{Cu}(\text{OH})_2$  and  $\text{Cu}(\text{OH})_2$ , leading to coagulation and forming, with aluminium hydroxide, large flocs whose separation is easily obtained [34]. In addition, colloids and hydroxides may also co-precipitate by replacing ions in the floc structure [33, 50].

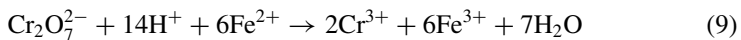
For instance, fluoride ions readily react with  $\text{Al}^{3+}$  ions forming  $\text{AlF}_6^{3-}$  [33, 68, 110] according to the following equation:



which could undergo more reactions, in the presence of sodium ions, to form salt as follows:



Chromium removal using iron electrodes is another good example of the high affinity of iron hydroxides metallic ions, where dichromate ions are readily reduced by ferrous ions according to the following equation [50]:



During the final stage of the electrocoagulation process, the formed aggregates will be separated from the liquid being treated by either flotation or sedimentation. Flotation is the separation of particles from an aqueous media by electrolytic gas; while the bubbles are moving upwards, aggregated colloids adhere to these bubbles and float to the surface of the liquid to be skimmed later [15, 32, 51]. While sedimentation takes place when the weight of the aggregated colloids become big enough to settle to the bottom of the EC unit due to the gravity, and this will be removed later as sludge [18, 32]. The dominant one of these two removal paths is determined by the magnitude of the applied current density; sedimentation is the dominant path at low current densities as the number of generated bubbles will not be enough to float the targeted pollutants. While, at high current densities, large amount of the electrolytic bubbles will be generated, which makes flotation is the predominant path [18, 51]. The number of bubbles produced in the EC unit explains this shift in removal mech-

anism; lower current densities produce an insufficient number of bubbles to float aggregates, making sedimentation predominant. As the current density increases, the number of bubbles increases, leading to aggregates floating to the surface, i.e. it gives the flotation path an edge over sedimentation [18, 51, 71].

The pollutants removal efficiency (Re%) can be calculated using the following formula [98]:

$$\text{Re\%} = \frac{C_0 - C_t}{C_0} \times 100\% \quad (10)$$

where  $C_0$  and  $C_t$  are the initial and final concentrations of the studied pollutant.

## 5 Energy Consumption of EC Units

Energy consumption is one of the most important parameters in water treatment as it determines the operating cost of any method, which in turn determines its applicability [14, 83]. Power consumption for EC units, which highly depends on the gap between the electrodes and conductivity of liquid being treated, can be calculated using the following equations [32, 98]:

$$\text{Power (W)} = V_{\text{cell}} \cdot I \quad (11)$$

where  $V_{\text{cell}}$  and  $I$  are the cell potential (V) and the applied electric current (A).

$$\text{Power consumption } (C_{\text{power}}) \text{ (kWh)} = \frac{I \cdot V_{\text{cell}} \cdot t}{1000} \quad (12)$$

where  $t$  is the treatment time (h).

The consumed power per cubic metre of treated solution is:

$$C_{\text{power}} \text{ (kWh/m}^3\text{)} = \frac{I \cdot V_{\text{cell}} \cdot t}{1000 \cdot \text{Vol.}} \quad (13)$$

where Vol. is volume of treated liquid ( $\text{m}^3$ ).

## 6 Dissolving Rate of Anode

The dissolved mass (dose) of the sacrificial anode is governed, as previously mentioned, by a number of parameters such as the magnitude of the applied current and treatment time. In fact, the applied current and treatment time are the most significant parameters in the anodic dissolving process as they determine the number of

liberated ions from the metallic anode [14, 32, 84, 103]. Theoretically, the dissolved amount of the anode can be calculated using Faraday's second Law [59, 83, 98, 103]:

$$C_{\text{material}} = \frac{I \cdot t \cdot m}{Z \cdot F \cdot \text{Vol.}} \quad (14)$$

where  $C_{\text{material}}$ ,  $t$ ,  $m$ ,  $Z$ , and  $F$  represent the dissolved mass from the anode (g/L), treatment time (second), molecular weight (g/mol) (26.98 for Al), number of electrons (3 for Al), and Faraday's constant (96,500 C/mol).

Experimentally, the consumed mass of electrodes can be calculated by measuring the difference between the anode before and after each run.

## 7 Operating Cost (OC) of EC Units

The operating cost of EC process consists of operating and fixed costs. The operating cost could be defined as all expenditures during the operation of the treatment process, such as the cost of electricity, consumed chemicals and electrodes material, and employment, while the cost of other parts of the EC plant, costs of equipment and construction, represent the fixed costs [14, 23, 39]. However, the operating cost of bench scale EC units (lab work) includes the costs of energy and materials [22, 39, 60, 83]. The following equation was recommended by Kobya et al. [60] to estimate the operating cost of the electrocoagulation process:

$$\text{OC} = \gamma_1 C_{\text{power}} + \gamma_2 C_{\text{electrodes}} + \gamma_3 C_{\text{chemicals}} \quad (15)$$

where  $C_{\text{power}}$  (kWh/m<sup>3</sup>),  $C_{\text{electrodes}}$  (kg/m<sup>3</sup>), and  $C_{\text{chemicals}}$  (kg/m<sup>3</sup>) are the consumed power, electrode material, and chemicals respectively. While  $\gamma_1$ ,  $\gamma_2$ , and  $\gamma_3$  represent the unit price of power, electrode material, and chemicals respectively.

## 8 Applications of EC Method in the Treatment of Water and Wastewater

It is well documented that the EC method has broadly been used in the water and wastewater treatment field to remove different pollutants such as heavy metals, dyes, oil, and bacteria [38, 89, 103, 105]. Overall, EC treatment method could remove as much as 95–99% of the targeted pollutants [15, 36, 41, 89, 103]. However, the performance of this technology is influenced by several parameters such as the chemistry of the liquid being treated, chemical properties and concentration of the targeted pollutant, and electrodes [29, 40, 57, 105].

Therefore, this section is devoted to presenting a quick review of earlier applications of EC technology in water and wastewater treatment. This literature survey



provides important information and data on the applications of the EC technology, which can be used as a guide to conduct future experimental works. The applications of EC technology discussed here were divided into the following five groups:

### **8.1 Removal of Dyes**

Treatment of water or wastewater containing dyes using EC method has become one of the most attractive methods during the last few decades due to its high efficiency and cost-effectiveness [9, 25, 58, 76]. For instance, Ogutverena et al. [80] used a bipolar packed bed EC unit supplied with soluble electrodes to remediate Acilan Blau dye from wastewater, taking into considerations the influence of several operating parameters such as pH and current density. 98–100% of dye was removed within 3–5 min and the power consumption was 2.24 kW/m<sup>3</sup>. Jia et al. [55] treated more than 20 types of dyes, such as sulphur brilliant green GB, Vat red F3B, and Vat blue RSN, using electrodes made from active carbon fibre. Overall, 90% of the studied dyes were removed within 60 min of electrolysis at voltage of 25 V and 0.5 g/L of Na<sub>2</sub>SO<sub>4</sub>. Daneshvar et al. [24] investigated the influence of dye concentration, initial pH, current density, and duration of electrocoagulation on the removal of Acid yellow 23 dye. The findings of this study demonstrated that the best removal efficiency (98%) was obtained after 5 min of electrolysis at an initial pH of 6, current density of 11.25 mA/cm<sup>2</sup>, and initial dye concentration of 50 mg/L.

Naje et al. [76] investigated the removal of Imperon violet KB dye from textile wastewater using a rotated bed EC unit (made from aluminium). 98.5% of this dye was removed after 10 min of electrolysis at a current density of 4 mA/cm<sup>2</sup>, initial pH of 4.57, and water temperature of 25 °C.

### **8.2 Removal of Heavy Metals**

Application of the EC method to treat water and wastewater containing heavy metals has gained substantial interest during the last few years, and removal efficiencies of 95–100% have been documented [50, 73, 79, 101, 108].

Öğütveren et al. [79] used a bipolar packed bed EC reactor with steel ring electrodes to treat water containing 100 mg/L chromium, taking into account the influences of some operating parameters such as time of treatment and the applied potential. The authors found that the chromium was completely removed after 20 min of electrolysis at a current of 160 mA, power consumption of 33.33 kW/m<sup>3</sup>, and 0.25 mol/L of NaCl (as electrolyte). Kumar et al. [62] used three different types of electrodes, namely iron, aluminium, and titanium, to treat water containing 2 mg/L arsenic, III and V. The results of their study showed that the most efficient electrode to remove arsenic was iron followed by aluminium and titanium, where, 99% of arsenic was removed using iron electrodes at a current density of 1.53 mA/cm<sup>2</sup>, for

a pH range 6–8. The simultaneous removal of two heavy metals, zinc and copper, from water using the EC method was investigated by Nouri et al. [78]. In this study, a batch flow EC reactor with four aluminium electrodes was applied to treat 5 mg/L of zinc and 5 mg/L of copper at different operating parameters such as the applied potential. The results obtained from this study showed that EC was able to remove 90.2% zinc and 97.7% of copper after 15 min at an initial pH of 7 and cell voltage of 30 V. Ouaisa et al. [82] used an EC unit provided with aluminium electrodes to investigate the ability of the EC method to remediate chromium Cr (VI) from synthetic water samples. The authors indicated that 97% of initial Cr (VI) concentration of 100 mg/L was achieved at a current density of 4.03 mA/cm<sup>2</sup>, with an initial pH of 3–6.

### 8.3 Removal of Organic Matter

Since the 1970s, EC technology has been practised in the treatment of organic-rich waters and wastewaters [27], such as the wastewater from coke plants, tanneries, and slaughterhouses, landfill leachate, seawater, and drinking water [21, 42, 61, 64, 87, 97]. For instance, Chiang et al. [21] used EC technology to treat wastewater from a coke plant containing 2143 mg/L of COD (chemical oxygen demand). The obtained results showed that the COD decreased from 2143 to 226 mg/L (89.5% removal efficiency) after 120 min of electrolysis using an EC cell supplied with a lead dioxide coated titanium anode. Remediation of the organic content of tannery wastewater is another application of the EC technology; Rao et al. [87] treated samples of tannery wastewater collected from the effluent of a treatment plant for 85 tanneries in India using a batch EC cell. The electrolysis process used three different pairs of electrodes, titanium/platinum (Ti/Pt), titanium/lead dioxide (Ti/PbO<sub>2</sub>), and titanium/manganese dioxide Ti/MnO<sub>2</sub>. The obtained results showed that the order of removal efficiency was Ti/Pt > Ti/PbO<sub>2</sub> > Ti/MnO<sub>2</sub>, where the COD concentration decreased from 515 to 189 g/m<sup>3</sup> (which the highest removal efficiency) after 240 min of electrolysis using Ti/Pt electrodes.

Tchamango et al. [96] used a batch EC reactor, provided with aluminium electrodes, to treat synthetic samples of dairy wastewater. The outcomes of this study showed that 61% of the initial COD was removed after 30 min of electrolysis at a current density of 4.3 mA/cm<sup>2</sup> and initial pH of 6.88–7. Aswathy et al. [10] conducted an investigation about the removability of organic matter from synthetic bilge water using the EC method. Synthetic bilge water samples with initial COD of 2.1120 g/L was treated using an EC cell supplied with Al electrodes and magnetic stirrer at different initial pHs (3–10), voltages (5–10 V), and gaps between electrodes (1–5 cm). The obtained results indicated that the 85% of the COD was removed after 120 min of electrolysis at initial pH of 7, with a mixing rate of 300 rpm, an applied voltage of 10 V, and a gap between electrodes of 1 cm.

## 8.4 Removal of Organisms and Pathogens

Beside the acknowledged efficiency of the EC technology to coagulate and remove colloids from water and wastewater, it has been found that this technology can eliminate several types of biological pollutants such as bacteria and algae [20, 63, 88]. Several trials have been made over the last four or five decades to use the EC method as a disinfection tool for water and wastewater. For instance, Matsunaga et al. [70] developed a new EC reactor using activated carbon fibre as electrodes to remediate *Escherichia coli* (*E. coli*) bacteria from drinking water. Water samples containing 22 cells of *E. coli*/L were treated using this type of electrodes at different voltages and durations, and the obtained results showed that the *E. coli* was completely removed from drinking water after 8 h of treatment at voltage of 0.8 V. The ability of the EC technology to remove algae from water was explored by Alfafara et al. [8]; the researchers used an EC reactor supplied with an aluminium anode and a titanium cathode to treat lake water containing *Chlorophyll*. The experimental work was conducted under different flow patterns (batch and continuous flow), taking into account the effect of several key parameters such as algae loading rate (from 2.4 to 22.9 mg/dm<sup>3</sup>·H) and applied power (60–155 W/dm<sup>3</sup>). The results showed that, under flow pattern conditions, algae removal efficiency was about 50%. Sarkka et al. [91] applied the EC technology to de-activate three types of paper mill bacteria (*Deinococcus geothermalis*, *Pseudoxanthomonas taiwanensis*, and *Meiothermus silvanus*). After 3 min of electrolysis, using an EC unit with stainless steel and mixed metal oxides electrodes, at current density of 50 mA/cm<sup>2</sup>, these three types of bacteria were efficiently de-activated (>2 log). Another study about the removal of *E. coli* from water by the EC method was conducted by Castro-Rios et al. [17]. In this study, a 500 mL batch EC cell having aluminium electrodes was used to treat synthetic water samples containing 10<sup>5</sup>–10<sup>6</sup> cfu/mL of *E. coli*. The outcomes of this investigation confirmed that a current density of 2.27 mA/cm<sup>2</sup> at initial pH of 4 and 2.5 mg/L of Na<sub>2</sub>SO<sub>4</sub> was enough to reduce the *E. coli* number by 1-log and 1.9-log after 40 min and 90 min respectively.

## 8.5 Removal of Other Pollutants

Beside the mentioned applications of EC, the literature survey showed that this technology has been applied to remove a vast number of other pollutants. For instance, Un et al. [98] using a batch EC reactor with aluminium electrodes for defluoridation of 5 mg/L fluoride-containing water. To obtain the best removal efficiency, the current density was changed between 0.5 and 2 mA/cm<sup>2</sup>, the initial pH range between 4 and 8, and electrolyte concentration between 0.01 and 0.03 mol of Na<sub>2</sub>SO<sub>2</sub>. The highest removal efficiency of 97.6% was achieved after 30 min of electrolysis at current density, initial pH, and electrolyte concentration of 2 mA/cm<sup>2</sup>, 4, and 0.01 mol respectively.

Additionally, the EC method was efficiently used to remove fluoride and nitrate from water and wastewater. Hashim et al. [45] studied fluoride removal from synthetic drinking water samples using EC technology. In this study, fluoride removal was performed using perforated aluminium electrodes taking into accounts the effects of the initial pH (4–8), current density (1–3 mA/cm<sup>2</sup>), inter-electrode distance (5–11 mm), treatment time (0–30 min), and the initial concentration of fluoride (10–20 mg/L). The results indicated that 98% of fluoride could be removed within 25 min of electrolysis at a current density of 2 mA/cm<sup>2</sup>, and inter-electrode distance of 5 mm.

Hashim et al. [46] used aluminium-based EC reactor to denitrify synthetic drinking water samples, under batch flow conditions, containing 100 mg/l of nitrate. The denitrification process was optimised for different current densities (1–3 mA/cm<sup>2</sup>), the inter-electrode distance (from 3 to 10 mm), treatment time (up to 70 min), and nitrate concentration ranging from 0.05 to 0.150 g/L. The authors indicated that the aluminium-based EC reactor removed 85% of nitrate (met the World Health Organization limitations for infants) within 55 min of electrolysis at current density of 2 mA/cm<sup>2</sup>, and inter-electrode distance of 5 mm.

## 9 Influence of Liquid Chemistry on the EC Method

In spite of the proven efficiency of the EC technology to remove a vast number of pollutants from aqueous media, its performance is highly influenced, negatively or positively, by the chemistry of the liquid being treated. It has been found that the presence of chloride or magnesium ions in water being treated enhances the performance of the EC units [50, 54]. Chloride inhibits the formation of the inert metallic film of the anode surface and accelerates anode dissolution rate by pitting corrosion, which enhances both generation of coagulants and current efficiency [54]. While, the presence of magnesium to a certain level enhances the performance of EC units by making the flocs bigger and denser, which greatly facilitates their precipitation [50].

Conversely, it has been well documented that the presence of some competitive ions (such as phosphate, silica, or organic matter) and/or the initial pH of liquid being treated can significantly decrease the efficiency of the EC cells [50, 53, 109]. For instance, Hu et al. [53] found, during defluoridation of water samples using aluminium-based EC reactor, that the presence of sulphate ions in water decreases the fluoride removal efficiency. The same negative impact of sulphate on the performance of the EC units was observed by Huang et al. [54], where the latter noticed, during cadmium removal from water, that no reaction took place during 10 min of electrolysis due to the presence of sulphate ions in the water being treated. The authors believed that sulphate ions inhibit the corrosion of Al electrodes, which in turn decreases the removal efficiency. Silicate and phosphate play a very negative role in the electrochemical removal of other pollutants such as arsenic [90, 104]. Where during the electrolysis of 0.5 mg/L arsenic containing water using iron electrodes, Roberts et al. [90] found that the presence of 30 mg/L of silicate in water

reduces arsenic removal by 90%. Moreover, the authors discovered that 3 mg/L of phosphate cause the same influence as 30 mg/L of silicate. Similar findings were obtained by Wan [104], the latter demonstrated that 0.04 g/L of phosphate, during the electrolysis of 0.1 mg/L of arsenic containing water, could inhibit arsenic removal. The authors explained this decrease in removal efficiency by competition between arsenic ions and phosphate and silicate ions to occupy the active sites on the surface of freshly generated coagulants.

## 10 Environmental Advantages of the Electrocoagulation Method

The electrocoagulation technology could be categorised as an eco-friendly water and wastewater treatment method as it bears several environmentally attractive merits. For example:

1. The EC method does not produce secondary pollutants as it does not require chemical additives, which makes it a green technology [18, 37].
2. In comparison with the traditional coagulation process, the flocs formed by the EC method have very low water content that significantly reduces the volume of the sludge produced [81, 111]. It has been found that the EC units produce about 50% less sludge than traditional coagulation processes [13]. This significant reduction in sludge volume greatly reduces the cost of sludge dewatering and handling, which in turn reduces the operating cost of the EC units [81].
3. Leaching of hazardous pollutants from waste landfills is a serious environmental problem [1, 2]. However, the heavy metals leaching from the EC sludge, according to the Toxicity Characteristic Leaching Procedure (TCLP), was within the permissible limits of the Environmental Protection Agency (EPA) [4]. These facts make the EC sludge one of the favourable additives for construction materials, and for instance, EC sludge was successfully used in the production of concrete [13], and cement mortar [11].
4. In comparison with traditional chemical and biological treatment methods, the EC units are able to remove very small particles, as the fine charged particles are more easily attracted to the electric field [75].
5. Due to the low electricity consumption, the required energy to perform the EC method can be driven from clean-energy resources such as the windmills or an attached solar panel [18, 28, 63]. Consequently, the EC method could reduce the carbon emission.
6. One of the main by-products of the EC units is hydrogen gas [65, 77], which is categorised as an eco-friendly fuel 122 kJ/g [30]. Therefore, recovery of hydrogen gas is considered to be one of the most important benefits of the EC treatment method, where Phalakornkule et al. [85] reported that 13% of the required power to operate the EC unit can be produced from the generated hydrogen gas.

## 11 Disadvantages of the Electrocoagulation Method

EC technology, like any other treatment technology, has some drawbacks that could influence its performance. For instance:

1. The electrodes should be periodically replaced as they dissolve into the solution due to the oxidation process [32, 95].
2. The formation of an oxide film on the surface of the anode during the electrolysis process reduces the anode dissolution, which in turn reduces the pollutants removal efficiency [49, 69]. Moreover, this film maximises energy consumption [50] and limits hydrogen recovery [107]. However, the negative influence of this film could be reduced by different techniques such as the addition of anti-passivation agents [72], aeration or increasing the turbulence [74], and periodically cleaning electrodes [63].
3. The EC technology still has a deficiency in the variety of reactor design [98], where most of the EC reactors have parallel plate monopolar or bipolar electrode configuration systems.
4. In addition, there is a real deficit in the modelling of EC performance, which is very important to design, optimise, and reproduce the performance of the EC units [43, 63].

## References

1. Abdulredha M, Al Khaddar R, Jordan D, Kot P, Abdulridha A, Hashim K (2018) Estimating solid waste generation by hospitality industry during major festivals: a quantification model based on multiple regression. *Waste Manag* 77:388–400
2. Abdulredha M, Rafid A, Jordan D, Hashim K (2017) The development of a waste management system in Kerbala during major pilgrimage events: determination of solid waste composition. *Procedia Eng* 196:779–784
3. Abuzaid NS, Bukhari AA, Al-Hamouz ZM (2002) Ground water coagulation using soluble stainless steel electrodes. *Adv Environ Res* 6:325–333
4. Addy SEA, Gadjil AJ, Genuchten CMV, Li L (2011) The future of water, sanitation and hygiene: innovation, adaption and engagement in a changing world. In: 35th WEDC international conference (pp 1–8), Loughborough, UK
5. Adhoum N, Monser L, Bellakhal N, Belgaied JE (2004) Treatment of electroplating wastewater containing  $\text{Cu}^{2+}$ ,  $\text{Zn}^{2+}$  and  $\text{Cr(VI)}$  by electrocoagulation. *J Hazard Mater* 112:207–213
6. Alattabi AW, Harris C, Alkhaddar R, Alzeyadi A, Hashim K (2017) Treatment of residential complexes' wastewater using environmentally friendly technology. *Procedia Eng* 196:792–799
7. Alattabi AW, Harris CB, Alkhaddar RM, Hashim KS, Ortoneda-Pedrola M, Phipps D (2017) Improving sludge settleability by introducing an innovative, two-stage settling sequencing batch reactor. *J Water Process Eng* 20:207–216
8. Alfafara CG, Nakano K, Nomura N, Igarashi T, Matsumura M (2002) Operating and scale-up factors for the electrolytic removal of algae from eutrophied lakewater. *J Chem Technol Biotechnol* 77:871–876
9. Aoudj S, Khelifa A, Drouiche N, Hecini M, Hamitouche H (2010) Electrocoagulation process applied to wastewater containing dyes from textile industry. *Chem Eng Process* 49:1176–1182

10. Aswathy P, Gandhimathi R, Ramesh ST, Nidheesh PV (2016) Removal of organics from bilge water by batch electrocoagulation process. *Sep Purif Technol* 159:108–115
11. Banerjee G, Chakraborty R (2005) Management of arsenic-laden water plant sludge by stabilization. *Clean Technol Environ Policy* 7:270–278
12. Bard AJ, Faulkner LR (2001) *Electrochemical methods: fundamentals applications*. Wiley, New York
13. Barrera-Diaz C, Martinez-Barrera G, Gencel O, Bernal-Martinez LA, Brostow W (2011) Processed wastewater sludge for improvement of mechanical properties of concretes. *J Hazard Mater* 192:108–115
14. Bayramoglu M, Kobya M, Can OT, Sozbir M (2004) Operating cost analysis of electrocoagulation of textile dye wastewater. *Sep Purif Technol* 37:117–125
15. Butler E, Hung Y-T, Yeh RY-L, Suleiman Al Ahmad M (2011) Electrocoagulation in wastewater treatment. *Water* 3:495–525
16. Cañizares P, Sáez C, Sánchez-Carretero A, Rodrigo MA (2008) Influence of the characteristics of p-Si BDD anodes on the efficiency of peroxodiphosphate electrosynthesis process. *Electrochem Commun* 10:602–606
17. Castro-Rios K, Taborda-Ocampo G, Torres-Palma RA (2014) Experimental design to measure *Escherichia coli* removal in water through electrocoagulation. *Int J Electrochem Sci* 9:610–617
18. Chaturvedi S, Dave PN (2012) Removal of iron for safe drinking water. *Desalination* 303:1–11
19. Chaturvedi SI (2013) Electrocoagulation: a novel waste water treatment method. *Int J Mod Eng Res* 3:93–100
20. Chen G (2004) Electrochemical technologies in wastewater treatment. *Sep Purif Technol* 38:11–41
21. Chiang LC, Chang JE, Wen TC (1995) Electrochemical oxidation process for the treatment of coke-plant wastewater. *J Environ Sci Health Part A Environ Sci Eng* 30:753–771
22. Chopra AK, Sharma AK (2012) Removal of turbidity, COD and BOD from secondarily treated sewage water by electrolytic treatment. *Appl Water Sci* 3:125–132
23. Dalvand A, Gholami M, Joneidi A, Mahmoodi NM (2011) Dye removal, energy consumption and operating cost of electrocoagulation of textile wastewater as a clean process. *CLEAN—Soil, Air, Water* 39:665–672
24. Daneshvar N, Khataee AR, Amani Ghadim AR, Rasoulifard MH (2007) Decolorization of C.I. acid yellow 23 solution by electrocoagulation process: investigation of operational parameters and evaluation of specific electrical energy consumption (SEEC). *J Hazard Mater* 148:566–572
25. Daneshvar N, Oladegaragoze A, Djafarzadeh N (2006) Decolorization of basic dye solutions by electrocoagulation: an investigation of the effect of operational parameters. *J Hazard Mater* 129:116–122
26. Den W, Huang C (2005) Electrocoagulation for removal of silica nano-particles from chemical–mechanical-planarization wastewater. *Colloids Surf, A* 254:81–89
27. Deng Y, Englehardt JD (2007) Electrochemical oxidation for landfill leachate treatment. *Waste Manag* 27:380–388
28. Deokate A (2015) Development of textile waste water treatment reactor to obtain drinking Water by solar powered electro-coagulation technique. *Int J Res Environ Sci Technol* 5:29–34
29. Dubrawski KL, Mohseni M (2013) Standardizing electrocoagulation reactor design: iron electrodes for NOM removal. *Chemosphere* 91:55–60
30. Eker S, Kargi F (2010) Hydrogen gas production from electrohydrolysis of industrial wastewater organics by using photovoltaic cells (PVC). *Int J Hydrogen Energy* 35:12761–12766
31. El-Naas MH, Alhajja MA, Al-Zuhair S (2014) Evaluation of a three-step process for the treatment of petroleum refinery wastewater. *J Environ Chem Eng* 2:56–62
32. Emamjomeh MM (2006) Electrocoagulation technology as a process for defluoridation in water treatment. Ph.D. thesis, University of Wollongong
33. Essadki AH, Gourich B, Vial C, Delmas H, Bennajah M (2009) Defluoridation of drinking water by electrocoagulation/electroflotation in a stirred tank reactor with a comparative performance to an external-loop airlift reactor. *J Hazard Mater* 168:1325–1333

34. Ferreira ADM, Marchesiello M, Thivel P-X (2013) Removal of copper, zinc and nickel present in natural water containing  $\text{Ca}^{2+}$  and  $\text{HCO}_3^-$  ions by electrocoagulation. *Sep Purif Technol* 107:109–117
35. Fogden J, Wood G (2009) Access to safe drinking water and its impact on global economic growth. A study for HaloSource, Inc. <http://faculty.washington.edu/categ/healthanddevgbf/wordpress/wp-content/uploads/2010/03/Access-to-Safe-Drinking-Water.pdf>
36. Gao S, Yang J, Tian J, Ma F, Tu G, Du M (2010) Electro-coagulation-flotation process for algae removal. *J Hazard Mater* 177:336–343
37. García-García A, Martínez-Miranda V, Martínez-Cienfuegos IG, Almazán-Sánchez PT, Castañeda-Juárez M, Linares-Hernández I (2015) Industrial wastewater treatment by electrocoagulation–electrooxidation processes powered by solar cells. *Fuel* 149:46–54
38. Genc A, Bakirci B (2015) Treatment of emulsified oils by electrocoagulation: pulsed voltage applications. *Water Sci Technol* 71:1196–1202
39. Ghosh DH, Solankiand Purkait MK (2008) Removal of Fe(II) from tap water by electrocoagulation technique. *J Hazard Mater* 155:135–143
40. Golder A, Samanta A, Ray S (2007) Removal of trivalent chromium by electrocoagulation. *Sep Purif Technol* 53:33–41
41. Gomes JA, Daida P, Kesmez M, Weir M, Moreno H, Parga JR, Irwin G, Mcwhinney H, Grady T, Peterson E, Cocke DL (2007) Arsenic removal by electrocoagulation using combined Al-Fe electrode system and characterization of products. *J Hazard Mater* 139:220–231
42. Hakizimana JN, Gourich B, Vial C, Drogui P, Oumani A, Naja J, Hilali (2016) Assessment of hardness, microorganism and organic matter removal from seawater by electrocoagulation as a pretreatment of desalination by reverse osmosis. *Desalination*
43. Hashim KS (2017) The innovative use of electrocoagulation-microwave techniques for the removal of pollutants from water. Ph.D., Liverpool John Moores University
44. Hashim KS, Khaddar RA, Jasim N, Shaw A, Phipps D, Kota P, Pedrola MO, Alattabi AW, Abdulredha M, Alawsh R (2018) Electrocoagulation as a green technology for phosphate removal from River water. *Sep Purif Technol* 210:135–144
45. Hashim KS, Shaw A, Al Khaddar R, Ortoneda Pedrola M, Phipps D (2017a) Defluoridation of drinking water using a new flow column-electrocoagulation reactor (FCER)—experimental, statistical, and economic approach. *J Environ Manage* 197:80–88
46. Hashim KS, Shaw A, Al Khaddar R, Pedrola MO, Phipps D (2017b) Energy efficient electrocoagulation using a new flow column reactor to remove nitrate from drinking water—experimental, statistical, and economic approach. *J Environ Manage* 196:224–233
47. Hashim KS, Shaw A, Al Khaddar R, Pedrola MO, Phipps D (2017c) Iron removal, energy consumption and operating cost of electrocoagulation of drinking water using a new flow column reactor. *J Environ Manage* 189:98–108
48. Hashim KS, Shaw A, Alkhaddar R, Pedrola MO (2015) Controlling of water temperature during the electrocoagulation process using an innovative flow columns—electrocoagulation reactor. *Int J Environ Chem Ecol Geol Geophys Eng* 9:869–872
49. Hashim KS, Shaw A, Alkhaddar R, Pedrola MO, Phipps D (2016) Effect of the supporting electrolyte concentration on energy consumption and defluoridation of drinking water in the electrocoagulation (EC) method. In: The 2nd BUiD doctoral research conference, The British University in Dubai
50. Heffron J (2015) Removal of trace heavy metals from drinking water by electrocoagulation. M.Sc. thesis, Marquette University
51. Holt PK, Barton GW, Mitchell CA (2005) The future for electrocoagulation as a localised water treatment technology. *Chemosphere* 59:355–367
52. Holt PK, Barton GW, Wark M, Mitchell CA (2002) A quantitative comparison between chemical dosing and electrocoagulation. *Colloids Surf A: Physicochem Eng Aspects* 211:233–248
53. Hu CY, Lo SL, Kuan WH (2003) Effects of co-existing anions on fluoride removal in electrocoagulation (EC) process using aluminum electrodes. *Water Res* 37:4513–4523
54. Huang C-H, Chen L, Yang C-L (2009) Effect of anions on electrochemical coagulation for cadmium removal. *Sep Purif Technol* 65:137–146



55. Jia J, Yang J, Liao J, Wang W, Wang Z (1999) Treatment of dyeing wastewater with ACF electrodes. *Water Res* 33:881–884
56. Katal R, Zare H, Rastegar SO, Mavaddat P, Darzi GN (2014) removal of dye and chemical oxygen demand (cod) reduction from textile industrial wastewater using hybrid bioreactors. *Environ Eng Manag J* 13:43–50
57. Kenova TA, Vasil'eva IS, Kornienko VL (2015) Removal of heavy metal ions from aqueous solutions by electrocoagulation using Al and Fe anodes. *Russ J Appl Chem* 88:693–698
58. Kim T-H, Park C, Shin E-B, Kim S (2002) Decolorization of disperse and reactive dyes by continuous electrocoagulation process. *Desalination* 150:165–175
59. Kobya M, Akyol A, Demirbas E, Oncel MS (2014) Removal of arsenic from drinking water by batch and continuous electrocoagulation processes using hybrid Al-Fe plate electrodes. *Environ Progress Sustain Energy* 33:131–140
60. Kobya M, Demirbas E, Parlak NU, Yigit S (2010) Treatment of cadmium and nickel electroplating rinse water by electrocoagulation. *Environ Technol* 31:1471–1481
61. Kobya M, Senturk E, Bayramoglu M (2006) Treatment of poultry slaughterhouse wastewaters by electrocoagulation. *J Hazard Mater* 133:172–176
62. Kumar PR, Chaudhari S, Khilar KC, Mahajan SP (2004) Removal of arsenic from water by electrocoagulation. *Chemosphere* 55:1245–1252
63. Kuokkanen V (2016) Utilization of electrocoagulation for water and wastewater treatment and nutrient recovery. Techno-economic studies. Ph.D. thesis, University of Oulu Graduate School; University of Oulu
64. Labanowski J, Pallier V, Feuillade-Cathalifaud G (2010) Study of organic matter during coagulation and electrocoagulation processes: application to a stabilized landfill leachate. *J Hazard Mater* 179:166–172
65. Lakshmi J, Sozhan G, Vasudevan S (2013) Recovery of hydrogen and removal of nitrate from water by electrocoagulation process. *Environ Sci Pollut Res* 20:2184–2192
66. Linares-Hernández I, Barrera-Díaz C, Roa-Morales G, Bilyeu B, Ureña-Núñez F (2009) Influence of the anodic material on electrocoagulation performance. *Chem Eng J* 148:97–105
67. Malakootian M, Mansoorian HJ, Moosazadeh M (2010) Performance evaluation of electrocoagulation process using iron-rod electrodes for removing hardness from drinking water. *Desalination* 255:67–71
68. Mameri N, Yeddou AR, Lounici H, Belhocine D, Grib H, Bariou B (1998) Defluoridation of septentrional Sahara water of North Africa by electrocoagulation process using bipolar aluminium electrodes. *Wat. Res.* 32:1604–1612
69. Mansour SE, Negim E-S, Hasieb IH, Desouky OA, Abdykalykova R, Beisebekov M (2013) Removal of cadmium pollutants in drinking water using alternating current electrocoagulation technique. *Glob J Environ Res* 7:45–51
70. Matsunaga T, Nakasono S, Kitajima V, Horiguchi K (1994) Electrochemical disinfection of bacteria in drinking water using activated carbon fibers. *Biotechnol Bioeng* 43:429–433
71. Maximova N, Dahl O (2006) Environmental implications of aggregation phenomena: current understanding. *Curr Opin Colloid Interface Sci* 11:246–266
72. Mechelhoff M, Kelsall GH, Graham NJD (2013) Electrochemical behaviour of aluminium in electrocoagulation processes. *Chem Eng Sci* 95:301–312
73. Mills D (2000) A new process for electrocoagulation. *Am Water Works Assoc J* 92:34–44
74. Mohora E, Rončević S, Agbaba J, Tubić A, Mitić M, Klačnja M, Dalmacija B (2014) Removal of arsenic from groundwater rich in natural organic matter (NOM) by continuous electrocoagulation/flocculation (ECF). *Sep Purif Technol* 136:150–156
75. Mollah MY, Morkovsky P, Gomes JA, Kesmez M, Parga J, Cocke DL (2004) Fundamentals, present and future perspectives of electrocoagulation. *J Hazard Mater* 114:199–210
76. Naje AS, Chelliapan S, Zakaria Z, Abbas SA (2016) Electrocoagulation using a rotated anode: a novel reactor design for textile wastewater treatment. *J Environ Manage* 176:34–44
77. Nasution MA, Yaakob Z, Ali E, Tasirin SM, Abdullah SR (2011) Electrocoagulation of palm oil mill effluent as wastewater treatment and hydrogen production using electrode aluminum. *J Environ Qual* 40:1332–1339

78. Nouri J, Mahvi AH, Bazrafshan E (2010) Application of electrocoagulation process in removal of zinc and copper from aqueous solutions by aluminum electrodes. *Int J Environ Res* 4:201–208
79. Ögütveren ÜB, Gönen N, Koparal S (1994) Removal of chromium from aqueous solutions and plating bath rinse by an electrochemical method. *Int J Environ Stud* 45:81–87
80. Ogutverena UB, Gonena N, Koparal S (1992) Removal of dye stuffs from waste water: Electrocoagulation of Acilan Blau using soluble anode. *J Environ Sci Health Part A Environ Sci Eng Toxicol* 27:1237–1247
81. Olmez T (2009) The optimization of Cr(VI) reduction and removal by electrocoagulation using response surface methodology. *J Hazard Mater* 162:1371–1378
82. Ouaisa YA, Chabani M, Amrane A, Bensmaili A (2013) Removal of Cr(VI) from model solutions by a combined electrocoagulation sorption process. *Chem Eng Technol* 36:147–155
83. Ozyonar F, Karagozoglul B (2011) Operating cost analysis and treatment of domestic wastewater by electrocoagulation using aluminum electrodes. *Polish J Environ Stud* 20:173–179
84. Pallier V, Feuillade-Cathalifaud G, Serpaud B (2011) Influence of organic matter on arsenic removal by continuous flow electrocoagulation treatment of weakly mineralized waters. *Chemosphere* 83:21–28
85. Phalakornkule C, Sukkasem P, Mutchimsattha C (2010) Hydrogen recovery from the electrocoagulation treatment of dye-containing wastewater. *Int J Hydrogen Energy* 35:10934–10943
86. Raju GB, Karuppiiah MT, Latha SS, Parvathy S, Prabhakar S (2008) Treatment of wastewater from synthetic textile industry by electrocoagulation–electrooxidation. *Chem Eng J* 144:51–58
87. Rao N, Somasekhar K, Kaul S, Szpyrkowicz L (2001) Electrochemical oxidation of tannery wastewater. *J Chem Technol Biotechnol* 76:1124–1131
88. Ricordel C, Darchen A, Hadjiev D (2010) Electrocoagulation–electroflotation as a surface water treatment for industrial uses. *Sep Purif Technol* 74:342–347
89. Ricordel C, Miramon C, Hadjiev D, Darchen A (2014) Investigations of the mechanism and efficiency of bacteria abatement during electrocoagulation using aluminum electrode. *Desalin Water Treat* 52:5380–5389
90. Roberts LC, Hug SJ, Ruettimann T, Billah MM, Khan AW, Rahman MT (2004) Arsenic removal with iron(II) and iron(III) in waters with high silicate and phosphate concentrations. *Environ Sci Technol* 38:307–315
91. Sarkka H, Vepsalainen M, Pulliainen M, Sillanpaa M (2008) Electrochemical inactivation of paper mill bacteria with mixed metal oxide electrode. *J Hazard Mater* 156:208–213
92. Shaw A, Hashim KS, Alkhaddar R, Pedrola MO, Phipps D (2017) Influence of electrodes spacing on internal temperature of electrocoagulation (EC) cells during the removal (Fe II) from drinking water. In: The 3rd BUId annual doctoral research conference, The British University, Dubai
93. Shim HY, Lee KS, Lee DS, Jeon DS, Park MS, Shin JS, Lee YK, Goo JW, Kim SB, Chung DY (2014) Application of electrocoagulation and electrolysis on the precipitation of heavy metals and particulate solids in washwater from the soil washing. *J Agric Chem Environ* 03:130–138
94. Swelam AA, El-Nawawy MA, Salem AMA, Ayman AA (2015) Adsorption characteristics of Co(II) onto ion exchange resins 1500H, 1300H and IRC 86: isotherms and kinetics. *Int J Sci Res* 4:871–875
95. Tamne GB, Nansau-Njiki CP, Bodoki E, Săndulescu R, Oprean R, Ngameni E (2015) Removal of nitroaniline from water/ethanol by electrocoagulation using response surface methodology. *Clean—Soil, Air, Water*
96. Tchamango S, Nansau-Njiki CP, Ngameni E, Hadjiev D, Darchen A (2010) Treatment of dairy effluents by electrocoagulation using aluminium electrodes. *Sci Total Environ* 408:947–952
97. Tsai CT, Lin ST, Shue YC, Su PL (1997) Electrolysis of soluble organic matter in leachate from landfills. *Water Res* 31:3073–3081
98. Un UT, Koparal AS, Bakir Ogutveren U (2013) Fluoride removal from water and wastewater with a batch cylindrical electrode using electrocoagulation. *Chem Eng J* 223:110–115

99. Van Genuchten CM, Peña J, Amrose SE, Gadgil AJ (2014) Structure of Fe(III) precipitates generated by the electrolytic dissolution of Fe(0) in the presence of groundwater ions. *Geochim Cosmochim Acta* 127:285–304
100. Vasudevan S, Lakshmi J, Sozhan G (2009) Studies on the removal of iron from drinking water by electrocoagulation—a clean process. *CLEAN—Soil, Air, Water* 37:45–51
101. Vasudevan S, Lakshmi J, Sozhan G (2011) Studies on the Al–Zn–In-alloy as anode material for the removal of chromium from drinking water in electrocoagulation process. *Desalination* 275:260–268
102. Vasudevan S, Lakshmi J, Sozhan G (2012) Optimization of the process parameters for the removal of phosphate from drinking water by electrocoagulation. *Desalin Water Treat* 12:407–414
103. Vidal J, Villegas L, Peralta-Hernandez JM, Salazar Gonzalez R (2016) Removal of acid black 194 dye from water by electrocoagulation with aluminum anode. *J Environ Sci Health A Tox Hazard Subst Environ Eng* 51:289–296
104. Wan W (2010) Arsenic Removal from Drinking Water by Electrocoagulation. Ph.D. thesis, Washington University
105. Wan W, Pepping TJ, Banerji T, Chaudhari S, Giammar DE (2011) Effects of water chemistry on arsenic removal from drinking water by electrocoagulation. *Water Res* 45:384–392
106. WHO/UNICEF (2000) Global water supply and sanitation assessment 2000 report. World Health Organization and United Nations Children's Fund, USA
107. Yang Z-H, Xu H-Y, Zeng G-M, Luo Y-L, Yang X, Huang J, Wang L-K, Song P-P (2015) The behavior of dissolution/passivation and the transformation of passive films during electrocoagulation: influences of initial pH, Cr(VI) concentration, and alternating pulsed current. *Electrochim Acta* 153:149–158
108. Yilmaz AE, Boncukcuoglu R, Kocakerim MM (2007) An empirical model for parameters affecting energy consumption in boron removal from boron-containing wastewaters by electrocoagulation. *J Hazard Mater* 144:101–107
109. You HJ, Han IS (2016) Effects of dissolved ions and natural organic matter on electrocoagulation of As(III) in groundwater. *Journal of Environmental Chemical Engineering* 4:1008–1016
110. Zhu J, Zhao H, Ni J (2007) Fluoride distribution in electrocoagulation defluoridation process. *Sep Purif Technol* 56:184–191
111. Zodi S, Potier O, Lapique F, Leclerc J-P (2009) Treatment of the textile wastewaters by electrocoagulation: effect of operating parameters on the sludge settling characteristics. *Sep Purif Technol* 69:29–36

# Wetland Dynamics Using Geo-Spatial Technology



Nilendu Das, Anurag Ohri, Ashwani Kumar Agnihotri, Padam Jee Omar and Sachin Mishra

**Abstract** Wetlands are very significant part of our environment. They improve water quality of its area and also makes local climate fairly moderate. Among the fertile areas of environment system, wetlands are the one. As the wetland decreases, it brings changes to weather pattern and diminution of water level below soil. Like many wetlands in India, wetland of Varanasi district is also facing with danger and diminishing day by day. Due to the rapid increase in urbanization of the city and population explosion over the last two decades, the encroachment process is taking place at a brisk rate; therefore, wetland area is reducing accordingly. So objective of this work is the mapping of wetland area in Varanasi district with the help of remote sensing using multi-date Landsat satellite data for two particular years 1990 and 2016. Water pixels have been demarcated by using *Normalized Difference Water Index* (NDWI). In the result of the study, it has been found that wetland area's reduction has been around 43% for the period spanning around 26 years. This is a cause of great concern that wetland area is reducing at a very fast rate; therefore, it is urgent need to protect these wetland area as this is one of the major components for sustaining balance in our ecosystem.

**Keywords** Wetlands · Remote sensing · Urbanization · NDWI · MNDWI

## 1 Introduction

Technology of remote sensing is very widely used to detect change in wetland area. Images taken in different dates are compared, analyzed and statistical computation based on indices were performed. These wetlands are very important for aquatic ecosystems [3]. Main features of wetland are that they remain waterlogged for a con-

---

N. Das · A. Ohri · A. K. Agnihotri (✉) · P. J. Omar  
Department of Civil Engineering IIT, BHU, Varanasi 221005, India  
e-mail: [ashwanika.rs.civ15@itbhu.ac.in](mailto:ashwanika.rs.civ15@itbhu.ac.in)

S. Mishra  
Department of Chemistry IIT, BHU, Varanasi 221005, India

© Springer Nature Singapore Pte Ltd. 2020  
R. AlKhaddar et al. (eds.), *Advances in Water Resources Engineering and Management*, Lecture Notes in Civil Engineering 39,  
[https://doi.org/10.1007/978-981-13-8181-2\\_18](https://doi.org/10.1007/978-981-13-8181-2_18)

237

siderable period of time. Their physico-chemical and biological behavior changes as they remain waterlogged for such a long period. It allows development of plant and animal communities on these wetlands. [6]. Different types of wetlands are peatlands, marshes, swamps, mangroves, shallow lakes (less than three meter deep), floodplains, littoral zones of lakes. These wetlands can be found mostly in the region starting from tropical zones to temperate zones. Most wetlands are extremely productive and support high biodiversity. The places which have abundance of wetland, those places have mostly home for successful human settlements, normal climates occur on those places and balanced ecosystem lies over there. Wetland performs several important functions such as controlling of floods, storage of water in abundance and its purification, protection of shorelines and hinterlands and economic sustenance to the people [5, 10]. Millions of people directly and indirectly depend on wetland system. They contribute to imperative processes such as flowing of water through the wetland into streams or sea; decomposition of organic matter; releasing sulfur, carbon, nitrogen to atmosphere; and breeding place for all the organism that requires wetland for living. The direct advantages of wetlands are water supply, timber, fish production; indirect advantages comes from the functions occurring inside the ecosystem such as ground water recharge, flood control and storm protection. Wetlands also are of great importance to indigenous people as a part of their cultural and ethical heritage. The areas, which have termed as wetlands, they will have less flooding during heavy rainfall as compared to areas which have no wetlands. There is retention capacity of wetland to hold extra flood water. Vegetation in wetland area acts as an important factor to control erosion which in turn becomes helpful for shoreline stabilization and storm protection. Parameters for strong eutrophication like phosphorous and nitrogen have been stored by wetland areas and thus wetland retains nutrients. They are also helpful in absorbing the sewage and thus purify the water supplies [8]. Ground-surveying methods for delineating wetlands are very old and traditional methods. These methods are very costly and very time-consuming. To save time and money, remote sensing technology and methodology can be implemented. Another form of remote sensing, i.e., aerial photography can also be helpful for identification and delineation of spatial extension of wetland (e.g., National Wetland Inventory). With periodical movement of satellites over a particular location, information of that location in the form of multi-date and multi-spectral images can be obtained. If environmental condition for earth surface changes, then that can be monitored and captured by satellites. Landsat series satellites like multi-spectral scanner (MSS) and later Thematic Mapper (TM) has become very cost-effective and easy for acquiring multi-date images over a greater variation of temporal and spatial scales than that was possible with aerial photography. For larger wetland monitoring purposes, Landsat MSS satellites have been used widely. But the use of this Landsat MSS satellite has been facing several constrain because the image acquired by this satellite has poor geometric accuracy along with poor spatial, spectral and radiometric resolutions of the acquired image. Landsat TM satellite launched during 1980s, and it has spatial resolution of 30 meters. So with this satellite data, it is quite convenient and more possible to analyze relatively smaller areas. Earlier with MSS satellites due to their poor spatial resolution, the remote sensing analysis for smaller

area was not possible [1, 2, 9, 11]. The main purpose of this study is to determine the spread of wetland area and temporal change in wetland area of Varanasi district for different years (only two years namely 1990 and 2016 considered here) with the help of satellite generated data.

## 2 The Study Area

In this work, Varanasi and its adjoining areas have been selected which is a famous Hindu holy city. The city and its adjoining areas (Varanasi district) lie between  $25^{\circ}14'$  to  $25^{\circ}23.5'$  N latitude and  $82^{\circ}56'$  to  $83^{\circ}03'$  E longitude. Ganga, Assi and Varuna rivers flow through this district. From 2001 census, the estimated population of this area is roughly around 32 lakhs. This district consists of two tehsils, eight blocks and 1336 villages. Climate of this area is humid subtropical type with extreme summer and winter temperatures. Summer season has very long duration with the monsoon season in between. The average temperature in summers hovers in the range of  $32-46^{\circ}\text{C}$ . Winters season lies from December to February. The average temperature in winters hovers around  $5-15^{\circ}\text{C}$ . The average annual rainfall is 1110 mm. Hot dry winds known as 'loo' is a common phenomena in summers season and fog is a typical phenomena of winter season [7]. The satellite data used in this study were Landsat TM for the year 1990 and Landsat OLI for the year 2016. All the satellite data that were used in this study was from the month of November.

## 3 Methodology

Creation of the database: The study area topographic sheet is downloaded from e-nakshe website [www.soinakshe.uk.gov.in](http://www.soinakshe.uk.gov.in) at a scale of 1:50,000 and the topo-sheet numbers which are covered in the study areas are as follows: G44Q10, 44Q11, 44Q12, G44Q14, G44Q15, G44Q16, G44R2, G44R3, G44R4, and topo-sheets are digitized and converted to vector map in Q-GIS software. The location map of study area is shown in Fig. 1.

### 3.1 Analysis of Remotely Sensed Data and Indices Calculation

Three major category defines wetland, i.e., wetland (aquatic vegetation), water and marshy land (waterlogged area), and these categories have to be mapped with the help of remotely sensed data. Spectral signature of water is quite different from other features of land like vegetation, agricultural lands, built-up lands but still the

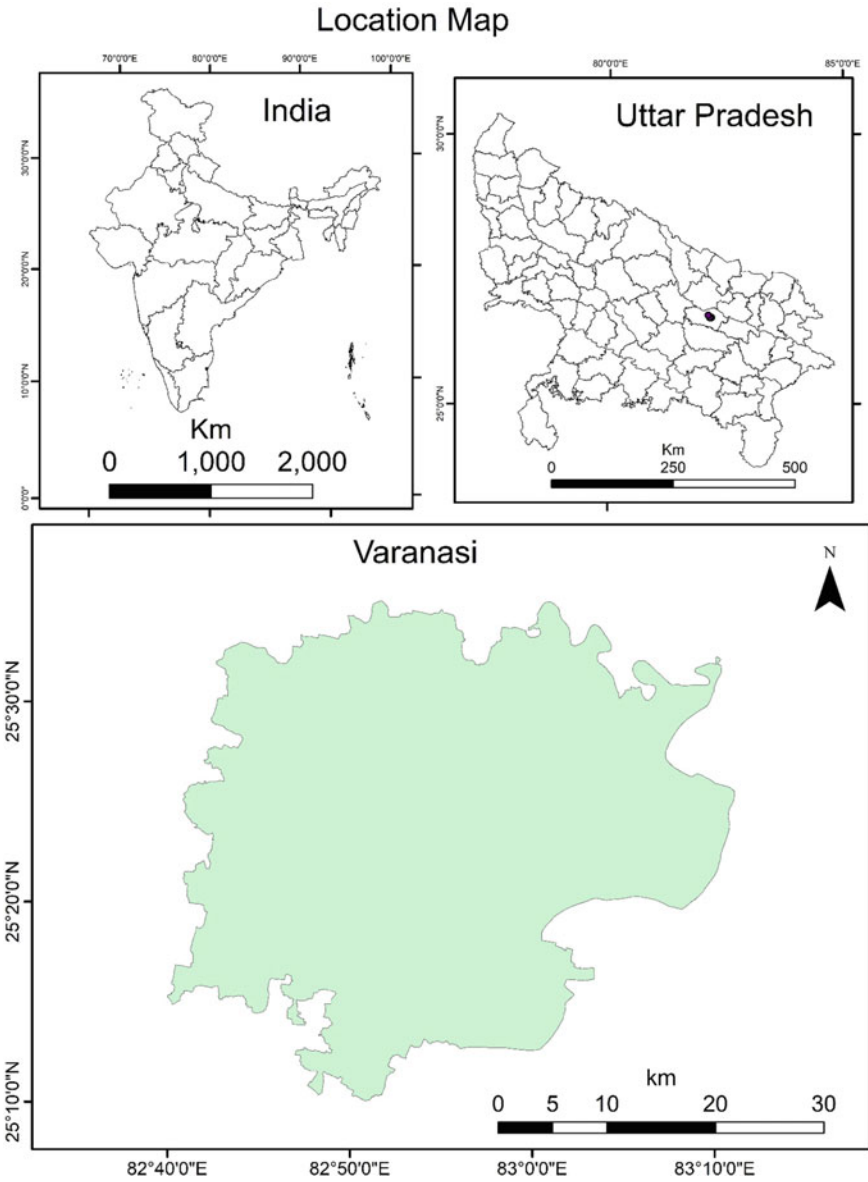


**Fig. 1** Location map of the study area

detection of pixels of water at the water/soil boundary is tough, and it requires good skills of analyst. Representation of deep water bodies in image is not a problem as spectral signatures of deep water bodies are quite different, but water bodies of shallow depth can easily confuse the interpreter with soil along the boundary of the water bodies. The pixel which is on the edge of water/soil boundary, is known as a mixed pixel in this case as it contained two features i.e. soil and water. So a proper indexing is required to highlight the water features in a more prominent manner. Thus an another band-ratioing index known as *Normalized Difference Water Index* (NDWI) is used. By following the formula, it is calculated:

$$NDWI = \frac{(GREEN - NIR)}{(GREEN + NIR)}$$

where GREEN is a wavelength that reflects green light and NIR is a wavelength that reflects near infrared light. When a multi-spectral image which has reflectance value in green and NIR band is processed by above formula, then water bodies in the image will show positive values of NDWI and non-water features will show zero or negative values of NDWI.

Since Varanasi is a densely populated area and it consist of large number of built-up land, so here efficient suppression cannot be done by NDWI because NDWI will give more or less the same reflectance value of mixed pixels that consist of both water and land features (mainly built-up pixels). So, a new index will be required to solve this problem, and hence, NDWI has to be modified or changed to tackle the above mentioned problem. A modified version of NDWI is used and in this index MIR (mid-infrared) band is used instead of NIR.

The modified NDWI (MNDWI) can be formulated like:

$$MNDWI = \frac{(GREEN - MIR)}{(GREEN + MIR)}$$

where MIR is the wavelength that reflects mid-infrared light. As one compute MNDWI, it will have more suppression of non-water body features because soil and vegetation will have negative values for MNDWI as they reflect more in MIR region of electromagnetic (EM) spectrum than in comparison with green region of EM spectrum. Same scenario happens for built-up pixels as well. But water bodies absorb more light in MIR region of EM spectrum, so water pixels will show large positive values. Thus, water and non-water features can be distinguished easily after applying MNDWI formula [4].

## 4 Result

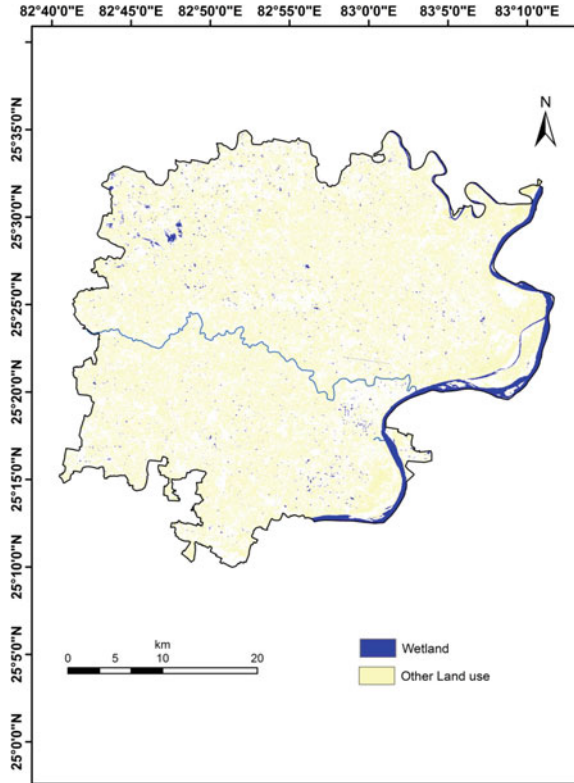
Instead of NDWI, the modified NDWI has been calculated and change in wetland has been tabulated in Varanasi and its adjoining areas. Classification done with the



**Table 1** Areal extent of the wetlands in different years

Year	Total wetland area (km <sup>2</sup> )
1990	90.41
2016	52.20

**Fig. 2** Wetland Area in 1990

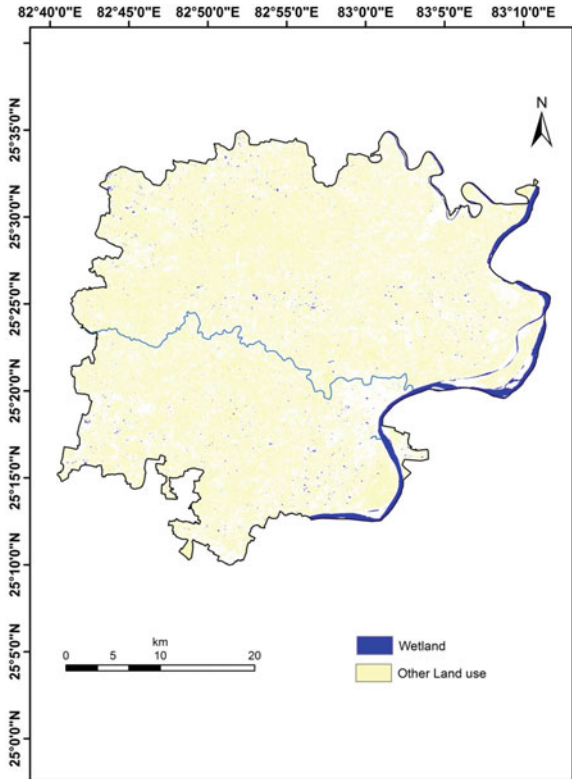


help of remote sensing images can be error prone. For this accuracy check has been done, and error in classification has been minimized. Field visit has been made for ground truth of data.

From Table 1, it can be seen that total wetland area has reduced from 90.41 km<sup>2</sup> in 1990 to 52.20 km<sup>2</sup> in 2016.

It can be clearly visible from the wetland area maps (Figs. 2 and 3) that in the year 1990, Varanasi and its adjoining areas had very large covering of wetlands, particularly several big patches of wetlands were found in north-western part of Varanasi district. Thereafter with due passage of time, wetland area gradually started to decrease, and then we can see that in the year 2016, it had been decreased almost half of the area that was in 1990. This rapid declination of wetland area is a major cause of concern for human society.

**Fig. 3** Wetland Area in 2016



## 5 Conclusion

Wetland area of Varanasi and its adjoining area are reducing due to various factors such as silting, excessive encroachment and urbanization. The wetland area mapping has been carried out using remote sensing for a period of 1990–2016 and wetland area in this time period has been computed. It has been found that about 42% total wetland area has reduced in these years. Varanasi city is the fastest growing city along with the most polluted city of the India. These reducing wetlands are very serious issue for the environmentalist and ecologist who are especially serious about the reducing rate of wetlands. This study can be helpful for their research purpose and can be useful in the conservation of these wetlands.

## References

1. Alsdorf DE, Smith LC, Melack JM (2001) Amazon floodplain water level changes measured with interferometric SIR-C radar. *IEEE Trans Geosci Remote Sens* 39(2):423–431
2. Chopra R, Verma VK, Sharma PK (2001) Mapping, monitoring and conservation of Harike wetland ecosystem, Punjab, India through remote sensing. *Int. J. Remote Sensing* 22(1):89–98
3. Gopal B (1994) Role of Ecotones in conservation and management of tropical inland waters. *Mitt Int Verein Theor Angew Limnol* 24:17–25
4. Hanqiu Xu (2006) Modification of normalized difference water index (NDWI) to enhance open water features in remotely sensed imagery. *Int J Remote Sens* 27(14):3025–3033
5. Jerath N (1992) The environs and problems of Harike wetland; some strategies for conservation. In wetlands of India. In: Chatrath KJS (ed) Ashish Publishing House, New Delhi, India, pp 103–124
6. Mitsch WJ, Gosselink JG (2000) *Wetlands*, 3rd edn. John Wiley, New York
7. NWIA (2006) *Uttar Pradesh Atlas*
8. Ramachandra TV (2001) Restoration and management strategies of wetlands in developing countries. *Electron Green J* (15) (December)
9. Saikh M, Green D, Cross H (2001) A remote sensing approach to determine environmental flows for wetlands of the Lower Darling River, New South Wales, Australia. *Int J Remote Sens* 22(9):1737–1751
10. Sarkar A, Jain SK (2008) Using remote sensing data to study wetland dynamics—a case study of Harike Wetland. In: Sengupta M, Dalwani R (ed) *Proceedings of Taal 2007: the 12th world lake conference*, pp 680–684
11. Shepherd I, Wilkinson G, Thompson J (2000) Monitoring surface water storage in the North Kent Marshes using landsat TM images. *Int J Remote Sens* 21(9):1843–1865

# Inland Waterway as an Alternative and Sustainable Transport in Kuttanad Region of Kerala, India



Madhuri Kumari, Sarath Syamaprasad and Sushmit Das

**Abstract** The purpose of this study is to illustrate the advantage of waterways over roadways in Kuttanad, Kerala. The paper also discusses how the neglect of waterways and growing preference over roadways has led to the environmental pollution in the area. The study area has been visited multiple times and interaction with the locals to understand the problems has been done for a comprehensive solution. Planning of waterways is done by collecting the data from the study area in focus. Travel times were estimated by travelling a route multiple times and distance is estimated from Google earth. Using the GPS device, tracks were saved while travelling by the route, on car and on boat. The tracks and the coordinates were then plotted in Google earth for representation. The study demonstrates how improvements in waterways can outrank roadways in the study area. The paper is also an attempt to prove the development of waterways can be an answer to the stagnant water in the locality.

**Keywords** Inland waterways · Sustainable transportation · Water pollution · Travel route · River and canal network

## 1 Introduction

The prospect of rapid industrialization in India has turned the focus towards the need to plan urbanization at an unprecedented rate. The speed and extent of urbanization should be such that it is sustainable. One very important aspect of urbanization is the prudent use of water and its resources. Rather than always thinking of purifying

---

M. Kumari (✉)

Department of Civil Engineering, Amity School of Engineering and Technology,  
Amity University Uttar Pradesh, Noida, India  
e-mail: [madhurikumari@gmail.com](mailto:madhurikumari@gmail.com); [mkumari@amity.edu](mailto:mkumari@amity.edu)

S. Syamaprasad  
Roberts Constructions, Dubai, United Arab Emirates

S. Das  
SingylStroke, Chennai, India

polluted water, it will be a step forward to find ways to prevent water pollution. The re-emergence of waterways will have dual benefit of improving the water quality of otherwise stagnant water bodies and a solution to sustainable transportation system. It will be beneficial to the environment as well as to the people living in the regions which has well-laid network of rivers and canals [6, 7].

Water transport is known to be cheaper. Many research studies support the fact that waterways can transport two to four times the tonnage per litre of fuel as compared to that of roadways. Though the speed of transportation is faster in the case of roadways, it requires considerable investment [3, 5]. With the advancement in recent technologies for design of water vessels and boats, the speed is no more a concern in waterways. In the current era of green and sustainable development, water transport presents a prospective alternate mode of transportation as it offers dual benefit of low energy consumption and low carbon emission.

There are abundant water bodies in India that can be used, but are neglected and are grossly unutilized. Insufficient information with respect to desirable routes for the boat inhibits the willingness of the investor in water transport system. The vehicular volume of passengers and human population in Kuttanad region of Kerala has continued to increase daily [4]. Hence, there is a need to complement travel demand on road to water as a strategy for efficient transportation network. The study focusses on water transportation because the purpose is to facilitate the proper use of water bodies in the area, encourage low-priced sustainable transportation and subsequently address neglect of travel by water. Focussing just on development of roads by neglecting the inland waterways in the regions with river and canal network clearly contradicts sustainable development.

## 2 Study Area

Kuttanad is a paddy-rich region and called as 'Rice bowl of Kerala'. It is spread in 875 km<sup>2</sup> and drained by network of four rivers originating from Western Ghats. The wetlands cover more than two-thirds of the land area. Vembanad, Ashtamudi and Shasthanamkota are three of its large lagoons forming wetlands of environmental importance.

Till 1970s farmers used to have only one crop a year, but with the introduction of new fertilizers and pesticides and also by constructing barrage (bund) that would cease the saline water, farmers successfully enacted the plan of two crops a year. After adoption of two-crop regime, lot of chemical input was applied to the fields which eventually got flushed as toxic contaminants to the adjoining river. The department of agriculture reported that pesticides used by the farmers of Kuttanad region for production of one tonne of rice is twice of that used by rest of the state. With the penetration of education in the villages, many people disowned farming and took up alternate employment options. Unlike in the past, the people in this region do not depend on water for their living. This change in dependency on water in the water-rich region needs thorough investigation. Most of the water ways are now covered



Fig. 1 Google earth image of the study region

with hyacinths and cannot be used for transportation. Extensive construction of roads has resulted in increased bus services thus resulting in decrease of boat services.

The roads were constructed over river beds blocking the flow of water, the roads have increased the monetary value of the land and more and more people supported the construction of roads even if the basic conditions were violated. Waterways were no more a basic necessity for the people in Kuttanad. Gradually they reduced their dependency on water. Though the main waterways seem to be clean and flowing freely, the small channels and canals connecting to the main waterways are flooded with hyacinth. This is posing a challenge to the people who engage in old traditional business activities that are dependent on waterways. Due to dumping of plastics and non-biodegradable waste into the canals, the water doesn't flow freely. The overall water quality in the waterway has degraded due to high degree of pollution.

All these factors have affected the river flow and thus water had become stagnant, which has become a breeding place for most of the parasites causing severe health problems [2]. Dumping of solid waste has resulted in raising the river bed. This poses a serious problem as the discharge of around 3000 mm gets added annually into the river. With the given state of river system, it is required that the advantages of waterways should be worked out and ways of restoration should be planned.

A portion of the Kuttanad region, i.e. AC canal, Ramankary, Mancombu, Kidangara, Nedumudi are taken for an extensive study as marked on Google earth image in Fig. 1.

### 3 Materials and Methods

The sites identified for samplings are extensively used for domestic and agricultural purposes. The water samples were collected from flowing and stagnant water. The samples were collected in pre-cleaned polythene bottles. The physical parameters were noted down at the time of collection. The water collected was then tested by standard procedures in the laboratory to determine its chemical characteristics. The coordinates of the points from where the water samples were taken is found by using a mobile GPS device. Using the GPS device, tracks were saved while travelling by the route, on car and on boat. The tracks and the coordinates were then plotted in Google earth for representation and planning of new waterways. The estimation of travel times on water as well as on road has been determined by travelling the specific route. The average speed of the car is taken as 25 km/h for entire course and average speed of boat is taken as 15 km/h. The time taken for water route is estimated by general enquiry from locals. The service route network is carried out using route analysis [1]. The environmental hazard posed by the river and water bodies in Kuttanad regions of Kerala is studied and solutions are suggested in this study.

### 4 Results and Discussions

The routes selected for this study are of three different types. First travel route exists and is functional, second one exists and is non-operational and third one exists partially. Table 1 lists the routes analysed and its distance via water and road travel, respectively. Table 2 presents the calculated timings in real-life situation with stoppage time for crossings and traffic allowance. Figure 2 shows water and road route along the routes being considered for analysis.

Terms used in Table 2 is explained below:

**Real road time:** The time taken after taking road allowance into account. It is the actual time noted by travelling through the route.

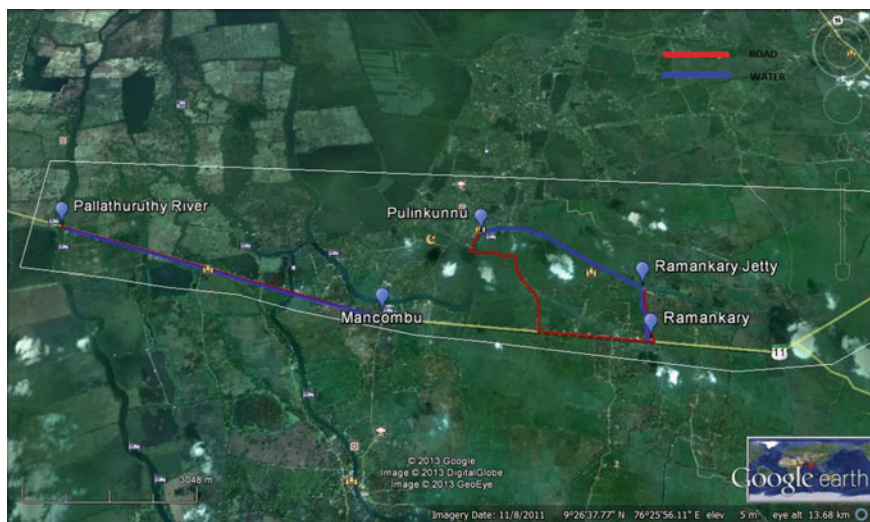
**Road allowance:** The average speed of the car during the run is taken as 25 kmph, the roads considered in this project involves street roads of width less than 3 m, thus smooth two-way traffic is restricted causing extra time to take over the vehicle in the opposite direction. The extra time taken for the additional traffic and conditions of road is taken as road allowance.

**Table 1** Description of selected routes and distance comparison between different modes of travel

Route name	Route description (from-to)	Road distance (km)	Water distance (km)
R1	Ramankary Jetty–Pulinkunnu	6.57	3.52
R2	Ramankary Jetty–Ramankary	1.16	1.12
R3	Mancombu–Pallathuruthi River	7	6.89

**Table 2** Travel speed and time comparison

Route name	Real road time (mins)	Road allowance (mins)	Best road time (mins)	Real water time (mins)	Water allowance (mins)	Best water time (mins)	PSI
R1	24.7	9	15.7	22.38	8.3	14.08	0.570
R2	4.784	2	2.784	15	10.52	4.48	0.936
R3	16.8	0	16.8	27.56	0	27.56	1.640

**Fig. 2** Google earth image showing routes selected for analysis (blue line indicates water route, red line indicates road route)

**Best road time:** It is the difference of best road time and road allowance.

**Real water time:** The real time taken by water is the time taken by boat or ferry to cover the distance mentioned.

**Water allowance:** The travel by water sometimes includes stopping at various substations and water allowance is the time taken for these stoppings en route. It also takes into account the variation in speed caused by motor.

**Best water time:** Time taken for travel by water, considering its average speed of 15 kmph.

**Passenger Service Index (PSI):** It is the ratio of time taken for travel by water to the time taken by road.

$$PSI = (\text{water time}/\text{road time})$$



## 4.1 Travel Route Analysis

### Travel Route 1

Travel route 1 (Fig. 1) is known for the conveyance of more than 200 children to their school every day. The time estimates clearly show that travel by boat is much time-saving. The real reason behind the option of choosing this water route is that though the distance by road is only 7 km the roads are narrow, 3 m width and there is a bridge of 2.5 m width which needs to be crossed. The width of the bridge being too narrow, the conveyance of more than 200 children in a school is not possible. This is the main reason why this water route is still operational in Kuttanad. The boat transport can be used effectively by the locals to go to the nearby villages and markets. At the moment, it is possible only for the people who own a ferry. Small boat services along this river during the peak time which is 7:30 am to 9 am and 4 pm to 5:30 pm will see more people using the route.

The real time taken by water travel is the time taken by State Water Transport Department (SWTD) boat along the route, and it includes four stops en route.

### Travel Route 2

Travel route 2 (Fig. 1) is a canal of 3.5 m width which existed and was used extensively by people to go to the AC canal. The AC canal connects Alleppey to Changanacherry both of which are the major commercial centres around the region. The canal traffic is now about one ferry per two hrs. It is mostly used by fishermen to take fish to the AC road. There are no public or private transport buses operating from this area to the main road. People living on the opposite side of Ramankary across the pampa tributary can use this canal extensively. At the moment, people hire an auto rickshaw from boat jetty after crossing the river by ferry. Thus small boat services which offer services to take the passengers from boat jetty to canal will help the individuals greatly. Ramankary Jetty itself is a significant landmark as it has a higher secondary school. Therefore, additional services offered by the small boats will definitely attract individuals.

The real time taken by water is taken after consulting the locals the time taken by manually operated ferry. Water allowance is provided for the increased speed by motors in this case.

### Travel Route 3

Travel route 3 (Fig. 1) is the AC canal itself. It is a man-made canal constructed in the 1980s to help the conveyance and agriculture. The dugout earth from the agricultural fields was used to make roads along the canal thus giving rise to bridges and a clear definite connectivity between Alleppey and Changanacherry by road. The road connectivity has increased over the years and is the number of bridges. The AC canal on the other hand did not serve its purpose completely. There are 124 homes on one side of the bank from Changanacherry to Kidangara. By rough estimation, there are about 500 individuals depending upon the canal in one way or the other. They use the water from AC canal for domestic and agricultural purposes and the canal is a part of their lifestyle. According to MS Swaminathan report, there are 171

illegal constructions causing the obstruction in the flow of the canal. The canal has to be connected to the Pallathuruthy River for a better flow and to avoid the extensive growth of weeds in the canal. It is to be noted that there was state transport boats in this region in the 1990s. Many bridges constructed across the river not only hampered the flow but also failed to give enough clearance for the boats plying in this route.

Water transport in this region declined steeply and in the course of time the encroachments increased by landfilling. Thus the canal which was used for transport and domestic activities has no more transport but still serves for the domestic purposes extensively. If this route is functional and had served its original idea, it can be used for the transport of materials between the two commercial hubs. The route can be used for tourist activities, and tourists can go from Alleppey backwaters to Changanacherry by boat which will increase the economic avenue of Changanacherry. At the moment, the tourists are taken from Alleppey to Kottayam. The development of AC canal is further necessary as it hosts boat races annually, and on every occasion prior to the race, the canal is cleared of weeds. KTDC (Kerala Tourism Development Corporation) owns a guest house in Changanacherry at the starting point of the AC canal. They have done considerable amount of development activities to promote tourism by constructing concrete platforms and small structures in the middle of the canal which would offer refreshments. The idea is very much appreciated, but the whole project was a failure as the canal is not in operation. Water transport in Kuttanad can further be developed by constructing canals to join the AC canal by taking the population into consideration. The economy of the region will improve by creating new jobs for the locals and encouraging them to create a small commercial hub based on waterways.

The time taken by water is calculated by taking into account the average speed of boat.

## 4.2 Summary of Route Analysis

Tables 3, 4 and 5 illustrate the comparison of water transport with road transport at varying speed. The development of motorboats and increased speeds will give numerous commendable scenarios. For calculation of  $PSI(X)$ , it is assuming that there is considerable development of motorboats in the study region.  $PSI(X)$  is calculated by using the increased speed by water and road time is kept constant (calculated at speed of 25 kmph). Figure 3 supports the comparison results. Key points to be noted in the analysis are

- $PSI$  value for a fully existing route is found to be 0.57. Thus when the value is close to 0.57, water travel is much efficient than road travel. Road may act as an alternative mode of transport.
- $PSI$  value for route 2 is found to be 0.93; thus for a route to act as an alternative mode, the  $PSI$  value need to be around this value.

**Table 3** Travel time and speed comparison for Route 1

Speed	Water distance	Road distance	Best water time	Best road time	PSI	PSI(X)
5	3.52	6.57	42.24	87.840	0.481	1.705
15	3.52	6.57	14.08	35.280	0.399	0.568
25	3.52	6.57	8.448	24.768	0.341	0.341
35	3.52	6.57	6.03	20.263	0.298	0.243
45	3.52	6.57	4.69	17.760	0.264	0.189
55	3.52	6.57	3.84	16.167	0.238	0.155
65	3.52	6.57	3.24	15.065	0.215	0.131
75	3.52	6.57	2.816	14.256	0.198	0.114

**Table 4** Travel time and speed comparison for Route 2

Speed	Water distance	Road distance	Best water time	Best road time	PSI	PSI(X)
5	1.12	1.16	13.440	15.920	0.844	2.809
15	1.12	1.16	4.480	6.640	0.675	0.936
25	1.12	1.16	2.688	4.784	0.562	0.562
35	1.12	1.16	1.920	3.989	0.481	0.401
45	1.12	1.16	1.493	3.547	0.421	0.312
55	1.12	1.16	1.222	3.265	0.374	0.255
65	1.12	1.16	1.034	3.071	0.337	0.216
75	1.12	1.16	0.896	2.928	0.306	0.187

**Table 5** Travel time and speed comparison for Route 3

Speed	Water distance	Road distance	Best water time	Best road time	PSI	PSI(X)
5	6.89	7	82.680	84.000	0.984	4.921
15	6.89	7	27.560	28.000	0.984	1.640
25	6.89	7	16.536	16.800	0.984	0.984
35	6.89	7	11.811	12.000	0.984	0.703
45	6.89	7	9.187	9.333	0.984	0.547
55	6.89	7	7.516	7.636	0.984	0.447
65	6.89	7	6.360	6.462	0.984	0.379
75	6.89	7	5.512	5.600	0.984	0.328

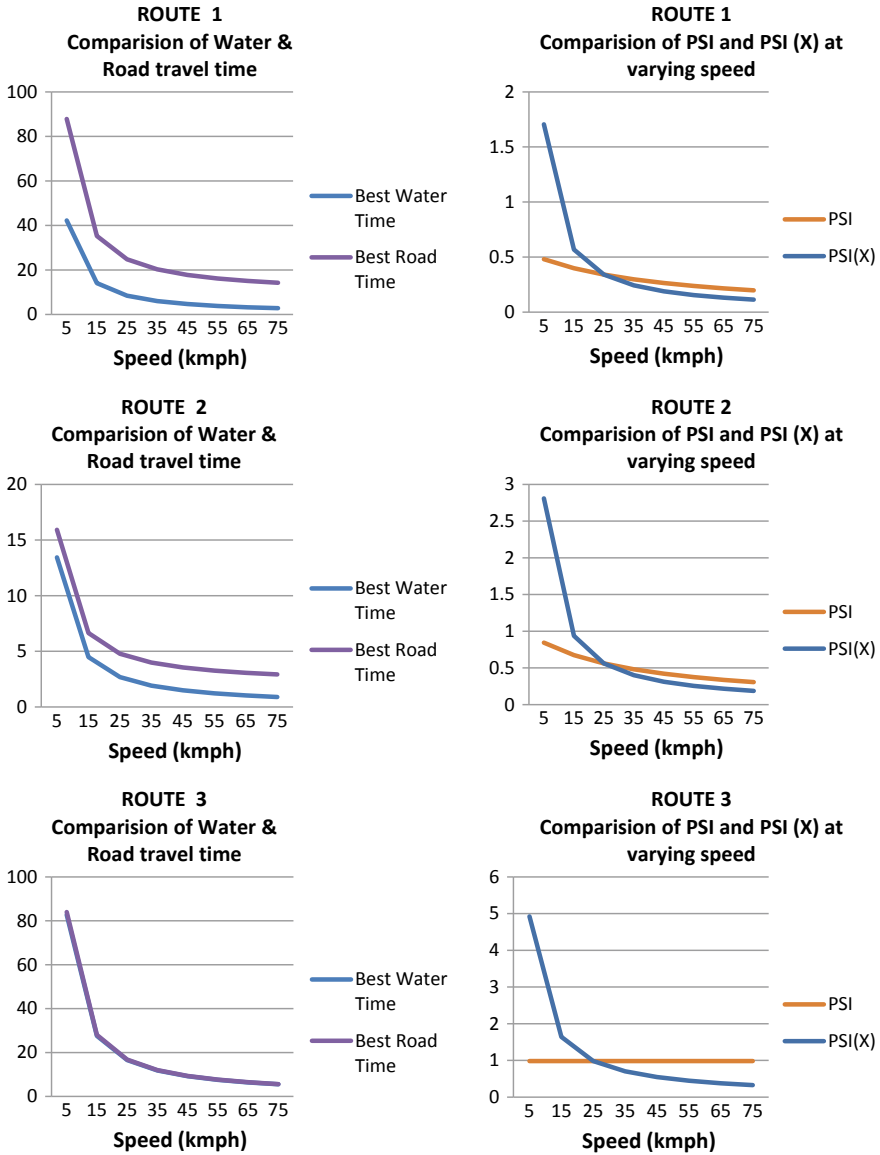


Fig. 3 Comparison result of different routes at varying speed

- PSI value for route 3 is found to be 1.64; in this case, water transport may act as a complementary mode of transport.
- Complementary water travel can be considered because of reduction in the travel cost, but complementary road transport does not work in the real scenario. It proves the non-usage of route 1 by road.

The value of  $PSI(X)$  indicates that the increased speed of boats can give different scenarios for alternative and complementary water networks.

### 4.3 Observation on Water Quality

Basic water quality tests like pH, hardness, alkalinity and dissolved oxygen have been carried out on the water samples collected from flowing water and stagnant water (Fig. 4).

#### Physical Characteristics

The characteristics of water samples at the time of collection are mentioned in Table 2. The temperature does not vary much as the sites are very close to one another. The variation from 27 to 31 °C is due to the collection of water samples on different days. Since the water was collected from the banks, the flowing water had some suspended particles scattered in it which caused the turbidity. Turbidity of water samples were categorized as less, medium and high. The colour is mentioned as it was observed at the time of collection.

#### Potential of Hydrogen (pH)

The pH values of water collected from stagnant water is slightly acidic and is falling out of the potable water standards. On the other hand, the water samples collected from flowing water is found to be within the limits of various standards issued by BIS and WHO. The slight acidity of the water is explained by the leaching effect of soils from agricultural fields, mainly paddy. The effect of leachates on the flowing water is temporary since the self-purification process of water regenerates its original quality.

#### Alkalinity

The total alkalinity of water samples was very low. There was not much variation between the flowing and stagnant water samples for alkalinity. The low values show the absence of carbonates and hydroxides in the water samples. Only bicarbonates are present in the water collected, thus the ability to neutralize acidity of these water samples is very low.

#### Dissolved Oxygen (DO)

The dissolved oxygen level for stagnant water was found to be about 3 mg/l. Meanwhile, the water samples collected from flowing water samples had DO of 5 mg/l. The dissolved oxygen levels for stagnant water is very low as the minimum DO content for the survival of fish is 4 mg/l. As mentioned earlier, the water after irrigation

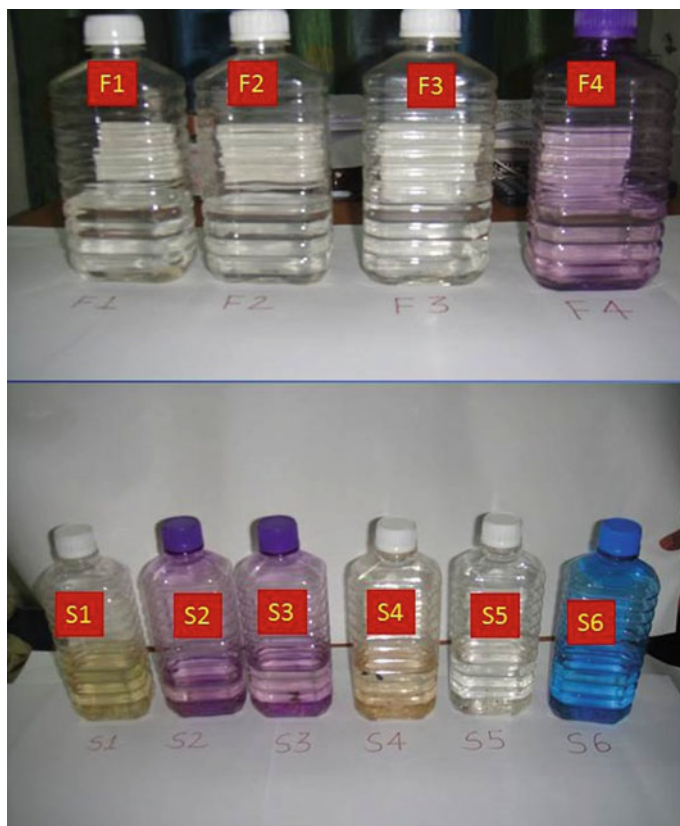


**Fig. 4** Water samples collected from flowing (F1, F2, F3, F4) and stagnant water sources (S1, S2, S3, S4, S5, S6)

activities are pumped back into the AC canal, thus the water is rich in pesticides and fertilizers. The nutrient-rich water is left stagnant and favours the growth of hyacinth and other weeds. This process has culminated into the process of eutrophication.

### Hardness

The hardness of water samples indicates the foaming ability of water. The flowing and the stagnant water samples were collected from sites where they are used extensively for domestic purposes like washing of clothes, utensils and bathing. The water samples collected from stagnant water samples showed that the water in the AC canal (stagnant) was ranging from moderately hard to medium hard. On the other hand, the flowing water has values showing it to be soft and on the lower side of moderate hardness.

## 5 Conclusion

Water transport was once an integral part of the people in Kuttanad. The advent of roads and motor vehicles has changed their lifestyles drastically. State water transport department has cancelled their services over the years due to low clearance provided by the bridges and thick vegetation which hamper the movement of vessels. The lack of advancement in the water transport in the Kuttanad region has further added to the cause of negligence of water resources. The study shows different types of water routes which can suit as a complementary and alternative mode of travel.

The inhabitants of villages living between Alleppey and Changanacherry have to reach AC road by some means and then wait for the bus services which originate from the town. Since this is the only option, it causes congestion during the peak hours. In today's scenario of rising prices, a cheaper alternative will be much appreciated by the people. Apart from conveyance, once functional the water courses will have many advantages in terms of economic and environmental perspective. Motor attached to the ferries can increase the speed of the vessel to a certain extent, and many programmes to encourage the residents to take-up water transport should be conducted by the authorities.

The present study on the water quality of the Kuttanad region has certain limitations due the non-availability of specific information on the epidemic outbreaks. However, the Alleppey medical college records of the past five years reveals that, of the total people admitted due to waterborne diseases, 70% belong to the study region. Also the waterborne diseases which used to occur only during the monsoon period are now all year round. Unscientific constructions of roads and bridges arresting the water flow cause the formation of large pools of stagnant and contaminate water which becomes a breeding ground for bacteria and mosquitoes. It is also to be noted that the quality of water standards when entering the AC canal is within the limits and along the course of the AC canal its quality depletes. The water used for agriculture is the same, which was flushed out in the previous season due to the absence of flow. This process has affected the agriculture sector dearly and immediate actions need to be taken.

## References

1. Adejare QA, Nwilo PC, Olusina OC, Opaluwa YD (2011) A study of ferry service route network in Lagos Lagoon Nigeria using graph theory. *J Geogr Reg Plann* 4(6):326–337
2. Meera S, Bijoy Nandan S (2010) Water quality status and primary productivity of Valanthatkadd backwater in Kerala. *Indian J Mar Sci* 39(1):105–113
3. Rangaraj N, Raghuram G (2007) Viability of inland water transport in India, INRM policy brief. Asian Development Bank, New Delhi
4. Swaminathan MS (2007) Measures to mitigate agrarian distress in Alleppey and Kuttanad Wetland Ecosystem: M S Swaminathan research foundation
5. Sriraman S (2009) Perspective on inland water transport in India. *Rites J*

6. UNESCAP (2004) Manual on modernization of inland water transport for integration within a multimodal transport system. <http://www.unescap.org/ttdw/PubsDetail.asp?IDNO=144>
7. World Bank (2002) Cities on the move: a world bank urban transport strategy review Washington DC, USA